



UNIVERSIDAD NACIONAL AUTÓNOMA DE MÉXICO

Maestría y Doctorado en Ciencias Bioquímicas

**EL PÉPTIDO VSAK DERIVADO DE LA REGIÓN CARBOXILO TERMINAL DE
CETPI COMO AGENTE TERAPÉUTICO EN SEPSIS Y CHOQUE SÉPTICO**

TESIS

QUE PARA OPTAR POR EL GRADO DE:

Doctor en Ciencias

PRESENTA:
ISMAEL LUNA REYES

TUTOR PRINCIPAL
Jaime Mas Oliva
Instituto de Fisiología Celular

MIEMBROS DEL COMITÉ TUTOR

Miguel Ángel Ávila Rodríguez
Facultad de Medicina

Alejandro Zentella Dehesa
Instituto Nacional de Ciencias Médicas y Nutrición Salvador Zubirán

Ciudad de México. Enero, 2024



UNAM – Dirección General de Bibliotecas

Tesis Digitales
Restricciones de uso

DERECHOS RESERVADOS ©
PROHIBIDA SU REPRODUCCIÓN TOTAL O PARCIAL

Todo el material contenido en esta tesis está protegido por la Ley Federal del Derecho de Autor (LFDA) de los Estados Unidos Mexicanos (Méjico).

El uso de imágenes, fragmentos de videos, y demás material que sea objeto de protección de los derechos de autor, será exclusivamente para fines educativos e informativos y deberá citar la fuente donde la obtuvo mencionando el autor o autores. Cualquier uso distinto como el lucro, reproducción, edición o modificación, será perseguido y sancionado por el respectivo titular de los Derechos de Autor.



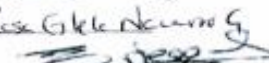
CGEP/PMDCBQ/1394
C4DBA6-65416ABE5287E
Asunto: Jurado de examen

SINODALES DESIGNADOS
Presente

Estimado académico:

Los miembros del Subcomité Académico en reunión extraordinaria **de octubre de 2023**, conocieron la solicitud de asignación de **JURADO DE EXAMEN** para optar por el grado de **Doctor en Ciencias** de la estudiante **LUNA REYES ISMAEL**, con la tesis "**El péptido VSAK derivado de la región carboxilo terminal de CETPI como agente terapéutico en sepsis y choque séptico**", dirigida por el/a Dr(a). **MAS OLIVA JAIME**.

De su análisis se acordó nombrar el siguiente jurado en el que se encuentra usted incluido:

			ACEPTE	FECHA	FIRMA
ALAGÓN CANO ALEJANDRO	PMDCBQ	PRESIDENTE	SI <input checked="" type="checkbox"/> NO <input type="checkbox"/>	13 / 11 / 23	
NAVARRO GONZÁLEZ ROSA ESTELA	PMDCBQ	SECRETARIO	SI <input checked="" type="checkbox"/> NO <input type="checkbox"/>	16 / 11 / 23	
ORTEGA SOTO ENRIQUE	PMDCBQ	VOCAL	SI <input checked="" type="checkbox"/> NO <input type="checkbox"/>	8 / 11 / 23	
SALCEDA SACANELLES ROCÍO	PMDCBQ	VOCAL	SI <input checked="" type="checkbox"/> NO <input type="checkbox"/>	7 / 11 / 23	
ZARAIN HERZBERG ANGEL ALFONSO	PMDCBQ	VOCAL	SI <input checked="" type="checkbox"/> NO <input type="checkbox"/>	9 / 11 / 23	

Una vez firmando este documento, favor de enviarlo a la coordinación del programa al correo ipalacios@posgrado.unam.mx

Sin otro particular por el momento, aprovecho la ocasión para enviarle un cordial saludo.

Atentamente
"POR MI RAZA HABLARÁ EL ESPÍRITU"
Cd. Universitaria, Cd. Mx., a 31 de octubre de 2023



Coordinadora
Dra. Claudia Lydia Treviño Santa Cruz

Agradecimientos institucionales

A CONAHCYT a través del programa de Becas de Estudios de Posgrado Nacionales en el periodo 01/Agosto/2019 - 31/Julio/2023. Número de apoyo: 749440

Al Programa de Maestría y Doctorado en Ciencias Bioquímicas, periodo 2020-1 – 2023-2

Al Programa de Apoyo a Proyectos de Investigación e Innovación Tecnológica por el apoyo financiero brindado a través de los proyectos IN205717 e IN206619

Al Programa de Apoyo a los Estudios del Posgrado por el apoyo brindado par la asistencia al “The 36th European and 12th International Peptide Symposium”, con el trabajo “Peptide VSAK Derived from the C-Terminal Region of CETPI Blocks LPS in an Animal Model of SIRS. Evidence Using PET-Imaging”

Al Dr. Arturo Avendaño Estrada y la M.V.Z Dafne Garduño de la unidad de MicroPET de la Unidad de PET/Ciclotrón de la Facultad de Medicina.

A la M.V.Z. Claudia Rivera Cerecedo y al M.V.Z Héctor Malagón de la Unidad de Bioterio del Instituto de Fisiología Celular

Al Dr. Jorge Ramírez de la Unidad de Microarreglos del Instituto de Fisiología Celular

Al Ing. Leobardo Itehua Rico Coordinador de Supercómputo de la DGTIC. Por el apoyo brindado en la super computadora Miztli con el proyecto LANCAD-UNAM-DGTIC-352

Al Taller De Mantenimiento Electrónico, Eléctrico y Mecánico del Instituto de Fisiología Celular

A la unidad de Biología Molecular del Instituto de Fisiología celular.

A la Unidad de Computo del Instituto de Fisiología Celular

Agradecimientos personales

A mi tutor el Dr. Jaime Mas Oliva por permitirme formar parte de su grupo de investigación y la confianza depositada durante el desarrollo de este proyecto, junto con su siempre optimista guía e instrucción.

A los integrantes de mi comité tutor, el Dr. Miguel Ángel Ávila Rodríguez y el Dr. Alejandro Zentella Dehesa, por los consejos y asesoría brindados a lo largo del proyecto.

A Blanca Delgado Coello, por todo el apoyo brindado en el laboratorio, su amistad y consejos.

A los integrantes del comité sinodal: Dr. Alejandro Alagón, Dra. Rosa E. Navarro, Dr. Enrique Ortega, Dra. Rocío Salceda y Dr. Ángel A. Zarain, por la revisión del trabajo de tesis y valiosos comentarios

A mis compañeras de laboratorio Roxana Gutiérrez, Eréndira Pérez y Sandra Calixto, por su amistad y apoyo en el trabajo del laboratorio.

A mis padres Venerando Luna y Yesenia Reyes y mis hermanos Octavio y Laura, por todo su apoyo y comprensión.

A mis amigos Silvia, Salomón e Isaí por todos los años de amistad y apoyo

A mis amigos biomédicos Emilio “Pastor”, Oscar, Josué y Cristian, por las siempre agradables pláticas de relevancia científica.

A la memoria de Teódulo “Teo” Arellano y el Dr. Alfredo Torres.

Yo grito que no creo en nada y que todo es absurdo, pero no puedo dudar de mi grito y tengo que creer por lo menos en protesta.

Je crie que je ne crois à rien et que tout est absurde, mais je ne puis douter de mon cri et il me faut au moins croire à ma protestation.

-Albert Camus

Lista de abreviaturas

[¹⁸ F]-FDG	2-[¹⁸ F]Fluoro-2-Desoxi-D-Glucosa
1L-1 β	Interleucina 1-Beta
ARNm	Ácido Ribonucleico mensajero
BPI	Proteína Incrementadora de la Permeabilidad Bactericida
CD14	Clúster de Diferenciación 14
CETP	Proteína de Transferencia de Esteres de Colesterol
CETPI	Proteína Transferidora de Esteres de Colesterol
DMEM	Dulbecco's Modified Eagle Medium
HDP	Péptidos de Defensa del Anfitrión
IL-1 α	Interleucina 1-Alfa
IL-8	Interleucina 8
IRAK-1	Cinasa Asociada al Receptor IL-1 1
IRAK-4	Cinasa Asociada al Receptor IL-1 4
I κ K	Cinasa del Inhibidor de κ B
KDO	ácido-ceto-desoxi-octuglucosídico
LBP	Proteína de Unión a LPS
LPS	Lipopolisacáridos
MAMPS	Patrones Moleculares Asociados Microorganismos
MAP-cinasas	Cinasas activadas por Mitógeno
MD2	Factor de Diferenciación 14
MIP-1 β	Proteína Inflamatoria de Macrófagos 1-beta
MSD	Desplazamiento cuadrado medio
MyD88	Gen 88 de respuesta primaria de Diferenciación Mieloide
NEO-3	Neoseptina-3
NF- κ B	Factor Nuclear κ B
pb	Pares de Bases
PCR	Reacción en cadena de la polimerasa
PLUNC	Proteínas Clon del Paladar, pulmón y epitelio Nasal
POPC	Fosfatidilcolina
POPS	Fosfatidilserina
PRR	Receptores de Reconocimiento de Patrones
TAK-1	Cinasa activada por el factor transformante β 1
TIR	Receptor TOLL-Interleucina-1
TLR-4	Receptor similar a TOLL-4
TNF α	Factor de Necrosis Tumoral Alfa
TRAF-6	Factor Asociado al Receptor TNF- 6
TRIF	Adaptador contenedor de dominio TIR inductor de IFN- β

ÍNDICE.

1. RESUMEN	1
2. ABSTRACT	2
3. INTRODUCCIÓN	2
3.1. Infección, sepsis y choque séptico	3
3.1.1. Reconocimiento de LPS por TLR-4.....	9
3.1.2. Señalización de TLR-4	11
3.2 Lipopolisacáridos.....	13
3.3. Péptidos de defensa del Anfitrión	16
3.4. CETP, CETPI y el péptido VSAK.....	19
4. PLANTEAMIENTO DEL PROBLEMA	25
5. HIPÓTESIS	26
6. OBJETIVO GENERAL.....	26
6.1. OBJETIVOS PARTICULARES	26
7. MATERIALES Y MÉTODOS	27
7.1. Péptido VSAK.....	27
7.2. Lipopolisacáridos.....	27
7.3. Simulaciones de dinámica molecular.....	27
7.4. Microscopía Electrónica	28
7.5. Ensayos de Hemólisis	29
7.6. Cultivo celular.....	30
7.7. Ensayos celulares.....	30
7.8. Viabilidad celular	31
7.9. PCR Tiempo real	31
7.10. Equipo de micro-PET	33
7.11. Estudio de PET	33
7.12. Protocolo de adquisición PET	35
7.13. Reconstrucción y análisis de datos de captura.....	35
7.14. Medición citocinas proinflamatorias.....	36
7.15. Análisis estadístico	36
8. RESULTADOS	37
8.1 Simulaciones de dinámica molecular.	37
8.1.1. Efecto de VSAK en la energía del sistema.....	37

8.1.2. Cambios en la fluidez de la membrana	41
8.2. Efecto de VSAK en la estructura de los LPS	42
8.3. Efecto hemolítico.....	44
8.4. Ensayos de viabilidad celular.....	46
8.5. Ensayos de estimulación con LPS y NEO-3	47
8.5.1. Células HAEC - Expresión de marcadores pro-inflamatorios.....	47
8.5.2. Células THP-1 - Expresión de marcadores pro-inflamatorios	49
8.6. Ensayos de PET.	51
8.6.1. Reconstrucción tridimensional.....	51
8.6.2. Valor de captación total	52
8.6.4. Marcadores proinflamatorios.....	55
8.6.5. Niveles de Glucosa e Insulina	57
9. DISCUSIÓN.....	58
10. CONCLUSIONES	71
11. PERSPECTIVAS.....	72
12. BIBLIOGRAFÍA.....	73
ANEXO I. Publicaciones generadas durante el proyecto de doctorado.....	92

1. RESUMEN

Durante este proyecto se analizó la capacidad del péptido VSAK para unir lipopolisacáridos (LPS) bacterianos y su efecto en el desarrollo de la respuesta inmune inducida por los LPS. VSAK es un péptido catiónico de dieciocho aminoácidos derivado del extremo carboxilo terminal de la proteína CETPI (Isoforma de la proteína de Transferidora de Esteres de colesterol). En estudios previos este péptido había mostrado capacidad de unirse a los LPS y limitar la producción de marcadores de inflamación.

A lo largo de este estudio nos enfocamos en entender a mayor profundidad las implicaciones de esta interacción de VSAK y los LPS, mediante ensayos *in silico*, *in vitro* e *in vivo*. Utilizando simulaciones de dinámica molecular se analizó la capacidad de VSAK para unirse selectivamente a membranas que contienen LPS en comparación con membranas únicamente constituidas por Fosfatidilcolina o Fosfatidilserina. Además, estos ensayos nos dieron información del efecto de VSAK en la estabilidad energética de las membranas de LPS y los cambios inducidos en las propiedades de estas por el péptido. Por otro lado, se generaron variantes del péptido para entender el efecto de las cargas positivas en la unión selectiva de VSAK a las estructuras de LPS. Experimentalmente, estos efectos de VSAK fueron validados con el apoyo de microscopía electrónica, en la que se observó como VSAK era capaz de alterar el patrón de agregación de los LPS en fibras cubicas para inducir la formación de agregados de LPS.

Por otro lado, a nivel celular mediante ensayos *in vitro*, se analizó la inocuidad del tratamiento de VSAK concentraciones muy altas de este péptido, mediante ensayos de citotoxicidad. Adicionalmente, se utilizaron células de las líneas THP-1 y HAEC para analizar los efectos de VSAK en la respuesta ante un reto con LPS. En estos ensayos se encontró una atenuación importante de la expresión de marcadores proinflamatorios, que fue más notable en las células THP-1 debido a su origen inmune. En adición, en esta línea celular se observó la capacidad de VSAK para atenuar el efecto inflamatorio de Neoseptina-3, un agonista no lipídico de TLR-4 con el que no se esperaba un efecto de VSAK.

Finalmente, utilizando un modelo animal de inflamación sistémica inducida por LPS, se analizó el papel de VSAK durante la respuesta sistémica. En estos ensayos se utilizó la Tomografía de Emisión de Positrones con [¹⁸F]-FDG para analizar cambios en el metabolismo ante el reto de LPS. Estos ensayos indicaron que VSAK puede atenuar la respuesta sistémica a nivel metabólico al tiempo que reduce la producción de marcadores inflamatorios en este modelo experimental.

En conjunto, los diferentes ensayos realizados soportan la capacidad de unión de VSAK a los LPS, la cual puede ocurrir inclusive cuando es administrado *in vivo*. Esta unión tiene un efecto atenuador de la respuesta a los LPS, lo cual disminuye el desarrollo de la respuesta inflamatoria. Por otro lado, los ensayos celulares utilizando Neoseptina-3 indican que VSAK puede tener otros efectos reguladores de la respuesta inflamatoria independientes a la interacción del péptido con los LPS, los cuales será necesario estudiar a profundidad en futuros proyectos

2. ABSTRACT

In this project, it was analyzed the ability of VSAK peptide to bind bacterial lipopolysaccharides (LPS) and their effects on the associated immune response. VSAK is an 18-amino acid length cationic peptide derived from the C-terminal region of CETPI (Cholesteryl Ester Transfer Protein Isoform). In previous work, the LPS-binding properties of this peptide as well as the associated decrease in the production of inflammation markers have been described.

Our present study focused on deeply understanding the implications of LPS-binding properties of VSAK, through *in silico*, *in vitro*, and *in vivo* approaches. By means of molecular dynamics simulations, we analyze the selective binding of VSAK to LPS-containing membranes compared to phosphatidylcholine-only or phosphatidylserine-only membranes. From these simulations, we analyzed changes in total energy, where an important change in energetic stability was observed in membranes containing LPS when VSAK was present. To further study the effect of VSAK on thermostability and the contribution of positive charges to LPS binding, we constructed a model of VSAK where positively charged amino acids were removed and replaced by uncharged amino acids. Experimentally, we showed by electronic microscopy techniques that by adding VSAK in different concentrations to LPS in solution, the loss of typical cubical fibrils of LPS and the formation of electrodense aggregates were produced.

In order to analyze possible deleterious effects of VSAK, we exposed different cell lines to high concentrations of the peptide, and no effects on viability were observed. On THP-1 and HAEC cells, we also analyzed the effects on proinflammatory markers, and it was found a decreased production when cells were treated with VSAK plus LPS, compared with LPS-alone. This effect was more noticeable in THP-1 due to its immune origin. Interestingly, on THP-1 cells we also observed a similar decrease after treatment with neoseptine-3 which is a TLR-4 agonist with no structural similarities with LPS.

Finally, using an animal model of systemic inflammation through LPS administration, we analyzed the systemic effects of VSAK *in vivo*. Positron Emission Tomography assays were performed to analyze metabolic changes using [¹⁸F]-FDG as the radiotracer. An important attenuation in the metabolic dysfunction produced by LPS was observed when animals were treated with VSAK along LPS.

Together, the variety of assays performed during this project supports the LPS-binding properties of VSAK, which can be observed even in *in vivo* models. The binding of LPS results in an attenuation of LPS response both *in vitro* and *in vivo*. On the other hand, during the cellular assays using Neoseptin-3, we found evidence indicating that some effects of VSAK on the inflammatory response could be not related to LPS-binding properties. This is an interesting finding that needs to be studied in further research.

3. INTRODUCCIÓN

3.1. Infección, sepsis y choque séptico

Las infecciones son uno de los principales problemas de salud pública de la actualidad, diversos factores han contribuido a los altos índices de mortalidad y morbilidad asociados a las infecciones. Uno de ellos es la propensión al desarrollo de estadios agravados como lo son las sepsis y el choque séptico, caracterizados por la respuesta desregulada del anfitrión ante la infección; lo cual tiene un papel antagónico en la resolución del proceso y pone en riesgo la vida de los individuos. En uno de los meta-análisis más recientes que analizó la morbilidad y mortalidad asociada al desarrollo de sepsis y choque séptico y el alto impacto de estas patologías en la salud pública. En este se observó que en 2017 hubo una incidencia mundial de 48.9 millones de casos de sepsis, además se reportó una mortalidad asociada al desarrollo sepsis en 11 millones de casos, lo cual constituye un 20% del total de muertes registradas en 2017 (Rudd et al., 2020). Fue en este mismo año durante la septuagésima reunión de la Organización Mundial de la Salud cuando la sepsis fue declarada una emergencia de salud pública, con una llamada urgente a la generación de estrategias para disminuir la incidencia y la mortalidad de estas patologías (Reinhart et al., 2017). Recientemente, este llamado a la acción fue reiterado a nivel hispanoamericano en el XXXIII Congreso Mundial de Medicina de Urgencias en Guadalajara, México (Julian-Jimenez et., al 2023).

La relevancia clínica de la sepsis está asociada a factores que favorecen la incidencia generalizada; en países de medios y bajos ingresos el desarrollo de sepsis suele ocurrir a partir de infecciones adquiridas comunitariamente; mientras que países desarrollados la incidencia es mayor en personas con una susceptibilidad mayor a las infecciones (Martin, 2012). Las cuales suelen adquirirse en un contexto nosocomial, en este escenario los más susceptibles suelen ser individuos afectados por enfermedades inmunosupresoras, trauma, quemaduras severas o bajo cuidados de terapia intensiva (Vincent et al., 2009). En las unidades de cuidados intensivo la sepsis y el choque séptico representan la principal causa de mortalidad a nivel mundial. En México el panorama clínico en este contexto es muy similar, uno de los estudios más recientes indica una incidencia de sepsis del

12.9% en las unidades de cuidados intensivos, con una mortalidad del 9.36%, la cual se incrementa hasta un 65.85% en los pacientes que desarrollan choque séptico (Gorordo-Delsol et al., 2020).

El progreso de una infección hacia sepsis y choque séptico está directamente relacionada a la forma en la que el individuo responde a la infección. Durante el curso de la infección, el organismo desarrolla una respuesta inflamatoria ante la invasión del patógeno (Angus & van der Poll, 2013; Van Der Poll et al., 2017). Esto incluye la activación coordinada de mecanismos de la inmunidad innata y adaptativa dirigidos a eliminar al microorganismo invasor. De forma paralela, se activan mecanismos antiinflamatorios que limitan el desarrollo de la respuesta inflamatoria y que permiten la reparación del daño producido por la inflamación y el regreso al estado homeostasis (Figura 1A) (Serhan et al., 2007). Este delicado balance entre la respuesta inflamatoria y los mecanismos antiinflamatorios permiten la correcta resolución de la infección.

Durante la sepsis estos mecanismos de regulación de la respuesta inflamatoria se ven sobrepasados. La carga microbiana resultante de la infección produce un efecto tóxico que conlleva a una hiperactivación de la respuesta inflamatoria, eventualmente la inflamación conduce a una disfunción celular generalizada y daño en distintos órganos (Figura 1B) (Vazquez-Grande, 2015). La respuesta hiperinflamatoria ocurre de forma aguda y está asociada a la mortalidad temprana durante sepsis y choque séptico. Por otro lado, la eventual activación de los mecanismos antinflamatorios contribuye a la patología de la sepsis en fases intermedias y tardías. Estos se activan en respuesta al proceso inflamatorio buscando limitar la inflamación, sin embargo, terminan teniendo efectos deletéreos y contribuyendo a la disfunción celular y el daño orgánico. Durante la sepsis y el choque séptico, el desbalance antinflamatorio está asociado a la disfunción crónica del sistema inmune (exhaustión inmune), lo cual conlleva una susceptibilidad incrementada a infecciones posteriores y la mortalidad en fases ulteriores (Figura 1A) (Cao et al., 2019).

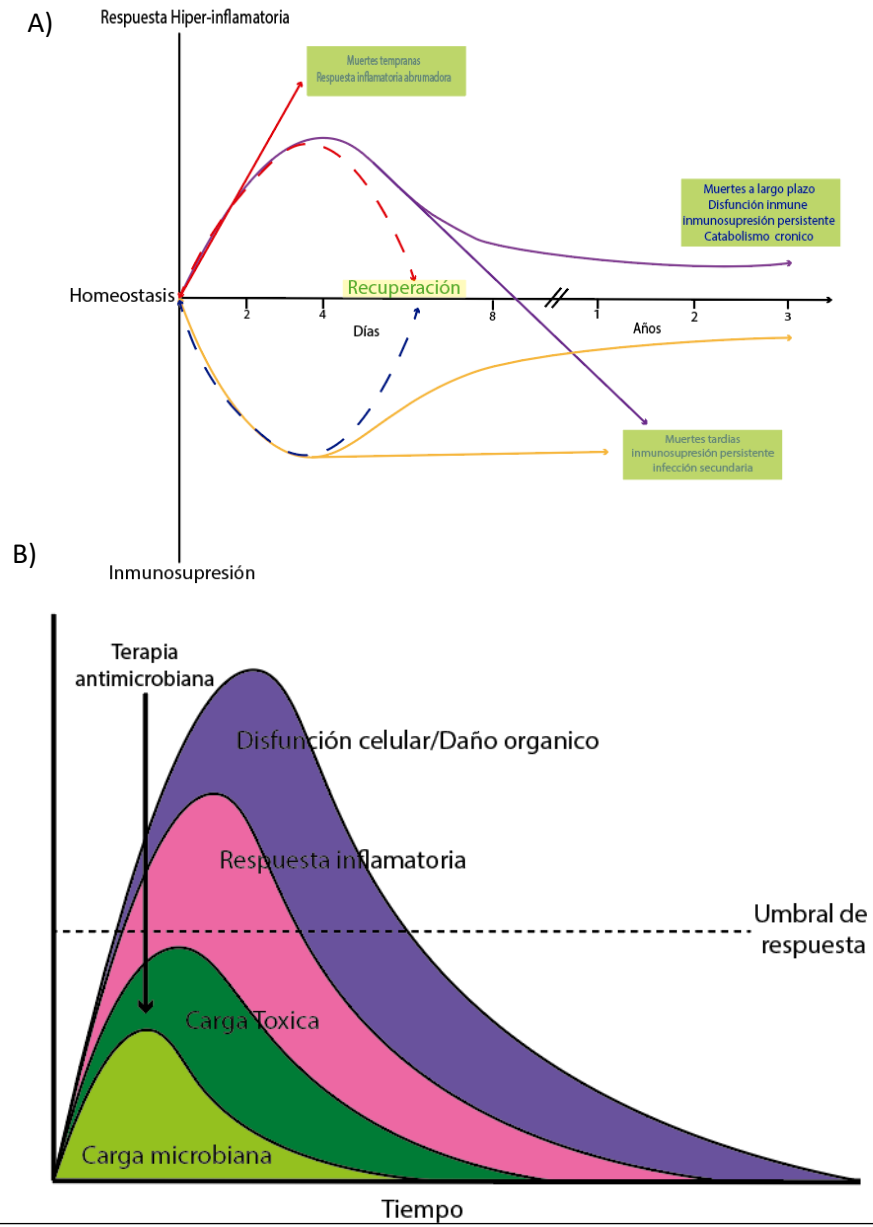


Figura 1 La respuesta del anfitrión en el desarrollo de sepsis y choque séptico. (A) Durante una infección la activación de las respuestas pro y antinflamatoria son necesarias para la correcta resolución de este proceso. Sin embargo, durante la sepsis y le choque séptico la perdida de la regulación de estas respuestas produce daño al anfitrión, al inicio se produce una respuesta hiper-inflamatoria que se asocia con la mortalidad temprana, esta se continua por una activación sostenida de la respuesta antinflamatoria; la cual se asocia a un estado de inmunosupresión y susceptibilidad aumentada a infecciones oportunistas y está relacionada con la mortalidad tardía en sepsis y choque séptico. Las alteraciones producidas en el individuo pueden producir secuelas en el funcionamiento del sistema inmune lo cual produce alteraciones a largo plazo, representando un tercer factor de mortalidad asociado a la sepsis y choque séptico. (B) Durante una infección los microrganismos producen moléculas tóxicas que favorecen la respuesta inmune del anfitrión; mientras esta respuesta se mantenga por debajo el umbral de regulación el proceso puede resolverse sin poner en riesgo al individuo (Cao et al., 2019; Vazquez-Grande Anand, 2015).

Esta respuesta desregulada en el anfitrión es común para la sepsis y el choque séptico, no obstante, en el choque séptico se presenta hipotensión sistémica que es resistente a la administración de vasopresores (Figura 2A) (Angus & van der Poll, 2013). La sepsis y el choque séptico son patologías altamente complejas, lo cual representa un reto importante para el diagnóstico y la aplicación de tratamientos, en el ámbito clínico es muy relevante la apropiada caracterización de los pacientes para brindar las opciones de tratamientos que garanticen un mejor pronóstico (Singer et al., 2016). (Figura 2B)

A pesar de que la sepsis y el choque séptico pueden desarrollarse a partir de la invasión cualquier tipo de microorganismo, la mayor incidencia de sepsis está asociado a infecciones producidas por bacterias (Vincent et al., 2009). Esto está asociado a fenómenos como la diseminación de patógenos que producen infecciones nosocomiales o bien, a países de bajos ingresos en los que la falta de acceso a condiciones adecuadas de higiene favorece la diseminación comunitaria de bacterias patógenas. Adicionalmente, la creciente resistencia a antibióticos se ha convertido en un adyuvante que favorece el desarrollo de sepsis y el choque séptico a partir de las infecciones bacterianas, debido a que la existencia de este tipo de bacterias dificulta la eliminación del patógeno aumentando el tiempo de exposición del anfitrión a subproductos bacterianos que favorecen la respuesta sistémica (Zaman et al., 2017).

En la actualidad las principales bacterias de relevancia clínica incluyen a aquellas especies conocidas como ESKAPE, las cuales están constituidas por: *Enterococcus faecium*, *Staphylococcus aureus*, *Klebsiella pneumoniae*, *Acinetobacter baumannii*, *Pseudomonas aeruginosa*, y *Enterobacter species*. Estas bacterias son especialmente relevantes debido a su amplia distribución y a la importante resistencia a antibióticos observada en estas (Bassetti et al., 2013; Santajit & Indrawattana, 2016). A pesar de que en los últimos años la incidencia de sepsis causada por bacterias Gram positivas, las infecciones por bacterias Gram negativas siguen representando la mayor incidencia para el desarrollo de sepsis y choque séptico (Trecarichi et al., 2015).

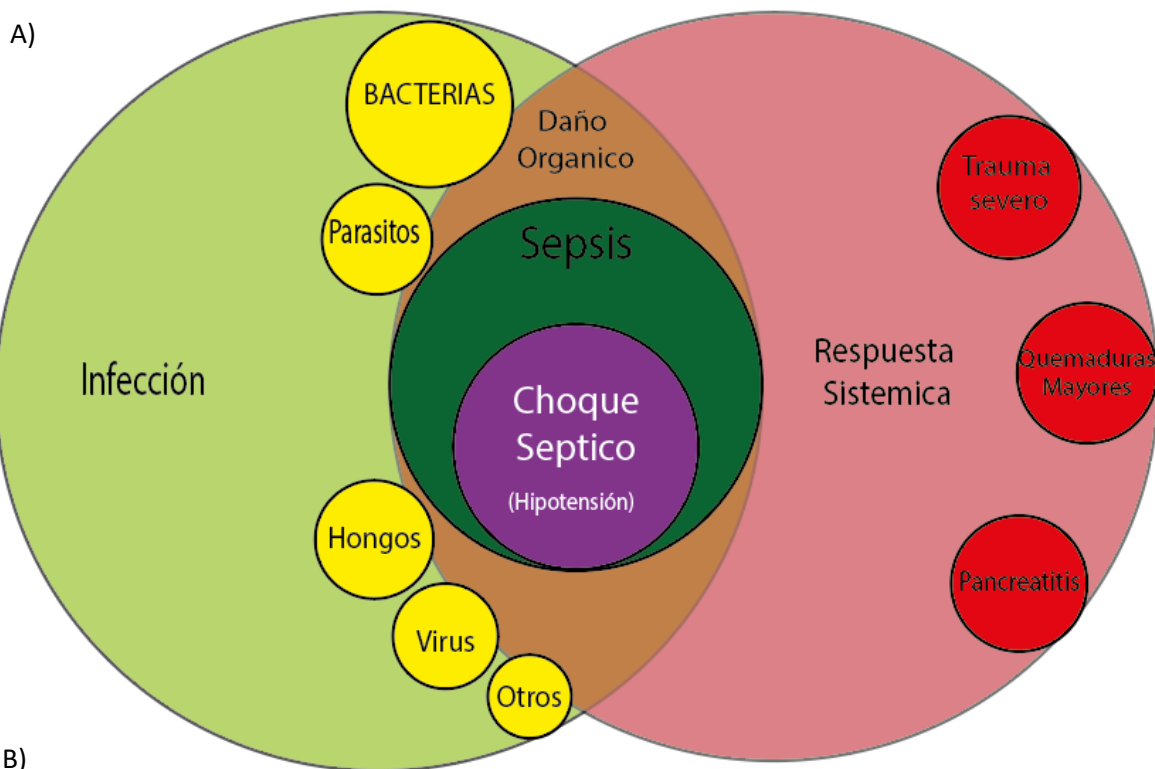


Figura 2. Definiciones internacionales de sepsis y choque séptico (SEPSIS-3). A) Representación esquemática de los procesos de sepsis y choque séptico. La sepsis incluye una infección que puede ser causada por distintos tipos de microorganismos, además de la presencia de la respuesta sistémica la cual no es exclusiva de la sepsis y también puede ser causada por quemaduras severas, trauma, pancreatitis y otras enfermedades. En la sepsis estos factores favorecen el desarrollo del daño celular y orgánico, mientras que el choque séptico presenta una hipotensión resistente a vasoconstrictores (Delano & Ward, 2016). B) Definiciones actuales para sepsis y choque séptico (SEPSIS-3) acorde al tercer consenso internacional para las definiciones de sepsis y choque séptico (Singer et al., 2016).

El desarrollo de la respuesta en el anfitrión depende de la capacidad de este para reconocer a los microorganismos patógenos y montar una respuesta ante ellos. Este reconocimiento es posible gracias a la presencia de un conjunto de receptores con la capacidad de reconocer moléculas que están presentes en los agentes patógenos, en conjunto estos receptores se conocen como Receptores de Reconocimiento de Patrones (PRR, del inglés Pattern Recognition Receptors), este conjunto de receptores es capaz de reconocer ácidos nucleicos, lípidos y proteínas presentes en los patógenos (Pop-Began et al., 2014). En conjunto las moléculas presentes en los microrganismos que pueden ser reconocidas por estos receptores reciben el nombre de Patrones Moleculares Asociados Microorganismos (MAMPS, del inglés Microbial-Associated Molecular Patterns). Los PRR están ampliamente distribuidos en distintos tipos celulares que están expuestos a microrganismos y en células del sistema inmune innato, teniendo un papel central en la respuesta inmune innata. Adicionalmente, estos receptores también reconocen moléculas indicadoras del daño celular conocidas como Patrones Moleculares Asociados a Daño (DAMPS, del inglés Damage-Associated Molecular Patterns) (Choi & Klessig, 2016). Esta capacidad para unir una amplia variedad de moléculas está asociada a la amplia diversidad de PRRs, además, la actividad de estos se complementa con la existencia de proteínas adaptadoras, la cuales favorecen la transferencia de los MAMPS y DAMPS hacia los PRR.

En la respuesta a bacterias los receptores tipo TOLL juegan un papel crítico para el reconocimiento de patrones moleculares presentes en bacterias como los son Lipopolisacáridos (LPS) de las bacterias Gram negativas, el Peptidoglicano de las bacterias Gram positivas y otras moléculas. En el reconocimiento de los LPS de las bacterias Gram negativas el Receptor similar a TOLL-4 (TLR-4, del inglés TOLL-like Recetor 4) tiene un papel central en este proceso y el desarrollo de la respuesta del anfitrión (Jerala, 2007).

3.1.1. Reconocimiento de LPS por TLR-4

El reconocimiento de los LPS mediado por TLR-4 involucra un conjunto de proteínas que permiten que estas moléculas puedan interaccionar con el receptor. En principio, los LPS son liberados de las bacterias una vez que estas son lisadas por la acción del sistema inmune innato o el tratamiento con antibióticos, los LPS pasan a la circulación en donde forman agregados heteromorfos que pueden ser captados por distintas proteínas acarreadoras (incluyendo lipoproteínas y proteínas de unión a LPS) (Shao et al., 2012). La captación de los LPS permite que una importante cantidad de estos puedan ser trasportados al hígado para ser metabolizados, sin embargo, existe otro grupo de proteínas que son capaces de unir LPS y que favorecen el desarrollo de la respuesta inflamatoria (Figure 3).

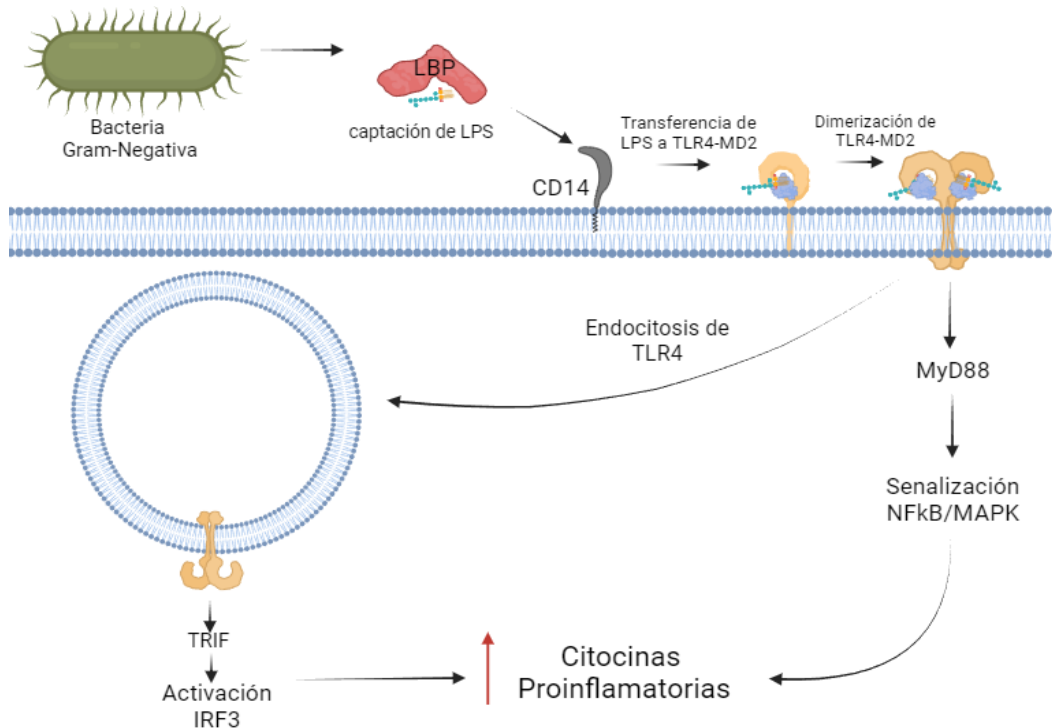


Figura 3. Papel de TLR-4 en la respuesta a LPS. Los LPS que son liberados a la circulación son captados por diferentes moléculas que favorecen el desarrollo de la respuesta del anfitrión. La proteína LBP es una de estas moléculas capaces de unir LPS, de forma posterior esta proteína forma un complejo con CD14 para trasferir los LPS al complejo de TLR4-MD2. Una vez que los LPS son transferidos al complejo TLR4-MD2 este receptor se dimeriza, lo cual favorece la activación de vías de señalización que favorecen la activación. Estas vías incluyen la activación de la vía dependiente de Myd88 o la vía independiente, asociada con TRIF e IRF3. adicionalmente, este receptor puede ser endocitado y mantenerse activado en el interior de la célula (Mazgaaen & Gurung, 2020).

Una de estas proteínas es la Proteína de Unión a LPS (LBP, del inglés Lipopolysaccharide Binding Protein), esta proteína es producida en hígado de forma constitutiva para después pasar a la circulación general. LBP actúa como una proteína de fase aguda por lo que su expresión aumenta de forma transitoria en las fases tempranas de la infección, favoreciendo la inflamación (Eckert et al., 2013). Otra proteína con funciones similares a LBP es la Proteína Incrementadora de la Permeabilidad Bactericida (BPI, del inglés Bactericidal-Permeability Increasing Protein), a diferencia de LBP esta proteína se produce en neutrófilos en donde es almacenada en los granos azurófilos y liberadas por la estimulación de estas células. Ambas proteínas tienen capacidad de unirse a los LPS, formando parte de los mecanismos de defensa ante infecciones por bacterias Gram negativas, estas proteínas presentan propiedades antimicrobianas, capacidad de funcionar como opsoninas y participan en la activación inducida por LPS (Weiss, 2003). LBP es capaz de unir los LPS que están presentes en la circulación tras la lisis de las bacterias, de forma posterior este complejo se asocia con CD14 (Clúster de Diferenciación 14, del inglés Cluster of Differentiation 14). La formación de este complejo favorece la interacción con TLR-4 en complejo con el correceptor MD2 (Factor de Diferenciación 14, del inglés Myeloid Differentiation factor 2), esto conduce a la activación de TLR-4 el cual promueve la inflamación y la respuesta del anfitrión a los patógenos. A pesar de que BPI también puede unirse a los LPS en circulación, la inducción de la respuesta del anfitrión parece no depender de la interacción con CD14 y la subsecuente activación de TLR-4-MD2 (Gallay et al., 1993) .

3.1.2. Señalización de TLR-4

Una vez que los LPS se unen a los LBP, estos pueden inducir la activación de vías de señalización que favorecen el desarrollo de la respuesta inflamatoria (Poltorak et al., 1998). Tras la unión de los LPS al receptor TLR-4 este se dimeriza, este evento resulta en cambios conformacionales que favorecen el reclutamiento de las proteínas adaptadoras implicadas en la señalización posterior. En este proceso los dominios TIR (Receptor TOLL-Interleucina-1, del inglés Toll-Interleukin-1 Receptor) presentes en el receptor TLR-4 son necesarios para el reclutamiento de otros factores mediante interacciones proteína-proteína. Las cuales incluyen a cinco miembros de proteínas que contienen dominios adaptadores para TIR (Lu et al., 2008).

En este punto la señalización de TLR-4 puede ocurrir en dos caminos: la vía dependiente de MyD88 (Gen 88 de respuesta primaria de Diferenciación Mieloide, del inglés Myeloid Differentiation primary response gene 88) y la vía independiente de MyD88 (Lu et al., 2008).

La vía dependiente de Myd88, incluye la interacción homotípica mediante dominios de muerte con cinasas. Estas cinasas incluyen IRAK-1 (IL-1 cinasa asociada al receptor-1, del inglés IL-1 receptor-associated kinase-1) e IRAK-4 (IL-1 cinasa asociada al receptor-4, del inglés IL-1 receptor-associated kinase-4) (Swantek et al., 2000). Estos eventos favorecen el reclutamiento de TRAF-6 (Factor Asociado al Receptor TNF- 6, del inglés TNF receptor-associated factor-6) el cual funciona como andamiaje para el reclutamiento de otras proteínas y cinasa (Gohda et al., 2004). Entre estas destaca el papel de TAK-1 (Cinasa activada por el factor transformante β 1, del inglés transforming growth factor- β -activated kinase 1). Esta última, está involucrada en la activación de las MAP-cinasas (Cinasas activadas por Mitógeno, del inglés Mitogen Activated Kinases) y de IkK (Cinasa del Inhibidor de κ B, del inglés κ B kinase), las cuales favorecen la producción de citocinas proinflamatorias y otros mediadores de la respuesta del anfitrión a través de la activación de NF- κ B (Factor nuclear κ B, del inglés Nuclear Factor κ B) y otros factores (Sato et al., 2005). Por otro lado, la vía independiente de MyD88 involucra a la proteína TRIF (Adaptador

contenedor de dominio TIR inductor de IFN- β , del inglés TIR domain-containing adaptor inducing IFN- β) y la activación de IRF-3 (factor de respuesta a interferón). Lo cual lleva a la producción de interferones de tipo 1 y una activación alternativa de MAP-cinasas y NF- κ B (Factor Nuclear κ B, del inglés Nuclear Factor κ B) (Akira & Hoshino, 2003).

En el desarrollo de sepsis la vía dependiente de MyD88 juega un papel central en el desarrollo de la respuesta ante LPS y al subsecuente desarrollo de la respuesta sistémica (Zhou et al., 2018).

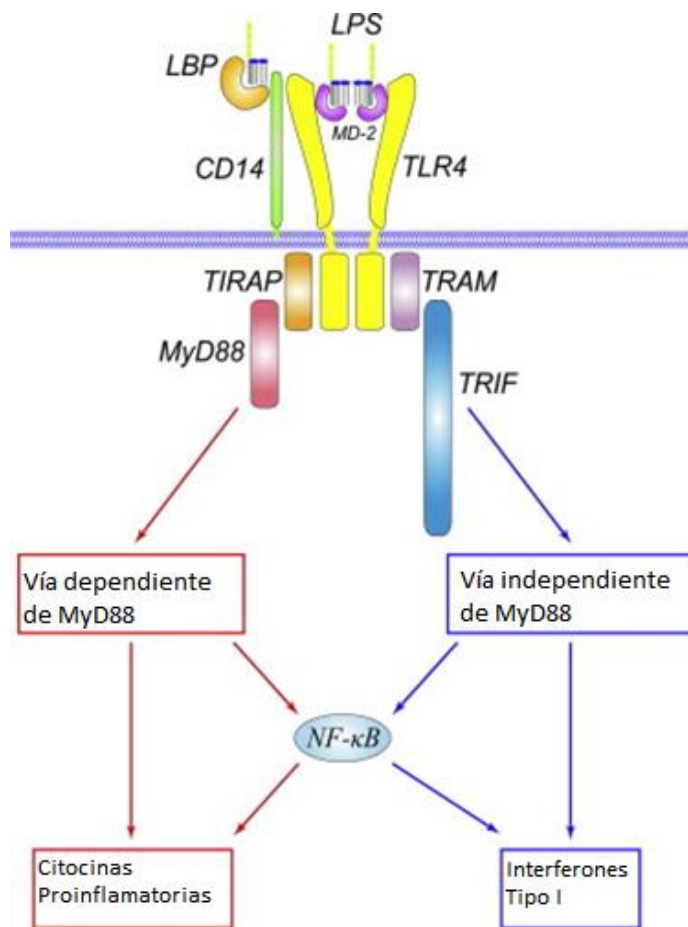


Figura 4. Señalización de TLR-4. Una vez que los LPS son reconocidos por TLR-4 este se dimeriza para activar su vía de señalización. Esta puede ser dependiente o independiente de MyD88. La vía dependiente incluye a la proteína TIRAP para el reclutamiento de Myd88, mientras que la vía independiente utiliza a TRAM como proteína adaptadora para el reclutamiento de TRIF. La vía independiente está asociada la producción de citocinas proinflamatorias, mientras que la vía independiente está asociada a la producción de interferones, sin embargo, ambas convergen a la activación de factor NF- κ B, el cual está ampliamente asociado con el desarrollo de la respuesta sistémica (Lu et al., 2008).

3.2 Lipopolisacáridos

El desarrollo de la respuesta sistémica a bacterias Gram negativas está ampliamente relacionada a los LPS, esta molécula es uno de los principales componentes de estas bacterias y es considerada una molécula con potentes propiedades estimulantes del sistema inmune. Esto le permite inducir la respuesta sistémica en el anfitrión, lo cual hace que los LPS sean especialmente relevantes para el desarrollo de la sepsis y el choque séptico (Cecconi et al., 2018; Jerala, 2007).

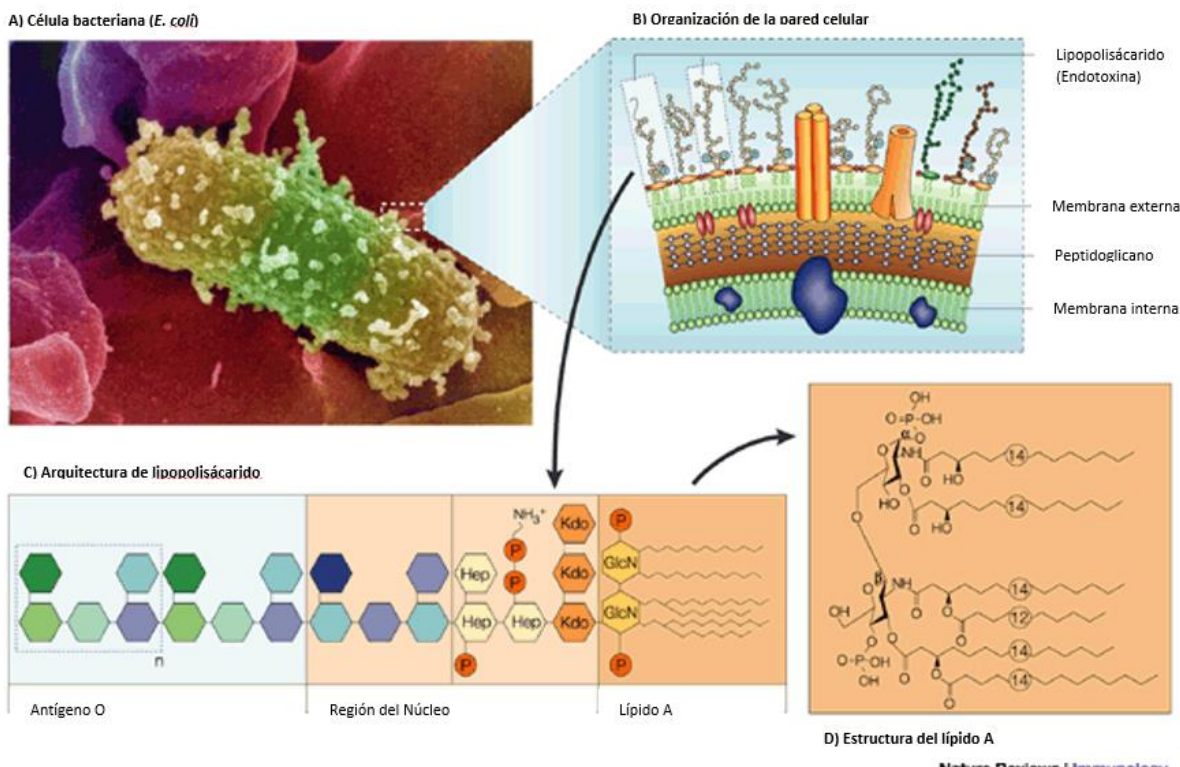


Figura 5. Lipopolisacáridos bacterianos. (A) Micrografía de *E. coli*, Las bacterias gran negativas son unas de los principales agentes causales de sepsis y coque séptico. (B) Esquema representativo de la doble membrana de las bacterias gran negativas. El LPS es uno de los principales componentes de la membrana externa. (C) Representación esquemática de LPS, en esta se observan las regiones características de los LPS: el lípido A, la región del núcleo y el antígeno O. (D) Diagrama del lípido A, esta es la región de mayor conservación en los LPS. Esta región puede ser reconocida por el sistema inmune y favorecer el desarrollo de la respuesta proinflamatoria (Beutler & Rietschel, 2003).

Los LPS están presentes exclusivamente en las bacterias Gram negativas, estos se localizan en la hemicapa externa de la membrana externa. Son un constituyente estructural muy importante llegando a representar hasta el noventa por ciento de los de esta hemicapa. Además, la presencia de los LPS en esta región está asociado a la capacidad de la bacteria para adaptarse a cambios ambientales, incluyendo modificaciones que les permiten evadir la respuesta inmune del organismo anfitrión (Beutler & Rietschel, 2003). La estructura general de los LPS está conformada por una región lipídica mayormente conservada y cadenas de oligosacáridos que presentan un mayor grado de variabilidad. Dentro de la estructura de los LPS se distinguen tres regiones: el lípido A, región del núcleo y el antígeno O; el lípido A constituye el elemento lipídico conservado, mientras que la región del núcleo y el antígeno O constituyen la región del menormente conservada del oligosacárido (Figura 5) (Erridge et al., 2002).

El lípido A es la región más interna de los LPS, esta región está constituida por disacárido de glucosamina unido por enlace β 1-6 glicosídico. Este dímero presenta carga negativa debido a la presencia de grupos fosfatos. Los ácidos grasos presentes en el lípido A están directamente unidos al dímero de glucosamina mediante enlaces éster presentando hasta cuatro ácidos grasos, estas cadenas tienen una longitud de 10 a 16 carbonos. Adicionalmente, existen cadenas de ácidos grasos unidas mediante enlaces éter a las cadenas unidas al dímero de glucosamina, la presencia de estas cadenas secundarias está asociada a la capacidad de lo LPS de inducir la respuesta inflamatoria del anfitrión (Netea et al., 2002).

La región localizada de forma inmediata al lípido A es la región del núcleo, esta región es un oligosacárido unido al dímero de glucosamina. Esta región a su vez puede dividirse en la región interna y la región externa. La región interna consiste en un oligosacárido con un moderado grado de conservación, la cual se caracteriza por la presencia de heptosas (Hep) y ácido-ceto-desoxi-octuglucosidico (KDO); además, esta región suele estar fosforilada por lo que contribuye a la carga negativa neta del LPS. Por otro lado, la región externa del núcleo está constituido por un

oligosacárido, los azúcares presentes en esta región muestran una mayor variabilidad en distintas variantes de LPS (Holst, 2011).

Finalmente, la región más externa de los LPS es el antígeno O el cual también es un oligosacárido que presenta un alto grado de variabilidad. Esta región presenta grupos de oligosacáridos conocidos como unidades repetidas, estas unidades están conformadas por 5 a 6 azúcares. Esta es la región más variable de los LPS debido a la combinación de diferentes azúcares en las unidades repetidas, además de que el número de unidades repetidas por LPS también puede variar pudiendo presentar de 1 a 8 unidades por cada molécula de LPS. La alta variabilidad estructural del antígeno O le permite cumplir funciones específicas para las bacterias, incluyendo la capacidad de evadir la respuesta inmune del anfitrión (Knirel, 2011; Pastelin-Palacios et al., 2011).

La conservación estructural que presenta la región del lípido A favorece el reconocimiento de motivos moleculares por proteínas y péptidos con capacidad de unión a LPS, como lo son LBP, BPI y los péptidos de defensa del anfitrión. (Van Der Poll et al., 2017)

3.3. Péptidos de defensa del Anfitrión

La capacidad de detectar y eliminar microorganismos invasores es un elemento necesario para la supervivencia de los organismos multicelulares. A través de la evolución los organismos han desarrollado diversos mecanismos que les han permitido combatir las infecciones producidas por organismos patógenos, la complejidad de estos sistemas presenta alta variabilidad, no obstante, existen elementos que se han conservado durante el proceso evolutivo (Peschel & Sahl, 2006; Zasloff, 2002).

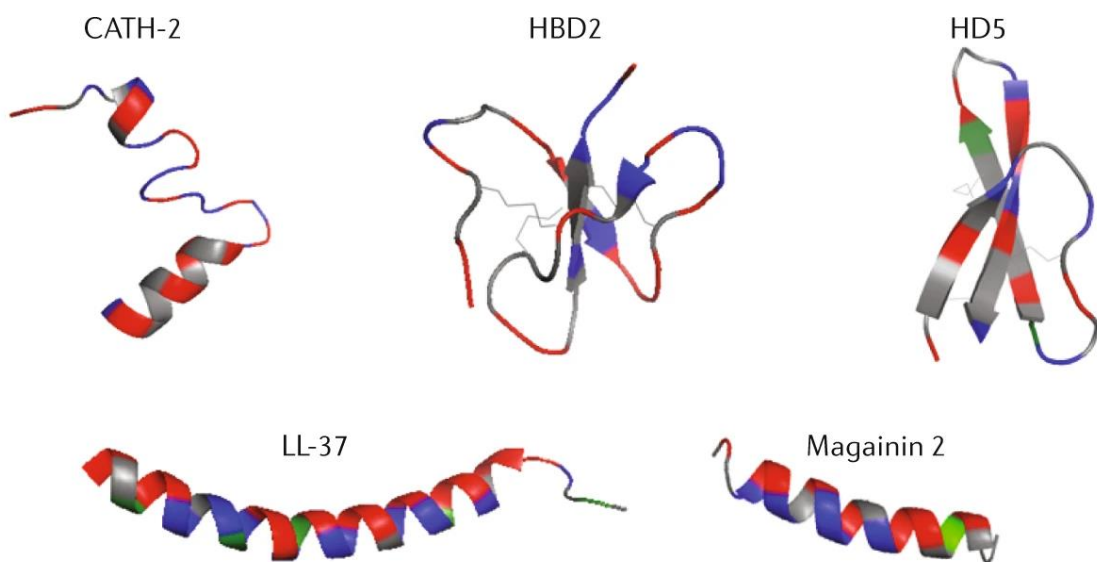


Figura 6. Variabilidad estructural de los HDPs. Los HDPs son un grupo heterogéneo de péptidos, entre ellos se encuentran algunos que presentan estructuras de alfa hélices, hojas beta, giros, horquillas, regiones desestructuradas o combinaciones de estas estructuras. Sin embargo, mantienen características comunes como la presencia de aminoácidos con carga positiva, residuos hidrofóbicos y un tamaño moderado. En la imagen se muestran catelicidinas LL-37, CATH-2 y Magainina 2, formados principalmente alfa hélices; también se muestran dos diferentes defensinas HBD2 y HD5, caracterizadas por la presencia de hojas B. En estos péptidos los aminoácidos hidrofóbicos se muestran en rojo, los cargados positivamente en azul y los cargados negativamente en verde.(Mookherjee et al., 2020)

Uno de estos mecanismos son los Péptidos de Defensa del Anfitrión (HDP, del inglés Host Defence Peptides), también conocidos como péptidos catiónicos antimicrobianos. Este grupo de péptidos está constituido por un gran número de miembros con características bastante heterogéneas, sin embargo, existen algunas

características comunes para la mayoría de los miembros: la mayoría son péptidos cortos con una longitud menor a cincuenta residuos, suelen presentar aminoácidos hidrofóbicos que llegan a constituir hasta el 50% de la secuencia del péptido; por último, presentan una carga neta positiva debido a la presencia de aminoácidos catiónicos como lisina y arginina (Hancock et al., 2016). Estructuralmente estos péptidos también presentan una alta variabilidad contando con miembros que presentan estructuras de hojas beta, alfa hélices horquillas, péptidos desestructurados y combinaciones de estas (Figura 6) (Rosenfeld et al., 2006).

Los HDPs tienen un muy importante papel en la inmunidad innata dado que estos pueden ser liberados de forma aguda ante la invasión de algún microorganismo, estos péptidos cumplen diversas funciones pudiendo actuar como opsoninas, agentes bacteriostáticos, bactericidas, neutralizando metabolitos tóxicos o mediante efectos inmunoreguladores (Mookherjee & Hancock, 2007). Algunos HDPs poseen una actividad bactericida directa, estos también son conocidos como péptidos antimicrobianos debido a esta capacidad para eliminar a los microorganismos. Este efecto suele estar asociado a la capacidad de los péptidos para unirse a la membrana de los microorganismos, este proceso esta mediado por la interacción de los péptidos con componentes conservados en estas membranas (como la presencia de LPS) lo cual induce cambios en la estructura promoviendo la desestabilización de la membrana, cambios en la permeabilidad de la membrana y la lisis de los microorganismos (Hancock et al., 2016; Shai, 2002). Por otro lado, existen HDPs que no poseen propiedades bactericidas, sin embargo, contribuyen a la resolución del proceso infeccioso al limitar el desarrollo de la respuesta del anfitrión; esto puede ocurrir mediante la unión de LPS y otros MAMPS para amortiguar el desarrollo de la respuesta o mediante efectos reguladores directos en diversos tipos celulares (Mansour et al., 2014).

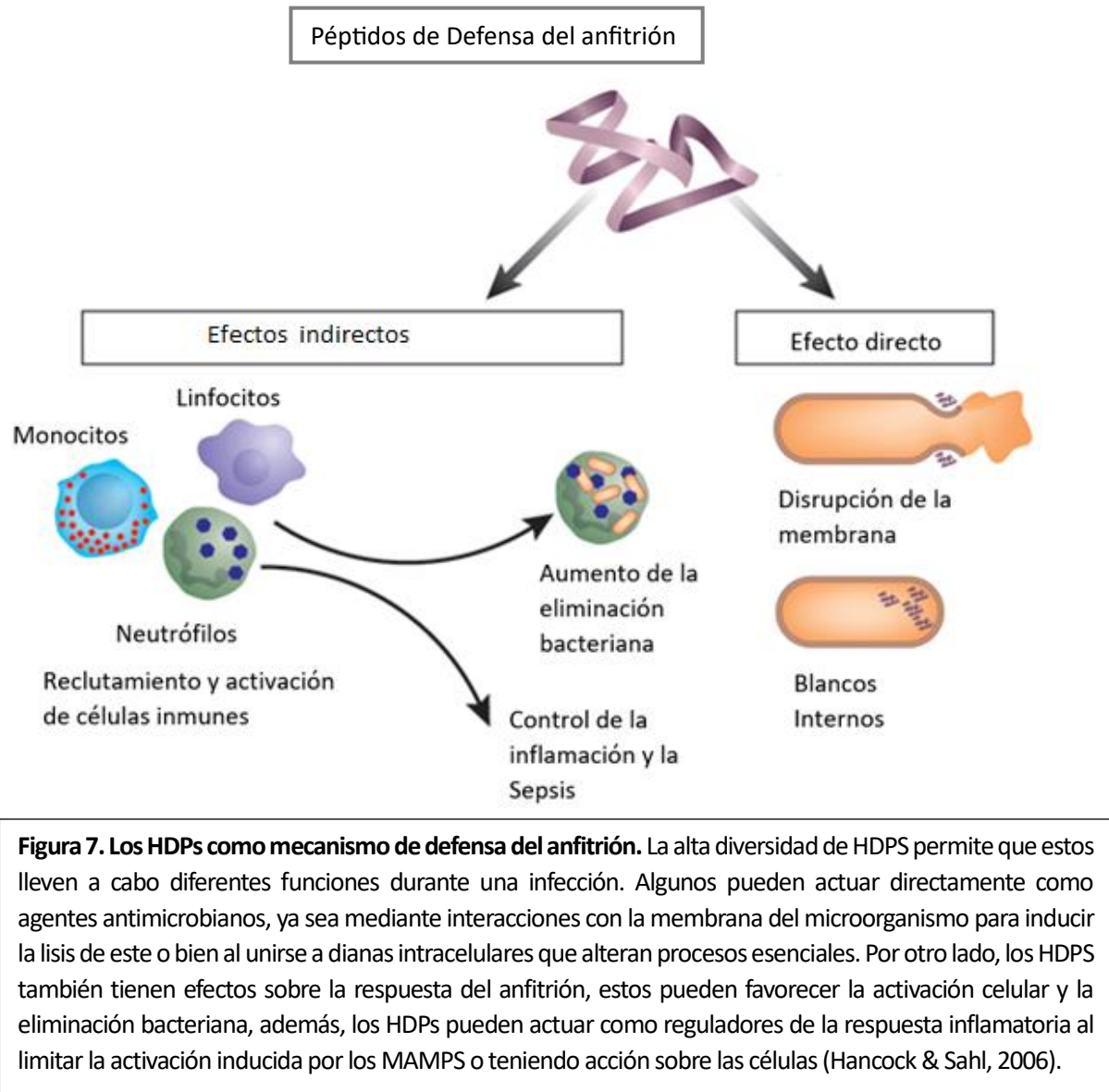


Figura 7. Los HDPs como mecanismo de defensa del anfitrión. La alta diversidad de HDPS permite que estos lleven a cabo diferentes funciones durante una infección. Algunos pueden actuar directamente como agentes antimicrobianos, ya sea mediante interacciones con la membrana del microorganismo para inducir la lisis de este o bien al unirse a dianas intracelulares que alteran procesos esenciales. Por otro lado, los HDPS también tienen efectos sobre la respuesta del anfitrión, estos pueden favorecer la activación celular y la eliminación bacteriana, además, los HDPS pueden actuar como reguladores de la respuesta inflamatoria al limitar la activación inducida por los MAMPS o teniendo acción sobre las células (Hancock & Sahl, 2006).

Debido a las interesantes propiedades que presentan los HDPS estos se han convertido en una plataforma interesante para el desarrollo de péptidos terapéuticos con capacidad antimicrobiana que pudieran funcionar como nuevos antibióticos para el tratamiento de infecciones resistentes a antibióticos tradicionales (Hamill et al., 2008; Hancock & Sahl, 2006). Además, la capacidad de regular la respuesta del anfitrión de estos péptidos al limitar la activación inducida por MAMPS presenta otra opción interesante para la generación de nuevas terapias que prevengan el desarrollo de sepsis y choque séptico, esto resulta especialmente relevante con los LPS los cuales pueden ser capturados por estos péptidos previniendo el reconocimiento por sus receptores (Giuliani et al., 2010).

3.4. CETP, CETPI y el péptido VSAK

Anteriormente se ha hablado de las proteínas de LBP y BPI, así como de su participación en la respuesta a LPS. Estas proteínas a su vez forman parte de una familia de proteínas que participan en la captura de LPS (LBP y BPI) y otros miembros que participan en la transferencia de lípidos, en este segundo grupo resaltan la Proteína de Transferencia de Fosfolípidos y la Proteína de Transferencia de Esteres de Colesterol (CETP, del inglés Cholestryl Ester Transfer Protein) (Bingle & Craven, 2004; Krasity et al., 2011). La similitud estructural de estas proteínas tiene rasgos particulares, a nivel de estructura primaria la identidad de estos miembros puede ser de apenas un 40% en algunos casos, sin embargo, la estructura terciaria de estas proteínas presenta una organización muy similar entre estas proteínas. A este nivel, las proteínas muestran tres dominios conservados: un barril N-terminal, un barril C-terminal y un domino central de bisagra (Figura 8). La conservación de esta estructura en los distintos miembros puede estar asociada a la capacidad de estas proteínas para interactuar con estructuras lipídicas en donde la flexibilidad sería necesaria para realizar el acoplamiento y la transferencia de estas moléculas (Schultz & Weiss, 2007). La presencia de estos dominios no solo abarca a las proteínas involucradas en la unión de LPS o transferencia de lípidos, ya que estas forman parte de un grupo aun mayor de proteínas conocidas como proteínas con motivos BPI/PLUNC (del inglés Palate, Lung and Nasal Epithelium Clone), cuyos miembros están relacionados con el sistema inmune innato y están involucradas en los sistemas de defensa en las vías respiratorias (Bingle & Craven, 2002; Ghafouri et al., 2004).

CETP es una proteína que participa en el metabolismo del colesterol, estando involucrada en el trasporte reverso de esta molécula. Esta función en particular, hace que CETP tenga relevancia en la fisiopatología de la aterosclerosis, una condición asociada a niveles elevados de colesterol en circulación que conllevan a la acumulación de este en las paredes de las arterias (de Groot et al., 2004). Debido a esto, CETP puede considerarse una proteína con efectos deletéreos para el organismo, convirtiéndola en un blanco importante en el desarrollo de terapias

enfocadas a prevenir esta condición. Sin embargo, el uso de inhibidores de esta proteína demostró su posible participación en la adecuada respuesta a infecciones, en estudios clínicos de fase 3 utilizando el inhibidor Torcetrapib se encontró un incremento de la mortalidad en el grupo tratado con este fármaco en el cual casi la mitad de las muertes estuvieron asociadas a procesos infecciosos (Clark et al., 2010). Debido a esto, el protocolo fue terminado dados los efectos adversos producidos por este inhibidor. Este evento indicaba una relación de CETP con la resolución de procesos infecciosos que no había sido abordada hasta ese entonces.

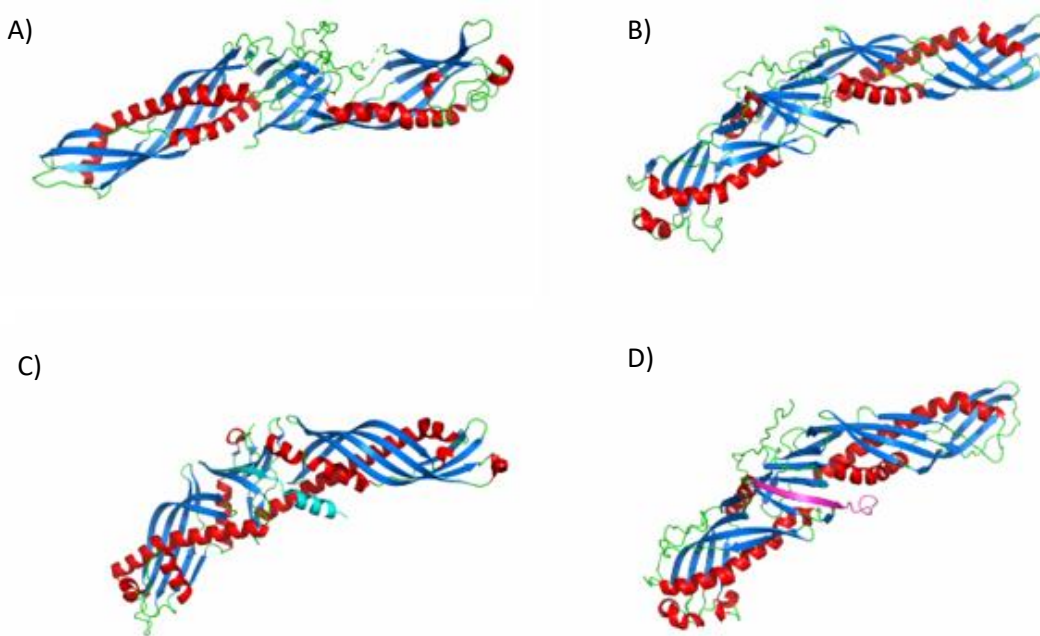


Figura 8. Proteínas de unión a LPS y transferencia de lípidos. (A) LBP, (B) BPI, y (C) CETP forman parte de la familia de proteínas de transferencia de lípidos y de unión a LPS, contenida a su vez en las proteínas con motivos BPI/PLUNC. Estas proteínas presentan una baja homología a nivel primario, sin embargo, mantienen una alta conservación de organización terciaria. D) Modelo predicho para CETPI mediante iTASSER, CETPI es una proteína con alto grado de identidad con CETP (96%) con un cambio mínimo en el extremo carboxilo terminal (rosa). (Beamer et al., 1997; Eckert et al., 2013; Liu et al., 2012)

En 2003, los estudios de la expresión de CETP en nuestro laboratorio condujeron al hallazgo de una nueva variante de CETP, la cual fue nombrada Isoforma de la Proteína Transferidora de Esteres de Colesterol (CETPI, del inglés Cholesteryl Ester Transfer Protein Isoform). La existencia de esta proteína fue descrita en primera instancia en conejos y posteriormente la existencia de la variante predicha fue corroborada en humanos. En un inicio esta nueva isoforma se observó como un

ARNm (Ácido Ribonucleico mensajero) cuya expresión es exclusiva del intestino delgado y el cual puede ser detectado con sondas específicas para CETP, sin embargo, este era de mayor longitud comparado con el ARNm típico de CETP. El análisis de la secuencia de estos transcritos indicó que el ARNm de CETPI tenía una longitud total de 1419 pb (pares de bases) conteniendo 108 nucleótidos adicionales en comparación con el transcripto de CETP. Originalmente esta secuencia adicional fue nombrada secuencia I, esta secuencia adicional corresponde a la región intrónica localizada entre los exones 15 y 16 del gen de CETP. La inclusión de esta secuencia en el ARNm de CETPI resulta en una proteína que conserva casi por completo la secuencia primaria de CETP, pero tendría un carboxilo terminal distinto. En CETP esta región codifica un carboxilo terminal de 23 aminoácidos, mientras que en CETPI esto son remplazados por 18 aminoácidos de la secuencia I y terminada debido a un codón de paro en la posición 55 de esta secuencia. Como resultado de estas modificaciones, CETP y CETPI mantienen una homología del 96% difiriendo solo en los aminoácidos de la región carboxilo terminal a partir del aminoácido 472 (Alonso-García et al., 2003). (Figura 8D)

A pesar de que la diferencia entre estas dos proteínas solo es una pequeña región del carboxilo terminal, esta modificación tiene repercusiones muy importantes en la funcionalidad. En CETP esta región se organiza como una alfa hélice anfipática, la cual se ha demostrado que está involucrada en el proceso de transferencia de esteroides de colesterol, siendo una región crítica para esta función de CETP (García-González et al., 2014). En contraste, en CETPI esta región es remplazada por un nuevo carboxilo, el cual está formado por 18 aminoácidos. Esta región se mantendría desestructurada debido a la alta presencia de prolina y de tres cargas positivas asociadas a la presencia de residuos catiónicos en las posiciones 4, 9 y 14. La modificación de esta región en CETPI implicaría la perdida de la capacidad de transferencia de esteroides de colesterol como se ha observado en una variante trunca de CETP conocida como delta-9, la cual solo incluye los primeros 9 exones del gen de CETP (Drayna et al., 1987). Sin embargo, a diferencia de esta variante CETPI mantiene intacta la estructura de la proteína, lo cual indicaba que esta proteína podría mantener la capacidad de interactuar con estructuras de lípidos.

diferentes a las lipoproteínas que transportan colesterol. Dada la cercanía de esta proteína con las proteínas de unión a LPS y las características del carboxilo de CETPI se planteó la posibilidad de que CETPI pudiera interactuar con los LPS teniendo una función similar a BPI y LPB. Esta hipótesis se ha visto favorecida por nuestros hallazgos más recientes, los cuales han demostrado que, en humanos, el nivel en circulación de CETPI se modifica durante procesos de infección, sepsis y choque séptico; en donde el nivel de esta proteína correlaciona con la severidad de la condición del individuo. Adicionalmente, hemos observado que el nivel en circulación de CETPI correlaciona con el nivel de algunas citocinas producidas durante la respuesta sistémica, lo cual podría indicar una regulación de esta proteína asociada a la respuesta del anfitrión (Pérez-Hernández et al., 2022).

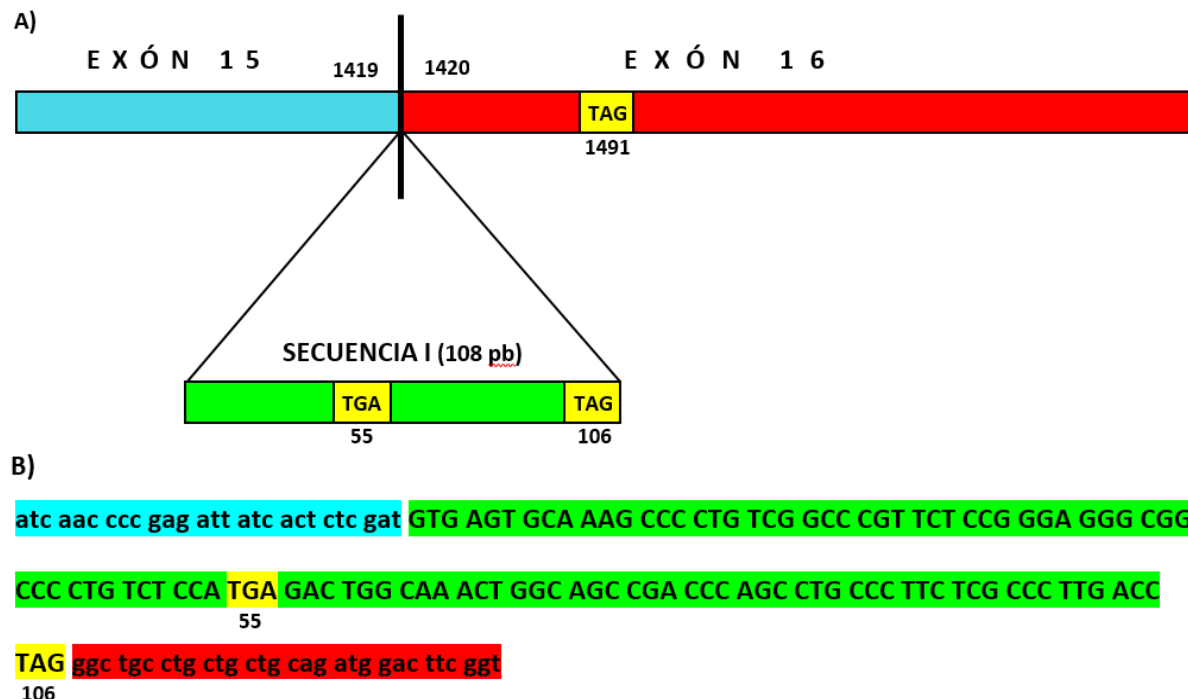


Figura 8. La Secuencia I de CETPI. A) Representación esquemática de la región límite entre los exones 15 (azul) y 16 (rojo) del mRNA de CETP. Entre las bases 1419 y 1420 ocurre la inserción de la secuencia I (verde) que da origen al mRNA de CETPI. Las regiones con codones de paro se muestran con resaltadas en amarillo. B) secuencia de la región terminal del mRNA de CETPI. El esquema muestra los tripletes presentes en la secuencia I, la presencia de un codón de paro en la posición 55 produce la pérdida de la región carboxilo terminal en CETPI y su sustitución por los aminoácidos codificados por las primeras 54 bases de la secuencia I. (Alonso-Garcia et al., 2003)

A) VSAKPLSARSPGGRPLSP
 B)

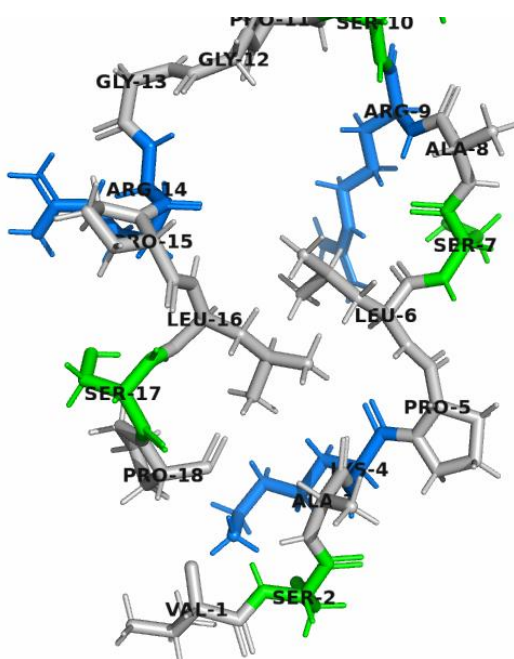


Figura 9. El péptido VSAK. A) Secuencia primaria del péptido VSAK los residuos hidrofóbicos están presentes en verde, en negro se presentan los residuos polares y en azul los aminoácidos con carga positiva. El péptido VSAK tiene una longitud de 18 aminoácidos correspondiendo con el carboxilo terminal característico de CETPI, este péptido posee un carácter anfipático y una importante carga neta positiva. B) Modelo representativo del péptido VSAK, Este péptido carece de una estructura secundaria manteniéndose desestructurado en solución. A pesar de la presencia de residuos hidrofóbicos (44%), este péptido mantiene una alta solubilidad en medios acuosos. El modelo fue generado con utilizando PEP-FOLD 3 (García-González et al., 2015; Shen et al., 2014)

En este sentido, el estudio de la capacidad de CETPI para unir LPS se ha realizado utilizando péptidos derivados del extremo carboxilo de CETPI, los cuales condujeron al desarrollo del péptido VSAK (VSAKPLSARSPGGRPLSP). Este péptido consiste en los 18 aminoácidos del carboxilo de CETPI el cual tienen capacidad de unirse a los LPS y neutralizar los efectos de estas moléculas. Esta capacidad de unión se estudió utilizando una batería de ensayos bioquímicos, la cual demostró una alta afinidad del péptido hacia los LPS de diferentes especies bacterianas. Adicionalmente, se observó que esta interacción tiene un carácter electrostático que depende en gran medida de las cargas positivas presentes en el péptido y la carga negativa de los LPS, ya que la interacción se pierde cuando se

trata a los LPS con fosfatasas, eliminando la mayor parte de las cargas negativas de esta molécula. Esta interacción entre VSAK y LPS presenta una gran avidez siendo capaz de soportar altas concentraciones de sales antes de verse afectada. Por otro lado, mediante ensayos *in vitro* se encontró que la unión del péptido VSAK disminuye la captación de LPS en macrófagos, así como la expresión de marcadores proinflamatorios (García-González et al., 2015).

Además, al utilizar un modelo de inflamación sistémica *in vivo* mediante la administración intravenosa de LPS se encontró que el péptido VSAK es capaz de reducir la producción de marcadores inflamatorios y del deterioro de los animales asociados al proceso de respuesta sistémica (García-González et al., 2015). En estos animales también se observó una reducción importante de la mortalidad posterior a la administración de los LPS. En conjunto estos resultados planteaban la posibilidad de que el péptido VSAK pudiera ser utilizado como plataforma para el desarrollo de tratamientos enfocados al tratamiento de sepsis y choque séptico (Luna-Reyes et al., 2021).

4. PLANTEAMIENTO DEL PROBLEMA

En la actualidad la sepsis y el choque séptico son una de las principales causas de muerte a nivel mundial; en conjunto estas son reconocidas como una de las más grandes amenazas de salud pública de nuestros tiempos.

La sepsis y el choque séptico son estadios agravados de una infección, en los cuales la incapacidad del organismo para lograr una resolución adecuada del proceso infeccioso lo lleva a un punto en el que la propia respuesta del individuo resulta dañina; produciendo daño a órganos y sistemas que terminan poniendo en riesgo la vida del organismo. Por tanto, la respuesta inmune al patógeno tiene un papel central en el desarrollo y desenlace de la sepsis y choque séptico.

En este sentido, en la implementación de estrategias enfocadas a combatir estas afecciones se debe considerar la regulación de respuesta del anfitrión durante la infección. Una de las estrategias enfocadas a limitar la respuesta del anfitrión al disminuir la cantidad de MAMPs a los que es expuesto el organismo. Debido a la relevancia clínica de las bacterias Gram negativas, los LPS son una de las principales moléculas objetivos de estas estrategias, las cuales están orientadas a limitar el reconocimiento de los LPS y la respuesta que estos inducen.

Ante este panorama, los HDPs presentan una importante plataforma para el desarrollo de moléculas terapéuticas con la capacidad de unir LPS para limitar la respuesta del anfitrión. No obstante, es necesario conocer a profundidad las propiedades de este tipo de péptidos para la generación de opciones seguras y funcionales.

Hace algunos años, nuestro grupo de investigación describió a la proteína CETPI a partir de la cual se generó el péptido VSAK, este péptido posee una capacidad de unirse a los LPS con una gran afinidad, por lo que podría ser una opción para el desarrollo de terapias enfocadas a limitar el desarrollo de la respuesta sistémica ante los LPS, la cual es un paso crítico en el desarrollo de sepsis y choque séptico.

5. HIPÓTESIS

El péptido VSAK puede ser utilizado de forma terapéutica en modelos de inflamación sistémica para mitigar los efectos deletéreos producidos por los LPS.

6. OBJETIVO GENERAL

Estudiar las propiedades del péptido VSAK enfocadas al desarrollo de una estrategia para el uso de VSAK como agente terapéutico en modelos de inflamación sistémica asociados con sepsis y choque séptico.

6.1. OBJETIVOS PARTICULARES

- Modelar mediante simulaciones de dinámica molecular el mecanismo de interacción del péptido VSAK con estructuras lipídicas de LPS y membranas eucariontes.
- Estudiar *in vitro* la toxicología y los efectos del péptido VSAK en células HAEC (células endoteliales aorticas humanas) y THP-1(células monocíticas humanas)
- Estudiar *in vitro* el efecto del péptido VSAK en células tratadas con LPS en comparación con agonistas no lipídicos de TLR-4
- Analizar mediante Tomografía de Emisión de Positrones los efectos sistémicos del péptido VSAK en condiciones normales y de inflamación sistémica inducida por LPS, junto con indicadores de la disfunción metabólica asociada a esta respuesta.

-

7. MATERIALES Y MÉTODOS

7.1. Péptido VSAK

El péptido VSAK utilizado en nuestros experimentos fue sintetizado por la empresa Genscript (Piscataway, NJ, USA) con una pureza mayor al 98%. El péptido VSAK tiene una longitud de 18 aminoácidos que corresponden a la región C-terminal comprendida entre V474-P491 (V S A K P L S A R S P G G R P L S P) de CETPI de conejo (García-González et al., 2015). Para la administración del péptido en animales utilizados en los estudios de PET se empleó una solución de trabajo con una concentración de 1mg/ml del VSAK suspendido en buffer salino de fosfatos (PBS) para su administración intravenosa (Thermofisher Scientific, Waltham, MA, USA).

7.2. Lipopolisacáridos

En los experimentos se utilizaron LPS de la variante O111:B4 los cuales son obtenidos de una cepa de *Escherichia coli* (Sigma, ST Luis, MO, USA). La cantidad de unidades de endotoxina presentes en esta variante de LPS fue cuantificada utilizando el sistema Endosafe (Charles River, Wilmington, MA, USA). Este sistema utiliza cartuchos con un sustrato coloreado que se procesa por el lisado de amebocito Limulus, en este ensayo la actividad de los LPS es proporcional a densidad óptica de observada en las muestras. La cuantificación determinó que existían 798 EU por nanogramo en los LPS utilizados en nuestros experimentos.

Los LPS utilizados en los experimentos fueron resuspendidos en un buffer Krebs-Ringer sin glucosa. Los LPS se homogenizaron disolviéndolos en H₂O_{dd} a una concentración inicial de 1mg/ml. Esta solución se agitó hasta disolver los agregados de LPS. Despues se calentó a 60°C durante 10 minutos, posteriormente se realizaron tres ciclos de sonicación de 5 minutos. Finalmente, la solución se agitó por dos minutos antes de ser utilizada.

7.3. Simulaciones de dinámica molecular

Los modelos de los péptidos utilizados en los sistemas de dinámica molecular fueron generados utilizando el servidor en línea de I-TASSER (Roy et al., 2010). Se seleccionaron aquellos modelos que reportaron mayores indicadores de la calidad

del modelo, incluyendo el C-escore, TM-escore y el RMSD ponderado de las plantillas.

Los sistemas fueron generados con el servidor en línea de CHARMMGUI (Jo et al., 2008), utilizando el generador de modelos de membrana basados en el campo de fuerza de MARTINI 3.0 para modelos de grano grueso (Siewert J. Marrink et al., 2007). Los sistemas generados consistieron en bicapas de lípidos donde cada hemicapa tuvo una constitución homogénea, con las combinaciones POPC (Fosfatidilcolina)-POPC, POPS-POPS (Fosfatidilserina) y LPS-POPC; para la hemicapa externa e interna respectivamente. En estos sistemas los péptidos se colocaron a 30 angstroms sobre la membrana externa. Se realizó una minimización en dos pasos utilizando los algoritmos de descenso rápido y de gradientes conjugados. Posteriormente se realizó el equilibrio de estos sistemas previo a la simulación. Los sistemas fueron simulados utilizando el barostato por reescalado de velocidad y el termostato Parinello-Rahman, los sistemas fueron simulados con ensambles NPT, a 1 bar de presión y 310.15K. Las simulaciones se realizaron hasta alcanzar 3μs de duración, utilizando pasos de tiempo de 2fs. La simulación se realizó de forma segmentada dividiendo en tiempo total en 100 fragmentos. Al término se realizó la unión de los archivos de trayectorias y registros de energía para los análisis posteriores.

El análisis de simulaciones incluyó el análisis de energía en los sistemas, fluctuaciones en los aminoácidos (RMSF) y cambios en la estructura de las membranas, estos últimos se realizaron en VMD (Humphrey et al., 1996) mediante el plugin MEMPLUGIN (Guixà-González et al., 2014).

7.4. Microscopía Electrónica

Las muestras de LPS y el péptido VSAK fueron preparadas en H₂O_{DD}, para evitar interferencia por sales en el buffer. Las concentraciones utilizadas en estos ensayos fueron 0.5 (0.5μM), 0.25 (0.25μM) y 0.125 mg/ml (0.125μM) para los LPS, mientras que el péptido VSAK se utilizó en una concentración de 8 mg/ml (4.5 μM) que se diluyó 1:1, 1:2 y 1:4 en solución de LPS al 1mg/ml (1 μM).

Para su observación las muestras fueron colocadas en rejillas de níquel (Supergrid Ni 3mm, SPI Supplies, West Chester, PA, USA) tratadas previamente con collodion y vapor de carbono, en donde dejaron secar por 5 minutos. Posteriormente se incubaron con una solución de acetato de uranilo (MERCK, Darmstadt, Alemania) durante tres minutos. Las muestras se secaron durante 15 minutos antes de ser observadas. Para la observación se utilizó el microscopio electrónico (JEM 1200EX II, Jeol, Tokio, Japón), el voltaje de utilizado fue de 80Kva. Las muestras se observaron en aumentos de 7500x, 15000x y 30000x.

7.5. Ensayos de Hemólisis

En todos los ensayos se utilizaron eritrocitos frescos, extraídos el mismo día de los ensayos. Estos fueron recuperados en tubos heparinizados para extracción de plasma. Después fueron centrifugados durante 5 minutos a 1500rpm (252g), mediante aspiración se desechó el plasma y el componente leucocitario. Los eritrocitos fueron resuspendidos en buffer salino (150mMKCl, 5mM Tris-HCl, pH 7.4) con una dilución 1:250 para generar la solución de trabajo.

La preparación de las muestras y estándares se realizó con un volumen final de 200 μ l, utilizando 20 μ l de muestras o estándares y 180 μ l de la solución de trabajo de eritrocitos. La curva estándar se generó utilizando 4 diluciones seriadas (1:2) de Triton X100 al 0.1% (Sigma, ST Luis, MO, USA) en buffer salino, como control negativo se utilizó buffer salino. En los ensayos de hemolisis se utilizaron concentraciones de 50, 100, 125, 150, 200 y 250 μ g/ml del péptido VSAK. En los ensayos de hemolisis con LPS se utilizaron 50, 100, 125, 150, 200 y 250 μ g/ml de LPS. Todas las muestras fueron preparadas por triplicado, estas se ajustaron para el volumen final (200 μ l) en las muestras utilizadas. Las muestras tratadas fueron incubadas durante dos horas a 37°C en agitación constante. Posteriormente, estas muestras fueron centrifugadas a 1500rpm (252 g) durante 5 minutos, 100 μ l del sobrenadante fue recuperado y trasferido a una microplaca para su análisis. La densidad óptica de estas muestras fue medida a 540nm utilizando un lector de placas (Synergy, Biotek, Santa Clara, CA, USA), esta longitud de onda corresponde

al valor de absorción de la hemoglobina libre. Los resultados se reportaron como el porcentaje de hemólisis con respecto a la curva estándar.

7.6. Cultivo celular

Todas las líneas celulares fueron mantenidas en condiciones estándar al 5% de CO₂, en una incubadora húmeda a 37°C (Panasonic, Wood Dale, IL, USA). En los ensayos se utilizaron células a un 80% de confluencia.

Las células HEPG2 y HEK 293 fueron cultivadas en medio DMEM (Dulbecco's Modified Eagle Medium) de alta glucosa (Thermofisher Scientific, Waltham, MA, USA) suplementado con 10% de suero fetal bovino (Thermofisher Scientific, Waltham, MA, USA) y 1% de Antibiotico-Antimicotico (Thermofisher Scientific, Waltham, MA, USA).

Las células THP-1 fueron mantenidas en medio RPMI 1640 (Thermofisher Scientific, Waltham, MA, USA) con 10% de suero fetal bovino, 1% de Antibiotico-Antimicotico y 0.05 mM 2-Mercaptoetanol (Sigma, ST Luis, MO, USA).

Finalmente, las células HAEC fueron cultivadas en medio basal celular (PCS-100-030, ATCC, Manassas, VA, USA), este medio fue complementado con el kit de suplementación para células endoteliales (PCS-100-041, ATCC, Manassas, VA, USA) de acuerdo a las instrucciones del fabricante.

7.7. Ensayos celulares

En estos ensayos se utilizaron células que fueron tratadas con LPS, VSAK o con ambas moléculas. Adicionalmente, se utilizó como control positivo Neoseptina-3 (NEO-3) (Sigma, ST Luis, MO, USA), un agonista de TLR-4 de carácter no lipídico. Las concentraciones de los tratamientos para las líneas celulares fueron: LPS 4μg/ml (4μM), VSAK 40μg/ml (22.5mM) y NEO-3 25μM

En estos ensayos, se sembraron 1x10⁶ células en cajas de 100 cm², estas se mantuvieron en los medios adecuados según el tipo celular durante 48 horas. Posteriormente las células fueron lavadas con PBS dos veces. En seguida, se colocaron los respectivos tratamientos, las células se mantuvieron en los tratamientos durante las 24 horas posteriores. Pasado este tiempo, los medios

celulares fueron recuperados y congelados. En paralelo, las células fueron lavadas tres veces con PBS para retirar restos del medio. Estas fueron utilizadas para extracción de proteínas mediante buffer RIPA o para extracción de RNA total utilizando el método de Trizol.

7.8. Viabilidad celular

Los ensayos de viabilidad celular se realizaron utilizando el protocolo de rojo neutro, en estos ensayos el colorante solo puede ser internalizado por células vivas por lo que la disminución en la captación de este puede ser asociada a cambios en la viabilidad celular (Repetto et al., 2008). En microplacas de 96 pozos se sembraron 10,000 células por pozo. Estas se mantuvieron durante 24 horas, después de 24 horas el medio se retiró, las células fueron lavadas con PBS tres veces para retirar restos del medio. Los tratamientos asignados fueron colocados durante 24 horas, una vez pasado este tiempo los tratamientos fueron removidos. Las células fueron lavadas tres veces con PBS, para después agregar 100 μ l de Solución de Rojo neutro al 0.0004%. Las células se incubaron durante 4 horas con esta solución, después fue removida y las células fueron lavadas con PBS dos veces. Posteriormente se agregó la solución de destilado (50% etanol, 29% H₂O_{dd}, 1% Ácido acético glacial), posteriormente las células se colocaron en un agitador para solubilizar el colorante. La densidad óptica fue medida a 540nm en un lector de microplacas (Synergy, Biotek, Santa Clara, CA, USA). En estos ensayos se generó una curva estándar utilizando diluciones seriadas (1:2) de Triton X100 al 0.1% (Sigma, ST Luis, MO, USA), como comparativa para analizar los cambios en la viabilidad celular.

7.9. PCR Tiempo real

La extracción de RNA total de las células tratadas se realizó mediante el método de Trizol (Thermofisher Scientific, Waltham, MA, USA), siguiendo las indicaciones del fabricante. La síntesis de cDNA se realizó utilizando el kit iScript RT Supermix (Biorad, Hercules, CA, USA) siguiendo el protocolo indicado por el fabricante. El cDNA de las muestras tratadas se prepararon para ser analizados mediante PCR de tiempo real utilizando el kit PowerUp Sybr Green Master Mix 2X (Thermofisher Scientific, Waltham, MA, USA), siguiendo las indicaciones del fabricante. Los ensayos se llevaron a cabo en el equipo

ABI PRISM 7000 (Applied Biosystems, Thermo Fisher Scientific, Waltham, MA, USA), utilizando un protocolo estándar sugerido por el fabricante de cuarenta ciclos, con 2 minutos a 50°C para inactivar UDG, 2 minutos a 95°C para el doble cierre de la polimerasa, además se incluyó un paso de 15 segundo a 95°C y un paso de 1 minuto a 60°C. En los ensayos se utilizó a *Gapdh* como gen reportero control, el procesamiento de los datos se realizó mediante la técnica de $2^{-\Delta\Delta Ct}$. Los oligonucleótidos utilizados en el análisis se muestran en la siguiente tabla:

<i>Tlr-4</i>	<i>E-Sele</i>
Sentido	Sentido
CACCACTAAAGGCAGGGATA	CTCAGTGTCCCTTCTACTC
Anti-sentido	Anti-sentido
GTGGCAGACCTGAATCCTAAA	GAGTCTTGGTCTCTCACCTTT
<i>Tlr-2</i>	<i>Nos2</i>
Sentido	Sentido
CCTACTGGGTGGAGAACCTTAT	GTCAGAGTCACCATCCTCTTG
Anti-sentido	Anti-sentido
CAGGAATGAAGTCCCGCTTATG	GCAGCTCAGCCTGTACTTATC
<i>Il-1 B</i>	<i>Nos3</i>
Sentido	Sentido
CAAAGGCCGCCAGGATATAA	GTTAGATTCCCTTGCCTCTCTC
Anti-sentido	Anti-sentido
CTAGGGATTGAGTCCACATTCA	GGCACAGTCCCTATGGTAAA
<i>Il-6</i>	<i>Cd274 (PDL1)</i>
Sentido	Sentido
GGAGACTTGCCTGGTGAAA	CTGTAACCACCCCTGTTGTGATA
Anti-sentido	Anti-sentido
CTGGCTTGTCCCTCACTACTC	GCAGCTGAGGTCTGCTATT
<i>Icam1</i>	<i>Il-10</i>
Sentido	Sentido
GTAGCAGCCGCAGTCATAAT	TTTCCCTGACCTCCCTCTAA
Anti-sentido	Anti-sentido
GGGCCTGTTGAGTCTGTATT	CGAGACACTGGAAGGTGAATTA
<i>Vcam1</i>	<i>Factor III</i>
Sentido	Sentido
GATTGGTGACTCCGTCTCATT	AAGCACTGTTGGAGCTACTG
Anti-sentido	Anti-sentido
CCTTCCCATTCACTGGACTATC	GGGTCTTCATGCTCCGAAATA

7.10. Equipo de micro-PET

Los experimentos de PET (Tomografía de Emisión de Positrones, del inglés Positron Emission Tomography) se realizaron en la unidad de PET-CT, de la Facultad de Medicina, UNAM. Se utilizó el equipo de MicroPET de cuarta generación FOCUS 120 (Concorde Microsystems, Knoxville, TN, USA) distribuido por SIEMENS. Este equipo cuenta con un anillo de detección de 15 cm de diámetro con 96 detectores. El cual cuenta con un detector formado por un arreglo de 12x12 cristales de Oxi-ortosilicato de Lutecio acoplados a un sistema fotomultiplicador. El equipo tiene una apertura de 12 cm de diámetro para la colocación de los animales de experimentación, el cual da lugar un campo de visión de 7.6 cm en dirección axial y 10 cm en dirección transaxial.

En nuestros experimentos utilizamos $[^{18}\text{F}]$ FDG (2-[18]Fluoro-2-Desoxi-D-Glucosa) como radiotrazador, esta molécula presenta el positrón en el segundo carbono del anillo del azúcar. Esta molécula es un análogo de la glucosa que puede ser captada por los transportadores de glucosa, pero no metabolizada. Una vez que esta molécula es captada el positrón del flúor interacciona con electrones del medio para producir el evento de aniquilación, esto produce la emisión de dos fotones de alta energía con trayectorias opuestas que pueden ser detectados

7.11. Estudio de PET

En este protocolo se utilizaron 14 conejos enanos machos, los conejos fueron obtenidos de una granja local con una edad de 35 días. A la llegada de los animales se realizó una evaluación de su estado de salud y la desparasitación de los mismos. Los conejos se mantuvieron por un periodo de 15 días, bajo condiciones controladas en el bioterio del instituto de Fisiología Celular, UNAM. Los animales se mantuvieron en ayuno las 12 horas previas a realizar los experimentos de microPET.

Los conejos fueron asignados aleatoriamente a alguno de los cuatro grupos siguientes:

1. Grupo CONTROL. Fue administrado con Solución salina (PBS) (3 animales)

2. Grupo VSAK. Fue administrado con el péptido VSAK (60 µg/kg) (3 animales)
3. Grupo LPS. Fue administrado con LPS (450 ng/kg) (4 animales)
4. Grupo VSAK+LPS. Fue administrado con péptido VSAK (60 µg/kg) y LPS (450 ng/kg) (4 animales)

La estimación para la administración de los distintos tratamientos se realizó con base al peso del animal. Los LPS se administraron en PBS con un volumen total de 300µl. El péptido VSAK se administró en PBS en un volumen final de 300ul. Los conejos del grupo control también fueron administrados con 300µl de PBS. Todos los tratamientos se administraron a través de las venas marginales de las orejas de los animales y la administración del tratamiento se hizo algunos minutos antes de la administración del radiofármaco para inmediatamente proceder a la captura de PET. Para los grupos CONTROL, LPS y VSAK; la administración del tratamiento fue seguida por la administración inmediata del radiofármaco y se procedió a iniciar la captura. En el caso del grupo VSAK+LPS, primero se administraron los LPS y de forma casi simultánea se administró el péptido VSAK por la oreja contraria, finalmente se administró el radiofármaco justo ante de iniciar con la captura de PET. En este ensayo se obtuvieron datos de captura dinámica de PET de la zona torácico-abdominal de los animales de experimentación de los 90 minutos posteriores a la administración del radiofármaco.

Al término de cada experimento el conejo se sacrificó por sobredosis de anestésico. Se recolectó sangre por punción cardiaca y se trajeron el hígado, intestino delgado, colon y estómago de los animales. Los órganos extraídos fueron pesados y se usó una muestra de los tejidos para el análisis de la actividad específica al final de experimento, el resto del tejido fue congelado en nitrógeno líquido con el objetivo de preservarlos para el análisis posterior. Todos los procedimientos fueron revisados y aprobados por el Comité Interno para el Cuidado y Uso de Animales de Laboratorio (CICUAL) del Instituto de Fisiología Celular con el número de protocolo JMO178-21.

7.12. Protocolo de adquisición PET

Los animales anestesiados se colocaron en el anillo de detección justo después de la administración de la [¹⁸F]-FDG, la posición de los animales se ajustó para enfocar la región comprendida entre del ápice del corazón y la parte superior de la vejiga. Con este cuadrante se obtuvo información de la captura de [¹⁸F]-FDG correspondiente a hígado, riñones y algunas regiones del intestino delgado. En ambos experimentos se realizaron capturas dinámicas de la región indicada.

El tiempo de captura utilizado fue de 90 minutos a partir de la administración de [¹⁸F]-FDG. En estos animales se recuperaron muestras de tejidos en las cuales se analizó la actividad residual de la [¹⁸F]-FDG para estimar el consumo específico por miligramo de tejido. Además, los órganos se pesaron antes de ser congelados para estimar el consumo específico total de los órganos.

Para los análisis posteriores se descartaron los datos obtenidos de animales con inconsistencias durante la captura o que murieron antes de finalizar el tiempo programado de captura.

7.13. Reconstrucción y análisis de datos de captura.

Todos los datos de captación obtenidos de los dos experimentos realizados fueron reconstruidos utilizando el algoritmo OSEM3D. Los datos se analizaron utilizando VOI (Volumen de Interés, del inglés Volume of Interest) esféricos con un diámetro de 5mm para analizar los datos de captación estándar (SUV, de inglés Estándar Uptake Value) de intestino delgado, hígado y riñones. Para la estimación del SUV en función del tiempo realizado en los riñones se analizaron los datos correspondientes a bloques de 30 segundos para cada animal, el análisis de SUV indica la captación cruda de la actividad radiactiva en los animales. Los datos de captación total se obtuvieron a partir del análisis del VOI durante los 90 minutos de captura en los órganos analizados. Para la determinación del porcentaje de dosis injectada por gramo de tejido (%ID/cc), se asumió una densidad de 1g/cm³ para cada tejido. Este ensayo nos permite conocer la actividad radiactiva específica considerando la actividad total administrada al inicio del estudio y el decaimiento en el tiempo.

7.14. Medición citocinas proinflamatorias

La medición de citocinas en suero se realizó utilizando un kit para detección múltiple de citocinas proinflamatorias Quantibody (Raybiotech, Norcross, GA, USA), el cual permite la detección simultánea de IL-1 α (Interleucina 1-Alfa), IL-1 β (Interleucina 1-Beta), IL-8 (Interleucina-8), MIP-1 β (Proteína Inflamatoria de Macrófagos 1-beta, del inglés Macrophage Inflammatory Protein) y TNF α (Factor de Necrosis Tumoral Alfa, del inglés Tumor Necrosis Factor Alpha) en muestras de plasma o suero. La medición se realizó directamente en el suero obtenido de los animales de acuerdo a las instrucciones del fabricante. La lectura de placa se realizó utilizando el lector de microarreglos GenePix 4000B (Molecular Devices, San Jose, CA, USA). La placa se leyó utilizando el canal Cy3 (verde) con una longitud de onda de excitación de 532nm.

La estimación de la concentración de las citocinas en plasma se realizó a mediante la extrapolación del valor de fluorescencia. Las curvas de concentración estándar también fueron generadas con los valores de fluorescencia media y ajustadas con ayuda del software Graphpad Prism (Graphpad Software, San Diego, CA, USA).

7.15. Análisis estadístico

El análisis estadístico se realizó utilizando el programa Graphpad Prism (Graphpad Software, San Diego, CA, USA). Los datos de hemólisis fueron analizados con pruebas T no pareadas. Los datos de viabilidad celular, expresión de marcadores inflamatorios, glucosa e insulina fueron analizados con ANOVAs de una vía. Los datos de %ID/cc total, SUV total y SUV renal fueron analizados con ANOVAs de dos vías.

8. RESULTADOS

8.1 Simulaciones de dinámica molecular.

8.1.1. Efecto de VSAK en la energía del sistema.

Las simulaciones de dinámica molecular buscaron analizar a detalle las estructuras involucradas en la interacción de VSAK con los LPS. En estas simulaciones el péptido VSAK fue colocado sobre las membranas dejando que este difundiera libremente para interactuar con cualquiera de las dos hemicapas. En estas simulaciones se observó la integración preferencial del péptido VSAK en membranas que estaban constituidas únicamente por LPS. Gracias al efecto de las condiciones periódicas que permiten la libre difusión del péptido al generar un continuo de la simulación permitiendo que este pueda difundir al lado opuesto de la posición inicial, se observó la aproximación de VSAK hacia cualquier tipo de membranas, incluyendo las constituidas por POPS-POPC y POPC-POPC. Sin embargo, la unión estable del péptido a la membrana se observó exclusivamente a las hemicapa de LPS en los sistemas LPS-POPC (Figura 10A), esta unión se mantuvo estable hasta el final de la simulación (Figura 10B). Mientras que en sistemas sin LPS, el péptido se mantuvo preferencialmente en la interfaz del solvente (Figura 10 C, D, E y F).

Considerando la participación de las cargas en el péptido en la selectividad y estabilización de estas interacciones, se generó un modelo de VSAK en el que los tres aminoácidos cargados fueron sustituidos por glutamina (VSAK Q3) (K4Q, R9Q y R14Q). Este péptido mostró una pérdida de la selectividad hacia los LPS (Figura 11A y B) y una tendencia a unirse a cualquier hemicapa de fosfolípidos, principalmente a POPC (Figura 11C, D, E y F). En estos sistemas el análisis de energía total indicó una disminución importante en los sistemas LPS-POPC en presencia del péptido VSAK (Figura 12A). Cambios de esta magnitud no fueron observados en sistemas POPC-POPC o POPS-POPC (Figura 12B y 12C). Por otro lado, el análisis de energía de los sistemas LPS-POPC en presencia de VSAK Q3 indicó una diferencia en la energía de estos en comparación con VSAK, siendo esta ligeramente menor a la del sistema en solitario (Figura 12A). No obstante, este cambio no es comparable al observado con VSAK; pudiendo atribuir este fenómeno

a la unión no selectiva de VSAK Q3 a la membrana LPS-POPC, en la hemicapa de POPC.

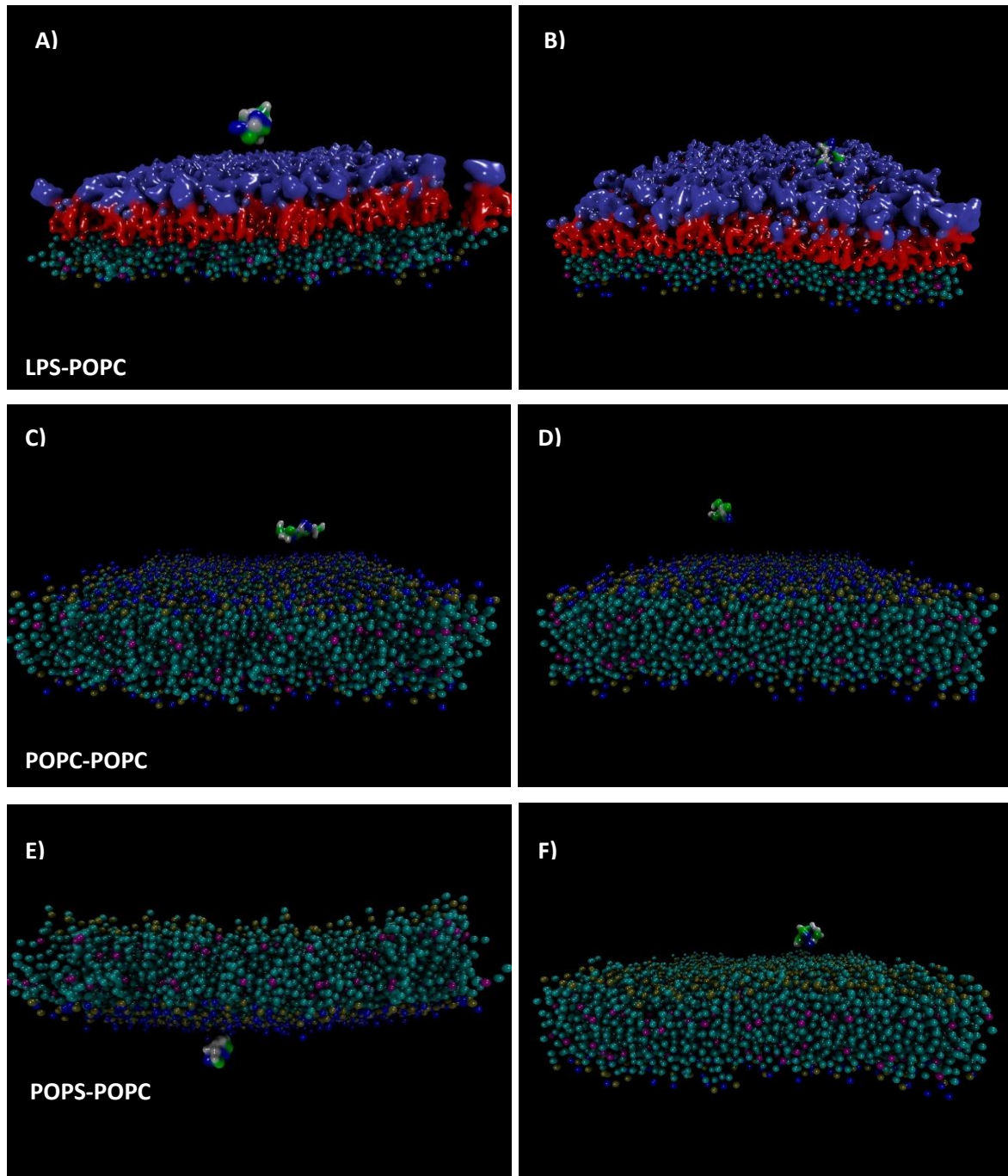


Figura 10. Simulaciones de dinámica molecular con el péptido VSAK. Los paneles (A) y (B) presentan el sistema LPS-POPC (superior-inferior) al inicio de la simulación ($t=0$) (A) y al final de la misma ($t=3\text{us}$) (B). Los paneles (C) y (D) presentan el sistema POPC-POPC (superior-inferior) al inicio de la simulación ($t=0$) (C) y al final de la misma ($t=3\text{us}$) (D). Los paneles (E) y (F) presentan el sistema POPS-POPC (superior-inferior) al inicio de la simulación ($t=0$) (E) y al final de la misma ($t=3\text{us}$) (F). VSAK: aa positivos (azul), aa hidrófobos (gris), aa hidrofílicos (verde); colas de fosfolípidos (cian); LPS: lípido A (rojo), región del núcleo (Purpura)

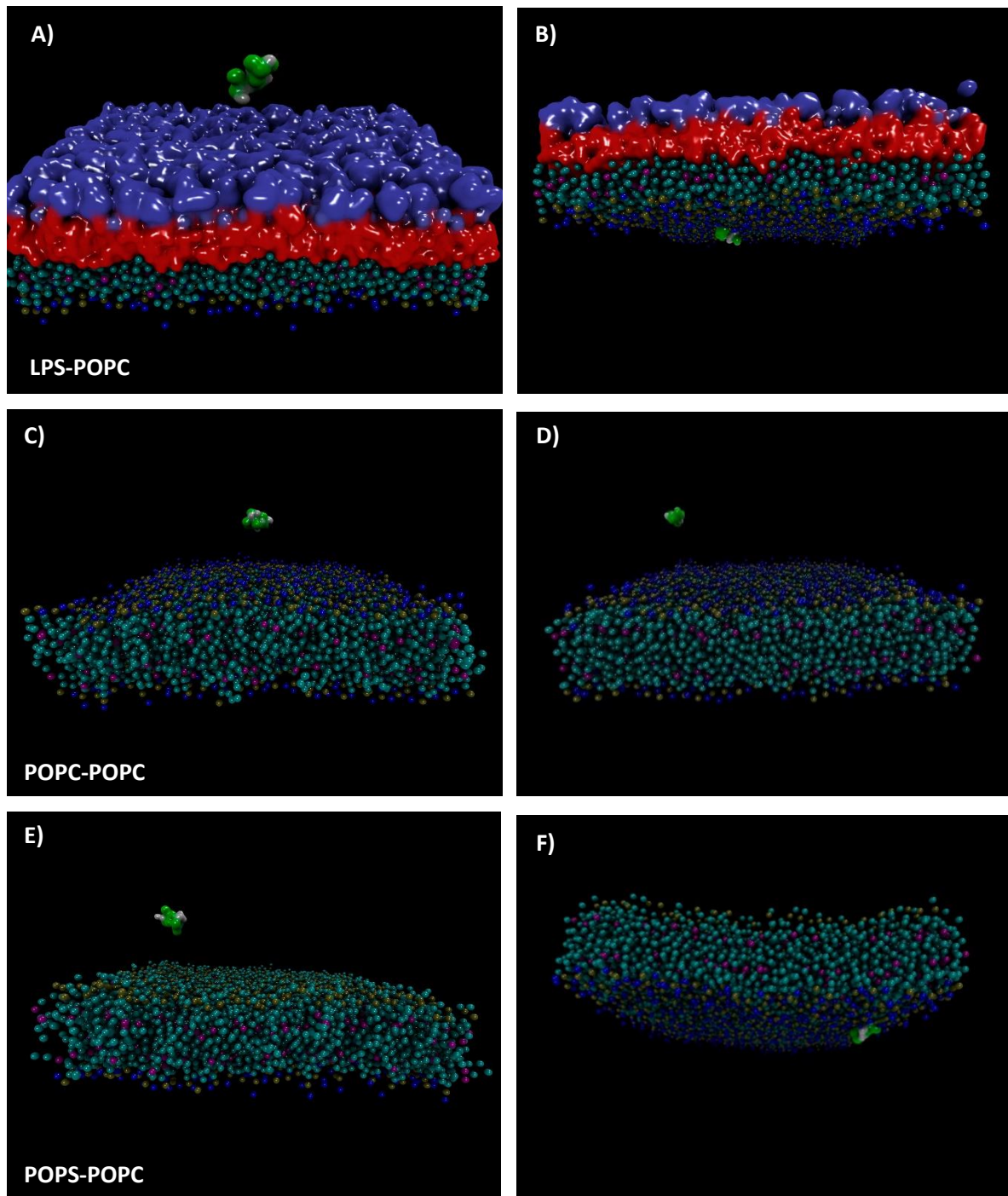


Figura 11. Simulaciones de dinámica molecular con el péptido VSAK Q3. Los paneles (A) y (B) presentan el sistema LPS-POPC (superior-inferior) al inicio de la simulación ($t=0$) (A) y al final de la misma ($t=3\text{us}$) (B). Los paneles (C) y (D) presentan el sistema POPC-POPC (superior-inferior) al inicio de la simulación ($t=0$) (C) y al final de la misma ($t=3\text{us}$) (D). Los paneles (E) y (F) presentan el sistema POPS-POPC (superior-inferior) al inicio de la simulación ($t=0$) (E) y al final de la misma ($t=3\text{us}$) (F). VSAK Q3: aa hidrófobos (gris), aa hidrofilicos (verde); colas de fosfolípidos (cian); LPS: lípido A (rojo), región del núcleo (Purpura)

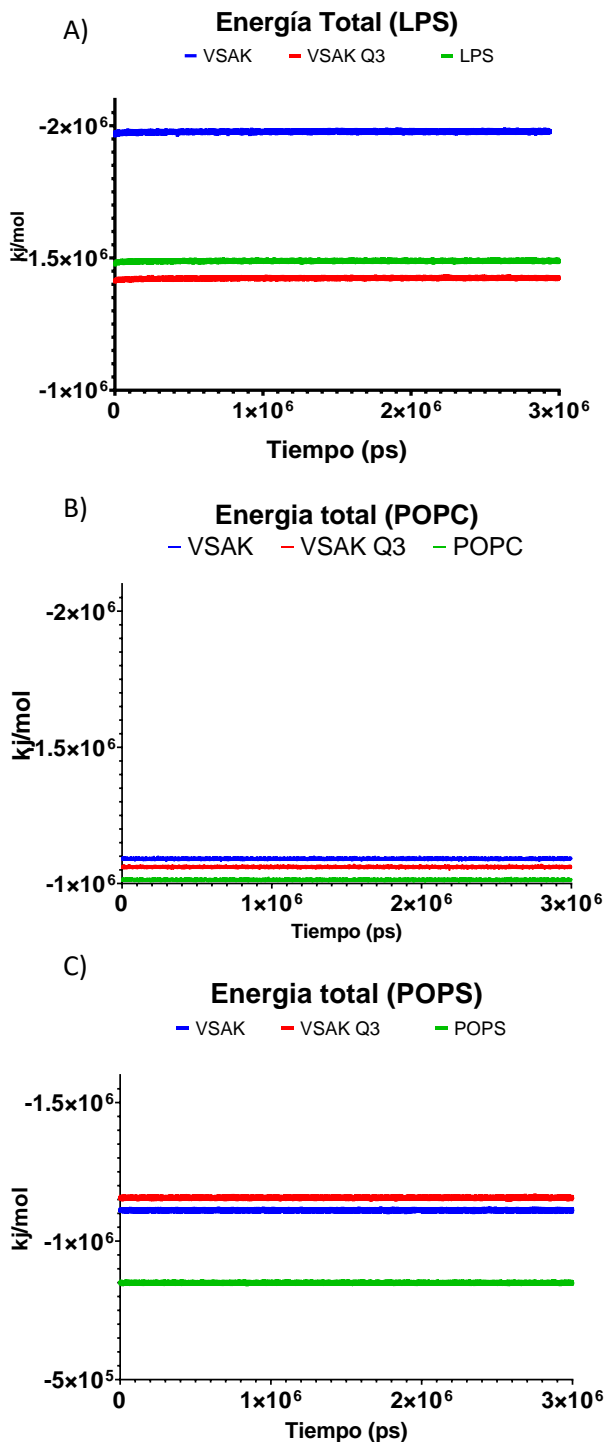


Figura 12. Energía total observada en las simulaciones de dinámica molecular. (A) Energía total observada en los sistemas LPS-POPC. Las energías promedio fueron: LPS ($-1.48 \times 10^6 \pm 2460$ Kj/mol), VSAK ($-1.97 \times 10^6 \pm 2968$ Kj/mol), VSAK Q3 ($-1.42 \times 10^6 \pm 2577$ Kj/mol). (B) Energía total observada en los sistemas POPC-POPC. Las energías promedio fueron: POPC ($-1.01 \times 10^6 \pm 2170$ Kj/mol), VSAK ($-1.09 \times 10^6 \pm 2281$ Kj/mol), VSAK Q3 ($-1.06 \times 10^6 \pm 2163$ Kj/mol). (C) Energía total observada en los sistemas POPS-POPC. Las energías promedio fueron: POPS ($-0.84 \times 10^6 \pm 1833$ Kj/mol), VSAK ($-1.11 \times 10^6 \pm 2130$ Kj/mol) y VSAK Q3 ($-1.15 \times 10^6 \pm 2167$ Kj/mol).

8.1.2. Cambios en la fluidez de la membrana

En paralelo al análisis de energía se realizó un análisis de fluidez de las membranas, en esto se utilizó el desplazamiento lateral de las cabezas de lípidos en la membrana. Mediante las herramientas de GROMACS se analizó el desplazamiento de los fosfolípidos o LPS en el plano lateral en función del tiempo.

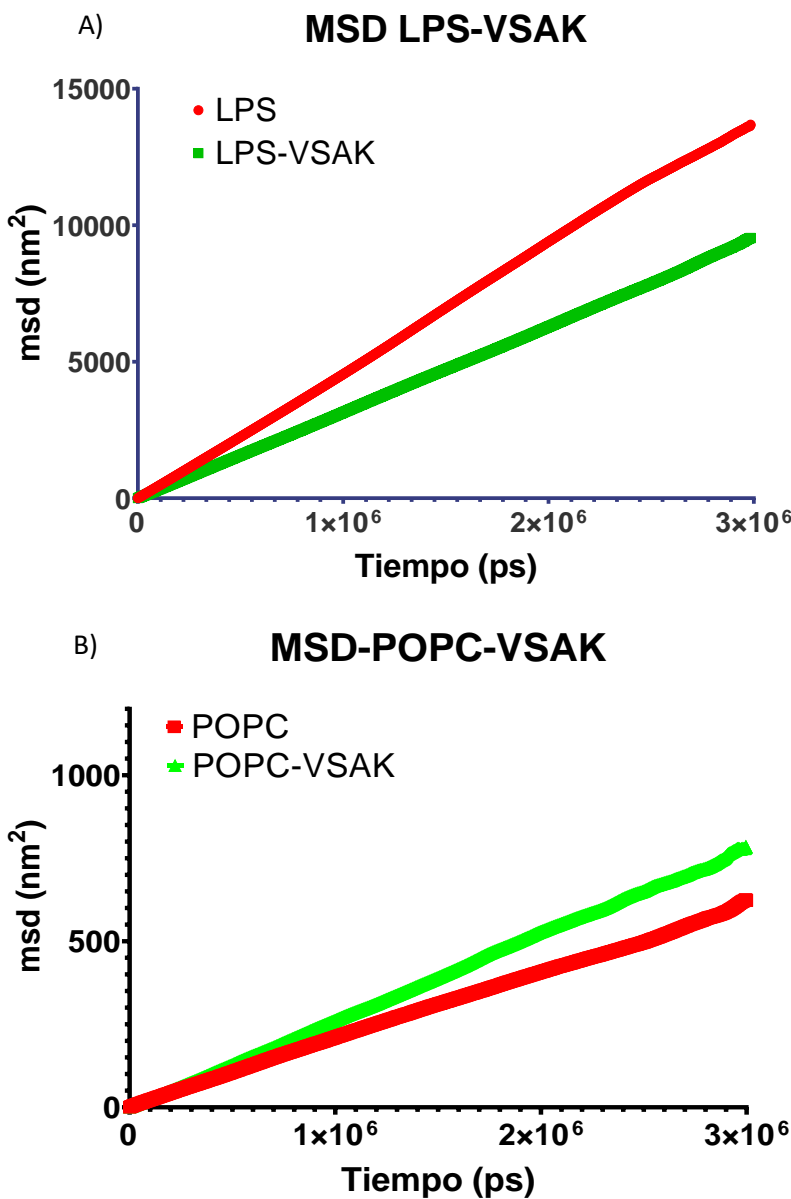


Figura 13. Cambios en la fluidez de la membrana analizados mediante MSD. (A) MSD observado en membranas LPS-POPC, en este análisis se observó una clara divergencia del MSD en presencia de VSAK en comparación con el sistema solo. (B) MSD observado en membranas POPC-POPC, el análisis de MSD indica que el MSD de estos sistemas era similar, presentando convergencia hacia el final de la simulación.

El desplazamiento cuadrado medio (MSD) fue calculado para sistemas que LPS-POPC y POPC-POPC en presencia del péptido VSAK y en los sistemas en solitario (Figura 13). En los sistemas LPS-POPC se observó que la presencia de VSAK disminuye el MSD de los LPS, efecto que puede ser atribuido a la diminución del desplazamiento en las moléculas de LPS que están en contacto con VSAK una vez que este se integra en la membrana (Figura 13A). Sin embargo, en los sistemas POPC-POPC no se observa un efecto de VSAK en el MSD, pudiendo observar una tendencia a converger en los puntos avanzados de la simulación (Figura 13B).

8.2. Efecto de VSAK en la estructura de los LPS

Por otro lado, los cambios inducidos en la estructura de LPS fueron analizados utilizando microscopía electrónica de transmisión. En estos ensayos se analizaron cambios en la estructura típica de los LPS inducidos por la presencia de VSAK.

En soluciones electro-neutras a concentraciones micromolares los LPS tienden a adoptar una estructura de fibras cubicas (Figura 14A). En las que el lípido A se localiza en la parte central de la estructura, mientras que la región del núcleo y el antígeno O rodea la estructura central formado una región electrodensa que rodea las fibras (Figura 14B).

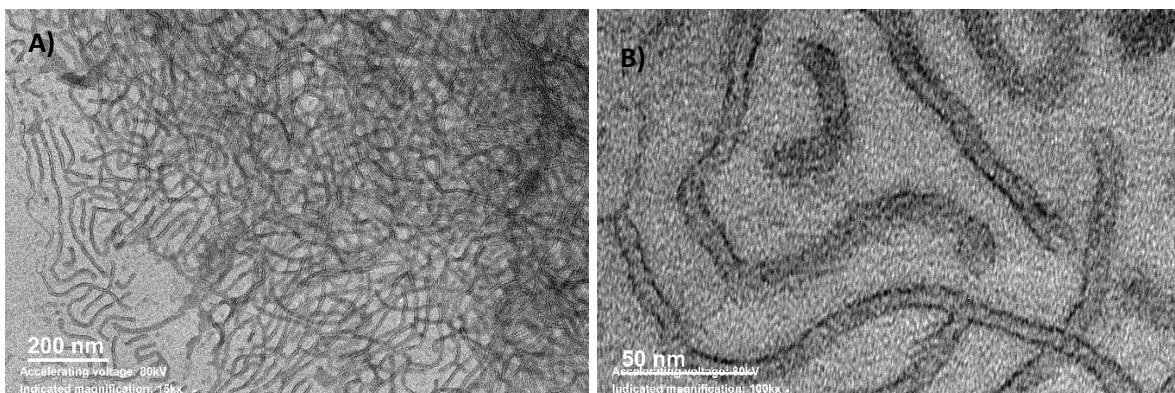
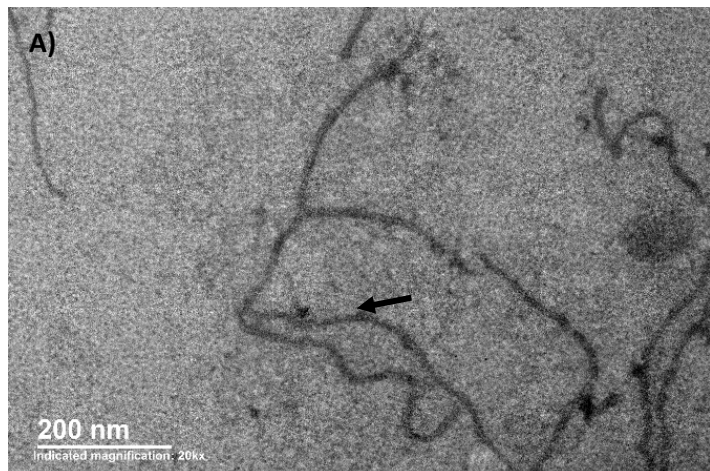
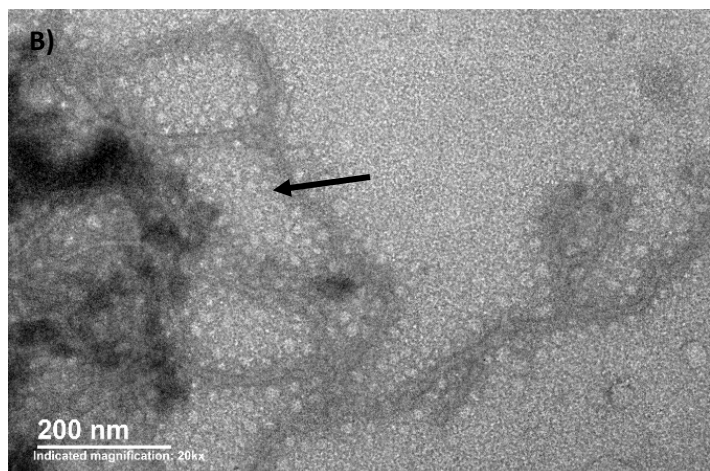


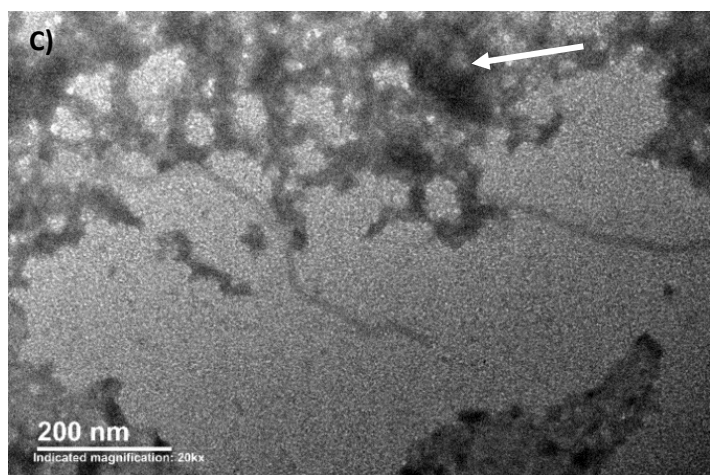
Figura 14. Estructura de los LPS. (A) Micrografía de los LPS a 7500x. En soluciones acuosas los LPS tienden a formar estructuras fibrilares, las cuales se acumulan en agregados mayores (B) Micrografía de los LPS 100000x. En las estructuras fibrilares de los LPS estos se alinean formando fibras cubicas. En esta estructura la región central menos electrodensa está correspondiente al lípido A, mientras que la región periférica más electrodensa está constituida por la región del núcleo y el antígeno O.



LPS($1\mu\text{M}$)
VSAK ($562.7\mu\text{M}$).



LPS($0.6\mu\text{M}$)
VSAK (1.12 mM)



LPS($0.5\mu\text{M}$)
VSAK (2.25 mM).

Figura 15. Efecto de VSAK en la estructura de los LPS. A) Micrografía electrónica a 20000x LPS($1\mu\text{M}$) y VSAK ($562.7\mu\text{M}$). En esta concentración se observó una disminución de la densidad de los cúmulos de fibras de LPS. (B) Micrografía electrónica a 20000x LPS($0.6\mu\text{M}$) y VSAK (1.12 mM). En estos ensayos se observó la pérdida de densidad de las fibras de LPS y la aparición de agregados micelares de LPS. (C) Micrografía electrónica a 20000x LPS($0.5\mu\text{M}$) y VSAK (2.25 mM). A esta concentración se observó una pérdida de la estructura de los LPS y la formación de agregados electrodensos.

Por otro lado, cuando los LPS son incubados en presencia del péptido VSAK se produce una alteración de la estructura típica de los LPS. A una concentración de 1mg/ml (562.7 μ M) del péptido VSAK se observa una disociación de los cúmulos de LPS disminuyendo a la densidad de fibras en estas regiones, además se observa una diminución del tamaño de las fibras y la densidad electrónica de estas (Figura 15A). En una concentración de 2mg/ml (1.12mM) de VSAK se observa una mayor perdida en la densidad electrónica de las paredes de las fibras y un menor grado de compactación en la estructura de las fibras cubica, adicionalmente, en esta concentración se observó la formación de agregados de tipo micelar en la cercanía de las fibras de LPS (Figura 15B). Finalmente, a una concentración de VSAK 4 mg/ml (2.25mM), se produjo una disociación casi total de las fibras de LPS, además de que a esta concentración se observa la formación de agregados electro densos que no presentan estructuras definidas (Figura 15C).

8.3. Efecto hemolítico

Algunos péptidos con capacidad de unión a LPS pueden llegar a producir efectos hemolíticos o citotóxicos, dada la capacidad de interacción con estructuras lipídicas. En este sentido se realizaron ensayos para estudiar posibles efectos hemolíticos y citotóxicos del péptido VSAK a distintas concentraciones del péptido.

En la figura A se muestra el ensayo de hemólisis utilizando el péptido VSAK, en estos ensayos no se observó un efecto hemolítico para ninguna de las concentraciones utilizadas en los ensayos (10-150 μ g/ml) (Figura 16A). Mientras que el efecto contrario fue observado con los LPS, en donde se observó un efecto hemolítico a partir de 100 μ g/ml (4%) que alcanzó un 100% de hemólisis a una concentración de 250 μ g/ml (Figura 16B).

Adicionalmente, cuando se evaluó la capacidad de VSAK para prevenir la hemólisis se observó que este disminuye de forma significativa la hemólisis inducida por LPS en una concentración de 100 μ g/ml de LPS ($1.93\pm0.04\%$) (Figura 16C), en comparación con LPS en solitario ($4.04\pm0.28\%$). Este efecto se mantiene en concentraciones altas de LPS (250 μ g/ml) ($98.89\pm0.87\%$), cuando los eritrocitos son tratados con una concentración de 150 μ g/ml de VSAK (78.31 ± 1.8) (Figura 16D).

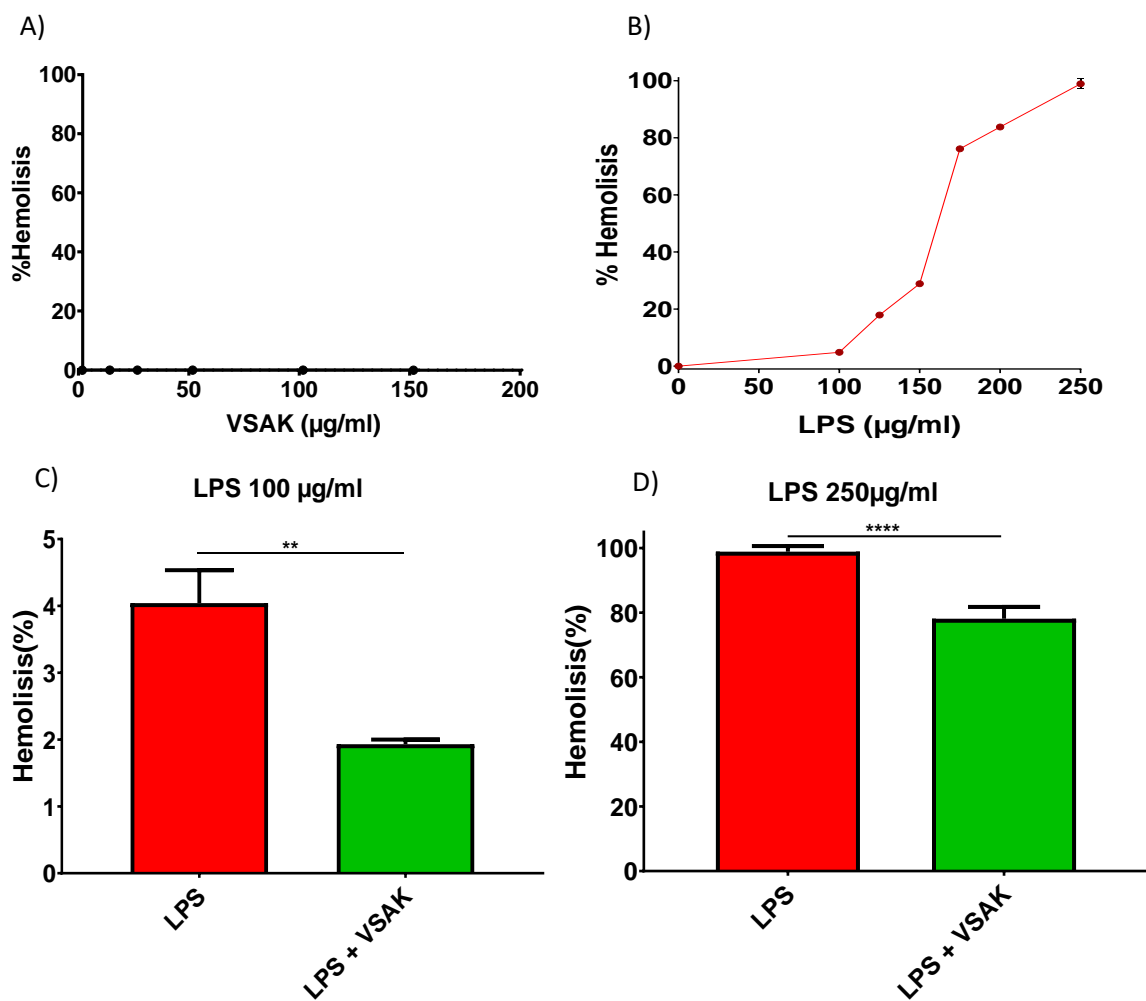


Figura 16. Efectos hemolíticos de VSAK y LPS. (A) Efecto hemolítico de LPS, el tratamiento con VSAK no presentó efectos hemolíticos en ninguna concentración. 10 $\mu\text{g/ml}$ (-0.04±0.003 %) a 150 $\mu\text{g/ml}$ (-0.06±0.003 %). (B) Efecto hemolítico de los LPS, en concentraciones elevadas se observó hemólisis asociada a los LPS: 100 μg (4.8±0.002%), 125 μg (17.8±0.01%), 150 μg (28±0.06%), 175 μg (76.1±0.04%), 200 μg (83.7±0.02%) y 250 μg (98.9±1.75%). (C) VSAK disminuye el efecto hemolítico de los LPS el tratamiento con VSAK (150 $\mu\text{g/ml}$) disminuyó de forma significativa la hemólisis inducida por LPS (1.9±0.04%), comparada con LPS en solitario (4.04±0.28, p=0.04, **). (D) un efecto similar fue observado en el tratamiento combinado utilizando 250 $\mu\text{g/ml}$ (98.89±0.87%) comparado con la aplicación en solitario de LPS (78.13±1.82%, p=<0.0001, ****). Las gráficas presentan el promedio ± error estándar. (n=4).

8.4. Ensayos de viabilidad celular

Para analizar la posible citotoxicidad asociada al tratamiento con el péptido VSAK, se realizaron ensayos de viabilidad celular mediante curvas dosis-respuesta. En estos ensayos se utilizó un detergente (Triton x100) para la elaboración de curvas de viabilidad celular control. En estos ensayos se midió el efecto de concentraciones crecientes de VSAK en la viabilidad celular, mediante cambios en la densidad óptica (O.D.) del colorante.

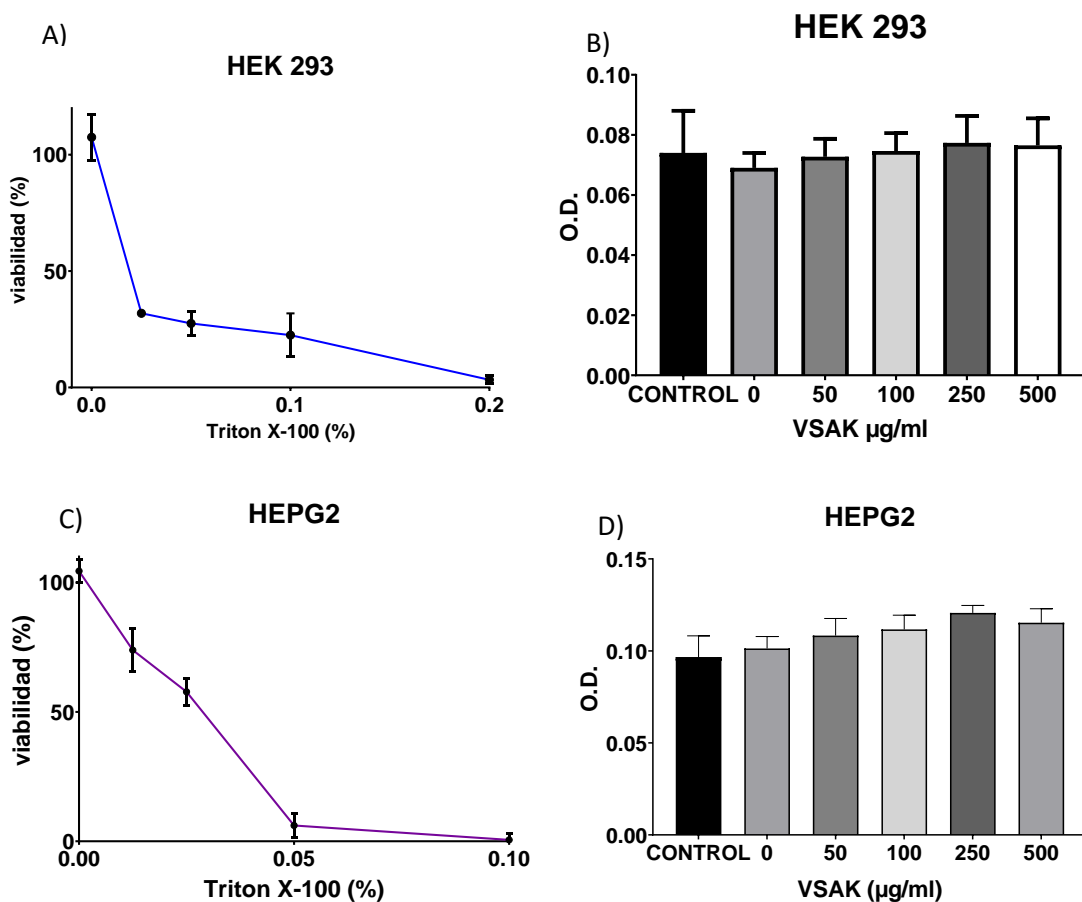


Figura 17. Ensayos de viabilidad celular con el péptido VSAK. (A) Curva de viabilidad celular en presencia de detergente Tritón en células HEK293. Los puntos de la curva incluyen 0 (107.5 ± 9.78), 0.025 (31.87 ± 3.14), 0.05 (27.5 ± 11.18), 0.1 (22.5 ± 9.3) y 0.2 (3.3 ± 1.76) porcentajes de Tritón x100 ($n=5$). (B) Viabilidad en células HEK293 en presencia de VSAK, en estos ensayos no se observaron cambios significativos en ningún tratamiento con el péptido VSAK ($n=4$). (C) Curva de viabilidad celular en células HEPG2 en presencia de Tritón x100. Los puntos de la curva incluyen 0 (104.4 ± 4.44), 0.0125 (73.88 ± 8.22), 0.025 (57.77 ± 5.35), 0.05 (6.1 ± 4.3) y 0.1 (0.55 ± 2.6) ($n=6$). (D) Viabilidad en células HEPG2 en presencia de VSAK, en estos ensayos no se observaron cambios significativos en ningún tratamiento con el péptido VSAK ($n=4$). Datos presentados como promedio ± error estándar.

La curva de viabilidad utilizada como control para las células HEK293 se muestra en la Figura 17A, en comparación, el tratamiento con el VSAK no produjo cambios en la viabilidad celular a ninguna de las concentraciones utilizadas (50-500 ug/ml) (Figura 17B). Las cuales incluyen concentraciones muy superiores a las utilizadas en los experimentos de estimulación.

Este efecto fue congruente con lo observado en las células HEPG2, en donde las células presentaron cambios en la viabilidad producidas por el detergente, con un efecto similar al observado en las células HEK293 (Figura 17C). En esta línea celular el tratamiento con VSAK a concentraciones elevadas tampoco produjo cambios en la viabilidad celular (Figura 17D)

8.5. Ensayos de estimulación con LPS y NEO-3

8.5.1. Células HAEC - Expresión de marcadores pro-inflamatorios

A nivel celular se analizaron cambios en la expresión de marcadores inflamatorios relacionados a la respuesta a LPS, estos marcadores se analizaron en las células HAEC y THP-1

Las células HAEC fueron estimuladas de acuerdo durante 24 horas con LPS, VSAK y VSAK+LPS, posteriormente se recuperaron la célula para la extracción de ARN total y el análisis de la expresión de marcadores de inflamación. Las gráficas muestran el resultado de cambios en la expresión de moléculas asociadas al proceso inflamatorio. En las gráficas se excluyó el grupo CONTROL, el cual fue utilizado para la normalización de los datos.

El análisis indicó un ligero incremento en la expresión de IL-1 β en los grupos tratados con LPS (2.56 ± 1.27) y LPS+VSAK (3.14 ± 1.16) con respecto al control y el grupo VSAK (0.952 ± 0.32), sin embargo, estos no fueron estadísticamente significativos (Figura 18A). El mismo efecto fue observado al analizar IL-6, un incremento en los grupos LPS (1.57 ± 0.2) y LPS+VSAK (1.45 ± 0.28) con respecto al grupo CONTROL y VSAK (0.55 ± 0.08), sin que estos fueran significativos (Figura 18B).

En el caso de ICAM-1, el análisis indicó un incremento significativo de esta molécula en el grupo LPS (2.83 ± 0.20) con respecto al grupo VSAK (0.84 ± 0.36). En el grupo LPS+VSAK (1.248 ± 0.14) se observó un nivel menor al del grupo LPS, sin embargo, este cambio no fue significativo (Figura 18C).

En el caso de Factor III, se observó, un mayor nivel de en la expresión de esta molécula en el grupo LPS (2.83 ± 0.2) en comparación con el grupo VSAK (0.84 ± 0.36) y el grupo LPS+VSAK (1.48 ± 0.14) (Figura 18D).

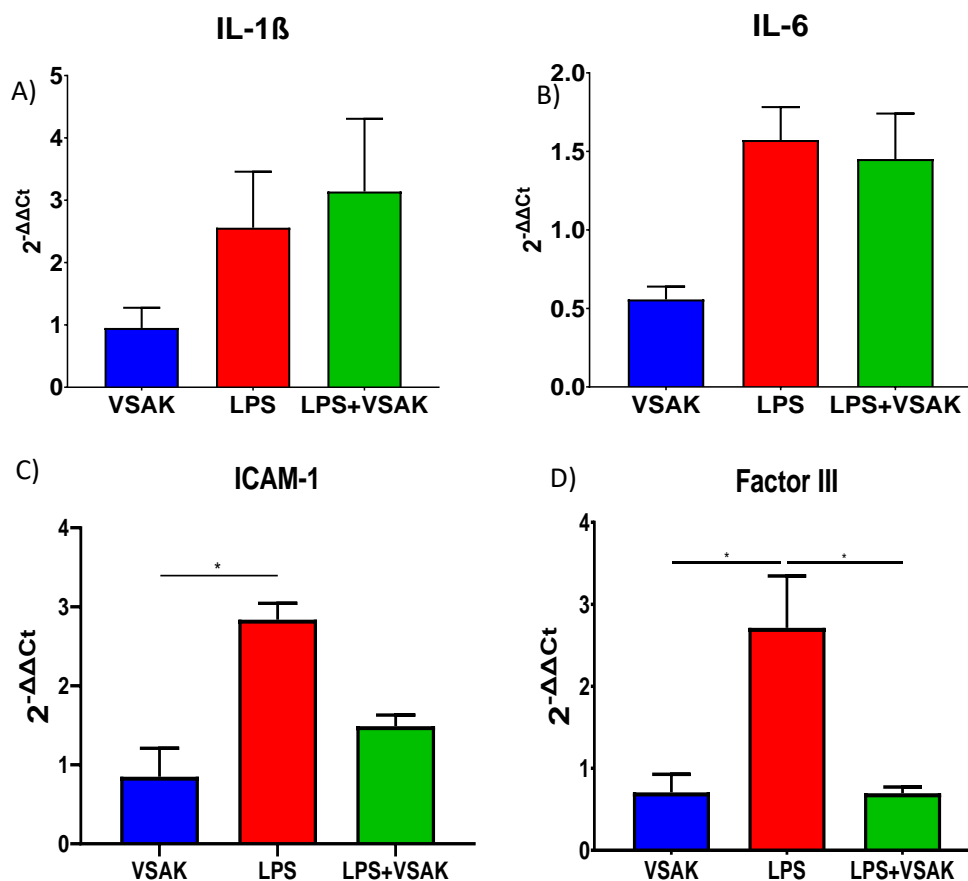


Figura 18. Expresión de marcadores proinflamatorios en células HAEC. (A) Niveles observados de IL-1 β , no se observaron resultados estadísticamente significativos. VSAK (0.952 ± 0.32), LPS (2.56 ± 1.27) y LPS+VSAK (3.14 ± 1.16) ($n=3$). (B) Expresión de IL-6, este análisis no presento diferencias estadísticamente significativas. VSAK (0.55 ± 0.08), LPS (1.57 ± 0.2) y LPS+VSAK (1.45 ± 0.28) ($n=3$). (C) Expresión de ICAM. Esta molécula presento una mayor expresión en el grupo LPS (2.83 ± 0.20) en comparación con el grupo VSAK (0.84 ± 0.36 , $p = 0.02$, *), pero esta no fue significativa al ser comparada con el grupo LPS+VSAK (1.248 ± 0.14) ($n=3$). (D) Niveles de Factor III. Esta molécula mostro un nivel estadísticamente mayor en el grupo LPS (2.83 ± 0.2) en comparación con el grupo VSAK (0.84 ± 0.36 , $p=0.02$, *) y el grupo LPS+VSAK (1.48 ± 0.14 , $p=0.02$, *) ($n=3$). Los datos se muestran como promedio ±error estándar.

8.5.2. Células THP-1 - Expresión de marcadores pro-inflamatorios

En esta línea celular el análisis del ARNm de IL-1 β indicó una mayor expresión de esta molécula en el grupo LPS (1.53 ± 0.008) en comparación con VSAK (0.68 ± 0.05) con LPS+VSAK (1.24 ± 0.43). Además, hubo un incremento considerable en el grupo NEO-3 (4.45 ± 2.98), que se vio atenuado en el grupo NEO-3+VSAK (2.96 ± 1.3), sin embargo, estos cambios no presentaron significancia estadística (Figura 19A).

Para IL-6, la expresión de esta molécula presentó un nivel mayor en el grupo LPS (7.9 ± 2.7) en comparación con el grupo VSAK (0.41 ± 0.008) y LPS+VSAK (3.9 ± 2.6). Sin embargo, el mayor incremento se observó en el grupo NEO-3 (209.9 ± 22.9), no obstante, este incremento fue parcialmente atenuado en el grupo NEO-3+VSAK (81.65 ± 23.3) (Figura 19B). En TLR-4 se observaron efectos similares a las dos moléculas previas, LPS (0.97 ± 0.06) presentó niveles mayores a los observados en los grupos VSAK (0.46 ± 0.06) y LPS+VSAK (0.53 ± 0.06), sin que estos fueran estadísticamente significativos. Mientras que el grupo NEO-3 (28.9 ± 10.4) mostro el mayor nivel de expresión de esta molécula, el cual se vio disminuido en el grupo NEO-3+VSAK (16.1 ± 13.1) (Figura 19C). En el caso de ICAM-1 se observó un incremento en el grupo LPS (3.5 ± 2.4) en comparación con el grupo VSAK (0.48 ± 0.24) y el grupo LPS+VSAK (0.72 ± 0.35), aunque este incremento no fue estadísticamente significativo (Figura 19D).

En NOS2 se observó un notable incremento en la expresión de esta molécula en el grupo LPS (81.66 ± 2.075) en comparación con los grupos VSAK (3.48 ± 0.2) y VSAK+LPS (1.96 ± 0.19) (Figura 19E). Un efecto similar se observó para NOS3, en donde hubo un incremento en el grupo LPS (50733 ± 12891) en comparación con el grupo VSAK (1.51 ± 0.03) y el grupo VSAK+LPS (80.95 ± 0.09) (Figura 19E). Un comportamiento muy similar al observado en E-SEL, en donde hubo un incremento significativo en el grupo LPS (6494 ± 1829) en comparación con los grupos VSAK (0.6 ± 0.3) y LPS (82.06 ± 0.51) (Figura 19F).

Finalmente, el análisis de IL-10 indicó un incremento importante en el grupo LPS (3.35 ± 0.74) con respecto al grupo VSAK (1.16 ± 0.16). Mientras que este no fue

significativo al ser comparado con el grupo LPS+VSAK (3.09 ± 0.22), el cual presento un nivel similar al del grupo LPS (Figura 19G).

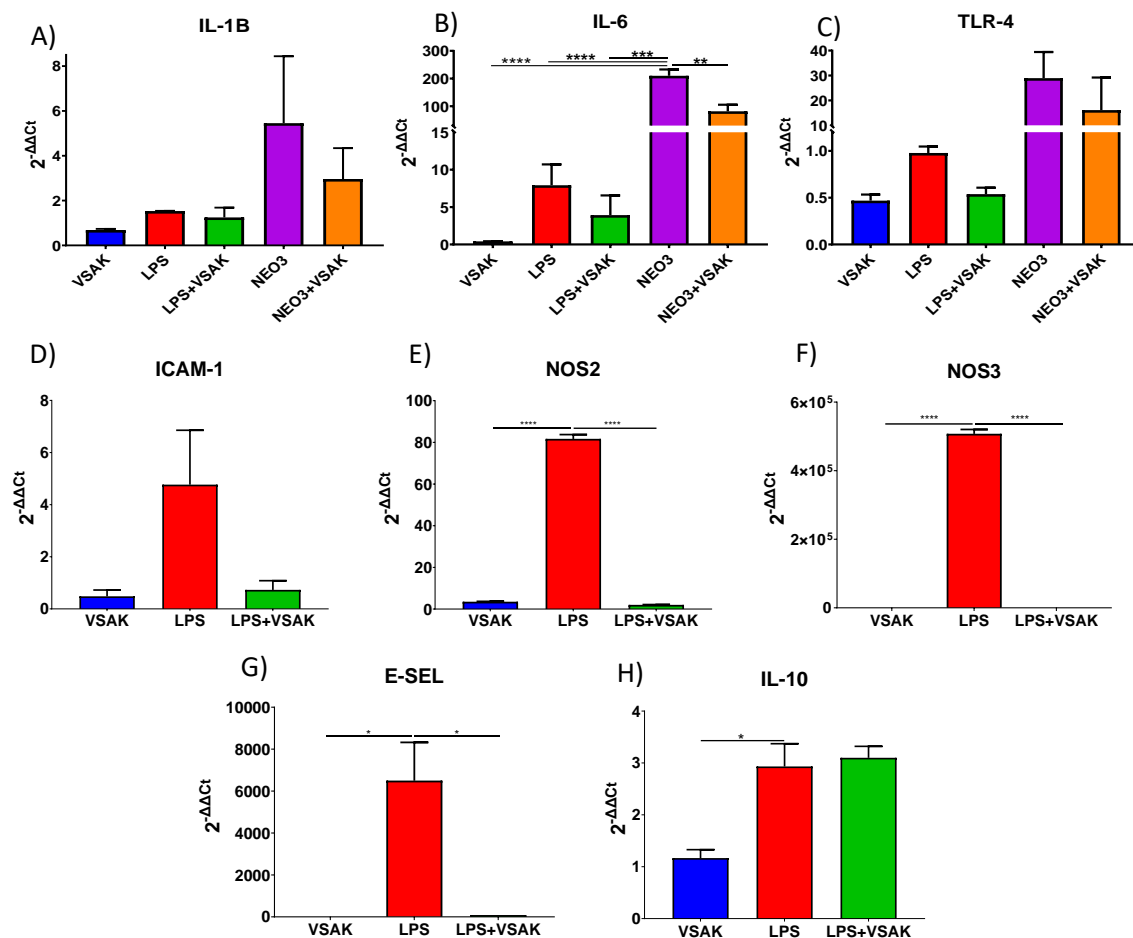


Figura 19. Expresión de marcadores proinflamatorios en células THP-1. (A)Expresión de IL-1B, en esta molécula no presento cambios significativos entre los grupos VSAK (0.68 ± 0.05), LPS (1.53 ± 0.008), LPS+VSAK (1.24 ± 0.43), NEO-3 (4.45 ± 2.98), NEO-3+VSAK (2.96 ± 1.3) (n=3). (B) Expresión de IL-6. En este análisis el grupo NEO-3 (209.9 ± 22.9) en comparación con los grupos VSAK (0.41 ± 0.008 , $p = <0.0001$, ****), LPS (7.9 ± 2.7 , $p = <0.0001$, ****), LPS+VSAK (3.9 ± 2.6 , $p=0.0001$, ***) y NEO-3+VSAK (81.65 ± 23.3 , $p=0.001$, **) (n=3). (C)Expresión de TLR-4. El análisis de esta molécula no presento diferencias significativas entre grupos. VSAK (0.46 ± 0.06), LPS (0.97 ± 0.06), LPS+VSAK (0.53 ± 0.06), NEO-3 (28.9 ± 10.4) y NEO-3+VSAK (16.1 ± 13.1) (n=3). (D) Expresión de ICAM-1. La expresión de esta molécula no mostro diferencias estadísticamente significativas. VSAK (0.48 ± 0.24), LPS (3.5 ± 2.4) y LPS+VSAK (0.72 ± 0.35) (n=3). (E) Expresión de NOS2. En este análisis el grupo LPS (81.66 ± 2.075) presento un incremento importante en comparación con VSAK (3.48 ± 0.2 , $p = <0.0001$, ****) y el grupo VSAK+LPS (1.96 ± 0.19 , $p = <0.0001$, ****) (n=3). (F) Expresión de NOS3. En esta molécula el grupo LPS (50733 ± 12891) tuvo un incremento significativo comparado con el grupo VSAK (1.51 ± 0.03 , $p = <0.0001$, ****) y el grupo VSAK+LPS (80.95 ± 0.09 , $p = <0.0001$, ****) (n=3). (G) Expresión de E-SEL. La expresión de esta molécula fue significativamente más elevada en el grupo LPS (6494 ± 1829) con parado con los grupos VSAK (0.6 ± 0.3 , $p=0.011$, *) y LPS (82.06 ± 0.51 , $p = 0.012$, *). (H)Expresión de IL-10. En esta molécula el grupo LPS (3.35 ± 0.74) presento un aumento significativo al ser comparado con el grupo VSAK (1.16 ± 0.16 , $p = 0.03$, *), pero no con el grupo LPS+VSAK (3.09 ± 0.22) (n=3).

8.6. Ensayos de PET.

8.6.1. Reconstrucción tridimensional.

A partir de los datos de captación obtenidos mediante PET, se realizó la reconstrucción de trayectorias para el análisis de la captación. Adicionalmente, estos datos se utilizaron para construir modelos tridimensionales para el análisis cualitativo de los cambios de captación. Como los mostrados en la Figura 20 en los que se muestra la reconstrucción de la captación observada en la región torácico-abdominal.

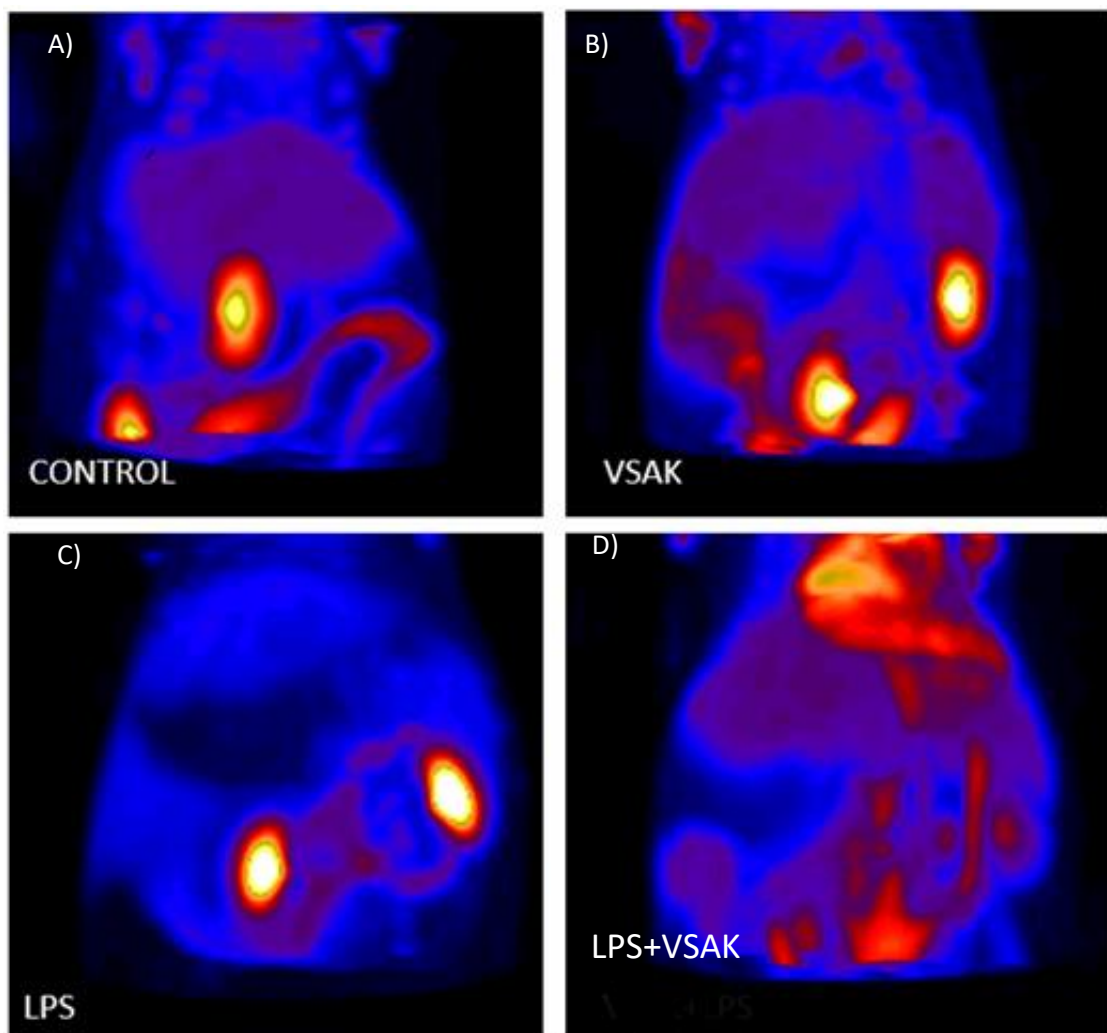


Figura 20. Imágenes representativas de animales pertenecientes a los grupos experimentales.

Los paneles muestran imágenes que corresponden a la captación observada en la región torácico-abdominal de los animales en los distintos grupos experimentales: (A) CONTROL, (B)VSAK, (C)LPS y (D)LPS+VSAK. En estas imágenes se pudo observar cambios en la captación, en particular en grupo LPS en donde ocurrió una disminución generalizada de la captación de $[^{18}\text{F}]\text{-FDG}$

El análisis cualitativo de la captura indica que en los animales del grupo LPS se produce una diminución generalizada de la captura de [¹⁸F]-FDG (Figura 20C). Esto en comparación con el patrón de captación que se observa en el grupo CONTROL, el cual es muy similar al que presenta el grupo VSAK. De forma interesante, en los animales del grupo LPS+VSAK (Figura 20D) parece haber un patrón de captación que es similar al de los grupos CONTROL y VSAK (Figura 20A y B).

8.6.2. Valor de captación total

El análisis de %ID/cc (porcentaje de dosis administrada por cm³) y el análisis de SUV (Valor de Captura Estándar) en órganos se realizó en aquellas áreas adecuadas para el uso de VOIs del tamaño indicado previamente. Los órganos analizados fueron los riñones, hígado e intestino delgado. Las mediciones de %ID/cc indicaron un incremento en la captación de glucosa a nivel renal en los animales tratados con LPS, este efecto se observó en ambos riñones, sin embargo, el cambio solo presentó diferencias estadísticamente significativas en el riñón derecho.

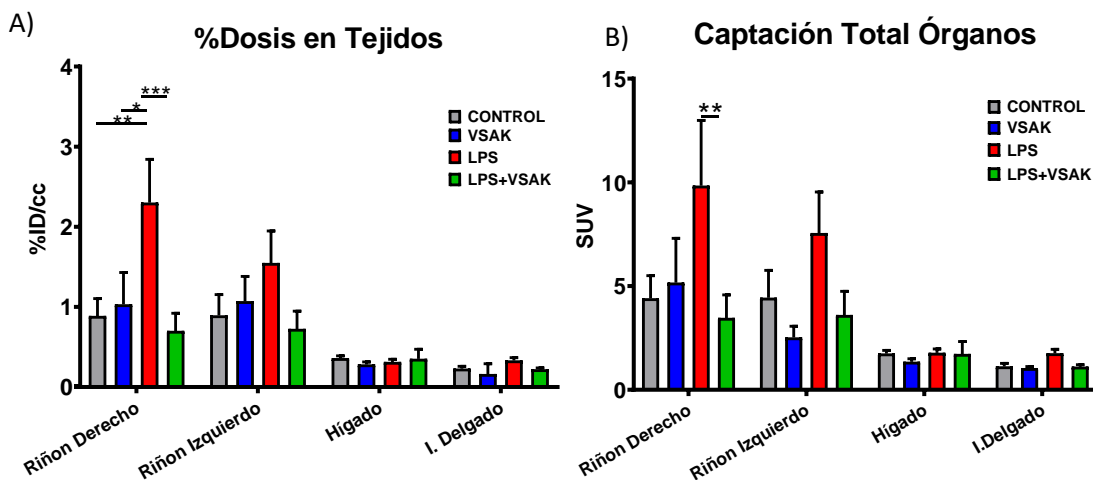


Figura 21. Análisis de Captación total de en órganos. A) Datos obtenidos del %ID/cc de los riñones, hígado e intestino delgado. Un incremento significativo fue observado en el SUV del riñón derecho en el grupo LPS (2.3 ± 0.54) en comparación con los otros grupos CONTROL (0.886 ± 0.21 , $p=0.005$ **), VSAK (1.03 ± 0.39 , $p=0.013$ *) y VSAK+LPS (0.7 ± 0.22 , $p=0.0005$ ***). Un efecto similar se observó en el riñón izquierdo sin que este fuera estadísticamente significativo. B) SUV total obtenido de los datos de captación. El SUV es significativamente mayor en el riñón derecho del grupo LPS (9.83 ± 3.15) con respecto al grupo VSAK+LPS (3.46 ± 1.11 , $p=0.008$ **). Un efecto muy similar se observó en el riñón izquierdo, sin que esté presentara cambios significativos. Los datos presentan el promedio \pm error estándar.

En el riñón derecho el grupo LPS presento el mayor nivel de captación de [¹⁸F]-FDG (2.3 ± 0.54), el cual fue significativamente más elevado al ser comparado con los grupos CONTROL (0.88 ± 0.21), VSAK (1.03 ± 0.39) LPS+VSAK (0.7 ± 0.22) (Figura 21A).

En el riñón izquierdo se observó una tendencia similar a la del riñón derecho, en donde el grupo LPS presento el mayor nivel de captación (1.54 ± 0.69), en comparación con los grupos CONTROL (0.89 ± 0.26), VSAK (1.07 ± 0.30) y LPS+VSAK (0.72 ± 0.22). Sin embargo, el análisis no indica diferencias estadísticas significativas (Figura 21A).

Por otro lado, el análisis de hígado e intestino delgado no presento diferencias significativas o tendencias relevantes en el análisis de %ID/cc para los distintos grupos experimentales (Figura 21A).

En este sentido, el análisis de SUV presento resultados muy similares a los observados en análisis de %ID/cc. En el riñón derecho de los animales del grupo LPS el SUV fue mayor a los observados en los otros grupos, este cambio fue estadísticamente significativo con respecto al grupo LPS+VSAK, pero no se encontraron diferencias significativas con los grupos CONTROL y VSAK (Figura 21B).

El riñón izquierdo presento un comportamiento muy similar, en este el SUV del grupo LPS (7.55 ± 1.55) fue mayor al de los grupos CONTROL (4.43 ± 1.32), VSAK (2.52 ± 0.54) y LPS+VSAK (3.6 ± 1.14), sin embargo, estas diferencias no fueron estadísticamente significativas (Figura 21B).

En concordancia con lo observado en el %ID/cc, el análisis de hígado e intestino delgado no presentaron diferencias estadísticamente significativas o tendencias resaltables (Figura 21B).

8.6.3. Valor de captura estándar renal

Dados los resultados observados en el análisis de SUV total, se realizó el análisis del SUV renal en función del tiempo. Este se realizó de forma individual para ambos riñones. En el riñón derecho el SUV del grupo LPS presento niveles mayores a los observados en los otros grupos. A partir del minuto 68 este cambio es estadísticamente significativo al ser comparado con el grupo LPS+VSAK. Al final de la captura este incremento en el grupo LPS (8.01 ± 3.2) es significativo con respecto al grupo VSAK (2.82 ± 1.01) y el grupo LPS+VSAK (2.3 ± 0.44), con el grupo CONTROL (4.69 ± 1.04) no se encontraron cambios significativos (Figura 22A). En el riñón izquierdo se observó el mismo patrón en donde el grupo LPS (7.76 ± 2.79) presento un mayor nivel de captura con respecto a los grupos CONTROL (4.53 ± 1.26), VSAK (2.93 ± 1.13) y LPS+VSAK (2.47 ± 0.65), sin embargo, este no presento diferencias significativas (Figura 22B). Es posible que esta diferencia pueda estar asociada al mayor flujo sanguíneo en el riñón derecho, permitiendo una mayor captación del radiotrazador.

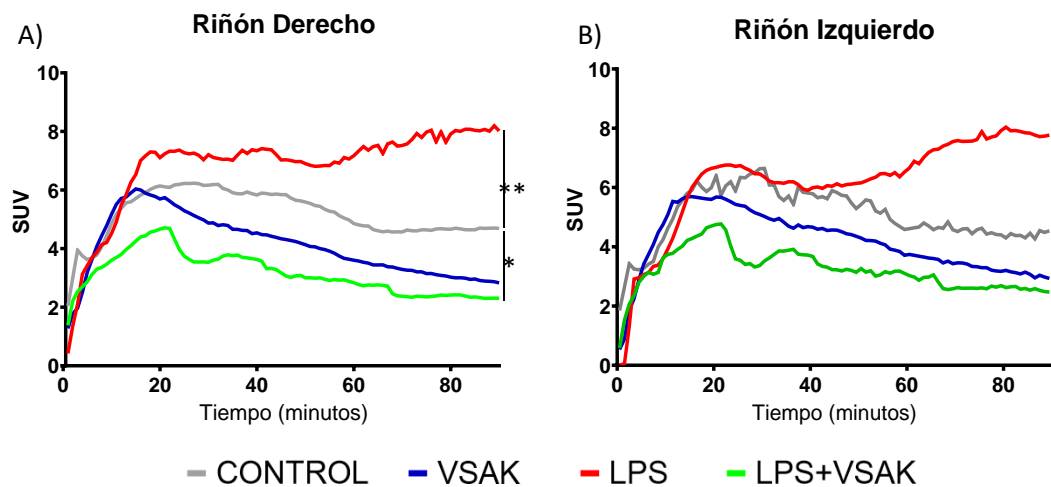


Figura 22. SUV renal. A) SUV del riñón derecho durante el tiempo captura. Para el caso del grupo LPS existe una diferencia significativa con respecto al grupo VSAK+LPS a partir del minuto 68; al final del experimento (minuto 90) la captación en el grupo LPS (8.01 ± 3.2) fue estadísticamente mayor a la observada en el grupo VSAK (2.82 ± 1.01) y el grupo LPS+VSAK (2.3 ± 0.44 , $p=0.008$, **), con el grupo CONTROL (4.69 ± 1.04 , $p=0.048$, *) no hubo diferencias significativas. B) Datos de SUV del riñón izquierdo. En este análisis se observa un comportamiento similar al del riñón derecho, sin embargo, no se encontraron diferencias significativas entre grupos al final del experimento. CONTROL (4.53 ± 1.26), VSAK (2.93 ± 1.13), LPS (7.76 ± 2.79) y VSAK+LPS (2.47 ± 0.65). Los datos se presentan como el promedio \pm error estándar. Barras de error no mostradas

8.6.4. Marcadores proinflamatorios

El análisis de marcadores proinflamatorios se realizó a partir de las muestras de suero recuperadas de los animales utilizados en los experimentos de PET. Estas se analizaron de forma simultánea utilizando un sistema de detección múltiple, como se describió anteriormente. En todas las moléculas analizadas se observó un patrón consistente, en el que la administración de LPS produjo un incremento de los marcadores con respecto a los grupos CONTROL y VSAK, mientras que el tratamiento con VSAK (en el grupo LPS+VSAK) disminuyó el nivel de estas moléculas.

En TNF α el nivel más alto de esta molécula se observó en el grupo LPS (13.48 ± 8.063), mientras que el nivel en los grupos CONTROL (0.55 ± 0.21), VSAK (0.67 ± 0.19) y LPS+VSAK (0.56 ± 0.13) fue considerablemente menor, sin embargo, el análisis indicó que esta diferencia no presentaba significancia estadística (Figura 23A).

El análisis de IL-1 α indicó que esta citocina presentaba mayores niveles en el grupo LPS (823.1 ± 350.5) en comparación con los otros tres grupos: CONTROL (314.9 ± 71.65), VSAK (439 ± 210.9) y LPS+VSAK (174.8 ± 48.69). No obstante, estos cambios no fueron estadísticamente significativos (Figura 23B).

En estas tres moléculas se observó un patrón con tendencias consistentes en el que tratamiento VSAK redujo la producción de las moléculas proinflamatorias producida por los LPS, aunque el análisis no indicó significancia estadística.

Un efecto similar fue observado en el análisis de IL-1 β , el mayor nivel de esta molécula se observó en el grupo LPS (4.06 ± 1.45), en comparación con los grupos CONTROL (1.73 ± 1.06), VSAK (1.78 ± 0.04) y LPS+VSAK (1.1 ± 0.92). El análisis indicó que las diferencias entre grupos no representaron un cambio significativo (Figura 23C).

En el caso de IL-8, el mayor nivel de esta citocina fue observado en el grupo LPS (75.34 ± 15.55), este cambio presentó una diferencia significativa con respecto al

grupo CONTROL (20.3 ± 7.44). En comparación con VSAK (42.57 ± 12.44) Y LPS+VSAK (54.65 ± 6.01), este cambio no fue significativo (Figura 23D).

El análisis de la proteína MIP-1 β indicó que el nivel de esta citocina fue más elevado en el grupo LPS (934.1 ± 170.6), este incremento fue estadísticamente significativo comparado con los grupos CONTROL (172.9 ± 49.9), VSAK (154.5 ± 27.37) y LPS+VSAK (446.4 ± 61.32) (Figura 23E).

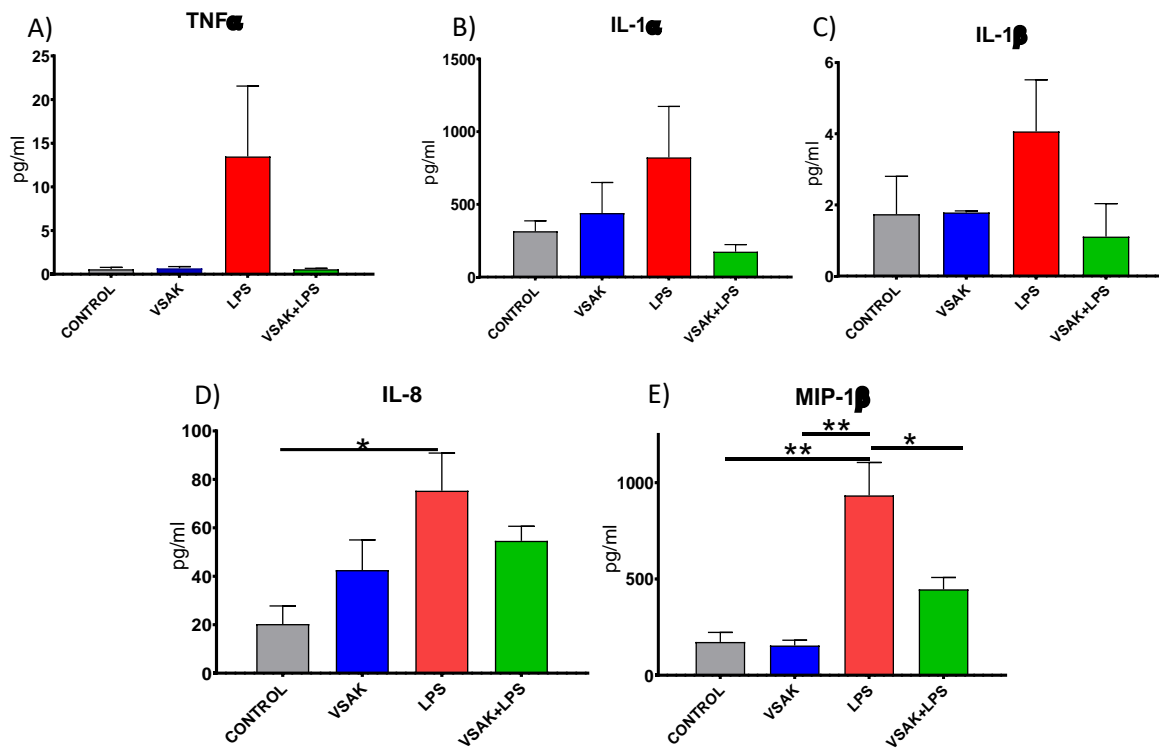


Figura 23. Marcadores pro-inflamatorios. (A) Niveles de TNF α . En este análisis no se encontraron diferencias significativas. CONTROL (0.55 ± 0.21), VSAK (0.67 ± 0.19), LPS (13.48 ± 8.063) y LPS+VSAK (0.56 ± 0.13). (B) Niveles de IL-1 α . Este análisis no indica cambios significativos. CONTROL (314.9 ± 71.65), VSAK (439 ± 210.9), LPS (823.1 ± 350.5) y LPS+VSAK (174.8 ± 48.69). (C) Niveles de IL-1 β . En este análisis no se encontraron diferencias CONTROL (1.73 ± 1.06), VSAK (1.78 ± 0.04) LPS (4.06 ± 1.45) y LPS+VSAK (1.1 ± 0.92). (D) Niveles de IL-8. En este análisis el grupo LPS (75.34 ± 15.55) mostró un nivel significativo respecto al grupo CONTROL (20.3 ± 7.44 , $p=0.03$, *), con los grupos VSAK (42.57 ± 12.44) y LPS+VSAK (54.65 ± 6.01), no hubo cambios significativos. (E) Niveles de MIP-1 β . En este análisis el grupo LPS (934.1 ± 170.6) presentó un nivel más elevado comparado con los grupos CONTROL (172.9 ± 49.9 , $p=0.002$, **), VSAK (154.5 ± 27.37 , $p=0.0018$, **) y LPS+VSAK (446.4 ± 61.32 , $p=0.027$, *). Datos presentados como promedio \pm error estándar.

8.6.5. Niveles de Glucosa e Insulina

A partir de los plasmas recuperados, se realizó el análisis de los niveles en circulación de glucosa e insulina, en los animales utilizados en los ensayos de PET.

El análisis de los niveles de Glucosa indicó que los animales del grupo LPS (191.5 ± 4.9) presentaron un nivel mayor de Glucosa en circulación en comparación con los animales de los grupos CONTROL (148.5 ± 0.86), VSAK (142 ± 4.3) y el grupo VSAK+LPS (152 ± 1.15) (Figura 24A).

Por otro lado, el análisis de Insulina indicó que el grupo LPS (5.4 ± 1.5) presentó un mayor nivel de esta molécula en comparación con lo observado en los otros grupos (CONTROL 1.5 ± 0.55 , VSAK 2.5 ± 0.8 y VSAK+LPS 3.8 ± 0.9). Sin embargo, esta diferencia no fue estadísticamente significativa (Figura 24B).

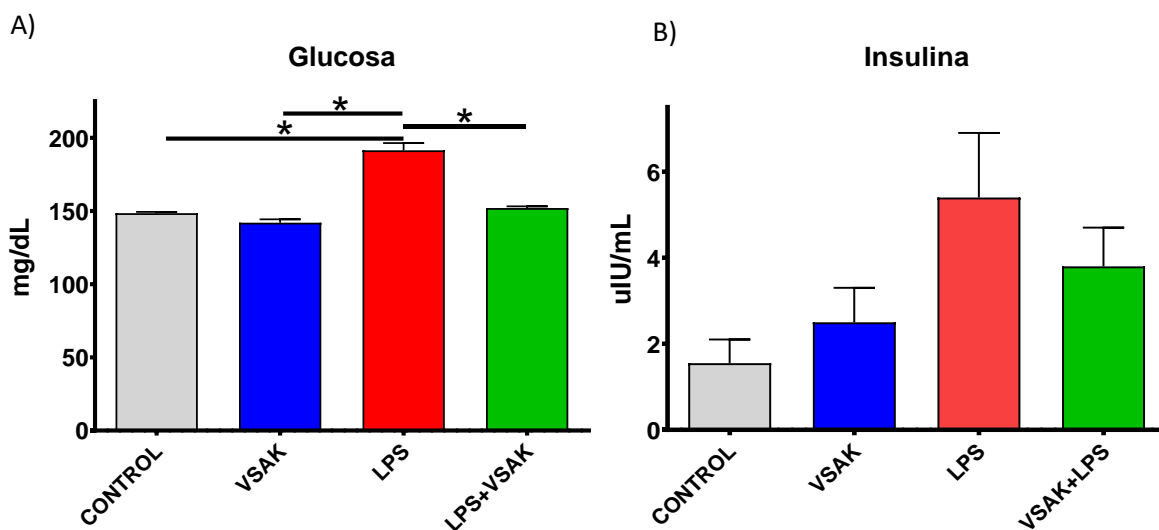


Figura 24. Niveles de insulina y glucosa en circulación. (A) Datos del nivel circulante de glucosa. Se observó un aumento en el nivel circulante en el grupo LPS (191.5 ± 4.9) con respecto al grupo CONTROL (148.5 ± 0.86 , $p=0.04$, *), VSAK (142 ± 4.3 , $p=0.016$, **) y el grupo VSAK+LPS (152 ± 1.15 , $p=0.03$, *), estos dos últimos también tuvieron valores más homogéneos en comparación. (B) Niveles de Insulina. En este análisis se puede apreciar que el nivel promedio de insulina en el grupo LPS (5.4 ± 1.5) es mayor al observado en los otros grupos (CONTROL (1.5 ± 0.55), VSAK (2.5 ± 0.8) y VSAK+LPS (3.8 ± 0.9)). Sin embargo, estos cambios no fueron estadísticamente significativos. Datos presentados como el promedio error ± estándar

9. DISCUSIÓN

En los diferentes ensayos que hemos realizado utilizando el péptido VSAK, hemos demostrado propiedades interesantes que permiten su unión a los LPS y la mitigación de los efectos producidos por los LPS.

En primera instancia, nuestros análisis *in silico* utilizando simulaciones de dinámica molecular de grano grueso nos han permitido comprender aspectos críticos de los ensayos del péptido. Uno de los efectos más notorios observados en las simulaciones al ser inspeccionadas visualmente, fue la unión selectiva de VSAK hacia los LPS. En los sistemas LPS-POPC se observa una clara preferencia de VSAK hacia la hemicapa de LPS, si bien, existen ocasiones el péptido puede hacer contacto con la membrana sin asociarse con esta, al avanzar la simulación este termina haciendo contacto con los LPS y uniéndose a esta hemicapa. Es interesante notar que el contacto de VSAK ocurre en la región superficial manteniéndose en la interfaz comprendida entre la región del núcleo y los dímeros de glucosamina del lípido A, en el tiempo de simulación utilizado no se observó que existiera una penetración de VSAK. Este comportamiento coincide con lo observado en el estudio de otros péptidos con capacidad de unión a LPS en donde inclusive a tiempo elevados de simulación (20μs) no se observa penetración en la membrana, a menos que esta se forzada por la aplicación de una fuerza dirigida (Montero Vega et al., 2022). Además, esta incapacidad de VSAK para penetrar hacia la interfaz de lípidos de la membrana, podría explicar la falta de actividad bactericida que fue observada en VSAK (García-González et al., 2015). En el caso los sistemas que estaban constituidos únicamente por fosfolípidos (POPC-POPC y POPS-POPC), en esto no se observó una incorporación del péptido VSAK en ninguna de las hemicapas. En estos sistemas también existen eventos en los que el péptido VSAK se aproxima a las hemicapas, sin embargo, estos contactos son transitorios y el péptido permanece en la interfaz del solvente durante la mayor parte de la simulación. En principio, las simulaciones aportan información sobre la capacidad de VSAK para unirse a membranas constituidas por LPS de forma selectiva, teniendo una interacción mínima con membranas constituidas por fosfolípidos, inclusive cuando estas están constituidas por fosfolípidos con carga negativa, como lo es POPS. Este

evento podría estar asociado a estructura primaria del péptido la cual presenta aminoácidos clave para la interacción con los elementos con carga negativa a nivel de la membrana, como son la lisina en posición cuatro, sin embargo, la falta de aminoácidos hidrofóbicos como triptófano limita la capacidad de interacción con la interfaz hidrofóbica del núcleo de lípidos de la membrana (Faya et al., 2019).

Por otro lado, el uso de la variante VSAK Q3 ha permitido explorar la contribución de las cargas positivas presentes en VSAK en su unión a LPS, en la estructura de VSAK la mayoría de los aminoácidos son apolares por lo que los aminoácidos con carga positiva tienen un papel relevante para la solubilidad del péptido y su afinidad por moléculas con carga negativa. En las simulaciones en las que se utilizó este péptido, se observó que este perdía la selectividad hacia los LPS pudiendo inclusive interactuar con la hemicapa compuesta de fosfolípidos (POPC). Sin embargo, esta interacción parece ser más lábil que la del péptido VSAK, debido a que en el sistema POPC-POPC el péptido VSAK Q3 se acercó de forma intermitente a la superficie de ambas hemicapas pero era posible que este regresara al solvente. Además, en los sistemas POPS-POPC se observó un acercamiento preferencial de VSAK Q3 hacia la hemicapa POPC, lo cual indica la preferencia de VSAK Q3 por lípidos electroneutros.

En estas simulaciones, el análisis de energía de los sistemas LPS-POPC indicó que la presencia del péptido produce una disminución de la energía total del sistema, en comparación con el sistema solo o el sistema POPS-POPC. Este efecto indicaría que la unión de VSAK a los LPS se ve energéticamente favorecida, lo cual no ocurre en el caso del péptido VSAK Q3. Este evento coincide con lo observado en análisis de Calorimetría de titulación isotérmica, utilizando un péptido similar a VSAK, el cual también se une a LPS. En estos ensayos se ha demostrado que esta reacción puede ocurrir de forma espontánea y esta energéticamente favorecida (datos no publicados). En el caso de los sistemas POPC, el cambio en energía es menor en comparación con lo observado con los LPS, estos cambios pueden ser atribuidos a una disminución de la entropía del solvente en el caso de VSAK y la unión de VSAK Q3 a las membranas de fosfolípidos. Los efectos observados podrían estar

asociados a una modificación en la organización de los LPS en los sitios del contacto del péptido, produciendo un estado de menor entropía que podría resultar en la reducción de energía, esto coincide con lo observado en otros péptidos que pueden inducir un cambio de fase en hemicapas de LPS (Jefferies et al., 2017). Este cambio en la estructura de los LPS, está asociado a lo observado en los análisis de difusión (MSD). En estos ensayos se observó una disminución en la difusión lateral de LPS, este efecto podría estar observado a esta transición hacia una estructura más compactada y de menor movilidad en los LPS que están contacto con el péptido VSAK. Un efecto similar ha sido observado en péptidos derivados de Polimixina B con capacidad de unión a LPS (Berglund et al., 2015; Fu et al., 2020).

Este efecto de VSAK para inducir producir perturbaciones en la estructura de los LPS fue observado mediante microscopía electrónica. En soluciones acuosas los LPS tienden a agregarse en forma de fibras cúbicas, en las que el lípido A se localiza en el centro mientras que la región del núcleo y el antígeno O se mantienen en la periferia (Castelletto et al., 2023). Este tipo de estructuras fueron claramente observadas en las micrografías de LPS en solitario, sin embargo, cuando estos eran coincubadas en presencia de VSAK, se observó la perdida de esta estructura hacia agregados, que podrían coincidir con la estructura multilaminar que producen otros HDPs y que es un evento asociado a la inhibición de la capacidad inmunoestimuladora de los LPS asociada la pérdida de la estructura típica (Brandenburg et al., 2011; Kaconis et al., 2011). En el caso de VSAK, en primera instancia se observó una disminución de los hace de fibras de LPS a la concentración de $567.7\mu\text{M}$; posteriormente al aumentar la concentración de VSAK (1.12mM), se observó la disminución de la densidad de las fibras de LPS y la aparición de estructuras micelares. En la concentración más alta de VSAK utilizada en nuestros ensayos (2.25mM), hubo una pérdida de la mayor parte de las fibras de LPS y la desaparición de los agregados micelares; además, en estos ensayos se observó la aparición de agregados amorfos de gran tamaño, estos podrían coincidir con agregados multilaminares de LPS (Hong et al., 2022).

Las simulaciones de dinámica molecular han aportado información relevante acerca de la capacidad de VSAK para interactuar con los LPS, especialmente en la importancia de las cargas positivas del péptido para esta interacción. Esto da indicios de la importancia de la estructura primaria de VSAK para esta interacción, la cual favorece al mismo tiempo la selectividad de VSAK hacia lípidos con cargas negativas importantes y la estabilización de la interacción con estas moléculas. En este sentido, el uso de simulaciones puede ser una herramienta muy útil para el estudio y desarrollo de HDPs y otros péptidos bioactivos. Por lo que la implementación de simulaciones atomísticas, acoplamiento molecular y muestreo computacional para posteriores estudios del mecanismo de interacción de VSAK con los LPS (Nicholas et al., 2021; Suzuki et al., 2010).

Otro de los aspectos que se han abordado para analizar los efectos de VSAK han sido sus efectos a nivel celular. En primera instancia estos sistemas se han utilizado para estudiar la inocuidad del tratamiento con el péptido VSAK, para descartar posibles efectos citotóxicos que pueden observarse en péptidos con capacidad de interactuar con membranas (Bhandari et al., 2020; Kumar et al., 2018). En este sentido se evaluó el efecto hemolítico y citotóxico de VSAK en un intervalo de concentraciones muy superiores a la que se ha establecido como terapéutica en otros ensayos celulares o la que es utilizada para administraciones en modelos animales. En los ensayos de hemólisis utilizando eritrocitos frescos, no se observó un efecto hemolítico asociado al péptido VSAK en el intervalo de concentraciones utilizadas (10-500 µg/ml), e inclusive el péptido VSAK es capaz de reducir el efecto hemolítico producido por altas concentraciones de LPS (Brauckmann et al., 2016). Las concentraciones de LPS necesarias para inducir hemólisis son demasiado elevadas en comparación con lo que se observa de manera normal durante una infección, por lo que el efecto hemolítico de los LPS no es un evento que ocurre de manera normal en el curso de una infección, en donde las concentraciones de LPS en circulación alcanzan unos cuantos nanogramos por kilogramo; aun así, siendo suficientes para inducir una respuesta sistémica severa (Dinges & Schlievert, 2001). Esta disminución del efecto hemolítico de los LPS respalda el hecho en el que la unión de VSAK a los LPS forma complejos LPS-VSAK con menor actividad, esto

coincidiría con la formación de agregados de LPS-VSAK observada en los ensayos de microscopia electrónica los cuales tendrían propiedades distintas a los agregados de LPS y presentarían una capacidad disminuida para interactuar con las membranas de los eritrocitos. Este evento coincide con la alteración de las propiedades típicas de los LPS al cambiar la estructura de los agregados.(Dijkstra et al., 1988).

En los ensayos de citotoxicidad con VSAK utilizamos dos líneas celulares que fueron sometidas a curvas dosis respuesta en concentraciones crecientes de VSAK. Como comparación utilizamos una curva con un detergente, considerando el efecto similar a detergente que tienen algunos péptidos antimicrobianos (Bechinger & Lohner, 2006). En estos ensayos no se encontró un efecto citotóxico que pudiera ser asociado con el péptido VSAK, inclusive a concentraciones muy elevadas del péptido VSAK. Estos resultados son un buen indicador del péptido VSAK, debido a que los efectos citotóxicos de los HDPs son unos de aspectos críticos en el desarrollo de estas moléculas (Bacalum & Radu, 2015).

En lo que respecta a los aspectos celulares del péptido VSAK sobre el desarrollo de la respuesta a LPS, se optó por el estudio del efecto de este tratamiento en dos líneas celulares: las células HAEC y las células THP-1. Estas células fueron estimuladas con LPS para analizar cambios en la expresión de marcadores proinflamatorios, moléculas de adhesión e indicadores de la disfunción endotelial. La elección de la línea THP-1 se basó en el fenotipo de estas células, el cual es similar al de las células mononucleares de sangre periférica y la capacidad que estas presentan para responder a la estimulación con LPS (Chanput et al., 2014).

En las células HAEC el protocolo de estimulación se realizó con LPS (4 µg/ml), se observaron cambios mínimos en la expresión de marcadores proinflamatorios como lo son IL-6 e IL-1 β , si bien estos fueron mayores en células estimuladas con LPS y LPS+VSAK, el nivel de expresión fue ligeramente mayor al de los controles y sin relevancia estadística. Los mayores cambios observados en esta línea celular fueron observados en el Factor III (factor tisular) e ICAM-1. Estos resultados son relevantes dado el papel de estas moléculas en el desarrollo de la respuesta

sistémica y el desarrollo del daño orgánico en sepsis y choque séptico. ICAM-1 es una molécula de adhesión que está relacionada a la infiltración de leucocitos hacia los tejidos. Sin embargo, la infiltración excesiva de estas células y la activación posterior, está asociada al daño tisular resultando en alteraciones que conducen al daño orgánico (Hildebrand et al., 2005). La expresión de esta molécula está regulada por MAMPS y citocinas proinflamatorias, por lo que el efecto de VSAK para disminuir a la expresión de esta molécula estaría asociado a su capacidad de unión a LPS y la estimulación producida por estas moléculas (Shi et al., 2010). En el caso de Factor III, esta molécula está implicada en la cascada de coagulación, teniendo un papel clave en el desarrollo de este proceso. Durante la sepsis, esta proteína está asociada al desarrollo del estado protrombótico por el procesamiento excesivo de fibrinógeno, además se ha asociado la actividad de esta molécula para favorecer la respuesta inflamatoria (Mackman, 2009). En este sentido, VSAK produjo una reducción muy importante en la expresión de esta molécula en células estimuladas con LPS y VSAK, esta inhibición es especialmente relevante debido a que las células endoteliales son una de las principales fuentes de Factor III, por lo que el endotelio tiene un papel critico en el desarrollo de la respuesta sistémica (Pawlinski & Mackman, 2010).

En los análisis realizados en las células THP-1, observamos un efecto similar de VSAK al atenuar los cambios en la expresión producidos por los LPS. En el análisis de IL-1 β se observó una disminución de la expresión de esta molécula cuando las células fueron tratadas con VSAK. Un efecto muy similar fue observado en la expresión de IL-6, en donde la expresión se vio reducida en células estimuladas con LPS y tratadas con VSAK. El papel de estas citocinas es muy relevante en la respuesta inicial, lo cual es un indicador de la capacidad de VSAK para mitigar el desarrollo de la respuesta temprana a los LPS (Waage et al., 1993). Los cambios en el receptor TLR-4 siguieron el patrón observado en IL-6 y IL-1 β , aunque la expresión total fue menor a la observada en estas dos moléculas analizadas previamente.

En estos análisis se utilizó NEO-3 como control positivo, esta molécula es un agonista selectivo de TLR-4 el cual no tiene estructuras similares a lípidos o cargas negativas (Wang et al., 2016). Con este tratamiento se buscaba evaluar la dependencia de la unión LPS por parte de VSAK para la mitigación de la expresión de la respuesta inflamatoria. En los ensayos en los que se utilizó NEO-3 se observó una respuesta mayor a la observada con el tratamiento con LPS, lo cual coincide con el potente efecto agonista de esta molécula para promover la activación de receptor TLR-4 (Wang et al., 2017). Sin embargo, el tratamiento combinado NEO-3 y el péptido VSAK presentó una disminución importante en la expresión de IL-16 e TLR-4, lo mismo ocurrió con IL-6 aunque el efecto general fue menor al observado en los otros dos marcadores. Este resultado es especialmente relevante, ya que podría indicar un papel regulador de VSAK sobre el desarrollo de la respuesta inflamatoria que no dependería de la capacidad de unión a LPS; esta podría estar dada por una posible interacción de VSAK con NEO-3 o con algún factor implicado en la respuesta inflamatoria. Este efecto de VSAK coincide con lo observado en nuestros últimos datos que hemos obtenido sobre el carboxilo de CETP, en donde el carboxilo de esta proteína tiene un efecto en la regulación de genes asociados al desarrollo de fibrosis; por lo que es posible que VSAK pudiera tener efectos similares, pudiendo regular cambios en la expresión de genes asociados al proceso inflamatorio. Este efecto parece plausible en el contexto de VSAK fungiendo como un HDP, ya que algunos de estos péptidos pueden presentar capacidades inmunoreguladoras directas (Choi et al., 2012; Hilchie et al., 2013; Mansour et al., 2014).

Adicionalmente, la estimulación con las LPS en las células THP-1 produjo un incremento en la expresión de esta molécula, la cual se vio atenuada por el tratamiento con VSAK (LPS+VSAK). Este aspecto coincide con lo observado anteriormente en las células HAEC y tiene implicaciones similares, asociadas al reclutamiento e infiltración de células inmunes. En monocitos y las células THP-1 se ha descrito que la expresión ICAM-1 está asociada a la polarización hacia un fenotipo inflamatorio, estando relacionado a la activación de NF-κB mediada por estimulación con LPS o TNF α (Wissink et al., 1997). Además, en estas células la

expresión de ICAM-1 está asociada con una mejor adhesión y un incremento de la capacidad fagocítica (Edwards & Thomas, 2017; Zhong et al., 2021).

Este efecto sobre ICAM-1 puede asociarse con los observado en la expresión de las sintetasas de óxido nítrico: NOS2 y NOS3. Estas moléculas están involucradas en la eliminación de patógenos a través de la generación de especies reactivas de nitrógeno, además, los efectos vasoactivos del óxido nítrico están asociados con el establecimiento de una vasodilatación sistémica observada en sepsis y choque séptico (Fernandes & Assreuy, 2008). En nuestros ensayos la estimulación con LPS produjo un incremento muy notable en la expresión de ambas sintetasas, mientras que las células que fueron tratadas con LPS+VSAK hubo una disminución muy importante en la expresión de ambas moléculas. Lo cual estaría asociado a una disminución en la generación de óxido nítrico y una disminución de la producción de radicales de nitrógeno. Por otro lado, los cambios en la expresión de NOS3 son especialmente llamativos, la expresión de esta sintasa en monocitos está asociada una producción de alta de óxido nítrico y un incremento de la producción de citocinas proinflamatorias; principalmente TNF α , la cual tiene un papel central en la respuesta temprana y el desarrollo de la respuesta sistemica (Connelly et al., 2003; Mühl & Pfeilschifter, 2003). En último lugar se analizó la expresión de IL-10, una citocina antinflamatoria. En nuestro análisis el nivel de esta citocina fue más elevado en el grupo LPS en comparación con VSAK, sin embargo, la expresión de esta molécula fue casi idéntica en el grupo LPS+VSAK. Esto puede indicar que la atenuación de los efectos de LPS no afecta los mecanismos de regulación de este marcador antinflamatorio, sin embargo, es necesario explorar más a fondo los efectos de VSAK sobre el proceso antinflamatorio (Azuma & Ohura, 2002).

Los efectos observados a nivel celular indican que VSAK es capaz de reducir el proceso inflamatorio asociado a la estimulación con LPS. Este efecto se pudo observar en distintos tipos celulares en los que VSAK demostró efectos particulares sobre distintos mediadores de la respuesta a LPS. Es necesario que en futuros proyectos se caracterice con mayor profundidad los efectos de VSAK sobre esta respuesta. Esto resulta especialmente importante debido al efecto observado en los

tratamientos con NEO-3 en las células THP-1, el cual es un indicador de una posible función reguladora de VSAK que no depende de la interacción con LPS y cuyo mecanismo es desconocido hasta el momento.

El último aspecto explorado durante este proyecto, fue la capacidad de VSAK para atenuar los efectos de LPS en un modelo animal de inflamación sistémica inducido por la administración intravenosa de LPS (García-González et al., 2015). En estos ensayos utilizamos PET para analizar a nivel sistémico los cambios en la captación de [¹⁸F] FDG, esta molécula es un análogo de la glucosa que puede ser utilizada como indicador de la actividad metabólica. Esta molécula es ampliamente utilizada en la detección de tumores, debido a la actividad metabólica de las células cancerosas. Sin embargo, el uso de estas técnicas también puede ser útil en la detección de focos de infección con infiltración de células inmunes o la disfunción metabólica observada en la sepsis (Gotthardt et al., 2010; Kluge et al., 2012; Sugawara et al., 1999).

En nuestros ensayos el grupo LPS se utilizó para recrear las condiciones de inflamación sistémica por lo que esperábamos que este presentara alteraciones en el patrón de captación de [¹⁸F] FDG. En los animales de este grupo el tratamiento con LPS produjo una disminución generalizada de la captación del radiotrazador y un incremento aparente de la captación en los riñones. Sin embargo, en los animales tratados con LPS y VSAK se atenuó este efecto, por lo que se observó un patrón de captación similar al del grupo CONTROL. Por otro lado, en estos análisis se observó que el tratamiento en solitario con VSAK no produjo cambios en el patrón de captación del radiofármaco.

Estos efectos coinciden con lo observado en el análisis cuantitativo del PET, si bien el análisis de %ID/cc y SUV del hígado e intestino, no indicó una diferencias importantes o tendencias características para los grupos. El análisis de %ID/cc y SUV en los riñones respaldo el efecto observado en la inspección visual de los datos. El %ID/cc indicó un claro incremento en la captación de glucosa en el riñón derecho de los animales del grupo LPS en comparación con los otros tres grupos, mientras que este mismo patrón fue observado en el riñón izquierdo sin que esta

diferencia fuera tan pronunciada. El análisis de SUV total fue congruente con los observado en el %ID/cc, en donde el grupo LPS presento una mayor captación renal, aunque las diferencias entre grupos fueron menos marcadas debido al incremento de la variación observada en este análisis. En este análisis, el tratamiento con LPS y VSAK (LPS+VSAK) presento niveles de captación menores a los del grupo LPS, tanto a nivel de %ID/cc como de SUV total. Este efecto sobre el SUV renal pudo ser observado con mayor claridad en el análisis de SUV en función del tiempo, en estos análisis se observó que el SUV de los animales del grupo LPS es considerablemente más elevado a partir de los 70 minutos. Esta diferencia se hace mayor conforme avanza el tiempo y se mantuvo hasta el final de la captura. Al igual que en los análisis de %ID/cc y SUV total, el tratamiento con el péptido VSAK en el grupo LPS+VSAK disminuyo el valor de capación, siendo más similar al observado en los grupos CONTROL y VSAK.

En conjunto, los análisis de PET indican que la administración de LPS produce un patrón alterado en la captación de [¹⁸F]-FDG, el cual podría estar relacionado con la disfunción metabólica que se produce en la respuesta durante el establecimiento de sepsis y choque séptico. Por lo que el patrón de captación observado en el grupo LPS podría asociarse a un incremento en la recaptura de [¹⁸F]-FDG en los riñones debido a que este no puede ser capturada en los tejidos periféricos (Mather & Pollock, 2011). Durante la sepsis y choque séptico esta disfunción metabólica está asociada al desarrollo del proceso inflamatorio en respuesta a la infección (Preau et al., 2021; Wasyluk & Zwolak, 2021).

Este efecto se relaciona con los efectos observados en la producción de marcadores de inflamación en los grupos experimentales. En estos análisis los animales del grupo LPS presentaron niveles elevados de TNF α , una de las principales citocinas proinflamatorias relacionadas al desarrollo de la respuesta sistémica inducida por LPS (Kothari et al., 2013), si bien el análisis estadístico no indicó diferencias con los grupos VSAK y VSAK+LPS debido a la variación observad dentro del grupo LPS, es resaltable el hecho de en estos grupos el nivel de esta citocina fue apenas detectable en comparación a lo observado con el grupo LPS. Además, es notable el

efecto del tratamiento con VSAK en el grupo LPS+VSAK, ya que este disminuye el nivel de TNF α a un valor cercano al de los grupos CONTROL y VSAK. Un efecto similar fue observado en los análisis de IL-1 α e IL-1 β , en donde el grupo LPS presentó mayores niveles de ambas citocinas. En estas moléculas el péptido VSAK también produjo una disminución en el nivel de estas citocinas al ser administrado en conjunto con LPS. Este efecto es relevante debido al papel que tienen estas citocinas en el desarrollo inicial de la respuesta inflamatoria, pudiendo indicar un posible papel regulador de VSAK en el inicio de la respuesta sistémica *in vivo* (Garlanda et al., 2013).

Los efectos más notables de VSAK sobre los marcadores de inflamación fueron observados sobre las quimiocinas IL-8 y MIP-1 β , estas citocinas están involucradas en el proceso de migración celular. Estas moléculas favorecen el reclutamiento de neutrófilos y monocitos hacia los sitios de infección, este proceso favorece la amplificación de la respuesta proinflamatoria ante la infección la cual está asociada al desarrollo de la respuesta sistémica en el anfitrión (Adams et al., 2001; Menten et al., 2002; Russo et al., 2014).

En nuestro análisis, IL8 y MIP-1 β mostraron un incremento notable en los animales que fueron tratados con LPS, este incremento fue menor en los animales tratados con LPS+VSAK. Este efecto fue especialmente notable en el caso de MIP-1 β donde la atenuación en la producción de esta citocina por el tratamiento con VSAK fue especialmente relevante (grupo LPS+VSAK).

En conjunto el análisis de los marcadores proinflamatorios indica que VSAK es capaz de disminuir la producción de estas moléculas inducida por los LPS. Esto es especialmente relevante, dado el papel que tienen estas moléculas en la respuesta sistémica y el subsecuente disfunción tisular y orgánica (Cavaillon et al., 2003; Devi Ramnath et al., 2006; López-Bojórquez et al., 2004). Es interesante notar que en este modelo el tratamiento con VSAK tuvo un efecto mitigador de la respuesta inmune, lo cual representan una ventaja en comparación con otros tratamientos en los que el uso de moléculas destinadas a inhibir la función de algún componente involucrado en la respuesta inmune terminan funcionando como inmunosupresores

y generando efectos deletéreos adicionales a los del proceso infeccioso, como lo ha sido el uso de anticuerpos para algunas citocinas (Cohen & Carlet, 1996).

En base a los cambios observados en la expresión de marcadores proinflamatorios, se consideró la posibilidad de que la respuesta inflamatoria estuviera asociada a los cambios en el patrón de captación observado en los animales del grupo LPS. En este sentido se realizó el análisis de glucosa e insulina en las muestras recuperadas. Este análisis indicó que en el grupo LPS el nivel de Glucosa en circulación fue mayor al de los otros tres grupos (CONTROL, VSAK, LPS+VSAK). Además, el análisis de insulina indicó que los animales del grupo LPS presentaron un mayor nivel de esta molécula en circulación en comparación, mientras que el tratamiento con VSAK disminuyó ligeramente el nivel de esta molécula en el grupo LPS+VSAK.

Al considerar la expresión de moléculas proinflamatorios junto con el patrón de distribución y los cambios en Glucosa e Insulina, se planteó la posibilidad de que la disfunción metabólica producida por los LPS estuviera produciendo un estado similar a la resistencia a la insulina (Carlson, 2003; Clemens et al., 1984; Clowes et al., 1978). Este efecto ha sido observado en otros ensayos en los que la respuesta inflamatoria se asocia a una insensibilización a los efectos de la insulina y es considerada un indicador negativo para el pronóstico de los individuos (Marik & Raghavan, 2004; Schetz et al., 2008). Este fenómeno está relacionado a la actividad de citocinas como TNF α , cuya activación está asociada a eventos que inducen una insensibilización a los efectos de la Insulina al alterar el mecanismo de señalización normal (Lassenius et al., 2011; Mehta et al., 2010; Nieto-Vazquez et al., 2008). Por tanto, la diminución del proceso inflamatorio producida por el tratamiento combinado con LPS y VSAK estaría asociada a una mitigación de las alteraciones que dan lugar del patrón de captación de [^{18}F]-FDG producido por los LPS. Indicando que VSAK para atenuar las alteraciones metabólicas producidas por los LPS *in vivo*.

En conjunto, los diferentes sistemas que hemos utilizado para entender los efectos del péptido VSAK indican que este péptido tiene una importante capacidad para mitigar los efectos de los LPS. Esta capacidad estaría dada por la capacidad de VSAK para unirse a los LPS con una alta afinidad y avidez. Esta unión a los LPS

produce una alteración de la estructura típica de estas moléculas, lo cual conllevaría a la formación de agregados de VSAK-LPS con una actividad reducida. Este efecto coincide con lo reportado por otros grupos, en los que cambios en la organización de los LPS conducen a la formación de agregados con capacidad estimulatoria reducida (Mueller et al., 2004). Esta capacidad de VSAK se mantendría en circulación, lo cual favorecería una diminución de la respuesta inflamatoria que se produce ante los LPS y otros efectos a nivel celular y tisular, como la disfunción metabólica observada en estas patologías. Adicionalmente, es posible que VSAK tenga propiedades aun no descritas que puedan tener un efecto sobre el proceso inflamatorio, las cuales serían independientes a la unión de LPS

Las propiedades observadas en VSAK hacen que sea un péptido con características prometedoras para la generación de tratamientos adyuvantes que puedan ser utilizados en conjunto con las estrategias tradicionales para prevenir el desarrollo de sepsis y choque séptico (Bárcena-Varela et al., 2017). Sin embargo, es necesario ampliar el repertorio de ensayos con el objetivo de entender a mayor profundidad los mecanismos moleculares de VSAK y los efectos de tratamiento. No obstante, durante el desarrollo de este proyecto se ha aportado valiosa información sobre las capacidades de VSAK y su potencial como molécula terapéutica (Luna-Reyes et al., 2021).

10. CONCLUSIONES

El péptido VSAK es capaz de unir a los LPS con una alta selectividad, la cual estaría dada por las cargas presentes en el péptido y prevendría la interacción de VSAK con lípidos neutrales, como los fosfolípidos presentes en las células eucariotas. Además, esta unión estaría estabilizada por la presencia de aminoácidos hidrofóbicos en VSAK, permitiendo la formación de un complejo estable de VSAK-LPS.

La unión de VSAK altera el patrón normal de agregación de los LPS, favoreciendo la formación de agregados micelares de menor tamaño. Estos agregados perderían propiedades típicas de los LPS, como su capacidad de desestabilizar las membranas de eritrocitos para inducir la lisis de estos.

A nivel celular, el tratamiento con VSAK no presenta efectos citotóxicos inclusive a concentraciones elevadas del péptido. Sin embargo, los ensayos con NEO-3 indican que VSAK puede tener efectos a nivel celular que deben ser estudiados en futuros proyectos.

En las células THP-1 y en las células HAEC, VSAK tuvo un efecto mitigador de los efectos producidos por los LPS, el cual se vio reflejado en la disminución generalizada de la expresión de los marcadores de inflamación analizados en estas células.

Mediante el uso de PET fue posible analizar la respuesta sistémica a los LPS en un modelo animal. En estos ensayos se observó un patrón de captación característico de la respuesta sistémica a LPS el cual pudo ser atenuado por el tratamiento con VSAK. En adición a los efectos observados mediante PET, *in vivo* el péptido VSAK atenuó la producción de marcadores proinflamatorios inducidos por los LPS, además de mitigar los cambios asociados a la disfunción metabólica que ocurre durante la respuesta sistémica.

Los efectos observados con el tratamiento con el péptido VSAK para mitigar la respuesta a los LPS, son un buen indicador del potencial de VSAK para ser utilizado durante el desarrollo de la respuesta inflamatoria sistémica durante una infección, y con ello prevenir la progresión hacia sepsis y choque séptico.

11. PERSPECTIVAS.

Durante el desarrollo de este proyecto se ha obtenido información muy importante sobre la interacción de VSAK a los LPS, no obstante, aún es necesario entender a mayor detalle como ocurre esta unión. En este aspecto, el uso de herramientas de biología computacional puede resultar especialmente útil para facilitar la exploración de estas propiedades. El uso de técnicas como la dinámica molecular y el acoplamiento pueden hacer más eficiente el desarrollo de estos análisis. Además, la incorporación de técnicas aún más novedosas como el uso de inteligencia artificial para realizar muestreos extensivos utilizando modelos moleculares, son opciones interesantes para desarrollar este aspecto de la investigación. Adicionalmente, hemos comenzado con la implementación de ensayos de calorimetría para, en conjunto con los ensayos de dinámica molecular y el uso de microscopía electrónica, determinar las características fisicoquímicas de la unión de VSAK a los LPS y los efectos que esto produce sobre la estructura de los LPS. En conjunto, es posible combinar el uso de estas metodologías para estudio y optimización de las propiedades del péptido VSAK.

A nivel celular, es necesario profundizar en los efectos del péptido VSAK, especialmente en tipos celulares relacionados con la respuesta inmune. En este sentido es necesario ampliar el análisis de marcadores de inflamación, para abarcar aspectos como el reclutamiento de leucocitos y el proceso antinflamatorio. Además de que será necesario explorar la producción de estas moléculas, más allá de la expresión, considerando los aspectos de regulación postranscripcional.

Otro aspecto relevante es la incorporación de nuevos modelos animales, la sepsis y el choque séptico son patologías exquisitamente complejas por lo que es necesario utilizar modelos que reproduzcan aspectos particulares de estos estados y en los cuales se puedan analizar los efectos terapéuticos de VSAK.

Entender a detalle los efectos de VSAK, permitirá plantear el uso de este péptido en ensayos clínicos en los cuales se pueda evaluar cómo la capacidad de VSAK para unir LPS puede tener un papel relevante durante el tratamiento de infecciones para prevenir el desarrollo de sepsis y choque séptico.

12. BIBLIOGRAFÍA

- Adams, J. M., Hauser, C. J., Livingston, D. H., Lavery, R. F., Fekete, Z., & Deitch, E. A. (2001). Early trauma polymorphonuclear neutrophil responses to chemokines are associated with development of sepsis, pneumonia, and organ failure. *The Journal of Trauma*, 51(3), 452–456; discussion 456-7. <http://www.ncbi.nlm.nih.gov/pubmed/11535890>
- Akira, S., & Hoshino, K. (2003). Myeloid Differentiation Factor 88—Dependent and —Independent Pathways in Toll-Like Receptor Signaling. *The Journal of Infectious Diseases*, 187(Supplement_2), S356-63. <https://doi.org/10.1086/374749>
- Alonso-Garcia, A. L., Zentella-Dehesa, A., & Mas-Oliva, J. (2003). Characterization of a naturally occurring new version of the cholesterol ester transfer protein (CETP) from small intestine. *Molecular and Cellular Biochemistry*, 245(1–2), 173–182. <http://www.ncbi.nlm.nih.gov/pubmed/12708757>
- Angus, D. C., & van der Poll, T. (2013). Severe Sepsis and Septic Shock. *New England Journal of Medicine*, 369(9), 840–851. <https://doi.org/10.1056/NEJMra1208623>
- Azuma, Y., & Ohura, K. (2002). Endomorphins 1 and 2 Inhibit IL-10 and IL-12 Production and Innate Immune Functions, and Potentiate NF-κB DNA Binding in THP-1 Differentiated to Macrophage-Like Cells. *Scandinavian Journal of Immunology*, 56(3), 260–269. <https://doi.org/https://doi.org/10.1046/j.1365-3083.2002.01128.x>
- Bacalum, M., & Radu, M. (2015). Cationic Antimicrobial Peptides Cytotoxicity on Mammalian Cells: An Analysis Using Therapeutic Index Integrative Concept. *International Journal of Peptide Research and Therapeutics*, 21(1), 47–55. <https://doi.org/10.1007/s10989-014-9430-z>
- Bárcena-Varela, S., Martínez-de-Tejada, G., Martin, L., Schuerholz, T., Gil-Royo, A. G., Fukuoka, S., Goldmann, T., Droemann, D., Correa, W., Gutsmann, T., Brandenburg, K., & Heinbockel, L. (2017). Coupling killing to neutralization:

combined therapy with ceftriaxone/Pep19-2.5 counteracts sepsis in rabbits. Experimental & Molecular Medicine, 49(6), e345. <https://doi.org/10.1038/emm.2017.75>

Bassetti, M., Merelli, M., Temperoni, C., & Astilean, A. (2013). New antibiotics for bad bugs: Where are we? In Annals of Clinical Microbiology and Antimicrobials (Vol. 12, Issue 1, pp. 1–15). BioMed Central. <https://doi.org/10.1186/1476-0711-12-22>

Beamer, L. J., Carroll, S. F., & Eisenberg, D. (1997). Crystal structure of human BPI and two bound phospholipids at 2.4 angstrom resolution. Science (New York, N.Y.), 276(5320), 1861–1864. <http://www.ncbi.nlm.nih.gov/pubmed/9188532>

Bechinger, B., & Lohner, K. (2006). Detergent-like actions of linear amphipathic cationic antimicrobial peptides. Biochimica et Biophysica Acta (BBA) - Biomembranes, 1758(9), 1529–1539. <https://doi.org/https://doi.org/10.1016/j.bbamem.2006.07.001>

Berglund, N. A., Piggot, T. J., Jefferies, D., Sessions, R. B., Bond, P. J., & Khalid, S. (2015). Interaction of the Antimicrobial Peptide Polymyxin B1 with Both Membranes of *E. coli*: A Molecular Dynamics Study. PLOS Computational Biology, 11(4), e1004180-. <https://doi.org/10.1371/journal.pcbi.1004180>

Beutler, B., & Rietschel, E. Th. (2003). Innate immune sensing and its roots: the story of endotoxin. Nature Reviews Immunology, 3(2), 169–176. <https://doi.org/10.1038/nri1004>

Bhandari, D., Rafiq, S., Gat, Y., Gat, P., Waghmare, R., & Kumar, V. (2020). A Review on Bioactive Peptides: Physiological Functions, Bioavailability and Safety. In International Journal of Peptide Research and Therapeutics (Vol. 26, Issue 1, pp. 139–150). Springer. <https://doi.org/10.1007/s10989-019-09823-5>

Bingle, C. D., & Craven, C. J. (2002). PLUNC: A novel family of candidate host defence proteins expressed in the upper airways and nasopharynx. Human Molecular Genetics, 11(8), 937–943. <https://doi.org/10.1093/hmg/11.8.937>

Bingle, C. D., & Craven, C. J. (2004). Meet the relatives: a family of BPI- and LBP-related proteins. *Trends in Immunology*, 25(2), 53–55. <https://doi.org/10.1016/J.IT.2003.11.007>

Brandenburg, K., Andrä, J., Garidel, P., & Gutsmann, T. (2011). Peptide-based treatment of sepsis. *Applied Microbiology and Biotechnology*, 90(3), 799–808. <https://doi.org/10.1007/s00253-011-3185-7>

Brauckmann, S., Effenberger-Neidnicht, K., de Groot, H., Nagel, M., Mayer, C., Peters, J., & Hartmann, M. (2016). Lipopolysaccharide-induced hemolysis: Evidence for direct membrane interactions. *Scientific Reports*, 6(1), 35508. <https://doi.org/10.1038/srep35508>

Cao, C., Yu, M., & Chai, Y. (2019). Pathological alteration and therapeutic implications of sepsis-induced immune cell apoptosis. *Cell Death & Disease*, 10(10), 782. <https://doi.org/10.1038/s41419-019-2015-1>

Carlson, G. L. (2003). Insulin resistance in sepsis. *British Journal of Surgery*, 90(3), 259–260. <https://doi.org/10.1002/bjs.4081>

Castelletto, V., Seitsonen, J., & Hamley, I. W. (2023). Effect of Glycosylation on Self-Assembly of Lipid A Lipopolysaccharides in Aqueous Solutions. *Langmuir*, 39(24), 8516–8522. <https://doi.org/10.1021/acs.langmuir.3c00828>

Cavaillon, J., Adib-conquy, M., Fitting, C., Adrie, C., & Payen, D. (2003). Cytokine Cascade in Sepsis. *Scandinavian Journal of Infectious Diseases*, 35(9), 535–544. <https://doi.org/10.1080/00365540310015935>

Cecconi, M., Evans, L., Levy, M., & Rhodes, A. (2018). Sepsis and septic shock. *The Lancet*, 392(10141), 75–87. [https://doi.org/10.1016/S0140-6736\(18\)30696-2](https://doi.org/10.1016/S0140-6736(18)30696-2)

Chanput, W., Mes, J. J., & Wichers, H. J. (2014). THP-1 cell line: An in vitro cell model for immune modulation approach. *International Immunopharmacology*, 23(1), 37–45. <https://doi.org/https://doi.org/10.1016/j.intimp.2014.08.002>

- Choi, H. W., & Klessig, D. F. (2016). DAMPs, MAMPs, and NAMPs in plant innate immunity. *BMC Plant Biology*, 16(1), 232. <https://doi.org/10.1186/s12870-016-0921-2>
- Choi, K.-Y., Chow, L. N. Y., & Mookherjee, N. (2012). Cationic Host Defence Peptides: Multifaceted Role in Immune Modulation and Inflammation. *Journal of Innate Immunity*, 4(4), 361–370. <https://doi.org/10.1159/000336630>
- Clark, R. W., Cunningham, D., Cong, Y., Subashi, T. A., Tkalcevic, G. T., Lloyd, D. B., Boyd, J. G., Chrunyk, B. A., Karam, G. A., Qiu, X., Wang, I.-K., & Francone, O. L. (2010). Assessment of cholesteryl ester transfer protein inhibitors for interaction with proteins involved in the immune response to infection [S]. *Journal of Lipid Research*, 51(5), 967–974. <https://doi.org/10.1194/jlr.M002295>
- Clemens, M. G., Chaudry, I. H., Daigneau, N., & Baue, A. E. (1984). Insulin resistance and depressed gluconeogenic capability during early hyperglycemic sepsis. *The Journal of Trauma*, 24(8), 701–708. <http://www.ncbi.nlm.nih.gov/pubmed/6381745>
- Clowes, G. H. A., Martin, H., Walji, S., Hirsch, E., Gazitua, R., & Goodfellow, R. (1978). Blood insulin responses to blood glucose levels in high output sepsis and septic shock. *The American Journal of Surgery*, 135(4), 577–583. [https://doi.org/10.1016/0002-9610\(78\)90040-5](https://doi.org/10.1016/0002-9610(78)90040-5)
- Cohen, J., & Carlet, J. (1996). INTERSEPT: an international, multicenter, placebo-controlled trial of monoclonal antibody to human tumor necrosis factor-alpha in patients with sepsis. International Sepsis Trial Study Group. *Critical Care Medicine*, 24(9), 1431–1440. <http://www.ncbi.nlm.nih.gov/pubmed/8797612>
- Connelly, L., Jacobs, A. T., Palacios-Callender, M., Moncada, S., & Hobbs, A. J. (2003). Macrophage Endothelial Nitric-oxide Synthase Autoregulates Cellular Activation and Pro-inflammatory Protein Expression *. *Journal of Biological Chemistry*, 278(29), 26480–26487. <https://doi.org/10.1074/jbc.M302238200>
- de Groot, G. J., Klerkx, A. H. E. M., Stroes, E. S. G., Stalenhoef, A. F. H., Kastelein, J. J. P., & Kuivenhoven, J. A. (2004). A review of CETP and its relation to

atherosclerosis. *Journal of Lipid Research*, 45(11), 1967–1974.
<https://doi.org/10.1194/jlr.R400007-JLR200>

Delano, M. J., & Ward, P. A. (2016). The immune system's role in sepsis progression, resolution, and long-term outcome. *Immunological Reviews*, 274(1), 330–353.
<https://doi.org/10.1111/imr.12499>

Devi Ramnath, R., Weing, S., He, M., Sun, J., Zhang, H., Singh Bawa, M., & Bhatia, M. (2006). Inflammatory mediators in sepsis: Cytokines, chemokines, adhesion molecules and gases. *Journal of Organ Dysfunction*, 2(2), 80–92.
<https://doi.org/10.1080/17471060500435662>

Dijkstra, J., Lerrick, J. W., Ryan, J. L., & Szoka, F. C. (1988). Incorporation of LPS in Liposomes Diminishes Its Ability to Induce Tumoricidal Activity and Tumor Necrosis Factor Secretion in Murine Macrophages. *Journal of Leukocyte Biology*, 43(5), 436–444. <https://doi.org/10.1002/jlb.43.5.436>

Dinges, M. M., & Schlievert, P. M. (2001). Comparative Analysis of Lipopolysaccharide-Induced Tumor Necrosis Factor Alpha Activity in Serum and Lethality in Mice and Rabbits Pretreated with the Staphylococcal Superantigen Toxic Shock Syndrome Toxin 1. *Infection and Immunity*, 69(11), 7169–7172.
<https://doi.org/10.1128/iai.69.11.7169-7172.2001>

Drayna, D., Jarnagin, A. S., McLean, J., Henzel, W., Kohr, W., Fielding, C., & Lawn, R. (1987). Cloning and sequencing of human cholesteryl ester transfer protein cDNA. *Nature*, 327(6123), 632–634. <https://doi.org/10.1038/327632a0>

Eckert, J. K., Kim, Y. J., Kim, J. I., Gürtler, K., Oh, D.-Y., Sur, S., Lundvall, L., Hamann, L., van der Ploeg, A., Pickkers, P., Giamarellos-Bourboulis, E., Kubarenko, A. V., Weber, A. N., Kabesch, M., Kumpf, O., An, H.-J., Lee, J.-O., & Schumann, R. R. (2013). The Crystal Structure of Lipopolysaccharide Binding Protein Reveals the Location of a Frequent Mutation that Impairs Innate Immunity. *Immunity*, 39(4), 647–660.
<https://doi.org/10.1016/J.IMMUNI.2013.09.005>

- Edwards, E. E., & Thomas, S. N. (2017). P-Selectin and ICAM-1 synergy in mediating THP-1 monocyte adhesion in hemodynamic flow is length dependent. *Integrative Biology*, 9(4), 313–327. <https://doi.org/10.1039/c7ib00020k>
- Erridge, C., Bennett-Guerrero, E., & Poxton, I. R. (2002). Structure and function of lipopolysaccharides. *Microbes and Infection*, 4(8), 837–851. [https://doi.org/https://doi.org/10.1016/S1286-4579\(02\)01604-0](https://doi.org/https://doi.org/10.1016/S1286-4579(02)01604-0)
- Faya, M., Kalhapure, R. S., Dhumal, D., Agrawal, N., Omolo, C., Akamanchi, K. G., & Govender, T. (2019). Antimicrobial cell penetrating peptides with bacterial cell specificity: pharmacophore modelling, quantitative structure activity relationship and molecular dynamics simulation. *Journal of Biomolecular Structure and Dynamics*, 37(9), 2370–2380. <https://doi.org/10.1080/07391102.2018.1484814>
- Fernandes D, Assreuy J. Nitric oxide and vascular reactivity in sepsis. *Shock*. 2008 Oct;30 Suppl 1:10-3. doi: 10.1097/SHK.0b013e3181818518. PMID: 18704016.
- Fu, L., Wan, M., Zhang, S., Gao, L., & Fang, W. (2020). Polymyxin B Loosens Lipopolysaccharide Bilayer but Stiffens Phospholipid Bilayer. *Biophysical Journal*, 118(1), 138–150. <https://doi.org/https://doi.org/10.1016/j.bpj.2019.11.008>
- Gallay, P., Heumann, D., Le Roy, D., Barras, C., & Glauser, M. P. (1993). Lipopolysaccharide-binding protein as a major plasma protein responsible for endotoxemic shock. *Proceedings of the National Academy of Sciences*, 90(21), 9935–9938. <https://doi.org/10.1073/pnas.90.21.9935>
- García-González, V., Gutiérrez-Quintanar, N., & Mas-Oliva, J. (2015). The C-terminal Domain Supports a Novel Function for CETPI as a New Plasma Lipopolysaccharide-Binding Protein. *Scientific Reports*, 5, 16091. <https://doi.org/10.1038/srep16091>
- García-González, V., Gutiérrez-Quintanar, N., Mendoza-Espinosa, P., Brocos, P., Piñeiro, Á., & Mas-Oliva, J. (2014). Key structural arrangements at the C-terminus domain of CETP suggest a potential mechanism for lipid-transfer

activity. Journal of Structural Biology, 186(1), 19–27.
<https://doi.org/10.1016/J.JSB.2014.02.002>

Garlanda, C., Dinarello, C. A., & Mantovani, A. (2013). The Interleukin-1 Family: Back to the Future. Immunity, 39(6), 1003–1018.
<https://doi.org/10.1016/J.IMMUNI.2013.11.010>

Ghafouri, B., Kihlström, E., Tagesson, C., & Lindahl, M. (2004). PLUNC in human nasal lavage fluid: multiple isoforms that bind to lipopolysaccharide. Biochimica et Biophysica Acta (BBA) - Proteins and Proteomics, 1699(1–2), 57–63.
<https://doi.org/10.1016/J.BBAPAP.2004.01.001>

Giuliani, A., Pirri, G., & Rinaldi, A. C. (2010). Antimicrobial Peptides: The LPS Connection (pp. 137–154). https://doi.org/10.1007/978-1-60761-594-1_10

Gohda, J., Matsumura, T., & Inoue, J. (2004). Cutting Edge: TNFR-Associated Factor (TRAF) 6 Is Essential for MyD88-Dependent Pathway but Not Toll/IL-1 Receptor Domain-Containing Adaptor-Inducing IFN- β (TRIF)-Dependent Pathway in TLR Signaling1. The Journal of Immunology, 173(5), 2913–2917.
<https://doi.org/10.4049/jimmunol.173.5.2913>

Gorordo-Delsol LA, Merinos-Sánchez G, Estrada-Escobar RA, Medveczky-Ordoñez NI, Amezcua-Gutiérrez MA, Morales-Segura MA, Uribe-Moya SE. Sepsis and septic shock in emergency departments of Mexico: a multicenter point prevalence study. Gac Med Mex. 2020;156(6):486-492. English. doi: 10.24875/GMM.M21000492. PMID: 33877101.

Gotthardt, M., Bleeker-Rovers, C. P., Boerman, O. C., & Oyen, W. J. G. (2010). Imaging of inflammation by PET, conventional scintigraphy, and other imaging techniques. Journal of Nuclear Medicine : Official Publication, Society of Nuclear Medicine, 51(12), 1937–1949. <https://doi.org/10.2967/jnumed.110.076232>

Guixà-González, R., Rodriguez-Espigares, I., Ramírez-Anguita, J. M., Carrión-Gaspar, P., Martínez-Seara, H., Giorgino, T., & Selent, J. (2014). MEMBPLUGIN: studying membrane complexity in VMD. Bioinformatics, 30(10), 1478–1480.
<https://doi.org/10.1093/bioinformatics/btu037>

Hamill, P., Brown, K., Jenssen, H., & Hancock, R. E. (2008). Novel anti-infectives: is host defence the answer? In Current Opinion in Biotechnology (Vol. 19, Issue 6, pp. 628–636). Elsevier Current Trends. <https://doi.org/10.1016/j.copbio.2008.10.006>

Hancock, R. E. W., Haney, E. F., & Gill, E. E. (2016). The immunology of host defence peptides: beyond antimicrobial activity. *Nature Reviews Immunology*, 16(5), 321–334. <https://doi.org/10.1038/nri.2016.29>

Hancock, R. E. W., & Sahl, H.-G. (2006). Antimicrobial and host-defense peptides as new anti-infective therapeutic strategies. *Nature Biotechnology*, 24(12), 1551–1557. <https://doi.org/10.1038/nbt1267>

Hilchie, A. L., Wuerth, K., & Hancock, R. E. W. (2013). Immune modulation by multifaceted cationic host defense (antimicrobial) peptides. *Nature Chemical Biology*, 9(12), 761–768. <https://doi.org/10.1038/nchembio.1393>

Hildebrand, F., Pape, H.-C., Harwood, P., Müller, K., Hoevel, P., Pütz, C., Siemann, A., Krettek, C., & van Griensven, M. (2005). Role of adhesion molecule ICAM in the pathogenesis of polymicrobial sepsis. *Experimental and Toxicologic Pathology*, 56(4), 281–290. <https://doi.org/https://doi.org/10.1016/j.etp.2004.09.004>

Holst, O. (2011). Structure of the Lipopolysaccharide Core Region. In Y. A. Knirel & M. A. Valvano (Eds.), *Bacterial Lipopolysaccharides: Structure, Chemical Synthesis, Biogenesis and Interaction with Host Cells* (pp. 21–39). Springer Vienna. https://doi.org/10.1007/978-3-7091-0733-1_2

Hong, L., Gontsarik, M., Amenitsch, H., & Salentinig, S. (2022). Human Antimicrobial Peptide Triggered Colloidal Transformations in Bacteria Membrane Lipopolysaccharides. *Small*, 18(5), 2104211. <https://doi.org/https://doi.org/10.1002/smll.202104211>

Humphrey, W., Dalke, A., & Schulten, K. (1996). VMD: Visual molecular dynamics. *Journal of Molecular Graphics*, 14(1), 33–38. [https://doi.org/https://doi.org/10.1016/0263-7855\(96\)00018-5](https://doi.org/https://doi.org/10.1016/0263-7855(96)00018-5)

- Jefferies, D., Hsu, P.-C., & Khalid, S. (2017). Through the Lipopolysaccharide Glass: A Potent Antimicrobial Peptide Induces Phase Changes in Membranes. *Biochemistry*, 56(11), 1672–1679. <https://doi.org/10.1021/acs.biochem.6b01063>
- Jerala, R. (2007). Structural biology of the LPS recognition. *International Journal of Medical Microbiology Microbiology*, 297(5), 353–363. <https://doi.org/10.1016/J.IJMM.2007.04.001>
- Jo, S., Kim, T., Iyer, V. G., & Im, W. (2008). CHARMM-GUI: A web-based graphical user interface for CHARMM. *Journal of Computational Chemistry*, 29(11), 1859–1865. <https://doi.org/10.1002/jcc.20945>
- Julián-Jiménez A, Gorordo-Delsol LA, Merinos-Sánchez G, Armando Santillán-Santos D, Rosas Romero FA, Sánchez Arreola D, López Tapia JD, Vázquez Lima MJ, García DE, González Del Castillo J, Menéndez E, Piñera Salmerón P, Candel González FJ, Rubio Díaz R, Juárez González R. The Guadalajara Declaration on sepsis: emergency physicians' constructive comments on the Surviving Sepsis Campaign's 2021 updated guidelines. *Emergencias*. 2023 Feb;35(1):53-64. English, Spanish. PMID: 36756917.
- Kaconis, Y., Kowalski, I., Howe, J., Brauser, A., Richter, W., Razquin-Olazarán, I., Iñigo-Pestaña, M., Garidel, P., Rössle, M., Martinez de Tejada, G., Gutsmann, T., & Brandenburg, K. (2011). Biophysical mechanisms of endotoxin neutralization by cationic amphiphilic peptides. *Biophysical Journal*, 100(11), 2652–2661. <https://doi.org/10.1016/j.bpj.2011.04.041>
- Kluge, S., Braune, S., Nierhaus, A., Wichmann, D., Derlin, T., Mester, J., & Klutmann, S. (2012). Diagnostic value of positron emission tomography combined with computed tomography for evaluating patients with septic shock of unknown origin. *Journal of Critical Care*, 27(3), 316.e1-316.e7. <https://doi.org/10.1016/J.JCRC.2011.10.004>
- Knirel, Y. A. (2011). Structure of O-Antigens. In Y. A. Knirel & M. A. Valvano (Eds.), *Bacterial Lipopolysaccharides: Structure, Chemical Synthesis, Biogenesis and*

Interaction with Host Cells (pp. 41–115). Springer Vienna.
https://doi.org/10.1007/978-3-7091-0733-1_3

Kothari, N., Bogra, J., Abbas, H., Kohli, M., Malik, A., Kothari, D., Srivastava, S., & Singh, P. K. (2013). Tumor Necrosis Factor gene polymorphism results in high TNF level in sepsis and septic shock. *Cytokine*, 61(2), 676–681.
<https://doi.org/https://doi.org/10.1016/j.cyto.2012.11.016>

Krasaty, B. C., Troll, J. V., Weiss, J. P., & McFall-Ngai, M. J. (2011). LBP/BPI proteins and their relatives: conservation over evolution and roles in mutualism. *Biochemical Society Transactions*, 39(4), 1039–1044.
<https://doi.org/10.1042/BST0391039>

Kumar, P., Kizhakkedathu, J. N., & Straus, S. K. (2018). Antimicrobial peptides: Diversity, mechanism of action and strategies to improve the activity and biocompatibility in vivo. In *Biomolecules* (Vol. 8, Issue 1, p. 4). MDPI AG.
<https://doi.org/10.3390/biom8010004>

Lassenius, M. I., Pietiläinen, K. H., Kaartinen, K., Pussinen, P. J., Syrjänen, J., Forsblom, C., Pörsti, I., Rissanen, A., Kaprio, J., Mustonen, J., Groop, P.-H., & Lehto, M. (2011). Bacterial Endotoxin Activity in Human Serum Is Associated With Dyslipidemia, Insulin Resistance, Obesity, and Chronic Inflammation. *Diabetes Care*, 34, 1809–1815. <https://doi.org/10.2337/dc10-2197>

Liu, S., Mistry, A., Reynolds, J. M., Lloyd, D. B., Griffor, M. C., Perry, D. A., Ruggeri, R. B., Clark, R. W., & Qiu, X. (2012). Crystal Structures of Cholesteryl Ester Transfer Protein in Complex with Inhibitors. *Journal of Biological Chemistry*, 287(44), 37321–37329. <https://doi.org/https://doi.org/10.1074/jbc.M112.380063>

López-Bojórquez, L. N., Dehesa, A. Z., & Reyes-Terán, G. (2004). Molecular mechanisms involved in the pathogenesis of septic shock. In *Archives of Medical Research* (Vol. 35, Issue 6, pp. 465–479). Elsevier Inc.
<https://doi.org/10.1016/j.arcmed.2004.07.006>

Lu, Y.-C., Yeh, W.-C., & Ohashi, P. S. (2008). LPS/TLR4 signal transduction pathway. *Cytokine*, 42(2), 145–151. <https://doi.org/10.1016/j.cyto.2008.01.006>

- Luna-Reyes, I., Pérez-Hernández, E. G., Delgado-Coello, B., Ávila-Rodríguez, M. Á., & Mas-Oliva, J. (2021). Peptide VSAK maintains tissue glucose uptake and attenuates pro-inflammatory responses caused by LPS in an experimental model of the systemic inflammatory response syndrome: a PET study. *Scientific Reports* 2021 11:1, 11(1), 1–13. <https://doi.org/10.1038/s41598-021-94224-2>
- Mackman, N. (2009). The many faces of tissue factor. *Journal of Thrombosis and Haemostasis*, 7, 136–139. <https://doi.org/10.1111/j.1538-7836.2009.03368.x>
- Mansour, S. C., Pena, O. M., & Hancock, R. E. W. (2014). Host defense peptides: Front-line immunomodulators. In *Trends in Immunology* (Vol. 35, Issue 9, pp. 443–450). Elsevier Ltd. <https://doi.org/10.1016/j.it.2014.07.004>
- Marik, P. E., & Raghavan, M. (2004). Stress-hyperglycemia, insulin and immunomodulation in sepsis. In *Intensive Care Medicine* (Vol. 30, Issue 5, pp. 748–756). Intensive Care Med. <https://doi.org/10.1007/s00134-004-2167-y>
- Martin, G. S. (2012). Sepsis, severe sepsis and septic shock: changes in incidence, pathogens and outcomes. *Expert Review of Anti-Infective Therapy*, 10(6), 701–706. <https://doi.org/10.1586/eri.12.50>
- Mather, A., & Pollock, C. (2011). Glucose handling by the kidney. *Kidney International*, 79, S1–S6. <https://doi.org/10.1038/ki.2010.509>
- Mazgaaen, L., & Gurung, P. (2020). Recent Advances in Lipopolysaccharide Recognition Systems. *International Journal of Molecular Sciences*, 21(2). <https://doi.org/10.3390/ijms21020379>
- Mehta, N. N., McGillicuddy, F. C., Anderson, P. D., Hinkle, C. C., Shah, R., Pruscino, L., Tabita-Martinez, J., Sellers, K. F., Rickels, M. R., & Reilly, M. P. (2010). Experimental endotoxemia induces adipose inflammation and insulin resistance in humans. *Diabetes*, 59(1), 172–181. <https://doi.org/10.2337/db09-0367>

Menten, P., Wuyts, A., & Van Damme, J. (2002). Macrophage inflammatory protein-1. Cytokine & Growth Factor Reviews, 13(6), 455–481.
<http://www.ncbi.nlm.nih.gov/pubmed/12401480>

Montero Vega, S., Booth, V., & Rowley, C. N. (2022). Interaction between Antimicrobial Peptide Magainin 2 and Nonlipid Components in the Bacterial Outer Envelope. *The Journal of Physical Chemistry B*, 126(29), 5473–5480.
<https://doi.org/10.1021/acs.jpcb.2c02768>

Mookherjee, N., Anderson, M. A., Haagsman, H. P., & Davidson, D. J. (2020). Antimicrobial host defence peptides: functions and clinical potential. In *Nature Reviews Drug Discovery* (Vol. 19, Issue 5, pp. 311–332). Nature Research.
<https://doi.org/10.1038/s41573-019-0058-8>

Mookherjee, N., & Hancock, R. E. W. (2007). Cationic host defence peptides: Innate immune regulatory peptides as a novel approach for treating infections. *Cellular and Molecular Life Sciences*, 64(7–8), 922–933. <https://doi.org/10.1007/s00018-007-6475-6>

Mueller, M., Lindner, B., Kusumoto, S., Fukase, K., Schromm, A. B., & Seydel, U. (2004). Aggregates Are the Biologically Active Units of Endotoxin*. *Journal of Biological Chemistry*, 279(25), 26307–26313.
<https://doi.org/https://doi.org/10.1074/jbc.M401231200>

Mühl, H., & Pfeilschifter, J. (2003). Endothelial nitric oxide synthase: a determinant of TNF α production by human monocytes/macrophages. *Biochemical and Biophysical Research Communications*, 310(3), 677–680.
<https://doi.org/https://doi.org/10.1016/j.bbrc.2003.09.039>

Netea, M. G., Van Deuren, M., Kullberg, B. J., Cavaillon, J. M., & Van Der Meer, J. W. M. (2002). Does the shape of lipid A determine the interaction of LPS with Toll-like receptors? *Trends in Immunology*, 23(3), 135–139.
[https://doi.org/10.1016/S1471-4906\(01\)02169-X](https://doi.org/10.1016/S1471-4906(01)02169-X)

Nicholas, P., A. M. J. R. M., T. T. M. D., & César, de la F.-N. (2021). Molecular Dynamics for Antimicrobial Peptide Discovery. *Infection and Immunity*, 89(4), 10.1128/iai.00703-20. <https://doi.org/10.1128/iai.00703-20>

Nieto-Vazquez, I., Fernández-Veledo, S., Krämer, D. K., Vila-Bedmar, R., García-Guerra, L., & Lorenzo, M. (2008). Insulin resistance associated to obesity: the link TNF-alpha. *Archives of Physiology and Biochemistry*, 114(3), 183–194. <https://doi.org/10.1080/13813450802181047>

Pastelin-Palacios, R., Gil-Cruz, C., Pérez-Shibayama, C. I., Moreno-Eutimio, M. A., Cervantes-Barragán, L., Arriaga-Pizano, L., Ludewig, B., Cunningham, A. F., García-Zepeda, E. A., Becker, I., Alpuche-Aranda, C., Bonifaz, L., Gunn, J. S., Isibasi, A., & López-Macías, C. (2011). Subversion of innate and adaptive immune activation induced by structurally modified lipopolysaccharide from *Salmonella typhimurium*. *Immunology*, 133(4), 469–481. <https://doi.org/10.1111/j.1365-2567.2011.03459.x>

Pawlinski, R., & Mackman, N. (2010). Cellular sources of tissue factor in endotoxemia and sepsis. *Thrombosis Research*, 125, S70–S73. <https://doi.org/https://doi.org/10.1016/j.thromres.2010.01.042>

Pérez-Hernández, E. G., De la Puente-Díaz de León, V., Luna-Reyes, I., Delgado-Coello, B., Sifuentes-Osornio, J., & Mas-Oliva, J. (2022). The cholestryler-ester transfer protein isoform (CETPI) and derived peptides: new targets in the study of Gram-negative sepsis. *Molecular Medicine*, 28(1), 1–14. <https://doi.org/10.1186/S10020-022-00585-3/FIGURES/6>

Peschel, A., & Sahl, H. G. (2006). The co-evolution of host cationic antimicrobial peptides and microbial resistance. In *Nature Reviews Microbiology* (Vol. 4, Issue 7, pp. 529–536). Nature Publishing Group. <https://doi.org/10.1038/nrmicro1441>

Poltorak, A., He, X., Smirnova, I., Liu, M.-Y., Huffel, C. Van, Du, X., Birdwell, D., Alejos, E., Silva, M., Galanos, C., Freudenberg, M., Ricciardi-Castagnoli, P., Layton, B., & Beutler, B. (1998). Defective LPS Signaling in C3H/HeJ and

C57BL/10ScCr Mice: Mutations in Tlr4 Gene. *Science*, 282(5396), 2085–2088.
<https://doi.org/10.1126/science.282.5396.2085>

Pop-Began, V., Păunescu, V., Grigorean, V., Pop-Began, D., & Popescu, C. (2014). Molecular mechanisms in the pathogenesis of sepsis. *Journal of Medicine and Life*, Spec Iss 2, 38–41. <http://www.ncbi.nlm.nih.gov/pubmed/25870671>

Preau, S., Vodovar, D., Jung, B., Lancel, S., Zafrani, L., Flatres, A., Oualha, M., Voiriot, G., Jouan, Y., Joffre, J., Uhel, F., De Prost, N., Silva, S., Azabou, E., & Radermacher, P. (2021). Energetic dysfunction in sepsis: a narrative review. *Annals of Intensive Care*, 11(1), 104. <https://doi.org/10.1186/s13613-021-00893-7>

Reinhart, K., Daniels, R., Kissoon, N., Machado, F. R., Schachter, R. D., & Finfer, S. (2017). Recognizing Sepsis as a Global Health Priority — A WHO Resolution. *New England Journal of Medicine*, 377(5), 414–417. <https://doi.org/10.1056/nejmp1707170>

Repetto, G., del Peso, A., & Zurita, J. L. (2008). Neutral red uptake assay for the estimation of cell viability/cytotoxicity. *Nature Protocols*, 3(7), 1125–1131. <https://doi.org/10.1038/nprot.2008.75>

Rosenfeld, Y., Papo, N., & Shai, Y. (2006). Endotoxin (lipopolysaccharide) neutralization by innate immunity host-defense peptides: Peptide properties and plausible modes of action. *Journal of Biological Chemistry*, 281(3), 1636–1643. <https://doi.org/10.1074/jbc.M504327200>

Roy, A., Kucukural, A., & Zhang, Y. (2010). I-TASSER: A unified platform for automated protein structure and function prediction. *Nature Protocols*, 5(4), 725–738. <https://doi.org/10.1038/nprot.2010.5>

Rudd, K. E., Johnson, S. C., Agesa, K. M., Shackelford, K. A., Tsoi, D., Kievlan, D. R., Colombara, D. V., Ikuta, K. S., Kissoon, N., Finfer, S., Fleischmann-Struzek, C., Machado, F. R., Reinhart, K. K., Rowan, K., Seymour, C. W., Watson, R. S., West, T. E., Marinho, F., Hay, S. I., ... Naghavi, M. (2020). Global, regional, and national sepsis incidence and mortality, 1990–2017: analysis for the Global

Burden of Disease Study. *The Lancet*, 395(10219), 200–211.
[https://doi.org/10.1016/S0140-6736\(19\)32989-7](https://doi.org/10.1016/S0140-6736(19)32989-7)

Russo, R. C., Garcia, C. C., Teixeira, M. M., & Amaral, F. A. (2014). The CXCL8/IL-8 chemokine family and its receptors in inflammatory diseases. *Expert Review of Clinical Immunology*, 10(5), 593–619.
<https://doi.org/10.1586/1744666X.2014.894886>

Santajit, S., & Indrawattana, N. (2016). Mechanisms of Antimicrobial Resistance in ESKAPE Pathogens. *BioMed Research International*, 2016, 2475067.
<https://doi.org/10.1155/2016/2475067>

Sato, S., Sanjo, H., Takeda, K., Ninomiya-Tsuji, J., Yamamoto, M., Kawai, T., Matsumoto, K., Takeuchi, O., & Akira, S. (2005). Essential function for the kinase TAK1 in innate and adaptive immune responses. *Nature Immunology*, 6(11), 1087–1095. <https://doi.org/10.1038/ni1255>

Schetz, M., Vanhorebeek, I., Wouters, P. J., Wilmer, A., & Berghe, G. Van den. (2008). Tight Blood Glucose Control Is Renoprotective in Critically Ill Patients. *Journal of the American Society of Nephrology: JASN*, 19(3), 571.
<https://doi.org/10.1681/ASN.2006101091>

Schultz, H., & Weiss, J. P. (2007). The bactericidal/permeability-increasing protein (BPI) in infection and inflammatory disease. *Clinica Chimica Acta*, 384(1), 12–23. <https://doi.org/https://doi.org/10.1016/j.cca.2007.07.005>

Serhan, C. N., Brain, S. D., Buckley, C. D., Gilroy, D. W., Haslett, C., O'Neill, L. A. J., Perretti, M., Rossi, A. G., & Wallace, J. L. (2007). Resolution of inflammation: state of the art, definitions and terms. *The FASEB Journal*, 21(2), 325–332.
<https://doi.org/https://doi.org/10.1096/fj.06-7227rev>

Shai, Y. (2002). Mode of action of membrane active antimicrobial peptides. In *Biopolymers - Peptide Science Section* (Vol. 66, Issue 4, pp. 236–248). John Wiley & Sons, Ltd. <https://doi.org/10.1002/bip.10260>

- Shao, B., Munford, R. S., Kitchens, R., & Varley, A. W. (2012). Hepatic uptake and deacylation of the LPS in bloodborne LPS-lipoprotein complexes. *Innate Immunity*, 18(6), 825–833. <https://doi.org/10.1177/1753425912442431>
- Shen, Y., Maupetit, J., Derreumaux, P., & Tufféry, P. (2014). Improved PEP-FOLD Approach for Peptide and Miniprotein Structure Prediction. *Journal of Chemical Theory and Computation*, 10(10), 4745–4758. <https://doi.org/10.1021/ct500592m>
- Shi, Q., Cox, L. A., Glenn, J., Tejero, M. E., Hondara, V., VandeBerg, J. L., & Wang, X. L. (2010). Molecular pathways mediating differential responses to lipopolysaccharide between human and baboon arterial endothelial cells. *Clinical and Experimental Pharmacology and Physiology*, 37(2), 178–184. <https://doi.org/https://doi.org/10.1111/j.1440-1681.2009.05260.x>
- Siewert J. Marrink, *,†, H. Jelger Risselada, †, Serge Yefimov, ‡, D. Peter Tieleman, § and, & Vries†, A. H. de. (2007). The MARTINI Force Field: Coarse Grained Model for Biomolecular Simulations. <https://doi.org/10.1021/JP071097F>
- Singer, M., Deutschman, C. S., Seymour, C. W., Shankar-Hari, M., Annane, D., Bauer, M., Bellomo, R., Bernard, G. R., Chiche, J.-D., Coopersmith, C. M., Hotchkiss, R. S., Levy, M. M., Marshall, J. C., Martin, G. S., Opal, S. M., Rubenfeld, G. D., Poll, T. van der, Vincent, J.-L., & Angus, D. C. (2016). The Third International Consensus Definitions for Sepsis and Septic Shock (Sepsis-3). *JAMA*, 315(8), 801. <https://doi.org/10.1001/JAMA.2016.0287>
- Sugawara, Y., Gutowski, T. D., Fisher, S. J., Brown, R. S., & Wahl, R. L. (1999). Uptake of positron emission tomography tracers in experimental bacterial infections: a comparative biodistribution study of radiolabeled FDG, thymidine, L-methionine, 67Ga-citrate, and 125I-HSA. *European Journal of Nuclear Medicine*, 26(4), 333–341. <http://www.ncbi.nlm.nih.gov/pubmed/10199938>
- Suzuki, M. M., Matsumoto, M., Yamamoto, A., Ochiai, M., Horiuchi, Y., Niwa, M., Omi, H., Kobayashi, T., & Takagi, T. (2010). Molecular design of LPS-binding

peptides. *Journal of Microbiological Methods*, 83(2), 153–155.
<https://doi.org/10.1016/j.mimet.2010.08.009>

Swantek, J. L., Tsen, M. F., Cobb, M. H., & Thomas, J. A. (2000). IL-1 Receptor-Associated Kinase Modulates Host Responsiveness to Endotoxin1. *The Journal of Immunology*, 164(8), 4301–4306.
<https://doi.org/10.4049/jimmunol.164.8.4301>

Trecarichi, E. M., Pagano, L., Candoni, A., Pastore, D., Cattaneo, C., Fanci, R., Nosari, A., Caira, M., Spadea, A., Busca, A., Vianelli, N., & Tumbarello, M. (2015). Current epidemiology and antimicrobial resistance data for bacterial bloodstream infections in patients with hematologic malignancies: an Italian multicentre prospective survey. *Clinical Microbiology and Infection*, 21(4), 337–343. <https://doi.org/https://doi.org/10.1016/j.cmi.2014.11.022>

Van Der Poll, T., Van De Veerdonk, F. L., Scicluna, B. P., & Netea, M. G. (2017). The immunopathology of sepsis and potential therapeutic targets. In *Nature Reviews Immunology* (Vol. 17, Issue 7, pp. 407–420). Nature Publishing Group.
<https://doi.org/10.1038/nri.2017.36>

Vazquez-Grande Anand, G. K. (2015). Optimizing Antimicrobial Therapy of Sepsis and Septic Shock: Focus on Antibiotic Combination Therapy. *Seminars in Respiratory and Critical Care Medicine*, 36(01), 154–166.
<https://doi.org/10.1055/s-0034-1398742>

Vincent, J.-L., Rello, J., Marshall, J., Silva, E., Anzueto, A., Martin, C. D., Moreno, R., Lipman, J., Gomersall, C., Sakr, Y., Reinhart, K., & EPIC II Group of Investigators, for the. (2009). International Study of the Prevalence and Outcomes of Infection in Intensive Care Units. *JAMA*, 302(21), 2323–2329.
<https://doi.org/10.1001/jama.2009.1754>

Waage, A., Redl, H., Schlag, G., & Schade, U. (1993). The Cytokine Network in Sepsis II: IL-1 and IL-6. In G. Schlag & H. Redl (Eds.), *Pathophysiology of Shock, Sepsis, and Organ Failure* (pp. 491–501). Springer Berlin Heidelberg.
https://doi.org/10.1007/978-3-642-76736-4_36

Wang, Y., Su, L., Morin, M. D., Jones, B. T., Whitby, L. R., Surakattula, M. M. R. P., Huang, H., Shi, H., Choi, J. H., Wang, K., Moresco, E. M. Y., Berger, M., Zhan, X., Zhang, H., Boger, D. L., & Beutler, B. (2016). TLR4/MD-2 activation by a synthetic agonist with no similarity to LPS. *Proceedings of the National Academy of Sciences*, 113(7), E884–E893. <https://doi.org/10.1073/pnas.1525639113>

Wang, Y., Su, L., Morin, M., Jones, B., Whitby, L., Surakattula, M., Huang, H., Shi, H., Choi, J. H., Wang, K., Moresco, E. M. Y., Berger, M., Zhan, X., Zhan, H., Boger, D., & Beutler, B. (2017). Identification of novel and potent synthetic TLR agonists. *The Journal of Immunology*, 198(1_Supplement), 129.3-129.3. <https://doi.org/10.4049/jimmunol.198.Supp.129.3>

Wasyluk, W., & Zwolak, A. (2021). Metabolic Alterations in Sepsis. *Journal of Clinical Medicine*, 10(11). <https://doi.org/10.3390/jcm10112412>

Weiss, J. (2003). Bactericidal/permeability-increasing protein (BPI) and lipopolysaccharide-binding protein (LBP): structure, function and regulation in host defence against Gram-negative bacteria. *Biochemical Society Transactions*, 31(4), 785–790. <https://doi.org/10.1042/bst0310785>

Wissink, S., Van De Stolpe, A., Caldenhoven, E., Koenderman, L., & Van Der Saag, P. T. (1997). NF-κB/Rel Family Members Regulating the ICAM-1 Promoter in Monocytic THP-1 Cells. *Immunobiology*, 198(1), 50–64. [https://doi.org/https://doi.org/10.1016/S0171-2985\(97\)80026-5](https://doi.org/https://doi.org/10.1016/S0171-2985(97)80026-5)

Zaman, S. Bin, Hussain, M. A., Nye, R., Mehta, V., Mamun, K. T., & Hossain, N. (2017). A Review on Antibiotic Resistance: Alarm Bells are Ringing. *Cureus*, 9(6). <https://doi.org/10.7759/cureus.1403>

Zasloff, M. (2002). Antimicrobial peptides of multicellular organisms. In *Nature* (Vol. 415, Issue 6870, pp. 389–395). Nature Publishing Group. <https://doi.org/10.1038/415389a>

Zhong, H., Lin, H., Pang, Q., Zhuang, J., Liu, X., Li, X., Liu, J., & Tang, J. (2021). Macrophage ICAM-1 functions as a regulator of phagocytosis in LPS induced

endotoxemia. Inflammation Research, 70(2), 193–203.
<https://doi.org/10.1007/s00011-021-01437-2>

Zhou, S., Wang, G., & Zhang, W. (2018). Effect of TLR4/MyD88 signaling pathway on sepsis-associated acute respiratory distress syndrome in rats, via regulation of macrophage activation and inflammatory response. Experimental and Therapeutic Medicine, 15(4), 3376. <https://doi.org/10.3892/ETM.2018.5815>

ANEXO I. Publicaciones generadas durante el proyecto de doctorado.

Luna-Reyes, I., Pérez-Hernández, E.G., Delgado-Coello, B. et al. Peptide VSAK maintains tissue glucose uptake and attenuates pro-inflammatory responses caused by LPS in an experimental model of the systemic inflammatory response syndrome: a PET study. *Sci Rep* 11, 14752 (2021).

<https://doi.org/10.1038/s41598-021-94224-2>

Luna-Reyes, I., Pérez-Hernández, E. G., Delgado-Coello, B., & Mas-Oliva, J. (2021). Peptides as Therapeutic Molecules to Neutralize Gram-negative Bacterial Lipopolysaccharides in Sepsis and Septic Shock. *Archives of Medical Research*, 52(8), 798–807.

<https://doi.org/10.1016/J.ARCMED.2021.08.001>

Pérez-Hernández, E. G., De la Puente-Díaz de León, V., Luna-Reyes, I., Delgado-Coello, B., Sifuentes-Osornio, J., & Mas-Oliva, J. (2022). The cholesteryl-ester transfer protein isoform (CETPI) and derived peptides: new targets in the study of Gram-negative sepsis. *Molecular Medicine*, 28(1), 1–14.

<https://doi.org/10.1186/s10020-022-00585-3>

Pérez-Hernández, E. G., Delgado-Coello, B., Luna-Reyes, I., & Mas-Oliva, J. (2021). New insights into lipopolysaccharide inactivation mechanisms in sepsis. *Biomedicine & Pharmacotherapy*, 141, 111890.

<https://doi.org/10.1016/J.BIOPHA.2021.111890>

Martínez-Navarro, I., Díaz-Molina, R., Pulido-Capiz, A., Mas-Oliva, J., Luna-Reyes, I., Rodríguez-Velázquez, E., Rivero, I. A., Ramos-Ibarra, M. A., Alatorre-Meda, M., & García-González, V. (2020). Lipid Modulation in the Formation of β -Sheet Structures. Implications for De Novo Design of Human Islet Amyloid Polypeptide and the Impact on β -Cell Homeostasis. *Biomolecules* 2020, Vol. 10, Page 1201, 10(9), 1201.

<https://doi.org/10.3390/BIOM10091201>



OPEN

Peptide VSAK maintains tissue glucose uptake and attenuates pro-inflammatory responses caused by LPS in an experimental model of the systemic inflammatory response syndrome: a PET study

Ismail Luna-Reyes¹, Eréndira G. Pérez-Hernández¹, Blanca Delgado-Coello¹, Miguel Ángel Ávila-Rodríguez² & Jaime Mas-Oliva¹✉

The present investigation using Positron Emission Tomography shows how peptide VSAK can reduce the detrimental effects produced by lipopolysaccharides in Dutch dwarf rabbits, used to develop the Systemic Inflammatory Response Syndrome (SIRS). Animals concomitantly treated with lipopolysaccharides (LPS) and peptide VSAK show important protection in the loss of radiolabeled-glucose uptake observed in diverse organs when animals are exclusively treated with LPS. Treatment with peptide VSAK prevented the onset of changes in serum levels of glucose and insulin associated with the establishment of SIRS and the insulin resistance-like syndrome. Treatment with peptide VSAK also allowed an important attenuation in the circulating levels of pro-inflammatory molecules in LPS-treated animals. As a whole, our data suggest that peptide VSAK might be considered as a candidate in the development of new therapeutic possibilities focused on mitigating the harmful effects produced by lipopolysaccharides during the course of SIRS.

During the last years, infections have re-emerged as one of the most important public health problems around the globe. Since nowadays the aggravated states of an infectious process, such as sepsis and septic shock are the main causes of death in Intensive Care Units worldwide, there is the imperative need to find new ways not only to diagnose but also to successfully treat these conditions^{1,2}. Sepsis is characterized by the presence of infection in association with a dysregulated host response and organ failure; while, septic shock also includes the development of systemic hypotension^{3,4}. Dysregulation of this response is mainly characterized by an imbalance in the systems that regulate the host's immune activation when the presence of the pathogen leads to the development of a hyper-inflammatory state followed by the exhaustion of the immune system to adequately respond⁵. With this concept in mind, and the goal to establish a set of guidelines that would allow to study the translational value of preclinical experimental models to the clinical setting, it is now established that the term Systemic Inflammatory Response Syndrome (SIRS), corresponds to a more appropriate term than experimental sepsis when LPS are used to trigger an inflammatory response⁶.

The recognition of molecules by the innate immune system has a leading role in the host's response through molecules present in most pathogenic organisms that stimulate the development of a systemic defense. As a whole, such molecules known as MAMPS for Microorganism Associated Molecular Patterns⁷, can be recognized through receptors that collectively are known as Pattern Recognition Receptors or PRR's. Toll-like receptors (TLRs) are considered one of the main families of receptors included among PRR's. Within the TLRs, the type

¹Instituto de Fisiología Celular, Universidad Nacional Autónoma de México, Circuito Exterior, Cd. Universitaria, 04510 Mexico, Mexico. ²Facultad de Medicina, Universidad Nacional Autónoma de México, 04510 Mexico, Mexico. ✉email: jmas@ifc.unam.mx

4 receptor (TLR4) plays an important role in the development of the host immune response during bacterial infection⁸ through the recognition of lipopolysaccharides (LPS), one of the most immunogenic MAMPs and responsible for the development of septic shock in infections caused by Gram-negative bacteria^{9–11}.

LPS molecules present three well-defined regions within their structure (lipid A, a core region and the O antigen), that show a large degree of variability independent of each other¹². Lipid A considered the most conserved region of LPS, presents special importance for recognition by the immune system. When this region binds to a member of the lipopolysaccharide-binding protein family, the complex is recognized by the TLR4 receptor, and the development of the host response initiates¹³.

Lipopolsaccharide-binding proteins are part of a family of proteins known as PLUNC-containing-motif proteins (PLUNC for Palate, Lung, Nasal-epithelium Clone-Protein). PLUNC proteins are involved in the defense system against pathogens of the upper airways and palate^{14–16}. Sharing a common structural motif, so far this family includes four members: the bactericidal permeability-increasing protein (BPI); the lipopolysaccharide-binding protein (LBP); the phospholipid-transfer protein (PLTP), the cholesterol-ester transfer protein (CETP), and the cholesterol-ester transfer protein intestinal isoform (CETPI) discovered by our group^{17–19}.

CETP corresponds to a plasma protein involved in the transfer of triacylglycerols and cholesterol-esters between lipoproteins, showing a critical role in the homeostasis of cholesterol metabolism and therefore being responsible for the reverse transport of cholesterol^{20–22}. Several years ago, studying this protein, our group discovered the presence in the human plasma of a new variant of CETP, called at that time cholesterol-ester transfer protein isoform from the intestine or CETPI¹⁷. Since then, we have reported that CETPI shares a very high degree of structural conservation with respect to CETP (~96%) while maintaining the same secondary and tertiary structures. The only difference found between these proteins resides in a change in the last 23 amino acids of the carboxy-end segment of CETP. Interestingly, despite being almost identical, this minimal difference allows both proteins to perform completely different functions²³.

By using a series of synthetic peptides derived from the carboxy-end segment of CETPI, we have established an important LPS binding property for this new protein. Therefore, employing a synthetic peptide containing 18 amino acids derived from this carboxy-end segment of CETPI (named VSAK for its first amino-end four amino acids), we have described that the interaction between peptide VSAK and LPS can neutralize LPS induced toxicity in vitro as well as in vivo. Moreover, the in vivo administration of peptide VSAK in an experimental animal model of septic shock, demonstrated that the intravenous administration of this peptide prevents the harmful effects of LPS associated with the development of this acute clinical condition¹⁸. As an extension of these results, the present investigation considered as proof of concept has allowed us to further test the in vivo action of peptide VSAK in LPS treated experimental animals using Positron Emission Tomography (PET), by measuring glucose metabolism through 2-deoxy-2-[¹⁸F]fluoro-D-glucose ([¹⁸F]FDG) tissue uptake in parallel with the study of pro-inflammatory cytokines, plasma glucose, and insulin. [¹⁸F]FDG corresponds to a radiolabeled glucose analogue that is actively incorporated into the cell through glucose transporters (GLUTs), then phosphorylated by hexokinases to FDG-6-phosphate, and trapped within the cell. The uptake of this radiotracer reflects tissue glucose uptake and metabolism.

Results

Peptide VSAK prevents the deleterious effects of circulating LPS allowing a normal tissue [¹⁸F]FDG permeation in a model of the systemic inflammatory response syndrome. Images were generated from data obtained during the PET experiment by using a dynamic scan data acquisition format (Fig. 1A). These images correspond to total [¹⁸F]FDG uptake observed at the end of the experiment (minute 70) in a representative animal from each experimental group (Fig. 1B, Supplementary Videos S1–S4)). Control groups consist of animals injected only [¹⁸F]FDG, or peptide VSAK (Fig. 1B, Supplementary Videos S1–S2). Consistently with the three animals studied, an important decrease in [¹⁸F]FDG uptake was observed in the LPS treated group with respect to controls (Fig. 1B, Supplementary Video S3). Remarkably, animals injected in the opposite ears within a 1-min interval with LPS and peptide VSAK, present [¹⁸F]FDG uptake values qualitatively similar to images seen in the control groups, demonstrating the LPS buffering capability of peptide VSAK (Fig. 1B, Supplementary Video S4).

Quantitative analysis performed on intestine and liver tissues from this set of animals is shown in Fig. 1C,D. Standard Uptake Values (SUV) for these tissues were normalized using the first 10 min as basal uptake. Related to the number of samples measured, although no statistical differences were found among experimental groups when SUV for [¹⁸F]FDG is measured in the intestine, there is an interesting trend showing an attenuation from the LPS effects carried out by peptide VSAK (Fig. 1C), results that agree with the PET images shown earlier.

When SUV for [¹⁸F]FDG from animals treated under the same referred experimental conditions was measured in the liver at 25 and 40 min after the start of the experiment, there are no significant differences in [¹⁸F]FDG uptake (Fig. 1D). Nevertheless, after 55 min had elapsed, a significant recovery in [¹⁸F]FDG uptake was found between the LPS and the VSAK + LPS group. These differences, maintained until the end of the experiment (70 min), again, are consistent with the PET images shown in Fig. 1B.

Since this experiment did not seem to present clear differences between experimental groups during the time frames evaluated, including the first 10 min of basal PET data acquisition, a second experiment was designed applying the administration of [¹⁸F]FDG and treatments at time zero, increasing the LPS concentration used, and the PET acquisition time from 70 to 90 min.

This new set of experiments employing a higher LPS dose (450 ng/kg) was conducted to evaluate the potential neutralizing effect of peptide VSAK under LPS saturating conditions (Fig. 2A). PET images from this experiment are shown in Fig. 2B, and supplementary videos S5–S8. In accordance to results obtained during the first experiment, a similar response can be observed, where tissue [¹⁸F]FDG perfusion dramatically drops when a higher

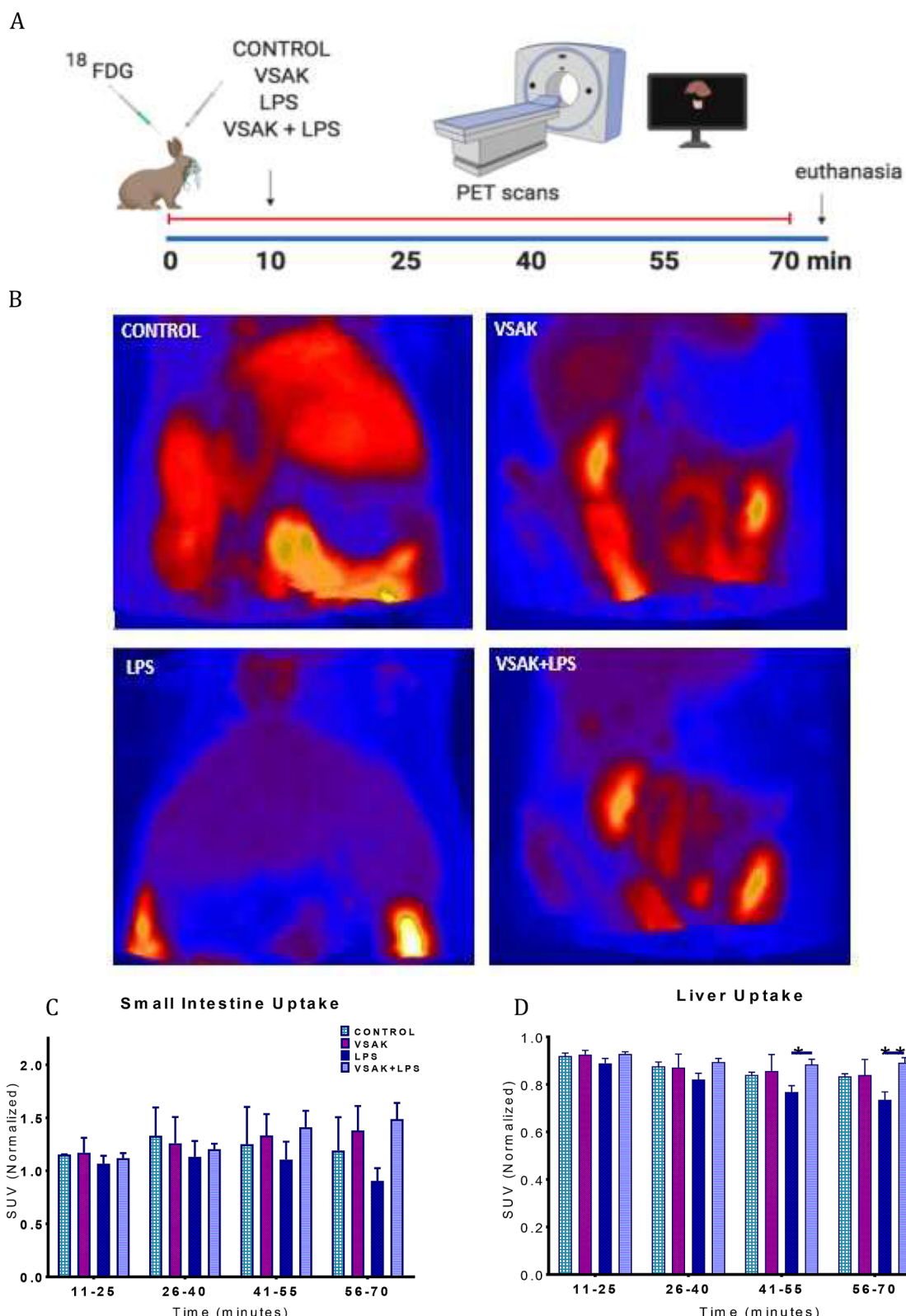


Figure 1. Systemic [¹⁸F]FDG uptake after the administration of LPS (300 ng/kg) and/or peptide VSAK (60 µg/kg). (A) Schematic representation showing the administration of treatments and PET acquisition procedures. (B) PET images showing the global [¹⁸F]FDG uptake of representative experimental rabbits during a 70 min acquisition time. Quantitative analysis for the small intestine (C) and the liver (D) during the different time intervals of PET acquisition (mean of normalized SUV ± SEM). Statistical differences were found in the liver between the LPS and LPS + VSAK groups at 55 min ($p=0.027^*$) and 70 min ($p=0.002^{**}$). Control, VSAK; LPS and VSAK + LPS groups, $n=3$ for each group. Differences assessed using two-way ANOVA with Tukey's multiple comparison tests.

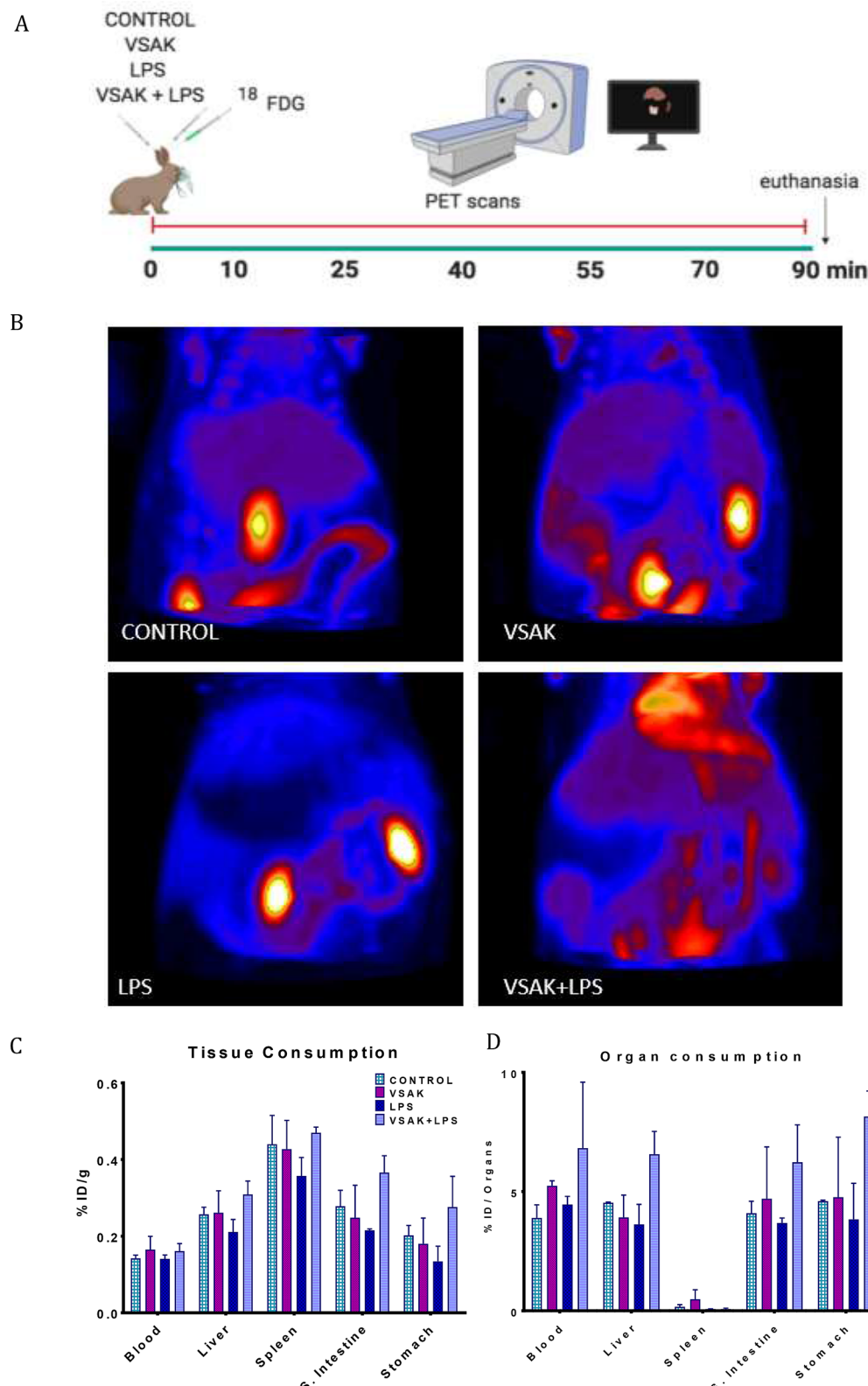


Figure 2. Systemic $[^{18}\text{F}]$ FDG uptake after the administration of LPS (450 ng/kg) and/or peptide VSAK (60 $\mu\text{g}/\text{kg}$). (A) Schematic representation showing the administration of treatments and PET acquisition procedures. (B) PET images showing the global $[^{18}\text{F}]$ FDG uptake of representative experimental rabbits during the 90-min acquisition time. (C) The quantitative analysis expressed as a percentage of the injected dose per gram of tissue (%ID/g). (D) percentage of injected dose per organ (%ID/organ). Control, VSAK; LPS and VSAK + LPS groups, $n = 3$. Differences assessed using two-way ANOVA with Tukey's multiple comparison tests.

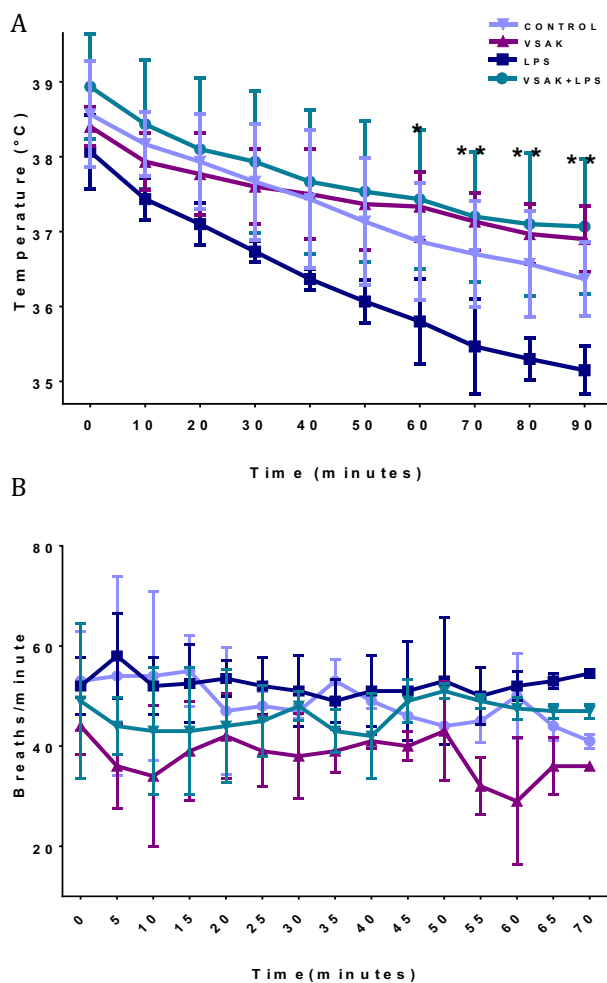


Figure 3. Vital signs of experimental animals under treatment with LPS (450 ng/kg) and/or peptide VSAK (60 µg/kg) registered throughout the PET study. (A) Temperature recordings were obtained every 5 min during the 90-min duration of the experiment. At 60 min significant differences started to be seen: LPS / VSAK + LPS groups ($*p=0.03$). Between 70–90 min: LPS / VSAK groups ($**p=0.007$); LPS / VSAK + LPS groups ($**p=0.003$). Control, VSAK; LPS and LPS + VSAK groups, $n=3$. (B) Respiratory frequency ($n=3$). Differences assessed using two-way ANOVA with Tukey's multiple comparison tests.

LPS concentration is used (Fig. 2B, Supplementary Video S7). This decrease in glucose perfusion is countered with the intravenous injection of peptide VSAK (Fig. 2B, Supplementary Video S8).

As shown in Fig. 2C, a direct measurement of Specific Tissue Activity (%ID/tissue) and Specific Organ Consumption (%ID/organ) from the same set of experimental animals was carried out in whole organs and samples from blood, liver, spleen, small intestine, and stomach (Fig. 2C,D). Even though due to the number of animals studied, no statistical significance was found among groups in both types of analysis, there is a clear tendency for LPS to decrease [^{18}F]FDG uptake, a situation that is reversed by the infusion of peptide VSAK. Again, there seems to be a protective trend against the action of LPS caused by the presence of peptide VSAK in circulation. Also, body temperature and respiratory frequency of animals from the different experimental groups were measured along with the PET experiments (Fig. 3). Although most probably due to the effect of the anesthetic, a continuous decrease in temperature could be observed in all animals from the different groups, there is a tendency for body temperature to decrease in all groups, and specially in the LPS group. At the end of the experiments, this last group showed severe hypothermia, a situation that was prevented when experimental animals were treated with peptide VSAK (Fig. 3A). These results indicate the ability of peptide VSAK to attenuate the continuous drop in temperature associated with hypothermia during the establishment of SIRS. On the other hand, since the parameter of respiratory frequency was employed to adjust the dosage of anesthetic and as an indicator of the effect of anesthesia during the procedure, there are no apparent changes between groups. Nevertheless, the group of animals treated with LPS and peptide VSAK seemed to present lower respiratory frequency values in comparison to the other groups (Fig. 3B).

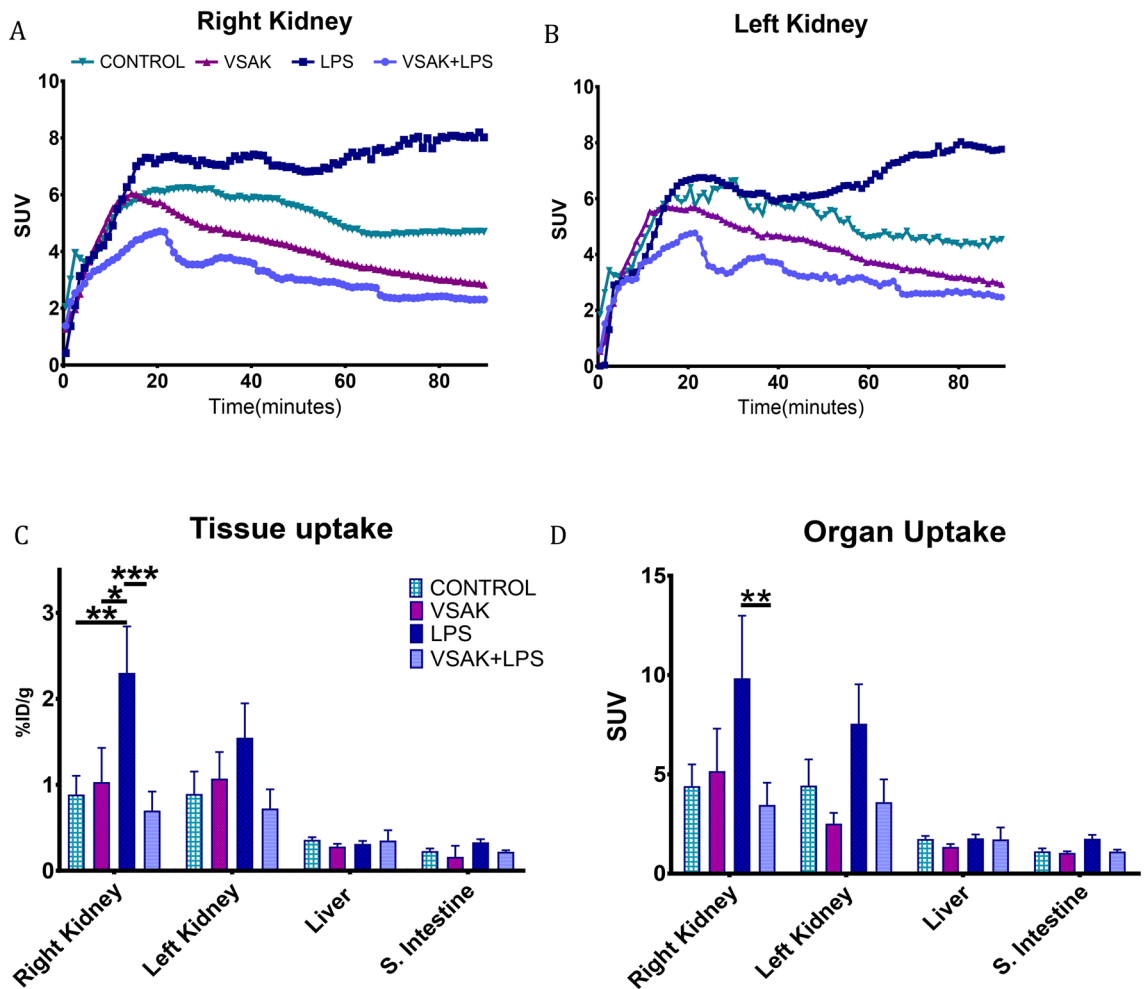


Figure 4. SUV analysis of organ throughout the experiment using 1-min frames. (A) Right kidney. LPS (7.33 ± 3.09); LPS + VSAK groups (2.77 ± 0.64) at minute 60 (* $p=0.04$). This difference was maintained during the 90 min of the experiment. VSAK (2.82 ± 1.42); LPS (8.02 ± 4.61) (* $p=0.04$); LPS + VSAK (2.3 ± 0.76) (** $p=0.008$). (B) Left kidney. (C) Percentage comparison of injected doses (%ID/g) observed in the kidney, liver, and small intestine. Right kidney: (** $p=0.005$); (* $p=0.013$); (** $p=0.0005$). Although a similar behavior was observed in the left kidney, non-significant differences were found. (D) SUV analysis. Right kidney; (* $p=0.0085$). (n = 3 in all groups studied). Differences assessed using two-way ANOVA with Tukey's multiple comparison tests.

Since a limitation of our study might be the number of experimental animals employed, it has to be mentioned that although a series of preliminary experiments were performed, these experiments that were not included in the study we report, showed the same protective role exerted by peptide VSAK upon LPS derived SIRS.

Peptide VSAK prevents an increase in glucose reuptake by the kidney. Changes in glucose renal reuptake were analyzed with data obtained from the kidneys of animals in all experimental groups (Fig. 4A,B). Although during the analysis of data throughout the 90-min duration of the PET experiments, we found slight differences in reuptake between the right and left kidneys, the group including LPS treated animals showed the highest value of kidney glucose reuptake. In contrast, over time, control groups show that renal glucose reuptake tends to decrease. Interestingly, the LPS/peptide VSAK group showed the lowest reuptake values. This result is most probably related to the fact that this group of animals presented a normal tissue glucose uptake, very much similar to what it is found with control groups.

To corroborate the effect observed in SUV through time, total values from both kidneys were studied in parallel to the liver and intestine (Fig. 4C,D). This analysis was performed using data acquisition parameters to obtain total %ID/cc and SUV from each organ. Following the previous analysis, we observed that the highest values for these parameters calculated in both kidneys correspond to the LPS treated group. Moreover, the protective effect carried out by the administration of peptide VSAK concomitantly with LPS is kept in all tissues studied. In concordance to the PET images presented earlier, the liver and the intestine showed much lower SUV and %ID/cc values than kidneys.

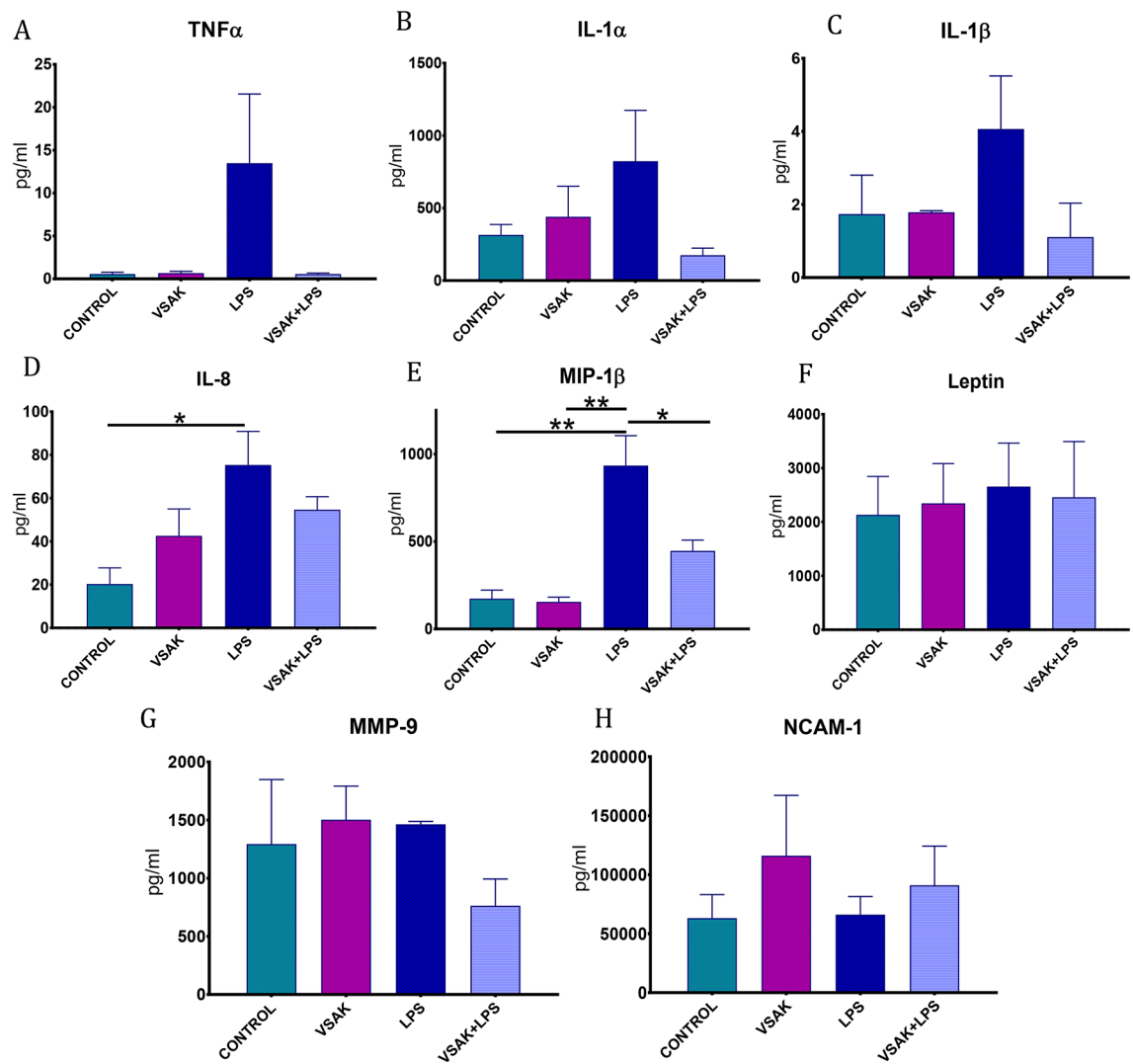


Figure 5. Quantitative estimation of pro-inflammatory cytokines in the plasma of rabbits treated with LPS (450 ng/kg). (A) TNF α . (B) IL-1 α . (C) IL-1 β . (D) IL-8. (* $p = 0.03$). (E) MIP-1 β . Control / LPS groups (** $p = 0.002$), LPS / LPS + VSAK groups (* $p = 0.027$). (F) Leptin. (G) MMP-9. (H) NCAM-1. Control, VSAK; LPS and VSAK + LPS groups, n = 3. Differences assessed using one-way ANOVA with Tukey's multiple comparison tests.

Peptide VSAK reduces the level of pro-inflammatory molecules in circulation. The level of a series of circulating cytokines investigated in all experimental groups directly associated with the pro-inflammatory response during the process of sepsis and septic shock are shown in Fig. 5. Studying the same animal groups employed for the PET analysis, we observed that while control groups show low levels of TNF α , IL-1 α , IL-1 β , IL-8, and MIP-1 β , the group of animals treated with LPS importantly increases the level of these cytokines. Interestingly, this response is prevented when peptide VSAK is in parallel infused with LPS.

When the circulating levels of Leptin, MMP-9, and NCAM-1 were measured in the different groups of animals, no differences among groups were observed. Nevertheless, the level of TNF- α that dramatically increases in the LPS treated group, is completely prevented by the intravenous infusion of peptide VSAK, as consistently observed by us¹⁸.

To further correlate the observation made by PET associating the neutralization of LPS carried out by peptide VSAK and the lowering effect in the levels of circulating cytokines, we also analyzed the levels of circulating glucose and insulin in association with the effects produced by LPS and LPS/peptide VSAK administration (Fig. 6). It can be appreciated that the level of glucose in the LPS group is significantly higher than that observed in the control groups (Fig. 6A). Again, the infusion of peptide VSAK in parallel with LPS allows glucose to be kept at levels similar to the ones measured in control groups. A similar correlation is found when insulin is studied, finding a tendency for insulin to increase in the LPS group and recovery close to control values observed after peptide VSAK treatment (Fig. 6B). Interestingly, despite the high level of insulin shown in animals from the LPS group, these experimental animals show the highest level of circulating glucose, a phenomenon that is prevented by the infusion of peptide VSAK.

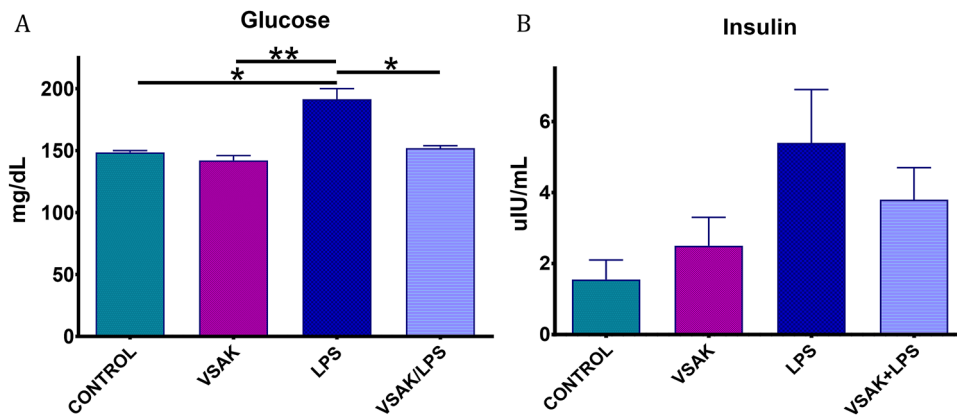


Figure 6. Plasma glucose and insulin levels from experimental rabbits after the administration of LPS (450 ng/kg). (A) Glucose level. (** $p=0.006$; * $p=0.015$). (B) Insulin level. ($n=3$ in all groups studied). Differences assessed using one-way ANOVA with Tukey's multiple comparison tests.

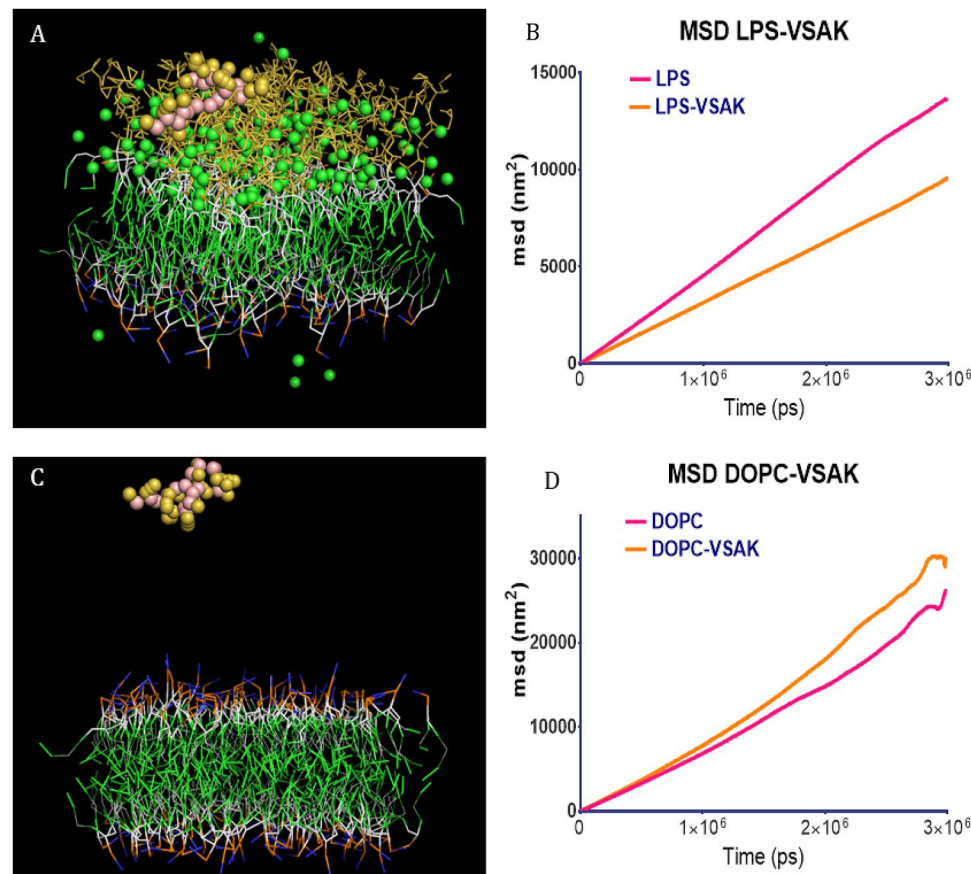


Figure 7. Molecular dynamics simulations employing lipid bilayers composed of LPS and/or DOPC. (A) Snapshot of a bilayer at 2250 ns containing LPS/DOPC interacting with peptide VSAK. (B) Mean square displacement (MSD) analysis of the LPS/DOPC system in the presence or absence of peptide VSAK. (C) Snapshot at 2250 ns of a bilayer made entirely of DOPC in the presence of peptide VSAK. (D) MSD values from the DOPC system in the presence or absence of peptide VSAK.

Molecular dynamics. The use of molecular dynamics has allowed us to start to understand the type of interactions that might be occurring *in vivo* between peptide VSAK and LPS. Figure 7A shows a captured frame of a dynamic system consisting of a bilayer whose external hemi-layer is made up of LPS, while the internal one is made up of DOPC. A simulation image frame obtained at 2250 ns shows peptide VSAK positioned in contact with the external hemi-layer of the bilayer, showing a slight bilayer penetration towards the core area of

LPS. During this simulation, it is observed that once peptide VSAK reaches the bilayer, it remains close to this region restricting its lateral movement (Fig. 7B, Supplementary Video S9). A mean square displacement (MSD) analysis for this set of simulations using a LPS/DOPC composite system shows the center of mass placed on the membrane, while the total movement in the lateral plane (z) analyzed as an indicator of a change in membrane fluidity is decreased by the presence of the peptide (Fig. 7B). Furthermore, to analyze whether this effect is directly related to the presence of LPS, bilayer systems consisting exclusively of DOPC were generated. Figure 7C shows a snapshot frame of one of these systems captured at 2250 ns corresponding to a simulation containing a membrane bilayer system composed of DOPC and no LPS in the presence of peptide VSAK. It is interesting to observe that MSD values are not affected when peptide VSAK apparently does not interact with the membrane (Fig. 7D, Supplementary Video S10).

Discussion

The use of functional imaging techniques such as PET nowadays has had a limited impact on the study of clinical conditions such as infection, sepsis, and septic shock. In many cases, the use of this technique has been limited as a diagnostic support tool when the source of the infection does not have a known origin. In basic research, the use of this technique for the study of these pathologies has also been quite limited and in a similar way to the clinical field, used mainly to study the development of infectious processes *in situ*^{24,25}.

During the present study, we continued with our strategy to use an experimental animal model closer to the human^{26–28}. Although in the past our research group used the New Zealand breed of rabbits to establish the preventive actions of peptide VSAK against the deleterious effects of LPS in experimental septic shock¹⁸, the present study has been carried out employing Dutch dwarf rabbits, that in the adult stage have a similar size to that of an adult Wistar rat. This strategy has permitted us to employ this animal model in a piece of micro PET equipment, originally designed to study mice and rats.

The most noticeable effect found in the experimental group of animals intravenously injected with LPS was the almost total absence of glucose uptake shown by most organs in two independent sets of PET experiments, an observation supported by the quantitative analysis of SUV data and %ID/cc values. Although most differences found to represent a relatively small change in the total capture of radiolabeled-glucose, our results still represent an important event in the context of the whole organism, something common when considering that one of the advantages of functional imaging techniques is to highlight very small variations in the specific region of study. This point is observed after the administration of LPS, associated with an important increase in glucose uptake by the kidneys. This effect became more noticeable as capture time advances reflected in the total uptake data for this organ. Nevertheless, the most dramatic effect found in our study is associated with the group simultaneously treated with LPS and peptide VSAK, where our experimental animals showed normal organ perfusion values and did not present any of the clinical signs associated with SIRS.

The decrease in organ glucose uptake due to the administration of LPS countered by the administration of peptide VSAK is not observed in the kidneys, where because of the administration of LPS an increase in glucose recapture was found. Since it has been proposed this late phenomenon is not associated with a change in the metabolic activity of the kidney²⁹, it can be related to the fact there is an increased recapture of glucose when most organs have become refractory to this sugar. All the changes observed in the uptake of radiotracer upon the administration of LPS, indicate there is an alteration in the mechanisms that regulate the entry of glucose into the cells. This alteration was confirmed by analyzing the circulating levels of glucose and insulin. While a slight increase in insulin associated with an important increase in the circulating level of glucose was observed, a phenomenon frequently related to metabolic dysfunction, the administration of peptide VSAK attenuated the increase of both parameters. Therefore, it is proposed that treatment with peptide VSAK might also prevent the establishment of an insulin-resistance-like condition^{30–32}.

This effect is consistent with observations from the clinical setting, where a transient appearance of insulin resistance is a characteristic event of sepsis and septic shock³³, and where the appearance of hyperinsulinemia and hyperglycemia associated with metabolic dysfunction have been considered as a negative indicator for the prognosis of sepsis and septic shock³⁴. During these clinical conditions, the establishment of an insulin resistance state is associated with the production of pro-inflammatory molecules, whose effects are known to interfere with the normal signaling pathway for insulin^{35–37}. Moreover, the appearance of hypothermia that regularly occurs during the critical phases of sepsis and septic shock³⁸ known to be exacerbated by the use of anesthetics³⁹, can be also related to the progressive decrease in tissue glucose uptake and the alteration of the cellular intermediate metabolism involved in the production of heat⁴⁰. Interestingly, independently of the origin of this harmful clinical sign, the administration of peptide VSAK preventing the onset of hypothermia maintains organs within their normal metabolic homeostasis.

Since there is evidence that hyperglycemia observed during the course of sepsis and septic shock, can be due in part to the inability for glucose to enter the cell, energy deficiency has been proposed among the mechanisms responsible for cell dysfunction in septic shock, where low ATP levels and phosphocreatine/ATP ratios have been associated to non-surviving cases of septic shock^{41,42}. This is supported by clinical studies where, for example, serum glucose measured in children presenting signs of septic shock and high plasma glucose levels, are associated to high mortality rates⁴³. By studying tissue [¹⁸F]FDG incorporation, our study supports the fact that by improving tissue glucose uptake, and in parallel reducing hyperglycemia close to normal levels as achieved here employing peptide VSAK, the chances for survival dramatically improve.

During the course of our study, the analysis of a series of pro-inflammatory molecules known to be involved in the pathophysiology of sepsis and septic shock were also studied. These included TNF α , IL-1 α , IL-1 β , IL-8, MIP-1 β , Leptin, soluble NCAM-1, and MMP-9. Among them, TNF α , IL-1 α , IL-1 β are known to intervene in the development of an acute inflammatory response and therefore associated with the early development of SIRS,

while chemokines MIP-1 β and IL-8 are produced in an intermediate phase of septic shock and associated with the migration of cells from the immune system to sites of infection to promote inflammation. TNF α that presents a central role in the response that leads to sepsis and septic shock, has been directly involved in the host's response to LPS mediated by the TLR4 receptor⁴⁴, and also associated to the development of insulin resistance^{45–47}.

The analysis of these pro-inflammatory markers was completed with Leptin, MMP-9, and NCAM-1. Unlike cytokines and chemokines, these molecules are associated with the later stages in the development of the inflammatory process. Since the analysis of these last three molecules showed no significant changes among the various groups of experimental animals studied, it can be considered that our model of SIRS corresponds to an acute model where the late phases of sepsis and septic shock are still not reached⁴⁸.

Interestingly, except for these three molecules, TNF α , IL-1 α , IL-1 β , IL-8, and MIP-1 β showed an important increase in their circulation level after the infusion of LPS, a response that is avoided if peptide VSAK is concomitantly administered. As shown before by us, TNF α one of the pro-inflammatory cytokines that importantly increase with LPS treatment is kept at basal control levels if peptide VSAK is employed, supporting the view that attenuation of the various pro-inflammatory molecules carried out by peptide VSAK occurs during the early stages of the inflammatory process. The potential beneficial effects of peptide VSAK during the late stages of SIRS will have to be further studied.

On the other hand, to explain not only the *in vitro* but the *in vivo* effects observed after the administration of peptide VSAK, we believe it is important to understand first the type of interactions that may occur between peptide VSAK and LPS. Therefore, in this study, we also decided to tackle this phenomenon through the use of molecular dynamics. Coarse grain molecular dynamics of VSAK peptide studied in association with LPS/DOPC composite systems shows there is a decrease of peptide displacement in the lateral plane of the membrane (MSD) representative of the membrane fluidity, in contrast to the normal displacement value when peptide VSAK interacts with a membrane composed only of DOPC. This result supports the possibility that interactions between peptide and LPS already located in a membrane, might be able to decrease membrane fluidity that in turn could interfere with the harmful cascade of cellular events known to be carried out by LPS^{49,50}.

The modulating effect of peptide VSAK showed in this study acquires special importance when considering that several of the experimental treatments investigated and designed to counteract sepsis and septic shock have failed during their study in clinical phases due mainly to the presence of immunosuppression^{51–54}. The LPS-neutralizing effect shown by peptide VSAK raises the possibility for the use of this peptide as a therapeutic agent in conjunction with the standard treatment approaches during the acute stages of SIRS in seriously ill patients at the intensive care unit^{55,56}.

Materials and methods

Study design. Based on the fact that VSAK peptide can bind LPS, the goal of the present study was to find additional evidence concerning the possibility that the intravenous administration of peptide VSAK results in a protective measure for animals exposed to LPS in a model of SIRS. In this study, we used as an experimental model, Dutch dwarf rabbits, found by us to be an appropriate model to evaluate the systemic effects of the administration of LPS employing micro-PET imaging. Since our investigation has been designed as an endpoint study, fluid resuscitation employing iso-osmolar crystalloid solutions which is a standard in patient management, was not carried out. Also, as a limitation of the study, it has to be mentioned that taking into account the duration of each experiment, and the fact that LPS are administered almost at the same time with peptide VSAK, our model is not 100% reflective of a clinical situation.

Reagents. Purified LPS from *Escherichia coli* O111: B4 was purchased from Sigma-Aldrich (St. Louis, MO, USA; Cat. L2630). LPS were solubilized at a final concentration of 10 mg/ml in glucose-free Krebs-Ringer buffer (125 mM NaCl, 2.5 mM KCl, 1.25 mM NaH₂PO₄, 2 mM CaCl₂, 1 mM MgCl₂, 25 mM NaHCO₃), at pH 7.4. VSAK peptide (VSAKPLSARSPGGRPLSP) was synthesized by GenScript USA Inc., (Piscataway, NJ, USA) with a purity of 98%. Peptide VSAK was diluted in PBS buffer at a final concentration of 1 mg/ml. The radiotracer 2-[¹⁸F]-fluoro-2-deoxy-D-glucose ([¹⁸F]FDG) was synthesized and provided by the Radiopharmacy-Cyclotron Unit located at Facultad de Medicina, Universidad Nacional Autónoma de México.

Experimental animals. All procedures with experimental animals were performed following the Guide for Care and Use of Laboratory Animals from the NIH, and the current Mexican Official Norm for the Use of Laboratory Animals (NOM-062-ZOO-199). All experimental protocols were revised and approved by the Animal Care and Use Committee of Instituto de Fisiología Celular, Universidad Nacional Autónoma de México (Protocol JMO2017-17).

Twenty-four male Dutch dwarf rabbits (45 days old) were purchased from a local certified farm. Rabbits were maintained in a quarantine period for 15 days under controlled conditions of temperature, humidity, light-dark cycles, and ad libitum access to food and water. Before the microPET assays, animals fasted for 12 h and were weighed 1 h before the start of the experiments to precisely estimate the corresponding doses of the radiotracer. All procedures were performed under gaseous anesthesia (isoflurane) administered through a breathing mask along with oxygen. For anesthesia induction, rabbits were placed in a closed chamber and administered with 5% isoflurane. The dose of anesthetic was adjusted using the respiratory rate that was kept at 50–60 breaths per minute and maintained with 1–2.5% isoflurane during the scan acquisitions. To prevent a drastic temperature drop caused by the anesthetic, animals were covered with a thermal coat during PET scans.

Experimental procedures. Rabbits were randomly assigned to four different experimental groups: Control, VSAK treatment, LPS treatment, and VSAK + LPS treatment. All treatments were administered via the

marginal veins of the ears. For the first experiment, the control group was administered only with a saline solution, and the VSAK/control group administered 60 µg/kg of the peptide, as previously reported¹⁸. Animals from the LPS group were administered with 300 ng/kg LPS, and the VSAK + LPS group administered with 60 µg/kg of peptide VSAK and 300 ng/kg LPS. For the first experiment, animals were first administered with [¹⁸F]FDG and 10 min later received the corresponding treatment. For the second experiment, doses for control and VSAK groups were administered as followed for the first experiment, whereas the LPS doses were adjusted to 450 ng/kg. For this experiment, animals were simultaneously administered with peptide VSAK and LPS on different ears. Once the animals received the treatments, they were administered [¹⁸F]FDG and microPET images acquired.

MicroPET equipment. The equipment employed for this study corresponds to a third-generation micro-PET Focus 120 Scanner (CTI-Concorde Microsystems LLC, Knoxville, TN, USA), designed for small animals. The microPET scanner is provided with a detection ring of 15 cm diameter with an array of 96 detector blocks, each of them consisting of a 12 × 12 array of lutetium oxyorthosilicate (LSO) crystals coupled to position-sensitive photomultiplier tubes. The equipment provides a field of view (FOV) of 7.6 cm by 11 cm in axial and transversal directions, respectively.

Data acquisition. Before [¹⁸F]FDG administration, anesthetized experimental animals were placed in the scanner bed and the FOV centered in the area between the apex of the heart and the topside of the bladder. With this alignment, the liver, kidneys, and part of the small intestine can be studied. After the radiotracer is intravenously administered, dynamic PET data starts in list mode.

For the first set of experiments, PET data were acquired for 70 min considering the administration of [¹⁸F]FDG as zero time. After this time had elapsed, a blood sample was obtained by cardiac puncture and animals euthanized with an overdose of pentobarbital. For the second experiment employing 450 ng/kg LPS, PET data were acquired for 90 min after the administration of [¹⁸F]FDG. At the end of both experiments, blood samples were collected as well as samples from the liver, small intestine, spleen, and kidneys. For the second experiment, collected organs were weighed to estimate the total uptake of the radiotracer. All tissue samples were stored in liquid nitrogen.

Image reconstruction and data analysis. PET images were reconstructed in a 3D mode with the ordered subset expectation maximization algorithm OSEM3D. Data analysis was carried out using spherical areas of 5 mm diameter to define the volume of interest (VOI) and to get the standardized uptake value (SUV) of the indicated organ. The 70 min scan acquisition data were analyzed in five frames: the first one comprising the initial 10 min (0–10 min), followed by four frames of 15 min each (10–25, 25–40, 40–55, and 55–70 min). To determine the percentage-injected dose per gram of tissue (%ID/g), density values of 1 g/cm³ were considered for all organs. Data from the first set of experiments were normalized with the SUV corresponding to the frame 0 to 10 min for each animal. To obtain the SUV of the second set of experiments, the data corresponding to 90 min of observation, were analyzed in 1-min frames. SUV estimations were obtained from the VOI data corresponding to the 90 min acquisition time. Image quantification was performed by the same person who acquired the images.

Measurement of pro-inflammatory cytokines. The antibody rabbit cytokine array 1 from Raybiotech (Norcross, GA, USA; Cat. QAL-CYT-1) was used to carry out the specific measurement of ten pro-inflammatory cytokines in serum samples, according to the manufacturer's instructions. The glass slide spotted with 28 wells was read in a microarray reader GenePix 4000B (Molecular Devices, San Jose, CA, USA) selecting the green channel for Cy3 at the 532 nm excitation wavelength. The fluorescence standard curves and quantitation of serum samples were processed with the GraphPad Prism software (GraphPad Software, San Diego, CA, USA).

Insulin and glucose measurements. The insulin and glucose levels were determined in serum by a certified clinical laboratory specialized in the management of animal samples (Laboratorios AIMS, ISO 15,189).

Molecular dynamics. For the study of molecular dynamics, we used a model of peptide VSAK generated by the I-TASSER server⁵⁷, at the highest TM server reporter. Simulations were performed employing a series of lipid bilayer systems generated by the CHARMM-GUI server and the MARTINI 22p modified forcefield^{58,59}. This forcefield allowed us the use of a polarizable water model and charged amino acids. For simulations, two different bilayers were constructed, the first one consisting of an array of 36 LPS molecules in the outer leaf and 92 molecules of DOPC in the inner leaf. The second one consisted of 92 DOPC molecules in both hemi-halves of the membrane. All simulations were performed for 3000 ns, and at the start, peptides were collocated at 30 Å above the top of the membrane. We analyzed the mean square displacement (MSD) in the lateral plane of the bilayers, as an indicator of membrane fluidity.

Statistical analysis. All statistical tests were performed with the GraphPad Prism software. Standard uptake value SUV, %ID, and temperature data were processed with a two-way ANOVA. Insulin, glucose, and cytokine measurements were evaluated by a one-way ANOVA. Statistical significance was considered at $p < 0.05$.

Received: 19 August 2020; Accepted: 7 July 2021
Published online: 20 July 2021

References

- Cecconi, M., Evans, L., Levy, M. & Rhodes, A. Sepsis and septic shock. *Lancet* **392**, 75–87 (2018).
- Singer, M. *et al.* The third international consensus definitions for sepsis and septic shock (sepsis-3). *JAMA* **315**, 801 (2016).
- Angus, D. C. & van der Poll, T. Severe sepsis and septic shock. *N. Engl. J. Med.* **369**, 840–851 (2013).
- López-Bojórquez, L. N., Dehesa, A. Z. & Reyes-Terán, G. Molecular mechanisms involved in the pathogenesis of septic shock. *Arch. Medical Res.* **35**, 465–479 (2004).
- Delano, M. J. & Ward, P. A. Sepsis-induced immune dysfunction: can immune therapies reduce mortality?. *J. Clin. Invest.* **126**, 23–31 (2016).
- Osuchowski, M. F. *et al.* Minimum quality threshold in pre-clinical sepsis studies (MQTiPSS): an international expert consensus initiative for improvement of animal modeling in sepsis. *Int. Care Med. Exp.* **6**, 26 (2018).
- Gentile, L. F. & Moldawer, L. L. DAMPs, PAMPs, and the origins of SIRS in bacterial sepsis. *Shock* **39**, 113–114 (2013).
- Tsujimoto, H. *et al.* Role of toll-like receptors in the development of sepsis. *Shock* **29**, 315–321 (2008).
- Jackson, J. J. & Kropf, H. β -Lactam Antibiotic-Induced Release of Free Endotoxin: In Vitro Comparison of Penicillin-Binding Protein (PBP) 2-Specific Imipenem and PBP 3-Specific Ceftazidime. *J. Infect. Dis.* **165**, 1033–1041 (1992).
- Jerala, R. Structural biology of the LPS recognition. *Int. J. Med. Microbiol.* **297**, 353–363 (2007).
- Rittirsch, D., Flierl, M. A. & Ward, P. A. Harmful molecular mechanisms in sepsis. *Nat. Rev. Immunol.* **8**, 776–787 (2008).
- Beutler, B. & Rietschel, E. T. Innate immune sensing and its roots: the story of endotoxin. *Nat. Rev. Immunol.* **3**, 169–176 (2003).
- Kaconis, Y. *et al.* Biophysical mechanisms of endotoxin neutralization by cationic amphiphilic peptides. *Biophys. J.* **100**, 2652–2661 (2011).
- Bingle, C. D. & Craven, C. J. PLUNC: a novel family of candidate host defence proteins expressed in the upper airways and nasopharynx. *Hum. Mol. Genet.* **11**, 937–943 (2002).
- Bingle, C. D. & Craven, C. J. Meet the relatives: a family of BPI- and LBP-related proteins. *Trends Immunol.* **25**, 53–55 (2004).
- Ghafouri, B., Kihlström, E., Tagesson, C. & Lindahl, M. PLUNC in human nasal lavage fluid: multiple isoforms that bind to lipopolysaccharide. *Biochim. Biophys. Acta Proteins Proteomics* **1699**, 57–63 (2004).
- Alonso-García, A. L., Zentella-Dehesa, A. & Mas-Oliva, J. Characterization of a naturally occurring new version of the cholesterol ester transfer protein (CETP) from small intestine. *Mol. Cell. Biochem.* **245**, 173–182 (2003).
- García-González, V., Gutiérrez-Quintanar, N. & Mas-Oliva, J. The C-terminal domain supports a novel function for CETPI as a new plasma lipopolysaccharide-binding protein. *Sci. Rep.* **5**, 16091 (2015).
- Luna-Reyes, I., Pérez-Hernández, E., Ávila-Rodríguez, M. Á. & Mas-Oliva, J. P38 the process of septic shock is attenuated by the intravenous administration of peptide VSAK: A FDG-PET study, sepsis 2018. *Intensive Care Med. Exp.* **6**, 1–33 (2018).
- Beamer, L. J., Carroll, S. F. & Eisenberg, D. Crystal structure of human BPI and two bound phospholipids at 2.4 angstrom resolution. *Science* **276**, 1861–4 (1997).
- Qiu, X. *et al.* Crystal structure of cholesteryl ester transfer protein reveals a long tunnel and four bound lipid molecules. *Nat. Struct. Mol. Biol.* **14**, 106–113 (2007).
- Eckert, J. K. *et al.* The crystal structure of lipopolysaccharide binding protein reveals the location of a frequent mutation that impairs innate immunity. *Immunity* **39**, 647–660 (2013).
- García-González, V. *et al.* Key structural arrangements at the C-terminus domain of CETP suggest a potential mechanism for lipid-transfer activity. *J. Struct. Biol.* **186**, 19–27 (2014).
- Via, L. E. *et al.* Infection dynamics and response to chemotherapy in a rabbit model of tuberculosis using [¹⁸F]2-fluoro-deoxy-D-glucose positron emission tomography and computed tomography. *Antimicrob. Agents Chemother.* **56**, 4391–4402 (2012).
- Odekerken, J. C. E. *et al.* (18)F-FDG microPET imaging differentiates between septic and aseptic wound healing after orthopedic implant placement: a longitudinal study of an implant osteomyelitis in the rabbit tibia. *Acta Orthop.* **85**, 305–313 (2014).
- Wichterman, K. A., Baue, A. E. & Chaudry, I. H. Sepsis and septic shock—a review of laboratory models and a proposal. *J. Surg. Res.* **29**, 189–201 (1980).
- Poli-de-Figueiredo, L. F., Garrido, A. G., Nakagawa, N. & Sannomiya, P. Experimental models of sepsis and their clinical relevance. *Shock* **30**, 53–59 (2008).
- Fink, M. P. Animal models of sepsis. *Virulence* **5**, 143–153 (2014).
- Mather, A. & Pollock, C. Glucose handling by the kidney. *Kidney Int.* **79**, S1–S6 (2011).
- Clowes, G. H. A. *et al.* Blood insulin responses to blood glucose levels in high output sepsis and septic shock. *Am. J. Surg.* **135**, 577–583 (1978).
- Clemens, M. G., Chaudry, I. H., Daigneau, N. & Baue, A. E. Insulin resistance and depressed gluconeogenic capability during early hyperglycemic sepsis. *J. Trauma* **24**, 701–708 (1984).
- Carlson, G. L. Insulin resistance in sepsis. *Br. J. Surg.* **90**, 259–260 (2003).
- Marik, P. E. & Raghavan, M. Stress-hyperglycemia, insulin and immunomodulation in sepsis. *Intensive Care Med.* **30**, 748–756 (2004).
- Schetz, M. *et al.* Tight blood glucose control is renoprotective in critically ill patients. *J. Am. Soc. Nephrol.* **19**, 571 (2008).
- Lassenius, M. I. *et al.* Bacterial endotoxin activity in human serum is associated with dyslipidemia, insulin resistance, obesity, and chronic inflammation. *Diabetes Care* **34**, 1809–1815 (2011).
- Mehta, N. N. *et al.* Experimental endotoxemia induces adipose inflammation and insulin resistance in humans. *Diabetes* **59**, 172–181 (2010).
- Nieto-Vazquez, I. *et al.* Insulin resistance associated to obesity: the link TNF-alpha. *Arch. Physiol. Biochem.* **114**, 183–194 (2008).
- Marik, P. E. & Zaloga, G. P. Hypothermia and cytokines in septic shock. *Intensive Care Med.* **26**, 716–721 (2000).
- Díaz, M. & Becker, D. E. Thermoregulation: physiological and clinical considerations during sedation and general anesthesia. *Anesth. Prog.* **57**, 25 (2010).
- Singer, M. Cellular dysfunction in sepsis. *Clin. Chest Med.* **29**, 655–660 (2008).
- Singer, M. The role of mitochondrial dysfunction in sepsis-induced multi-organ failure. *Virulence* **5**, 66–72 (2014).
- Vogt, J. A. *et al.* Effects of glycemic control on glucose utilization and mitochondrial respiration during resuscitated murine septic shock. *Intensive Care Med. Exp.* **2**, 19 (2014).
- Branco, R. G. *et al.* Glucose level and risk of mortality in pediatric septic shock. *Ped. Crit. Care Med.* **6**, 470–472 (2015).
- Lu, Y.-C., Yeh, W.-C. & Ohashi, P. S. LPS/TLR4 signal transduction pathway. *Cytokine* **42**, 145–151 (2008).
- Hoareau, L. *et al.* Signaling pathways involved in LPS induced TNFalpha production in human adipocytes. *J. Inflamm. (Lond.)* **7**, 1 (2010).
- Shi, H. *et al.* TLR4 links innate immunity and fatty acid-induced insulin resistance. *J. Clin. Invest.* **116**, 3015–3025 (2006).
- Moller, D. E. Potential role of TNF- α in the pathogenesis of insulin resistance and type 2 diabetes. *Trends Endocrinol. Metab.* **11**, 212–217 (2000).

48. Devi Ramnath, R. *et al.* Inflammatory mediators in sepsis: cytokines, chemokines, adhesion molecules and gases. *J. Organ. Dysfunct.* **2**, 80–92 (2006).
49. Hancock, R. E. W. & Scott, M. G. The role of antimicrobial peptides in animal defenses. *Proc. Natl. Acad. Sci. U. S. A.* **97**, 8856–8861 (2000).
50. Scott, M. G., Vreugdenhil, A. C., Buurman, W. A., Hancock, R. E. & Gold, M. R. Cutting edge: cationic antimicrobial peptides block the binding of lipopolysaccharide (LPS) to LPS binding protein. *J. Immunol.* **164**, 549–553 (2000).
51. Brown, K. *et al.* Neutrophils in development of multiple organ failure in sepsis. *Lancet* **368**, 157–169 (2006).
52. Cohen, J. & Carlet, J. INTERSEPT: an international, multicenter, placebo-controlled trial of monoclonal antibody to human tumor necrosis factor-alpha in patients with sepsis. International Sepsis Trial Study Group. *Crit. Care Med.* **24**, 1431–40 (1996).
53. Cohen, J. *et al.* Sepsis: a roadmap for future research. *Lancet Infect. Dis.* **15**, 581–614 (2015).
54. Opal, S. M. *et al.* Confirmatory interleukin-1 receptor antagonist trial in severe sepsis: a phase III, randomized, double-blind, placebo-controlled, multicenter trial. The interleukin-1 receptor antagonist sepsis investigator group. *Crit. Care Med.* **25**, 1115–24 (1997).
55. Bárcena-Varela, S. *et al.* Coupling killing to neutralization: combined therapy with ceftriaxone/Pep19–2.5 counteracts sepsis in rabbits. *Exp. Mol. Med.* **49**, 345 (2017).
56. Brandenburg, K., Heinbockel, L., Correa, W. & Lohner, K. Peptides with dual mode of action: killing bacteria and preventing endotoxin-induced sepsis. *Biochim. Biophys. Acta Biomembr.* **1858**, 971–979 (2016).
57. Roy, A., Kucukural, A. & Zhang, Y. I-TASSER: a unified platform for automated protein structure and function prediction. *Nat. Protoc.* **5**, 725–738 (2010).
58. Jo, S., Kim, T., Iyer, V. G. & Im, W. CHARMM-GUI: a web-based graphical user interface for CHARMM. *J. Comput. Chem.* **29**, 1859–1865 (2008).
59. Qi, Y. *et al.* CHARMM-GUI martini maker for coarse-grained simulations with the martini force field. *J. Chem. Theory Comput.* **11**, 4486–4494 (2015).

Acknowledgements

We thank M.Sc. Victoria López and V.M.D. Dafne Garduño for experimental assistance and helpful discussions. I.L-R received a scholarship from CONACYT during his M.Sc. studies, and currently is receiving a scholarship from the same source for the development of his Ph.D. studies (45060). E.P-H is currently also receiving a scholarship from CONACYT (465348) in support of her Ph.D. studies.

Author contributions

I.L-R. designed, conducted both in vitro and in vivo experimentation, carried out data analysis and participated in writing the paper. E.G.P-H. participated in all aspects involving in vitro experimentation and discussion of results. B.D-C. participated with the organization of all the logistics of the project, experimentation and discussion of results. M.A.A-R. supervised all PET experimentation, contributed with material, logistics and expert use of the microPET equipment, and participated in data analysis and discussion of results. J.M-O. designed, participated with in depth analysis of results, supervised all aspects of the investigation, and wrote the paper.

Funding

This work was supported by grants awarded to J-M-O from CONACYT (255778), and UNAM-PAPIIT (IN205717 and IN206619). J.M-O thanks Dirección General de Cómputo y de Tecnologías de Información y Comunicación (Universidad Nacional Autónoma de México) for access to the supercomputer Miztli (grant: LANCAD-UNAM-DGTIC-352), and Fundación Miguel Alemán AC through its program Estímulos a Investigaciones Médicas "Miguel Alemán Valdés".

Competing interests

J.M-O. is inventor on patent application PCT/MX2014/00087 related to this study, "Peptides derived from the C-Terminal domain of CETPI as molecules blocking the lipopolysaccharide-induced effect in sepsis and septic shock", submitted to the World Intellectual Property Organization and held by Universidad Nacional Autónoma de México. I.L-R., E.P-H., B.D-C., and M.A.A-R. declare no competing conflict of interest.

Additional information

Supplementary Information The online version contains supplementary material available at <https://doi.org/10.1038/s41598-021-94224-2>.

Correspondence and requests for materials should be addressed to J.M.-O.

Reprints and permissions information is available at www.nature.com/reprints.

Publisher's note Springer Nature remains neutral with regard to jurisdictional claims in published maps and institutional affiliations.



Open Access This article is licensed under a Creative Commons Attribution 4.0 International License, which permits use, sharing, adaptation, distribution and reproduction in any medium or format, as long as you give appropriate credit to the original author(s) and the source, provide a link to the Creative Commons licence, and indicate if changes were made. The images or other third party material in this article are included in the article's Creative Commons licence, unless indicated otherwise in a credit line to the material. If material is not included in the article's Creative Commons licence and your intended use is not permitted by statutory regulation or exceeds the permitted use, you will need to obtain permission directly from the copyright holder. To view a copy of this licence, visit <http://creativecommons.org/licenses/by/4.0/>.

© The Author(s) 2021



ELSEVIER

Archives
of Medical
Research

Archives of Medical Research 52 (2021) 798–807

REVIEW ARTICLE

Peptides as Therapeutic Molecules to Neutralize Gram-negative Bacterial Lipopolysaccharides in Sepsis and Septic Shock

Ismael Luna-Reyes, Eréndira Guadalupe Pérez-Hernández, Blanca Delgado-Coello and Jaime Mas-Oliva

Departamento de Bioquímica y Biología Estructural, Instituto de Fisiología Celular, Universidad Nacional Autónoma de México, Ciudad de México, México

Received for publication July 25, 2021; accepted August 3, 2021 (ARCMED-D-21-00954).

During the last years, infections have become a global health emergency, where the appearance of bacteria highly resistant to traditional antibiotics have set off an alarm worldwide. Moreover, the increased incidence and mortality resulting from its aggravated states, sepsis, and septic shock, have been observed with growing concern. In this context, knowing the need for a new concept for treatment, peptides such as antimicrobial peptides (AMP) and host defense peptides (HDP), have started to show interesting properties in the development of new antimicrobial agents and host response modulatory therapies. Nevertheless, since it is a well-known fact that a peptide-based drug development is a long process that consumes a significant number of resources, recent approaches that tend to mitigate these obstacles, have included the implementation of novel *in silico* strategies for the optimization of naturally occurring AMP and HDP. In this review, we analyze these strategies that seek to improve not only peptide design, but also production, by including the incorporation of computational biology techniques such as molecular dynamics. © 2021 The Authors. Published by Elsevier Inc. on behalf of Instituto Mexicano del Seguro Social (IMSS). This is an open access article under the CC BY-NC-ND license (<http://creativecommons.org/licenses/by-nc-nd/4.0/>)

Keywords: Sepsis, Septic shock, Lipopolysaccharides (LPS), Antimicrobial peptides (AMP), Host defense peptides (HDP), Peptide VSAK.

Introduction

Nowadays, infection has become one of the main concerns in public health. Due to factors such as antimicrobial resistance associated in the last years with a slowdown in the development of new antibiotics, has resulted in an increase in the morbidity and mortality attributable to the absence of new effective treatments (1). Infection-related mortality has been directly associated with the presence of sepsis and septic shock; conditions characterized by the development of a hyper-inflammatory state followed by immunosuppression.

The host response to an infection is mediated through the recognition of pathogen microorganisms, a process that involves the ability of the immune system to recognize molecular structures known as Microorganism-Associated Molecular Patterns (MAMPs) or Pathogen-Associated Molecular Patterns (PAMPs) (2). The recognition of these patterns is carried out through Pattern Recognition Receptors (PRR) grouped in different families, as part of the innate immune system (3). The MAMPs and PRR interaction induces the activation of the innate immune system through signaling pathways leading to inflammatory processes and metabolic changes aimed at the elimination of the pathogen (4). However, during sepsis and septic shock, this response overcomes the host's regulatory mechanisms resulting in an uncontrolled inflammatory response, followed by organ damage and systemic failure (5). In later stages, the initial hyper-inflammatory response concludes in immunosuppression associated with immune

Address reprint requests to: Jaime Mas-Oliva, Departamento de Bioquímica y Biología Estructural, Instituto de Fisiología Celular, Universidad Nacional Autónoma de México, Apartado Postal 70-243, 04510, Ciudad de México, México; Phone: (+52) (55) 56225584; FAX: (+52) (55) 56225611; E-mail: jmas@ifc.unam.mx

system exhaustion (6). Under these circumstances, it can be recognized that the development of new strategies focused on the treatment of both conditions, should consider the regulation of the immune host response, along with the efficient elimination of the pathogen (7–9).

As mentioned earlier, antibiotic resistance has hampered the development of effective antibiotic therapies, the reason why sepsis and septic shock are now recognized as major causes of death worldwide and a public health emergency situation (10,11). Since the development of new antibiotic molecules has been affected by the appearance of cross-resistance to the newest variants of current antibiotics (12,13), the use of peptides represents a viable option in the design and development of new molecules against particular molecular targets to treat sepsis and septic shock (14–16).

Peptides are especially relevant due to the existence of naturally occurring peptides with antimicrobial and immunomodulatory properties (17). Currently, a variety of peptides with this kind of properties have been described in different organisms. In general, these peptides have been called antimicrobial peptides (AMP), based on their antimicrobial properties observed *in vitro* (18). Among AMP, there is a group of peptides that lack antimicrobial properties, but show instead, immuno-regulatory properties over the host immune system. Thus, several authors have classified these peptides into two main groups: AMP, comprising peptides with antimicrobial properties, and host defense peptides (HDP), including peptides without direct antimicrobial properties (19) (Figure 1). The main property of AMP is related to their ability to induce the lysis of microorganisms mainly through direct interaction with the membrane, resulting in an altered permeability, pore formation, and/or changes in the mechanical properties of the membrane. In contrast, HDP exert their action using diverse mechanisms, such as MAMPs neutralization, immune cell recruitment, and a series of activation effects upon the white cell population (20).

Despite the differences between AMP and HDP, peptides included in both groups share similar characteristics; for example, most of them are short peptides between 9 and 50 amino acids showing a positive net charge, associated with an amphipathic character (21). The secondary structure of these molecules shows high variability, with peptides structured as α -helices, β -sheets, extended structures, and mixed conformations including these last structures. In this sense, it seems that HDP presents a major dependence on their primary structure, while changes in the primary structure of AMP, apparently can be better tolerated for function. This difference can be explained by the specificity required for the interactions carried out by HDP, while for AMP, it is instead critical to maintain the charge and the integrity of hydrophobic regions to warranty an efficient interaction with bacterial structures. Given the properties observed with AMP and HDP, they represent

an interesting option as a platform for the development of molecules with the potential to be used as antimicrobial agents and/or therapeutic molecules during the course of sepsis and septic shock (22).

Antimicrobial and Immunomodulatory Properties of AMP

As mentioned before, AMP action lies in the peptide ability to interact with the pathogen microorganism, inducing membrane lysis, or to accomplish peptide internalization (23). These actions are facilitated by the presence of lipids with a negative charge such as lipopolysaccharides (LPS) in Gram-negative bacteria, and lipoteichoic acid (LTA) in Gram-positive bacteria (24). Interestingly, a group of fungi presenting negatively charged molecules in their membranes, also show interaction properties with AMP (25,26).

As a result of the interaction between AMP and the pathogen membrane, peptides induce physicochemical changes in the membrane that provoke pore formation, osmotic changes, membrane fragmentation, and finally, pathogen lysis. Moreover, several AMP have been reported to bind to internal targets to achieve their antimicrobial activities (27–30). The interaction required for AMP action does not need a specific interaction with membrane targets, since usually this binding involves non-specific electrostatic and hydrophobic forces. For example, in Gram-negative bacteria, many AMP are able to interact with LPS through negative charges and the hydrophobic regions located in lipid A (31). These interactions although necessary for AMP action, do not involve specific recognition between AMP and LPS, and therefore can be replicated with other pathogen membranes with similar characteristics (29). This particularity of AMP make bacteria to be less prone to develop resistance against these molecules (26).

In contrast, HDP participate in infection resolution through the modification of the host immune system, showing no microbicide action upon the pathogen (32). Several *in vitro* studies have demonstrated that HDP enhance the host immune cell ability for the clearance of pathogens (33,34). HDP can also influence white cell migration by mechanisms that promote changes in chemokine production, such as CXCL8 (35). Additionally, HDP influence immune cell survival through inhibition of several cell death mechanisms (36). These aspects of HDP action open the possibility to develop strategies to prevent immune exhaustion in the late stages of sepsis.

HDP can also affect the host recognition of pathogens by stimulating or limiting interactions that involve changes in MAMPs that eventually affect their recognition by PRR. The enhancing of the host recognition process involves an increased pro-inflammatory response associated with improved MAMPs recognition properties (30). On the other hand, it is known that HDP mediate immune-regulation

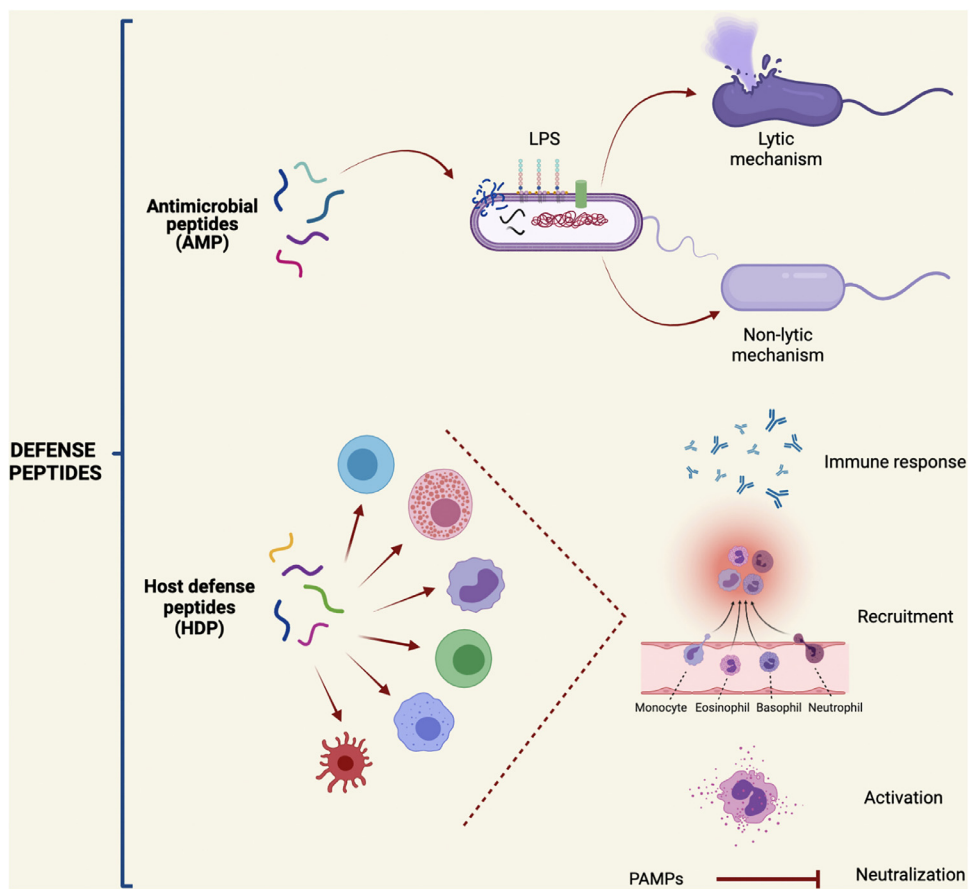


Figure 1. Mechanisms performed by antimicrobial peptides (AMP) and host defense peptides (HDP) to neutralize pathogen microorganism. These groups of short molecules include a myriad of peptides with high structural diversity. Nevertheless, they share common features such as a net positive charge and amphiphilicity. AMP show direct antimicrobial activity through lytic mechanisms involving membrane disruption, or by using non-lytic mechanisms, which usually target intracellular pathogen molecules. HDP contribute by regulating the host response, the modulation of immune cells, and the blocking of PAMPs signaling pathways.

processes based on the ability of peptides to block recognition of MAMPs by PRR (37).

The ability of HDP to block and neutralize MAMPs has been well documented for LPS produced by Gram-negative bacteria. LPS considered one of the most immunogenic MAMPs, are mainly recognized by Toll-like receptor 4 (TLR-4), and associate with several proteins present in circulation (38,39). Since LPS recognition promotes TLR-4 induced inflammation as part of the host response, the presence of LPS in circulation is important in the establishment of sepsis and septic shock. In this scenario, HDP interacting with circulating LPS, but also competing with several other plasma LPS-binding proteins, limit the activation of TLR-4 by LPS (40), and promote other regulatory effects upon the host's immune system (20).

Peptide Therapeutics

Despite the field of peptide therapeutics represents an interesting option for the development of new antimicrobial molecules and novel treatments, the generation of new con-

cepts based on these molecules has not yet reached the expected relevance (41). This phenomenon is partially attributable to outdated policies related to the more common practices of classical drug development. Peptides such as AMP and HDP could be considered a midpoint between a traditional drug developed through chemical synthesis, and a biomolecule, more related to biotechnology. As shown during the early stages of development for pexiganan and omiganan, it is clear that the middle ground between the regulation for drug development, their establishment, and usage, represented an obstacle for their clinical testing (22,42). However, recent changes in the legislation for drug development in the U.S. Food and Drug Administration (FDA), and several European countries, have achieved major changes aimed to improve and ease the development of new antimicrobial drugs. These changes have resulted in initiatives such as FDASIA in the USA, and COMBACTE in Europe (43,44).

At present, the DRAMP 2.0 database, is one of the most complete with more than 20,000 therapeutic peptide entries, where more than seventy trials at different stages

Table 1. Approved peptides with antimicrobial properties

Peptide	Mechanism of Action	Administration	Year
Colistin	Alters external membrane stability through interactions with LPS	Intravenous	1959 (47)
Dalbavancin	Inhibits cell wall synthesis, interfering by cross-linking and polymerization	Topical	2014 (48)
Daptomycin	Alters membrane permeability	Intravenous	1986 (49,50)
Gramicidin	Alters membrane permeability	Topical	1939 (51)
Oritavancin	Inhibits cell wall synthesis	Topical	2014 (52)
Telavancin	Interferes in cell wall peptidoglycan synthesis	Topical	2009 (53)
Vancomycin	Inhibits cell wall synthesis	Intravenous	1958 (54)

of development are included for the clinical application of AMP and HDP (45). Currently, seven peptide-based pharmaceutical products have been approved by the FDA for commercial usage (Table 1) (46–54). Although this might appear as a minor advance in drug development, it represents a noticeable progress in the development of treatments based on AMP and HDP.

Another relevant aspect for peptide development is their design and production. Usually, AMP and HDP are produced by Solid-Phase Peptide Synthesis (SPPS), where the use of advanced computational methods has represented a very useful tool implementing key findings related to peptide structural properties and peptide-ligand interactions.

Since an important group of molecules have been produced as pro-peptides, and therefore are dependent on proteolytic enzymes for their conversion into an active form (55,56), the use of these computational systems has represented a very useful tool in the understanding of their structure in close relationship to their therapeutic targets. Therefore, the design of new AMP and HDP has mainly focused on peptide optimization through a process known as sequence optimization. This process has shown to be extremely useful when considering the study of potential side effects, the reduction of toxicity, the improvement of molecule stability, and the finding of the lowest activity loss, associated to an optimum therapeutic effect (57).

Considering that an important number of AMP and HDP are naturally occurring peptides present in almost all organisms, currently, several databases account for thousands of these peptides. Although these peptides share many characteristics, they also present great variability regarding, for example, primary and secondary structure. Although such variability might represent a major challenge for peptide optimization, the elucidation of the general motifs or structural arrangements needed to produce their optimal effect, will represent an important breakthrough in the design of new molecules (58). In this sense, to improve peptide optimization, there is the need for new strategies related with peptide analysis to generate a structure-function classification for AMP and HDP.

A second major challenge for optimization arises when sequence changes are introduced. These changes could result in improved or reduced activities, associated

to important changes in toxicity and/or stability. Since traditional methods for sequence modification normally present extended time frameworks, and high resource costs, prediction of the net secondary effects following the introduction of sequence changes, is a major issue that needs to be addressed with novel strategies (Figure 2). The implementation of such strategies nowadays involve the use of deep learning and machine learning techniques (59,60). These methods represent viable options for optimization mainly due to the existence of highly complex databases able to feed and develop algorithms oriented to facilitate the operation (61). The incorporation of these methods will undoubtedly facilitate not only the study of structural predictions, but also the relationship structure/function as a guidance in the generation of better candidates as AMP or HDP (21).

On the other hand, the *in vivo* stability shown by AMP and HDP is one of the biggest concerns within the field of peptide therapeutics. Since this type of peptides are mainly short amphipathic molecules, containing a large proportion of positive charges and the lack of bulky structures, make these peptides accessible to attack by the host serum proteases (62). Since protease susceptibility of AMP and HDP is an aspect that needs to be considered for viable treatment development, the introduction of structural modifications addressed to confer proteolytic resistance against serum proteases and pathogen proteases, has lately been implemented. Such modifications include the use of non-naturally occurring amino acid substitutions and peptide cyclization. The substitution of key amino acids in HDP and AMP by non-naturally occurring amino acids such as D-amino acids, can improve endopeptidase resistance by altering recognition of proteolytic sites (63). On the other hand, with certain specific molecules, peptide cyclization confers minimum changes to the overall structure, therefore improving peptide stability and proteolytic resistance as shown for carboxypeptidases and aminopeptidases (64,65). Even though pathogen resistance to AMP is not a common event due in part to the fact that non-specific interactions with AMP require major changes in the targeted pathogen molecules, it is possible to observe adjusted pathogen responses, as in the case of nisin, an effective antimicrobial peptide used for years as a food preservative (66). The main mechanisms of pathogen re-

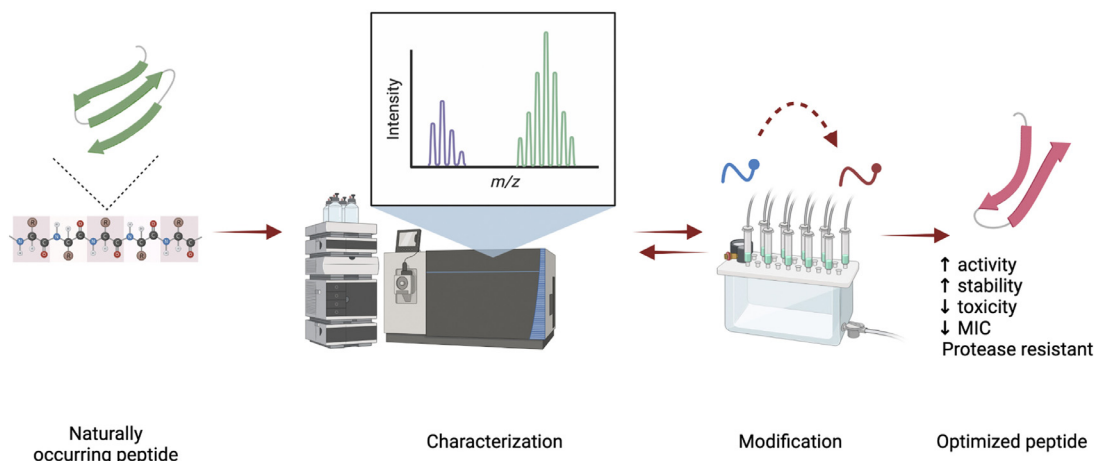


Figure 2. Traditional process employed for peptide design and function optimization. During the peptide optimization process, a naturally occurring peptide is frequently used as a template. After the properties of this peptide are characterized, modifications can take place according to the desirable effects seek after.

sistance present with peptides that localize intracellularly, include peptide extrusion events through membrane pumps (67). Since the presence of membrane pumps represents a major challenge for AMP activity, a combined treatment with pump inhibitors has been visualized as a viable option in the improvement of antimicrobial peptide activity (68,69).

Although several clinical protocols along the development of AMP and HDP have been stopped due to the appearance of side effects (70), these events are usually more related to AMP due to their ability to interact with lipid membranes in general (71). It has been identified that this unspecific interaction, may result toxic for host cells, especially when treatment requires higher doses to achieve a therapeutic effect (27,72). To overcome this kind of risk, it is still necessary to have a better understanding of how peptides might differentially interact between specific lipid membranes from the host, and membranes from the pathogen microorganism (73).

Peptide Production

Even when peptide production seems to be a non-relevant factor in the development of peptide therapeutics, the increase in the demand observed in the last years, has revealed relevant concerns that need to be addressed in the coming years. Among the relevant aspects for improved peptide production are the optimization of SPPS, and the development of new strategies for peptide production (42).

Since as mentioned above, AMP and HDP are frequently produced as pro-peptides or as part of a protein, they require proteolytic cleavage for conversion into their active forms. This fact represents a limitation in the production of candidate peptides, due to the need of specific enzymes required in the production of the functional form (74,75). A different strategy might be the administration

of pro-peptides that can be cleaved by serum proteases to achieve their active form (76). This pathway has been considered a viable option as shown by us during the study of normal volunteers in comparison to patients with signs of infection, sepsis, and septic shock (Pérez-Hernández, EG, et al. 2021, in editorial evaluation). In this sense, we have shown a direct correlation between the severity of the disease and the level of serum proteolysis, allowing peptide VSAK, a LPS-binding peptide derived from the carboxy-end terminal sequence of the Cholesteryl-ester Transfer Protein Isoform (CETPI) synthesized in the intestine, to be present in circulation (77). Therefore, by demonstrating this phenomenon, we have proposed that CETPI and peptide VSAK, can be considered as protective molecules against the deleterious effects of LPS, and also, as a new set of biomarkers useful in the recognition of the progression from infection to sepsis and septic shock (77).

Although SPPS has become the most used method for peptide synthesis, it is clear that laboratory production - possess several problems (72). This technique is a good option for the introduction of peptide modifications, but major concerns are related to yield and production costs. Currently, SPPS yield is less than fifty per cent, depending on the type of synthesized peptide. SPPS consumes an important amount of resources, where the amount of waste increases for longer peptides, resulting in high economic costs (78). Another relevant issue related to SPPS, is the production of toxic waste coming from solvents, anti-racemic agents, and catalytic agents used during the process. Therefore, the need for optimization of SPPS, and the development of environment-friendly compounds that can substitute toxic agents in SPPS, has gained great relevance in recent years (79).

Strategies for the Elucidation of Action Mechanisms

During the last years, the use of computational methods in research has increased in close relationship with an increase in computational power and access to high-performance computers. This situation has favored the development of new software in the implementation of computational methods with better performance and user-friendly interfaces (80,81). Among the computational methods employing high-performance computers that can be used to finely study action mechanisms, and the interactions that underlie peptide efficacy, we find the use of molecular dynamic simulations (MDS), and molecular docking (MDO), to be extremely useful tools for peptide research (82).

MDS are carried out as atomistic simulations or coarse-grained simulations, each one comprising advantages and limitations. Atomistic simulations are based on detailed structure models that allow an accurate study of structural rearrangements and molecule interactions. This kind of systems is suitable for the study of changes in structure induced by sequence modifications in AMP and HDP during their optimization process. Additionally, atomistic simulations permit the study of peptide interactions with lipid structures of moderate size (73,83,84). Nevertheless, atomistic simulation presents as a major limitation the possibility to achieve long simulation times.

On the other hand, even when coarse grain simulation employs less detailed models, this approach is very useful during long time simulations, allowing larger and more complex systems to be studied. Also, this kind of simulation can be suitable for the elucidation of events such as peptide aggregation in membranes, or to help speed up candidate molecule testing (85). Additionally, coarse grain simulations present the potential to study the interaction between AMP and HDP with larger structures, such as LPS or other membrane components of pathogens (86,87). Remarkably, in the last few years, MDS has shown important progress with the improvement in force-field refinement, and software development, offering results with biological relevance.

One such case of MDS has been developed in our laboratory studying peptide VSAK (Figure 3). This peptide contains the last 18 amino acids from the carboxy-end segment of CETPI (named VSAK for its first amino-end four amino acids) (88,89). We used a model of peptide VSAK generated by the I-TASSER server (81). Simulations were performed employing a series of lipid bilayer systems generated by the CHARMM-GUI server and the MARTINI 22p modified force-field (80,90). This force-field allowed us the use of a polarizable water model and charged amino acids. For simulations, different bilayers were constructed consisting of an array of LPS molecules in the outer leaf and molecules of dioleoyl-phosphatidylcholine (DOPC) in the inner leaf (Figure 4). Simulations performed for 3000

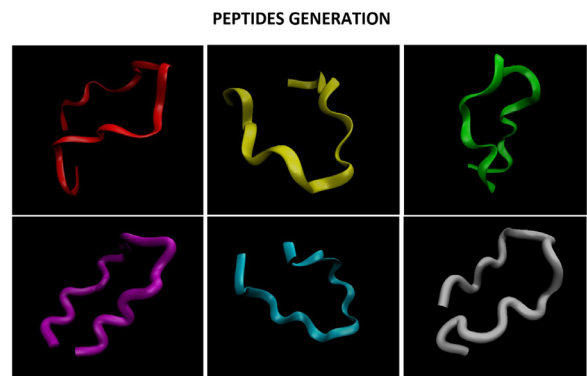


Figure 3. Molecular dynamic simulations (MDS) applied in the development of improved peptides. After a natural peptide is chosen as a model, it can be modeled and characterized *in silico* to improve, for example, the structure for an antimicrobial peptide (AMP) or host defense peptide (HDP), that might better interact with relevant molecules such as Gram-negative bacteria derived lipopolysaccharides. Here, peptide VSAK is shown as a natural occurring peptide, and the structural changes that might be carried out by changing specific amino acids.

ns start with peptides placed at 30 Å from the membrane surface. Employing this methodology, we were able to establish the strong binding properties of peptide VSAK with LPS (Figure 5; Supplementary Video 1).

On the other hand, another computational method that has gained importance in the last years is MDO, mainly because it has less computing power requirements and larger sampling capabilities than MDS. This technique is suitable for the study of protein-peptide and peptide-peptide interactions; therefore, facilitating the study of target proteins involved in HDP action (91). In addition, MDO allows the use of libraries favoring fast testing of multiple compounds, including peptides. Nevertheless, one of the main disadvantages of MDO is the dependence of a putative binding site, which needs to be determined by experimental means, or with the aid of additional software (92).

Advances in the *in vivo* Analysis of Peptide Therapeutics

A key aspect in the understanding of how AMP and HDP interact with the host organism, is also related to the way these interactions might change during the different clinical conditions of patients. Nowadays, although there are a series of protocols to study peptide bio-distribution, pharmacodynamics and pharmacokinetics, the particular characteristics of AMP and HDP, such as their short plasma half-life and non-specific organ uptake, require the implementation of novel strategies in order to properly carry out these studies (93). An interesting possibility has been developed in the study of the *in vivo* effects of peptides using Positron Emission Tomography (PET). This imaging technique allows the dynamic analysis of the distribution of molecules coupled with a radionuclide. Since radionuclides are short molecules that cause minimum changes in

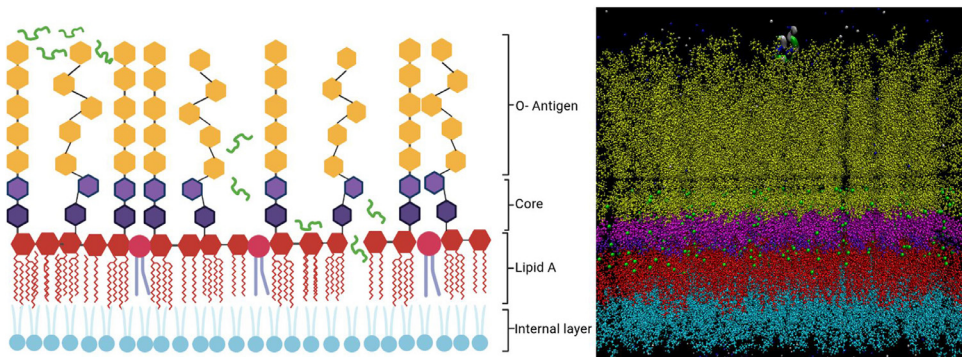


Figure 4. Lipopolysaccharide (LPS) arrangement in the outer membrane layer of a Gram-negative bacteria. Left: Cartoon of a LPS molecule arrangement associated to a series of peptides, showing important segments such as the core region and lipid A, the most conserved region of these molecules, and the region that plays a central role in the recognition by the immune system. Right: MDS of the same LPS arrangement showing an associated peptide placed at 30 Å above the membrane. The different regions for this arrangement are shown with the same color code as shown in the left panel.

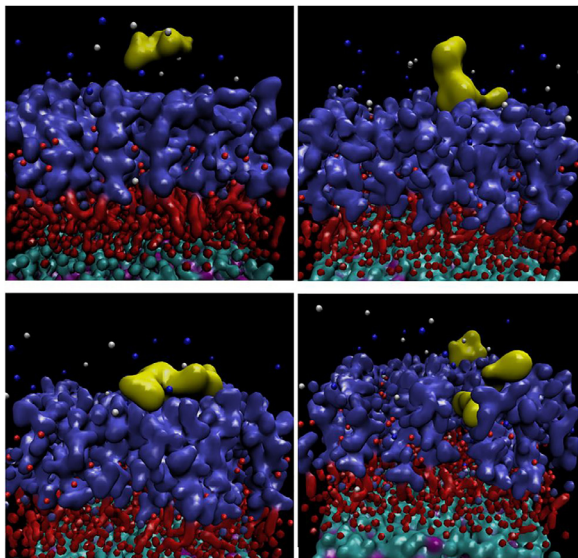


Figure 5. Coarse grain simulation of peptide VSAK interaction with an LPS arrangement. The panels show a coarse-grained simulation of a system composed of a LPS membrane and its association to a single peptide VSAK. Left upper panel shows peptide VSAK still in solution. Right upper panel, the initial interaction of peptide VSAK with the core region of the LPS membrane. Left lower panel, complete surface binding of peptide VSAK with the LPS membrane. Right lower panel, entire integration of peptide VSAK in the core region and its association with lipid A. Color code: Yellow –VSAK; Purple-LPS core; Red-lipid A; Cyan-DOPC.

the structure of peptides, this technique has started to be successfully employed (28,94). PET presents several advantages when peptides are tested, since small amounts of peptide are required, usually associated to rapid-decay radioactive labeled-tags. Although the use of PET presents limitations mainly related to the high costs involved in peptide-radionuclide production (95), this technique appears to be a valuable option for the *in vivo* analysis of AMP and HDP.

In this respect, we have established employing PET, and an experimental animal model of the Systemic Inflammatory Response Syndrome (SIRS), an important LPS-binding property for peptide VSAK (88). We demonstrated that the intravenous administration of peptide VSAK, followed by the interaction between peptide VSAK/LPS, neutralizes LPS induced toxicity preventing the development of septic shock in the experimental animals (88,96). This proof-of-concept related to the LPS-neutralizing effect shown by peptide VSAK, raises the possibility for the future use of this type of molecules as novel therapeutic agents. We believe, in conjunction with the established treatment carried out during the initial acute stages of SIRS shown in sepsis and septic shock patients (97), this new class of molecules undoubtedly will improve the outcome of severely-ill patients. It is our belief, that newly discovered AMP will play an important part in the development of novel strategies designed with the only purpose to substantially improve the way we treat sepsis, especially in the current scenario of antibiotic resistance shown by pathogen bacteria. Moreover, if we take into account the involvement of LPS in related pathologic conditions such as atherosclerosis, obesity, and metabolic syndrome (98), there is no doubt the impact LPS-neutralizing peptides might have in medicine, would be enormous.

Acknowledgments

I.L-R received a scholarship from CONACYT during his M.Sc. studies, and currently is receiving a scholarship from the same source (45060), for the development of his Ph.D. studies. E.G.P-H received a scholarship from CONACYT (465348) in support of her Ph.D. studies. This work was supported by grants awarded to J.M-O from CONACYT (255778), and UNAM-PAPIIT (IN205717 and IN206619). J.M-O thanks Dirección General de Cómputo y de Tecnologías de Información y Comunicación (Universidad Na-

cional Autónoma de México) for access to the supercomputer Miztli (grant: LANCAD-UNAM-DGTIC-352). J.M.-O also thanks Fundación Miguel Alemán A.C., for support through the program “Incentives for Medical Research, Miguel Alemán Valdés”.

Supplementary Materials

Supplementary material associated with this article can be found, in the online version, at doi:[10.1016/j.arcmed.2021.08.001](https://doi.org/10.1016/j.arcmed.2021.08.001).

References

- Bin Zaman S, MA Hussain, Nye R, et al. A Review on Antibiotic Resistance: Alarm Bells are Ringing. *Cureus* 2017;9:e1403. doi:[10.7759/cureus.1403](https://doi.org/10.7759/cureus.1403).
- Gentile LF, Moldawer LL. DAMPs, PAMPs, and the origins of SIRS in bacterial sepsis. *Shock* 2013;39:113–114. doi:[10.1097/SHK.0b013e318277109c](https://doi.org/10.1097/SHK.0b013e318277109c).
- Van Amersfoort ES, Van Berkel TJC, Kuiper J. Receptors, mediators, and mechanisms involved in bacterial sepsis and septic shock. *Clin Microbiol Rev* 2003;16:379–414. doi:[10.1128/CMR.16.3.379-414.2003](https://doi.org/10.1128/CMR.16.3.379-414.2003).
- López-Bojórquez LN, Dehesa AZ, Reyes-Terán G. Molecular mechanisms involved in the pathogenesis of septic shock. *Arch Med Res* 2004;35:465–479. doi:[10.1016/j.arcmed.2004.07.006](https://doi.org/10.1016/j.arcmed.2004.07.006).
- Ramnath R, Weing S, He M, et al. Inflammatory mediators in sepsis: Cytokines, chemokines, adhesion molecules and gases. *J Organ Dysfunct* 2006;2:80–92. doi:[10.1080/17471060500435662](https://doi.org/10.1080/17471060500435662).
- Delano MJ, Ward PA. The immune system's role in sepsis progression, resolution, and long-term outcome. *Immunol Rev* 2016;274:330–353. doi:[10.1111/imr.12499](https://doi.org/10.1111/imr.12499).
- Cohen J, Vincent J-L, Adhikari NKJ, et al. Sepsis: a roadmap for future research. *Lancet Infect Dis* 2015;15:581–614. doi:[10.1016/S1473-3099\(15\)70112-X](https://doi.org/10.1016/S1473-3099(15)70112-X).
- Dellinger RP, Levy MM, Rhodes A, et al. Surviving Sepsis Campaign: International Guidelines for Management of Severe Sepsis and Septic Shock. *Intensive Care Med* 2013;39:165–228. doi:[10.1007/s00134-012-2769-8](https://doi.org/10.1007/s00134-012-2769-8).
- Devasahayam G, Scheld WM, Hoffman PS. Newer antibacterial drugs for a new century. *Expert Opin Investig Drugs* 2010;19:215–234. doi:[10.1517/13543780903505092](https://doi.org/10.1517/13543780903505092).
- Rudd KE, Johnson SC, Agesa KM, et al. Global, regional, and national sepsis incidence and mortality, 1990–2017: analysis for the Global Burden of Disease Study. *Lancet* 2020;395:200–211. doi:[10.1016/S0140-6736\(19\)32989-7](https://doi.org/10.1016/S0140-6736(19)32989-7).
- Reinhart K, Daniels R, Kissoon N, et al. Recognizing Sepsis as a Global Health Priority — A WHO Resolution. *N Engl J Med* 2017;377:414–417. doi:[10.1056/nejmp1707170](https://doi.org/10.1056/nejmp1707170).
- Bassetti M, Merelli M, Temperoni C, et al. New antibiotics for bad bugs: Where are we? *Ann Clin Microbiol Antimicrob* 2013;12:1–15. doi:[10.1186/1476-0711-12-22](https://doi.org/10.1186/1476-0711-12-22).
- Gilbert DN, Guidos RJ, Boucher HW, et al. The 10 X 20 initiative: Pursuing a global commitment to develop 10 new antibacterial drugs by 2020. *Clin Infect Dis* 2010;50:1081–1083. doi:[10.1086/652237](https://doi.org/10.1086/652237).
- Álvarez-Martínez FJ, Barrajón-Catalán E, Micol V. Tackling Antibiotic Resistance with Compounds of Natural Origin: A Comprehensive Review. *Biomedicines* 2020;8:405. doi:[10.3390/biomedicines8100405](https://doi.org/10.3390/biomedicines8100405).
- Derakhshankhah H, Jafari S. Cell penetrating peptides: A concise review with emphasis on biomedical applications. *Biomed Pharmacother* 2018;108:1090–1096. doi:[10.1016/j.biopha.2018.09.097](https://doi.org/10.1016/j.biopha.2018.09.097).
- Zakeri B, Lu TK. Synthetic biology of antimicrobial discovery. *ACS Synth Biol* 2013;2:358–372. doi:[10.1021/sb300101g](https://doi.org/10.1021/sb300101g).
- Fjell CD, Hiss JA, Hancock REW, et al. Designing antimicrobial peptides: form follows function. *Nat Rev Drug Discov* 2012;11:37–51. doi:[10.1038/nrd3591](https://doi.org/10.1038/nrd3591).
- Choi K-Y, Chow LNY, Mookherjee N. Cationic Host Defence Peptides: Multifaceted Role in Immune Modulation and Inflammation. *J Innate Immun* 2012;4:361–370. doi:[10.1159/000336630](https://doi.org/10.1159/000336630).
- Wieczorek M, Jenssen H, Kindrachuk J, et al. Structural studies of a peptide with immune modulating and direct antimicrobial activity. *Chem Biol* 2010;17:970–980. doi:[10.1016/j.chembiol.2010.07.007](https://doi.org/10.1016/j.chembiol.2010.07.007).
- Hancock REW, Haney EF, Gill EE. The immunology of host defence peptides: beyond antimicrobial activity. *Nat Rev Immunol* 2016;16:321–334. doi:[10.1038/nri.2016.29](https://doi.org/10.1038/nri.2016.29).
- Hilpert K, Volkmer-Engert R, Walter T, et al. High-throughput generation of small antibacterial peptides with improved activity. *Nat Biotechnol* 2005;23:1008–1012. doi:[10.1038/nbt1113](https://doi.org/10.1038/nbt1113).
- Fox JL. Antimicrobial peptides stage a comeback. *Nat Biotechnol* 2013;31:379–382. doi:[10.1038/nbt.2572](https://doi.org/10.1038/nbt.2572).
- Hancock REW, Rozek A. Role of membranes in the activities of antimicrobial cationic peptides. *FEMS Microbiol Lett* 2002;206:143–149. doi:[10.1111/j.1574-6968.2002.tb11000.x](https://doi.org/10.1111/j.1574-6968.2002.tb11000.x).
- Scott MG, Gold MR, Hancock REW. Interaction of cationic peptides with lipoteichoic acid and gram- positive bacteria. *Infect Immun* 1999;67:6445–6453. doi:[10.1128/iai.67.12.6445-6453.1999](https://doi.org/10.1128/iai.67.12.6445-6453.1999).
- De Luca AJ, Bland JM, Jacks TJ, et al. Fungicidal and binding properties of the natural peptides cecropin B and dermaseptin. *Med Mycol* 1998;36:291–298. doi:[10.1080/02681219880000461](https://doi.org/10.1080/02681219880000461).
- Jenssen H, Hamill P, Hancock REW. Peptide antimicrobial agents. *Clin Microbiol Rev* 2006;19:491–511. doi:[10.1128/CMR.00056-05](https://doi.org/10.1128/CMR.00056-05).
- Shai Y. Mechanism of the binding, insertion and destabilization of phospholipid bilayer membranes by α -helical antimicrobial and cell non-selective membrane-lytic peptides. *Biochim Biophys Acta-Biomembr* 1999;1462:55–70. doi:[10.1016/S0005-2736\(99\)00200-X](https://doi.org/10.1016/S0005-2736(99)00200-X).
- Lee T-H, N Hall K, Aguilar M-I. Antimicrobial Peptide Structure and Mechanism of Action: A Focus on the Role of Membrane Structure. *Curr Top Med Chem* 2015;16:25–39. doi:[10.2174/156802661566150703121700](https://doi.org/10.2174/156802661566150703121700).
- Shai Y. Mode of action of membrane active antimicrobial peptides. *Biopolym-Pept Sci Sect* 2002;66:236–248. doi:[10.1002/bip.10260](https://doi.org/10.1002/bip.10260).
- Kumar P, Kizhakkedathu JN, Straus SK. Antimicrobial peptides: Diversity, mechanism of action and strategies to improve the activity and biocompatibility in vivo. *Biomolecules* 2018;8:4. doi:[10.3390/biom8010004](https://doi.org/10.3390/biom8010004).
- Epanet RM, Vogel HJ. Diversity of antimicrobial peptides and their mechanisms of action. *Biochim Biophys Acta-Biomembr* 1999;1462:11–28. doi:[10.1016/S0005-2736\(99\)00198-4](https://doi.org/10.1016/S0005-2736(99)00198-4).
- Scott MG, Dullaghan E, Mookherjee N, et al. An anti-infective peptide that selectively modulates the innate immune response. *Nat Biotechnol* 2007;25:465–472. doi:[10.1038/nbt1288](https://doi.org/10.1038/nbt1288).
- Mookherjee N, Hancock REW. Cationic host defence peptides: Innate immune regulatory peptides as a novel approach for treating infections. *Cell Mol Life Sci* 2007;64:922–933. doi:[10.1007/s0018-007-6475-6](https://doi.org/10.1007/s0018-007-6475-6).
- Morton B, Mitsi E, Pennington SH, et al. Augmented Passive Immunotherapy with P4 Peptide Improves Phagocyte Activity in Severe Sepsis. *Shock* 2016;46:635–641. doi:[10.1097/SHK.0000000000000715](https://doi.org/10.1097/SHK.0000000000000715).
- Nijnik A, Madera L, Ma S, et al. Synthetic Cationic Peptide IDR-1002 Provides Protection against Bacterial Infections through Chemokine Induction and Enhanced Leukocyte Recruitment. *J Immunol* 2010;184:2539–2550. doi:[10.4049/jimmunol.0901813](https://doi.org/10.4049/jimmunol.0901813).
- Mansour SC, Pena OM, Hancock REW. Host defense peptides: Front-line immunomodulators. *Trends Immunol* 2014;35:443–450. doi:[10.1016/j.it.2014.07.004](https://doi.org/10.1016/j.it.2014.07.004).
- Mookherjee N, Brown KL, Bowdish DME, et al. Modulation of the TLR-Mediated Inflammatory Response by the Endogenous Hu-

- man Host Defense Peptide LL-37. *J Immunol* 2006;176:2455–2464. doi:[10.4049/jimmunol.176.4.2455](https://doi.org/10.4049/jimmunol.176.4.2455).
38. Lu Y-C, Yeh W-C, Ohashi PS. LPS/TLR4 signal transduction pathway. *Cytokine* 2008;42:145–151. doi:[10.1016/J.CYTO.2008.01.006](https://doi.org/10.1016/J.CYTO.2008.01.006).
 39. Jerala R. Structural biology of the LPS recognition. *Int J Med Microbiol* 2007;297:353–363. doi:[10.1016/J.IJMM.2007.04.001](https://doi.org/10.1016/J.IJMM.2007.04.001).
 40. Rosenfeld Y, Papo N, Shai Y. Endotoxin (lipopolysaccharide) neutralization by innate immunity host-defense peptides: Peptide properties and plausible modes of action. *J Biol Chem* 2006;281:1636–1643. doi:[10.1074/jbc.M504327200](https://doi.org/10.1074/jbc.M504327200).
 41. Zhang L, Falla TJ. Antimicrobial peptides: Therapeutic potential. *Expert Opin Pharmacother* 2006;7:653–663. doi:[10.1517/14656566.7.6.653](https://doi.org/10.1517/14656566.7.6.653).
 42. Hancock REW, Sahl H-G. Antimicrobial and host-defense peptides as new anti-infective therapeutic strategies. *Nat Biotechnol* 2006;24:1551–1557. doi:[10.1038/nbt1267](https://doi.org/10.1038/nbt1267).
 43. Bettoli E, Wetherington JD, Schmitt N, et al. Challenges and solutions for clinical development of new antibacterial agents: Results of a survey among pharmaceutical industry professionals. *Antimicrob Agents Chemother* 2015;59:3695–3699. doi:[10.1128/AAC.00638-15](https://doi.org/10.1128/AAC.00638-15).
 44. Sinha MS, Kesselheim AS. Regulatory Incentives for Antibiotic Drug Development: A Review of Recent Proposals. *Bioorganic Med Chem* 2016;24:6446–6451. doi:[10.1016/j.bmc.2016.08.033](https://doi.org/10.1016/j.bmc.2016.08.033).
 45. Kang X, Dong F, Shi C, et al. DRAMP 2.0, an updated data repository of antimicrobial peptides. *Sci Data* 2019;6:1–10. doi:[10.1038/s41597-019-0154-y](https://doi.org/10.1038/s41597-019-0154-y).
 46. Chen CH, Lu TK. Development and Challenges of Antimicrobial Peptides for Therapeutic Applications. *Antibiotics* 2020;9:24. doi:[10.3390/antibiotics9010024](https://doi.org/10.3390/antibiotics9010024).
 47. Falagas ME, Kasiakou SK. Colistin: The revival of polymyxins for the management of multidrug-resistant gram-negative bacterial infections. *Clin Infect Dis* 2005;40:1333–1341. doi:[10.1086/429323](https://doi.org/10.1086/429323).
 48. Billeter M, Zervos MJ, Chen AY, et al. Dalbavancin: A novel once-weekly lipoglycopeptide antibiotic. *Clin Infect Dis* 2008;46:577–583. doi:[10.1086/526772](https://doi.org/10.1086/526772).
 49. Straus SK, Hancock REW. Mode of action of the new antibiotic for Gram-positive pathogens daptomycin: Comparison with cationic antimicrobial peptides and lipopeptides. *Biochim Biophys Acta - Biomembr* 2006;1758:1215–1223. doi:[10.1016/j.bbamem.2006.02.009](https://doi.org/10.1016/j.bbamem.2006.02.009).
 50. Eliopoulos GM, Willey S, Reiszner E, et al. *In vitro* and *in vivo* activity of LY 146032, a new cyclic lipopeptide antibiotic. *Antimicrob Agents Chemother* 1986;30:532–535. doi:[10.1128/AAC.30.4.532](https://doi.org/10.1128/AAC.30.4.532).
 51. Dubos RJ. Studies on a bactericidal agent extracted from a soil bacillus: I. Preparation of the agent. Its activity *in vitro*. *J Exp Med* 1939;70:1–10. doi:[10.1084/jem.70.1.1](https://doi.org/10.1084/jem.70.1.1).
 52. Allen NE, Nicas TI. Mechanism of action of oritavancin and related glycopeptide antibiotics. *FEMS Microbiol Rev* 2003;26:511–532. doi:[10.1111/j.1574-6976.2003.tb00628.x](https://doi.org/10.1111/j.1574-6976.2003.tb00628.x).
 53. Higgins DL, Chang R, Debabov DV, et al. Telavancin, a multi-functional lipoglycopeptide, disrupts both cell wall synthesis and cell membrane integrity in methicillin-resistant *Staphylococcus aureus*. *Antimicrob Agents Chemother* 2005;49:1127–1134. doi:[10.1128/AAC.49.3.1127-1134.2005](https://doi.org/10.1128/AAC.49.3.1127-1134.2005).
 54. Griffith RS. Introduction to Vancomycin. *Clin Infect Dis* 1981;3:S200–S204. doi:[10.1093/clinids/3.Supplement_2.S200](https://doi.org/10.1093/clinids/3.Supplement_2.S200).
 55. Bhandari D, Rafiq S, Gat Y, et al. A Review on Bioactive Peptides: Physiological Functions, Bioavailability and Safety. *Int J Pept Res Ther* 2020;26:139–150. doi:[10.1007/s10989-019-09823-5](https://doi.org/10.1007/s10989-019-09823-5).
 56. Zasloff M. Antimicrobial peptides of multicellular organisms. *Nature* 2002;415:389–395. doi:[10.1038/415389a](https://doi.org/10.1038/415389a).
 57. Hilpert K, Elliott MR, Volkmer-Engert R, et al. Sequence Requirements and an Optimization Strategy for Short Antimicrobial Peptides. *Chem Biol* 2006;13:1101–1107. doi:[10.1016/j.chembiol.2006.08.014](https://doi.org/10.1016/j.chembiol.2006.08.014).
 58. Li J, Koh JJ, Liu S, et al. Membrane active antimicrobial peptides: Translating mechanistic insights to design. *Front Neurosci* 2017;11:73. doi:[10.3389/fnins.2017.00073](https://doi.org/10.3389/fnins.2017.00073).
 59. Fjell CD, Jenssen H, Hilpert K, et al. Identification of novel antibacterial peptides by chemoinformatics and machine learning. *J Med Chem* 2009;52:2006–2015. doi:[10.1021/jm8015365](https://doi.org/10.1021/jm8015365).
 60. Cherkasov A, Hilpert K, Jenssen H, et al. Use of artificial intelligence in the design of small peptide antibiotics effective against a broad spectrum of highly antibiotic-resistant superbugs. *ACS Chem Biol* 2009;4:65–74. doi:[10.1021/cb800240j](https://doi.org/10.1021/cb800240j).
 61. Jenssen H, Lejon T, Hilpert K, et al. Evaluating Different Descriptors for Model Design of Antimicrobial Peptides with Enhanced Activity Toward *P. aeruginosa*. *Chem Biol Drug Des* 2007;70:134–142. doi:[10.1111/j.1747-0285.2007.00543.x](https://doi.org/10.1111/j.1747-0285.2007.00543.x).
 62. Nguyen LT, Chau JK, Perry NA, et al. Serum Stabilities of Short Tryptophan- and Arginine-Rich Antimicrobial Peptide Analogs. *PLoS One* 2010;5:e12684. doi:[10.1371/journal.pone.0012684](https://doi.org/10.1371/journal.pone.0012684).
 63. Hamamoto K, Kida Y, Zhang Y, et al. Antimicrobial activity and stability to proteolysis of small linear cationic peptides with D-amino acid substitutions. *Microbiol Immunol* 2002;46:741–749. doi:[10.1111/j.1348-0421.2002.tb02759.x](https://doi.org/10.1111/j.1348-0421.2002.tb02759.x).
 64. Moncla BJ, Pryke K, Rohan LC, et al. Degradation of naturally occurring and engineered antimicrobial peptides by proteases. *Adv Biosci Biotechnol* 2011;2:404. doi:[10.4236/ABB.2011.26059](https://doi.org/10.4236/ABB.2011.26059).
 65. Rozek A, Powers J-PS, Friedrich CL, et al. Structure-based design of an indolicidin peptide analogue with increased protease stability. *Biochemistry* 2003;42:14130–14138. doi:[10.1021/bi035643g](https://doi.org/10.1021/bi035643g).
 66. Sobrino-López A, Martín-Belloso O. Use of nisin and other bacteriocins for preservation of dairy products. *Int Dairy J* 2008;18:329–343. doi:[10.1016/j.idairyj.2007.11.009](https://doi.org/10.1016/j.idairyj.2007.11.009).
 67. Mookherjee N, Anderson MA, Haagsman HP, et al. Antimicrobial host defence peptides: functions and clinical potential. *Nat Rev Drug Discov* 2020;19:311–332. doi:[10.1038/s41573-019-0058-8](https://doi.org/10.1038/s41573-019-0058-8).
 68. Maria-Neto S, De Almeida KC, Macedo MLR, et al. Understanding bacterial resistance to antimicrobial peptides: From the surface to deep inside. *Biochim Biophys Acta-Biomembr* 2015;1848:3078–3088. doi:[10.1016/j.bbamem.2015.02.017](https://doi.org/10.1016/j.bbamem.2015.02.017).
 69. Peschel A, Sahl HG. The co-evolution of host cationic antimicrobial peptides and microbial resistance. *Nat Rev Microbiol* 2006;4:529–536. doi:[10.1038/nrmicro1441](https://doi.org/10.1038/nrmicro1441).
 70. Kollef M, Pittet D, García MS, et al. A randomized double-blind trial of iseganan in prevention of ventilator-associated pneumonia. *Am J Respir Crit Care Med* 2006;173:91–97. doi:[10.1164/rccm.200504-656OC](https://doi.org/10.1164/rccm.200504-656OC).
 71. Matsuzaki K. Why and how are peptide-lipid interactions utilized for self-defense? Magainins and tachyplesins as archetypes. *Biochim Biophys Acta-Biomembr* 1999;1462:1–10. doi:[10.1016/S0005-2736\(99\)00197-2](https://doi.org/10.1016/S0005-2736(99)00197-2).
 72. Eckert R. Road to clinical efficacy: Challenges and novel strategies for antimicrobial peptide development. *Future Microbiol* 2011;6:635–651. doi:[10.2217/fmb.11.27](https://doi.org/10.2217/fmb.11.27).
 73. Tsai CW, Hsu NY, Wang CH, et al. Coupling Molecular Dynamics Simulations with Experiments for the Rational Design of Indolicidin-Analogous Antimicrobial Peptides. *J Mol Biol* 2009;392:837–854. doi:[10.1016/j.jmb.2009.06.071](https://doi.org/10.1016/j.jmb.2009.06.071).
 74. Yount NY, Bayer AS, Xiong YQ, et al. Advances in antimicrobial peptide immunobiology. *Biopolymers* 2006;84:435–458. doi:[10.1002/bip.20543](https://doi.org/10.1002/bip.20543).
 75. Tyo KE, Alper HS, Stephanopoulos GN. Expanding the metabolic engineering toolbox: more options to engineer cells. *Trends Biotechnol* 2007;25:132–137. doi:[10.1016/j.tibtech.2007.01.003](https://doi.org/10.1016/j.tibtech.2007.01.003).
 76. Forde ÉB, Kelly G, Makki H, et al. Using Disease-Associated Enzymes to Activate Antimicrobial Peptide Prodrugs. Hansen PR, editor. *Antimicrob. Pept. Methods Protoc.*, New York, NY: Springer New York 2017:359–368. doi:[10.1007/978-1-4939-6737-7_26](https://doi.org/10.1007/978-1-4939-6737-7_26).
 77. Alonso-Garcia AL, Zentella-Dehesa A, Mas-Oliva J. Characterization of a naturally occurring new version of the cholesterol ester

- transfer protein (CETP) from small intestine. *Mol Cell Biochem* 2003;245:173–182.
78. Isidro-Llobet A, Kenworthy MN, Mukherjee S, et al. Sustainability Challenges in Peptide Synthesis and Purification: From R&D to Production. *J Org Chem* 2019;84:4615–4628. doi:[10.1021/acs.joc.8b03001](https://doi.org/10.1021/acs.joc.8b03001).
79. Varnava KG, Sarojini V. Making Solid-Phase Peptide Synthesis Greener: A Review of the Literature. *Chem – An Asian J* 2019;14:1088–1097. doi:[10.1002/asia.201801807](https://doi.org/10.1002/asia.201801807).
80. Jo S, Kim T, Iyer VG, et al. CHARMM-GUI: A web-based graphical user interface for CHARMM. *J Comput Chem* 2008;29:1859–1865. doi:[10.1002/jcc.20945](https://doi.org/10.1002/jcc.20945).
81. Roy A, Kucukural A, Zhang YI-TASSER. A unified platform for automated protein structure and function prediction. *Nat Protoc* 2010;5:725–738. doi:[10.1038/nprot.2010.5](https://doi.org/10.1038/nprot.2010.5).
82. Kumar N, Sood D, Tomar R, et al. Antimicrobial Peptide Designing and Optimization Employing Large-Scale Flexibility Analysis of Protein-Peptide Fragments. *ACS Omega* 2019;4:21370–21380. doi:[10.1021/acsomega.9b03035](https://doi.org/10.1021/acsomega.9b03035).
83. Chen CH, Melo MC, Berglund N, et al. Understanding and modelling the interactions of peptides with membranes: from partitioning to self-assembly. *Curr Opin Struct Biol* 2020;61:160–166. doi:[10.1016/j.sbi.2019.12.021](https://doi.org/10.1016/j.sbi.2019.12.021).
84. Almeida JG, Preto AJ, Koukos PI, et al. Membrane proteins structures: A review on computational modeling tools. *Biochim Biophys Acta-Biomembr* 2017;1859:2021–2039. doi:[10.1016/j.bbamem.2017.07.008](https://doi.org/10.1016/j.bbamem.2017.07.008).
85. Cirac AD, Moiset G, Mika JT, et al. The molecular basis for antimicrobial activity of pore-forming cyclic peptides. *Biophys J* 2011;100:2422–2431. doi:[10.1016/j.bpj.2011.03.057](https://doi.org/10.1016/j.bpj.2011.03.057).
86. Shi Y, Wan M, Fu L, et al. Peptide-Lipid Interaction Sites Affect Vesicles' Responses to Antimicrobial Peptides. *Biophys J* 2018;115:1518–1529. doi:[10.1016/j.bpj.2018.08.040](https://doi.org/10.1016/j.bpj.2018.08.040).
87. Zhou J, Thorpe IF, Izvekov S, et al. Coarse-grained peptide modeling using a systematic multiscale approach. *Biophys J* 2007;92:4289–4303. doi:[10.1529/biophysj.106.094425](https://doi.org/10.1529/biophysj.106.094425).
88. García-González V, Gutiérrez-Quintanar N, Mas-Oliva J. The C-terminal Domain Supports a Novel Function for CETPI as a New Plasma Lipopolysaccharide-Binding Protein. *Sci Rep* 2015;5:16091. doi:[10.1038/srep16091](https://doi.org/10.1038/srep16091).
89. Luna-Reyes I, Pérez-Hernández EG, Delgado-Coello B, et al. Peptide VSAK maintains tissue glucose uptake and attenuates pro-inflammatory responses caused by LPS in an experimental model of the systemic inflammatory response syndrome: a PET study. *Sci Rep* 2021;11:14752. doi:[10.1038/s41598-021-94224-2](https://doi.org/10.1038/s41598-021-94224-2).
90. Qi Y, Ingólfsson HI, Cheng X, et al. CHARMM-GUI Martini Maker for Coarse-Grained Simulations with the Martini Force Field. *J Chem Theory Comput* 2015;11:4486–4494. doi:[10.1021/acs.jctc.5b00513](https://doi.org/10.1021/acs.jctc.5b00513).
91. Meng X-Y, Zhang H-X, Mezei M, et al. Molecular Docking: A Powerful Approach for Structure-Based Drug Discovery. *Curr Comput Aided-Drug Des* 2012;7:146–157. doi:[10.2174/157340911795677602](https://doi.org/10.2174/157340911795677602).
92. Pagadala NS, Syed K, Tuszyński J. Software for molecular docking: a review. *Biophys Rev* 2017;9:91–102. doi:[10.1007/s12551-016-0247-1](https://doi.org/10.1007/s12551-016-0247-1).
93. Welling MM, Paulusma-Annema A, Balter HS, et al. Technetium-99m labelled antimicrobial peptides discriminate between bacterial infections and sterile inflammations. *Eur J Nucl Med* 2000;27:292–301. doi:[10.1007/s002590050036](https://doi.org/10.1007/s002590050036).
94. Morris O, Fairclough M, Grigg J, et al. A review of approaches to ¹⁸ F radiolabelling affinity peptides and proteins. *J Label Compd Radiopharm* 2019;62:4–23. doi:[10.1002/jlcr.3634](https://doi.org/10.1002/jlcr.3634).
95. Ebenhan T, Gheysens O, Kruger HG, et al. Antimicrobial Peptides: Their Role as Infection-Selective Tracers for Molecular Imaging. *Biomed Res Int* 2014 2014. doi:[10.1155/2014/867381](https://doi.org/10.1155/2014/867381).
96. Mas-Oliva J, Gutiérrez Quintanar N, García-González V. Peptídos derivados del dominio C-terminal de CETPI como moléculas bloqueadoras del efecto citotóxico inducido por lipopolisacáridos en septicemia y choque séptico. *PCT/MX2014/000087; WO2015190903A1*. (Patent) 2014.
97. Pérez-Hernández EG, Delgado-Coello B, Luna-Reyes I, et al. New insights into lipopolysaccharide inactivation mechanisms in sepsis. *Biomed Pharmacother* 2021;141:111890. doi:[10.1016/j.biopha.2021.111890](https://doi.org/10.1016/j.biopha.2021.111890).
98. Munford RS. Endotoxemia-menace, marker, or mistake? *J Leukoc Biol* 2016;100:687–698. doi:[10.1189/jlb.3RU0316-151R](https://doi.org/10.1189/jlb.3RU0316-151R).

RESEARCH ARTICLE

Open Access



The cholesteryl-ester transfer protein isoform (CETPI) and derived peptides: new targets in the study of Gram-negative sepsis

Eréndira G. Pérez-Hernández¹, Víctor De la Puente-Díaz de León², Ismael Luna-Reyes¹, Blanca Delgado-Coello¹, José Sifuentes-Osornio³ and Jaime Mas-Oliva^{1*}

Abstract

Background: Sepsis is a syndrome where the dysregulated host response to infection threatens the life of the patient. The isoform of the cholesteryl-ester transfer protein (CETPI) is synthesized in the small intestine, and it is present in human plasma. CETPI and peptides derived from its C-terminal sequence present the ability to bind and deactivate bacterial lipopolysaccharides (LPS). The present study establishes the relationship between the plasma levels of CETPI and disease severity of sepsis due to Gram-negative bacteria.

Methods: Plasma samples from healthy subjects and patients with positive blood culture for Gram-negative bacteria were collected at the Intensive Care Unit (ICU) of INCMNSZ (Mexico City). 47 healthy subjects, 50 patients with infection, and 55 patients with sepsis and septic shock, were enrolled in this study. CETPI plasma levels were measured by an enzyme-linked immunosorbent assay and its expression confirmed by Western Blot analysis. Plasma cytokines (IL-1 β , TNF α , IL-6, IL-8, IL-12p70, IFN γ , and IL-10) were measured in both, healthy subjects, and patients, and directly correlated with their CETPI plasma levels and severity of clinical parameters. Sequential Organ Failure Assessment (SOFA) scores were evaluated at ICU admission and within 24 h of admission. Plasma LPS and CETPI levels were also measured and studied in patients with liver dysfunction.

Results: The level of CETPI in plasma was found to be higher in patients with positive blood culture for Gram-negative bacteria than in control subjects, showing a direct correlation with their SOFA values. Accordingly, septic shock patients showing a high CETPI plasma concentration, presented a negative correlation with cytokines IL-8, IL-1 β , and IL-10. Also, in patients with liver dysfunction, since higher CETPI levels correlated with a high plasma LPS concentration, LPS neutralization carried out by CETPI might be considered a physiological response that will have to be studied in detail.

Conclusions: Elevated levels of plasma CETPI were associated with disease severity and organ failure in patients with Gram-negative bacteraemia, defining CETPI as a protein implicated in the systemic response to LPS.

Keywords: CETPI, LPS, Gram-negative bacteria, Sepsis, Septic shock, CETP

Background

Each year an elevated number of people worldwide experience an episode of sepsis, where millions die as a result of its associated complications (Singer et al. 2016; Reinhart et al. 2017). In low- and middle-income countries, the burden of sepsis is even higher and represents

*Correspondence: jmas@ifc.unam.mx

¹ Instituto de Fisiología Celular, Universidad Nacional Autónoma de México, 04510 Ciudad de Mexico, Mexico
Full list of author information is available at the end of the article



© The Author(s) 2022. **Open Access** This article is licensed under a Creative Commons Attribution 4.0 International License, which permits use, sharing, adaptation, distribution and reproduction in any medium or format, as long as you give appropriate credit to the original author(s) and the source, provide a link to the Creative Commons licence, and indicate if changes were made. The images or other third party material in this article are included in the article's Creative Commons licence, unless indicated otherwise in a credit line to the material. If material is not included in the article's Creative Commons licence and your intended use is not permitted by statutory regulation or exceeds the permitted use, you will need to obtain permission directly from the copyright holder. To view a copy of this licence, visit <http://creativecommons.org/licenses/by/4.0/>.

one of the leading causes of death in the general population, where a complex interaction of factors such as the causative pathogen, timely diagnosis, host immunity, and access to quality care, determine lethality in sepsis (Cecconi et al. 2018; Rudd et al. 2020). Sepsis occurs when the host produces an unbalanced response to an infection, that if not diagnosed and treated early, can lead to profound circulatory and cellular dysfunction, progressing to septic shock (Cecconi et al. 2018). Gram-negative bacteria are the most frequent etiological agents of sepsis worldwide (Font et al. 2020), presenting in their outer membrane LPS. The physiological response to LPS is mediated by stimulation of the Toll-like receptor 4, that includes the release of pro-inflammatory cytokines and reactive oxygen species, causing endothelial damage and vasodilation, leading to hypo-perfusion and capillary fluid leakage. Additionally, cytokines activate the coagulation cascade, resulting in capillary microthrombi, and ultimately organ ischemia (Van Der Poll et al. 2017). LPS released into the circulation interact with lipoproteins, such as the High-Density Lipoproteins (HDL) and Low-Density Lipoproteins (LDL), but importantly with lipopolysaccharide-binding proteins (Vreugdenhil et al. 2001), which eventually promote LPS clearance through the hepatobiliary system (Pérez-Hernández et al. 2021). The LPS-binding protein and the bactericidal/permeability-increasing protein are closely related proteins that bind LPS, and present an important role in the host response to acute infections involving Gram-negative bacteria (Krasity et al. 2011). These proteins are members of the LTP/LPS-binding family of lipid binding and transfer proteins which also includes the cholesteryl-ester transfer protein (CETP), the phospholipid transfer protein (Beamer 2003), and now the cholesteryl-ester transfer protein isoform (CETPI), originally described by our research group years ago (Alonso et al. 2003; García-González et al. 2015).

CETPI was identified and found to be synthesized in the small intestine, and it is present in human plasma (Alonso et al. 2003). The only structural difference between CETP and CETPI resides in their C-terminal domain, where human CETPI presents a 41 C-terminal segment containing prolines, and a disordered conformation, instead of the normal 24 residues present as an α -helix in CETP (Alonso et al. 2003). Peptides derived from the C-terminal domain of CETPI bind LPS through electrostatic interactions, and the intravenous administration of one of these peptides, called VSAK, attenuates the harmful effects produced by LPS in a model of the systemic inflammatory response syndrome (Luna-Reyes et al. 2021). In addition, considering that the expression of CETPI in intestinal cells is upregulated in the presence of LPS (García-González et al. 2015), we aimed to

evaluate the relation of the CETPI plasma levels with disease severity in Gram-negative sepsis. For this purpose, during the present study we collected plasma samples along a period of two years at the ICU of Instituto Nacional de Ciencias Médicas y Nutrición “Salvador Zubirán” (INCMNSZ), a tertiary care center located in Mexico City. In comparison to healthy subjects, we measured the plasma CETPI concentration in patients presenting infection, sepsis, and septic shock, and examined the correlation between CETPI with the plasma levels of LPS and a series of cytokines in all patients.

Our results suggest that an increased plasma level of CETPI in patients, associated to the presence of peptides derived from this protein, in correlation with their ability to bind and inactivate LPS, might be considered as a defense mechanism involved in the emergency host response to a Gram-negative infection, and therefore, also as indicators of disease severity.

Materials and methods

Study design

For this study, plasma samples from healthy subjects and patients with infection, sepsis, and septic shock with positive blood culture for Gram-negative bacteria were collected over a period of two years at the ICU of INCMNSZ (Mexico City). To quantify CETPI in plasma we employed an enzyme-linked immunosorbent assay (ELISA). The pro- and anti-inflammatory plasma cytokines were measured using the human cytokine magnetic bead panel Milliplex Map Kit. We determined the relationship between plasma levels of LPS and CETPI in patients with liver dysfunction. Also, the expression of CETPI in plasma was confirmed by Western Blot analysis, and the bands recognized by the anti-CETPI antibody identified by HPLC-mass spectrometry. Depletion of plasma albumin was used to determine the possible binding of peptides derived from the C-terminal domain of CETPI to this protein.

Study population

For the development of this study at INCMNSZ, 47 healthy subjects, and 105 patients with infection, sepsis, and septic shock between 18 and 65 years of age were enrolled. All subjects provided written informed consent prior to the participation in the study. As controls, a total of 47 samples were obtained from healthy volunteer blood donors at the blood bank of INCMNSZ. The inclusion criteria were body mass index < 30 kg per m^2 , normal vital signs, oxygen saturation $> 90\%$, with no evidence of infection or acute/chronic illnesses. Exclusion criteria included having consumed any drug seven days before sample collection, and the presence of an

infection, inflammatory, and traumatic process in the six weeks before the acceptance for inclusion in the study.

Patients were divided into three groups: infection, sepsis, and septic shock. Baseline values for SOFA scores were determined upon patient arrival at the ICU, and the Delta SOFA score was calculated as the change in total SOFA score between baseline values and values obtained 24 h after ICU admission. The infection group included 50 subjects without evidence of organ failure defined by the Delta SOFA score lower than 2 points. The sepsis group comprised 28 sepsis patients with infection and organ failure defined as Delta SOFA score of 2 points or more. The septic shock group included 27 patients with sepsis and persisting hypotension requiring vasopressors to maintain a mean arterial pressure of 65 mmHg or greater and having a serum lactate level greater than 2 mmol/L (>18 mg/dL) in the absence of hypovolemia. All patients had positive blood cultures for Gram-negative bacteria. Patients with trauma, renal replacement therapy, or patients that have received anti-inflammatory drugs 48 h prior to sample collection were excluded from the study.

Patients were clinically assessed by recording vital signs, mean arterial pressure, C-Reactive Protein (CRP), hemoglobin, albumin, procalcitonin (PCT), bilirubin, lactate, creatinine, HDL, leucocytes, platelets, and time of antibiotic treatment. Also, demographic data and baseline comorbidities (heart disease, lung disease, chronic liver dysfunction, immunosuppression, cancer, endocrinopathy, dyslipidemia, and autoimmune disease) were collected at the time of the patient's admission. Patients were considered immunocompromised if they had severe neutropenia, and/or received steroid treatment or cytotoxic drugs. The source of infection was categorized into eight groups: abdomen, lung, urinary tract, soft tissue, sinusitis, empyema, central nervous system, and intravenous catheter. The criteria employed to define patients with liver dysfunction were: patients with known liver disease, basal SOFA score ≥ 1 in liver and coagulation item, or a previous diagnosis of cirrhosis.

This study was reviewed and approved by the Ethics Committee of the INCMNSZ (Reference number: 2252).

Sample collection

All plasma samples were collected within 12 h of ICU admission, then samples were centrifuged for 10 min at 1500 rpm, and aliquots were immediately stored at -80°C . Blood cultures were taken in all patients upon arrival to the ICU. Only samples with positive blood culture for Gram-negative bacteria were included in the study.

Western blot analysis

Protein from plasma samples was measured using the DC Protein Assay (Bio-Rad, Hercules, CA, USA). A total of 30 μg of protein were loaded and separated on 8% SDS-PAGE, and further transferred to PVDF membranes (Immobilon-P, Merck Millipore, Billerica, MA, USA). Membranes were blocked using 10% of Blotting-Grade Blocker (Bio-Rad), incubated with anti-CETPI (1:4000) overnight at 4°C , and washed six times with TBST. Anti-CETPI antibodies from Alpha Diagnostic International Inc. (San Antonio, TX, USA), consist of antibodies raised using a synthetic peptide that corresponds to the last 12 amino acids of the C-terminal segment of CETPI. Membranes were incubated with a rabbit peroxidase-conjugated anti-chicken IgY secondary antibody (1:30,000) (Thermo Fisher Scientific, Waltham, MA, USA) for 60 min at room temperature (RT). Antibodies were diluted in a 5% of Blotting-Grade Blocker (Bio-Rad) solution. Protein bands were visualized using Immobilon[®] Western from Merck Millipore on X-OMAT autoradiographic plates (Kodak, Rochester, NY, USA).

Plasma cytokine measurements

For the measurement of cytokine levels in plasma, the human cytokine magnetic bead panel Milliplex[®] Map Kit (Merck Millipore) was used to assess the levels of IL-1 β , TNF α , IL-6, IL-8, IL-12 (p70), IFN γ , and IL-10. Plasma samples were analyzed in duplicate, and the procedure was carried out according to the manufacturer instructions. Briefly, 25 μL of control and patient plasmas were incubated with antibody-immobilized beads overnight at 4°C . Bead-complexes, after being rinsed, were incubated with 25 μL of biotinylated detection antibody for 1 h with agitation. Next, 25 μL of Streptavidin–Phycoerythrin were added and incubated for 30 min at RT with agitation. After washing the plate, 150 μL of Drive Fluid were added to all wells. Plates were read on a MAGPIX employing the xPONENT software, and the Median Fluorescent Intensity analyzed.

Plasma CETPI measured by ELISA

CETPI plasma levels were measured by an ELISA test employing 96-well Maxisorp plates (Thermo Fisher Scientific). 50 μL of dilutions of plasma samples were added into the appropriate wells and incubated overnight at 4°C , then the plate washed out one time with Phosphate-Buffered Saline (PBS). The plate was blocked for 2 h using 2.5% Bovine Serum Albumin plus 2.5% of Blotting-Grade Blocker (Bio-Rad), and then washed out three times with PBS. Next, anti-CETPI (1:5000) antibodies were added into each well and the plate incubated for 90 min at 37°C . The plate was washed out three times with PBS and

further incubated with a rabbit peroxidase-conjugated anti-chicken IgY secondary antibody (Thermo Fisher Scientific) for 30 min at 37 °C. Finally, the plate was washed with PBS, TMB substrate was added to each well, and incubated for 15 min at RT. To stop the reaction, 50 µL of 2 M H₂SO₄ were added and the absorbance of samples measured at 450 nm using the Synergy HT microplate reader (BioTek Instruments, Inc., Winooski, VT, USA). CETPI plasma concentration of all samples was determined using a standard curve.

Casein protease activity assay

Plasma protease activity was determined employing the Protease Activity Assay Kit (Abcam, Cambridge, UK), which uses FITC-Casein as a general protease substrate. Plasma samples were incubated with the protease substrate for 30 min at 25 °C, and fluorescence was measured at Ex/Em = 485/ 550 nm immediately after the protease substrate addition (R1) and at 30 min, after the incubation time (R2). Differences between both lectures (R2–R1), indicated the fluorescence of the unquenched FITC generated by the proteolytic digestion of the substrate. The plasma protease activity was reported as mU/mL. One unit was defined as the amount of protease that cleaves the substrate, to yield an amount of fluorescence equivalent to 1.0 µmol of unquenched FITC per minute at 25 °C.

Plasma LPS quantification

Plasma LPS was measured using a competitive inhibition enzyme immunoassay (Cloud-Clone Corp, Houston, TX, USA). This assay employs a monoclonal antibody specific to lipopolysaccharide pre-coated onto a microplate. 50 µL of dilutions of standard, blank, and samples were added into the appropriate wells. A competitive inhibition reaction was launched between biotin-labeled lipopolysaccharide and the unlabeled lipopolysaccharide present in the samples with the pre-coated antibody. After incubation for 1 h at 37 °C, the unbound conjugate is washed off, and then Avidin conjugated to HRP added to each well. The plates were incubated for 30 min at 37 °C and washed five times. The substrate solution was added to each well and after the incubation time (30 min at 37 °C), 50 µL of stop reaction solution were added. The absorbance was measured at 450 nm using a Synergy HT microplate reader (BioTek Instruments, Inc.). The intensity of color developed represents the amount of bound HRP that is inversely proportional to the concentration of LPS in the sample.

Albumin depletion

Albumin depletion of plasma samples was performed using the Pierce Albumin Depletion Kit (Thermo Fisher

Scientific). The kit consists of a high-capacity, immobilized Cibacron Blue dye agarose resin, which binds the albumin present in the plasma. Briefly, the resin was transferred into a spin column to be washed employing the Binding/Wash Buffer. After, the plasma sample was added and incubated for 1–2 min at RT. The spin column was centrifuged, and the flow-through was re-applied to the spin column and incubated for another 1–2 min at RT to ensure maximal albumin binding. After centrifugation, we stored the flow-through and placed the spin column in a new collection tube. The column was washed to release unbound proteins and albumin eluted with a solution of 20 mM sodium phosphate, 250 mM sodium thiocyanate, pH 7.2. The protein content was determined in the collected fractions and were further analyzed by SDS-PAGE.

Statistical analysis

Data are expressed as frequencies for categorical variables and as a mean with standard deviation (SD) or median with interquartile range (IQR) for continuous variables according to their distribution as assessed by Shapiro–Wilk normality test. When variables were not normally distributed, differences between groups were analyzed employing the Mann Whitney U-test, or the Kruskal–Wallis test with the Dunn's Multiple Comparison Test. In the case of variables with a normal distribution, the statistical analysis was performed using Student's t-tests.

The plasma values of CETPI and cytokines were transformed to logarithm (log 10) before performing the correlations analysis to normalize the distribution of data. Correlations between cytokines and CETPI plasma levels were assessed by the Pearson's correlation coefficient. Statistical test, significance level, n-numbers for each analysis are stated in figure legends. Differences were considered statistically significant at p < 0.05. The statistical analyses were performed employing the GraphPad Prism software (GraphPad Software, La Jolla, CA), and JMP 16.1.0 (SAS Institute, Cary NC, USA).

Results

Subjects and clinical parameters

Blood samples from 47 healthy subjects attending the blood bank at INCMNSZ for blood donation, were collected as controls, this group included 22 males and 25 females. Also, a total of 105 ICU patients were enrolled in this study; 50 patients with infection (Delta SOFA score < 2), and 55 patients with sepsis and septic shock (Delta SOFA score > 2), all patients with positive blood culture for Gram-negative bacteria (Table 1). The mean age in the overall population was 50.00 years

Table 1 Demographic, clinical and laboratory parameters of patients

	Total (n = 105)	Patients with Delta SOFA score < 2 (n = 50)	Patients with Delta SOFA score > 2 (n = 55)	p value
Gender, male	50 (47.62%)	27 (54.00%)	23 (41.82%)	0.24
Gender, female	55 (52.38%)	23 (46.00%)	32 (58.18%)	
Age (years)	50.00 (37.50–57.50)	54.50 (39.00–58.00)	47.00 (35.00–55.00)	0.17
Etiologic agent (%)				
<i>Escherichia coli</i>	61 (58.10%)	28 (56.00%)	33 (60.00%)	0.36
<i>Klebsiella pneumoniae</i>	12 (11.43%)	7 (14.00%)	5 (9.09%)	
<i>Pseudomonas aeruginosa</i>	12 (11.43%)	8 (16.00%)	4 (7.27%)	
Site of infection (%)				
Abdominal	71 (67.62%)	32 (64.00%)	39 (70.91%)	0.15
Urinary tract	20 (19.05%)	12 (24.00%)	8 (14.55%)	
Intravenous catheter	5 (4.76%)	3 (6.00%)	2 (3.64%)	
Pulmonary	4 (3.81%)	0 (0.00%)	4 (7.27%)	
Comorbidities				
Dyslipidemia	61 (58.10%)	32 (64.00%)	29 (52.73%)	0.89
Immunosuppression	55 (52.38%)	26 (52.00%)	29 (52.73%)	
Cancer	55 (52.38%)	28 (56.00%)	27 (49.09%)	
Liver dysfunction	27 (25.71%)	12 (24.00%)	15 (27.27%)	
Laboratory tests				
CRP (mg/L)	14.00 (7.30–19.80)	10.75 (4.80–16.87)	15.20 (9.47–21.50)	< 0.05
PCT (ng/mL)	7.40 (1.80–17.90)	3.10 (1.33–8.58)	11.40 (3.90–24.33)	< 0.01
Hemoglobin (g/dL)	10.27 ± 2.63	10.38 ± 2.62	10.17 ± 2.66	0.47
Serum Albumin (g/dL)	3.17 ± 0.73	3.26 ± 0.70	3.09 ± 0.76	0.23
Total bilirubin (mg/dL)	1.40 (0.62–4.90)	0.90 (0.60–2.93)	2.20 (0.90–7.40)	< 0.01
Lactate (mmol/L)	2.40 (1.40–4.00)	1.65 (1.18–2.60)	3.45 (1.63–4.20)	< 0.01
Creatinine (mg/dL)	0.90 (0.65–1.40)	0.80 (0.50–1.06)	1.00 (0.70–1.90)	< 0.01
White blood cells ($\times 10^9$ /L)	6.95 (0.35–12.30)	7.25 (0.60–12.18)	6.65 (0.10–12.30)	0.87
Platelet ($\times 10^3$ /μL)	107.0 (21.00–243.00)	162.50 (26.25–265.00)	100.00 (16.00–216.00)	0.19
HDL (mg/dL)	35.19 ± 17.71	36.88 ± 17.57	33.65 ± 17.89	0.40
Total cholesterol (mg/dL)	138.50 (113.30–181.80)	139.50 (109.00–201.30)	136.00 (115.80–165.50)	0.56
LDL (mg/dL)	75.00 (48.25–109.30)	77.00 (48.75–118.30)	73.00 (47.50–101.50)	0.46
Delta SOFA score	0–11	0–1	2–11	

Data are reported as mean (\pm SD), median (IQR), and n (%). Comparisons were performed with Fisher's exact test or Pearson's Chi-squared test, and either Mann-Whitney U test or Student's t-test. C-reactive protein (CRP); procalcitonin (PCT); High-Density Lipoprotein (HDL); Low-Density Lipoprotein (LDL); sequential organ failure assessment (SOFA)

(37.50–57.50), of which 55 (52.38%) were female and 50 (47.62%) male.

In all patients, the most prevalent bacteria isolated from the bloodstream was *Escherichia coli* (58.10%), and the main sites of infection were the abdomen (67.62%), and the urinary tract (19.05%) (Table 1). In patients with Delta SOFA score < 2, the main comorbidities corresponded to dyslipidemia (64.00%), cancer (56.00%), immunosuppression (52.00%), and liver dysfunction (24.00%). In patients with Delta SOFA score > 2, dyslipidemia (52.73%), immunosuppression (52.73%), cancer (49.09%), and liver dysfunction (27.27%) were also the principal comorbidities (Table 1).

The main clinical parameters of patients are shown in Table 1, CRP levels were lower in patients with Delta SOFA score < 2 (10.75 [4.80–16.87]), than in patients with Delta SOFA score > 2 (15.20 [9.47–21.50], $p < 0.05$). PCT levels were also higher in patients with Delta SOFA score > 2 (11.40 [3.90–24.33]) compared to patients with Delta SOFA score < 2 (3.10 [1.33–8.58], $p < 0.01$). Also, significant differences were observed in the levels of total bilirubin, lactate, and creatinine between patients with Delta SOFA score > 2, and those with Delta SOFA score < 2 (Table 1).

The concentration of CETPI in plasma is higher in patients with Gram-negative bacteraemia

To explore the relation between CETPI and disease severity in infections due to Gram-negative bacteria, circulating levels of CETPI were measured in the plasma from controls and patients with infection (Delta SOFA score < 2), sepsis, and septic shock (Delta SOFA score > 2) employing ELISA. We found that patients with an infectious process due to Gram-negative bacteria had elevated circulating levels of CETPI when compared to control subjects (15.21 nM [10.52–26.23] vs 11.58 nM [8.05–14.71], $p < 0.001$) (Fig. 1A), showing a clear difference in the distribution of the data between controls and patients above 18 nM (Additional file 1: Fig. S1). Although differences in CETPI plasma levels were found between control subjects and patients with Delta SOFA score < 2 (11.58 nM [8.05–14.71] vs 13.54 nM [9.99–26.65],

$p < 0.05$), and with those with Delta SOFA score > 2 (11.58 nM [8.05–14.71] vs 16.00 nM [11.30–26.11], $p < 0.001$), no differences were observed between patients grouped according with the Delta SOFA score greater or less than 2 (Fig. 1B). Patients who had a severe outcome (in-hospital death), did not have significantly differences in CETPI levels than those with a non-severe outcome (Fig. 1C).

CETPI and plasma cytokines correlate with SOFA score in patients with Gram-negative bacteraemia

In parallel to the determination of plasma levels of CETPI, plasma cytokine concentrations of IL-1 β , TNF α , IL-6, IL-8, IL-12 (p70), IFN γ , and IL-10 were also measured (Fig. 2). Given that higher CETPI levels were found in patients compared with healthy subjects, and considering its ability to bind LPS, a correlation between

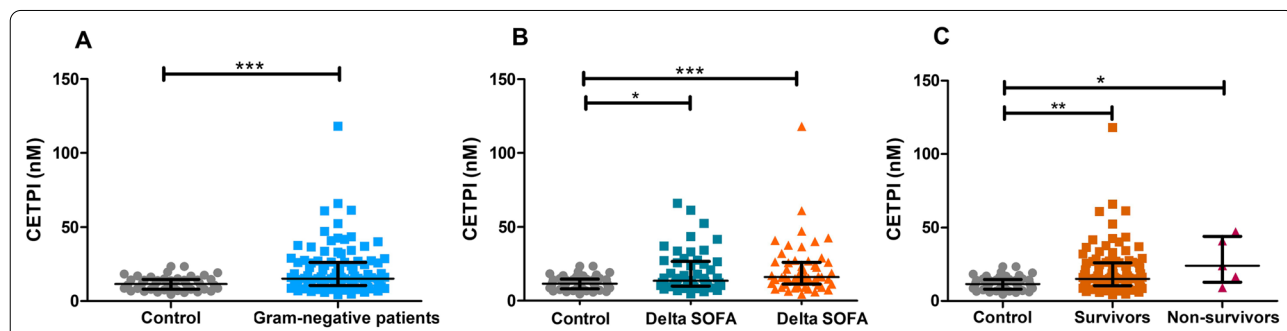


Fig. 1 CETPI plasma levels in patients with Gram-negative bacteraemia. **A** CETPI plasma concentration of patients with a positive blood culture for Gram-negative bacteria ($n = 105$) and control subjects ($n = 47$). **B** CETPI plasma concentration of patients with Delta SOFA score ≤ 2 ($n = 50$), or > 2 ($n = 55$) and control subjects ($n = 47$). **C** CETPI plasma concentration between survivors ($n = 100$), non-survivors ($n = 5$), and control subjects ($n = 47$). Data are shown as median with IQR. * $p < 0.05$, ** $p < 0.01$, *** $p < 0.001$. Differences between groups were assessed using Mann-Whitney test or Kruskal-Wallis test and subsequent Dunn's Multiple Comparison test. Samples were assessed in duplicate in ELISA assays

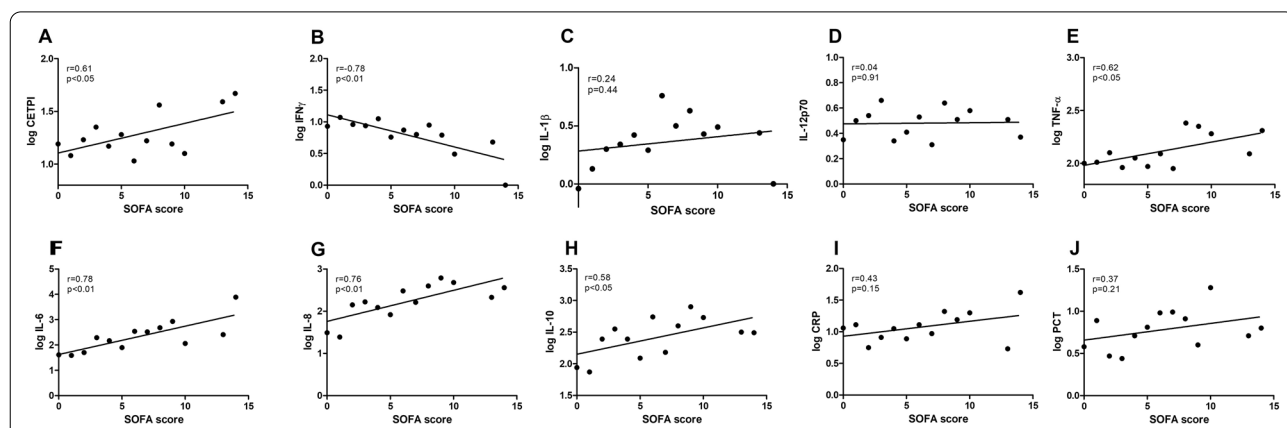


Fig. 2 Correlation between SOFA score measured within 12 h of ICU admission with CETPI and cytokines in patients with Gram-negative bacteraemia. Pearson correlations show associations between SOFA score with the mean values of CETPI and relevant cytokines in patients. **A** CETPI. **B** IFN γ . **C** IL-1 β . **D** IL-12p70. **E** TNF- α . **F** IL-6. **G** IL-8. **H** IL-10. **I** CRP. **J** PCT. The levels of the 7 cytokines and CETPI, CRP, PCT were transformed to common logarithm values for the correlations. SOFA: Sequential Organ Failure Assessment; CRP: C-Reactive Protein; PCT: Procalcitonin

SOFA scores (measured within 12 h of ICU admission) with CETPI, and plasma cytokines were carried out. We found that SOFA scores positively correlate with CETPI ($r=0.61$, $p<0.05$), TNF- α ($r=0.62$, $p<0.05$), IL-6 ($r=0.78$, $p<0.01$), IL-8 ($r=0.76$, $p<0.01$), and IL-10 ($r=0.58$, $p<0.05$); whereas a negative correlation was found with IFN γ ($r=-0.78$, $p<0.01$) (Fig. 2A–J).

CETPI plasma levels negatively correlate with IL-1 β , IL-8, and IL-10 in septic shock patients

To explore the association between CETPI plasma levels with cytokines implicated in the pathophysiology of Gram-negative infections, a correlation was carried out. First, we analyzed CETPI and cytokine expression in patients with infection, sepsis, and septic shock (Fig. 3A–H). Although no differences in CETPI levels were found in the three patient groups, in septic shock patients CETPI levels tend to increase (Fig. 3A) (Additional file 1: Fig. S1); also, significant differences in the levels of IL-6, IFN γ , and IL-8 were found. IL-6 levels were found to be fivefold higher in septic shock patients, and 2.7-fold

higher in sepsis patients, compared with patients with infection (319.00 pg/mL [105.1–1870.00] and 61.81 pg/mL [56.98–1033.00] vs 61.81 pg/mL [21.56–370.5]; $p<0.01$ and $p<0.05$) (Fig. 3B). IFN γ levels were 2.7-fold lower in septic shock patients compared with patients with infection (3.2 pg/mL [2.23–9.21] vs 8.58 pg/mL [3.84–27.01], $p<0.05$) (Fig. 3D). IL-8 levels were 3.2-fold higher in septic shock patients compared with patients with infection (182.60 pg/mL [97.34–621.70] vs 55.40 pg/mL [21.74–218.30], $p<0.01$) (Fig. 3F).

We next assessed the correlation between the full set of cytokines and CETPI in patients with infection, sepsis, and septic shock through the Pearson correlation coefficient. There were positive correlations between the pro-inflammatory cytokines in infection patients, and more importantly, in sepsis patients (Fig. 3I, J) (Additional file 1: Table S1 and S2). However, in septic shock patients, the correlation between IFN γ and IL-12 (p70) with CETPI, IL-1 β , TNF- α , IL-6, IL-8, and IL-10, were not significant (Fig. 3K). IL-10 showed positive correlations with the other six cytokines studied in patients

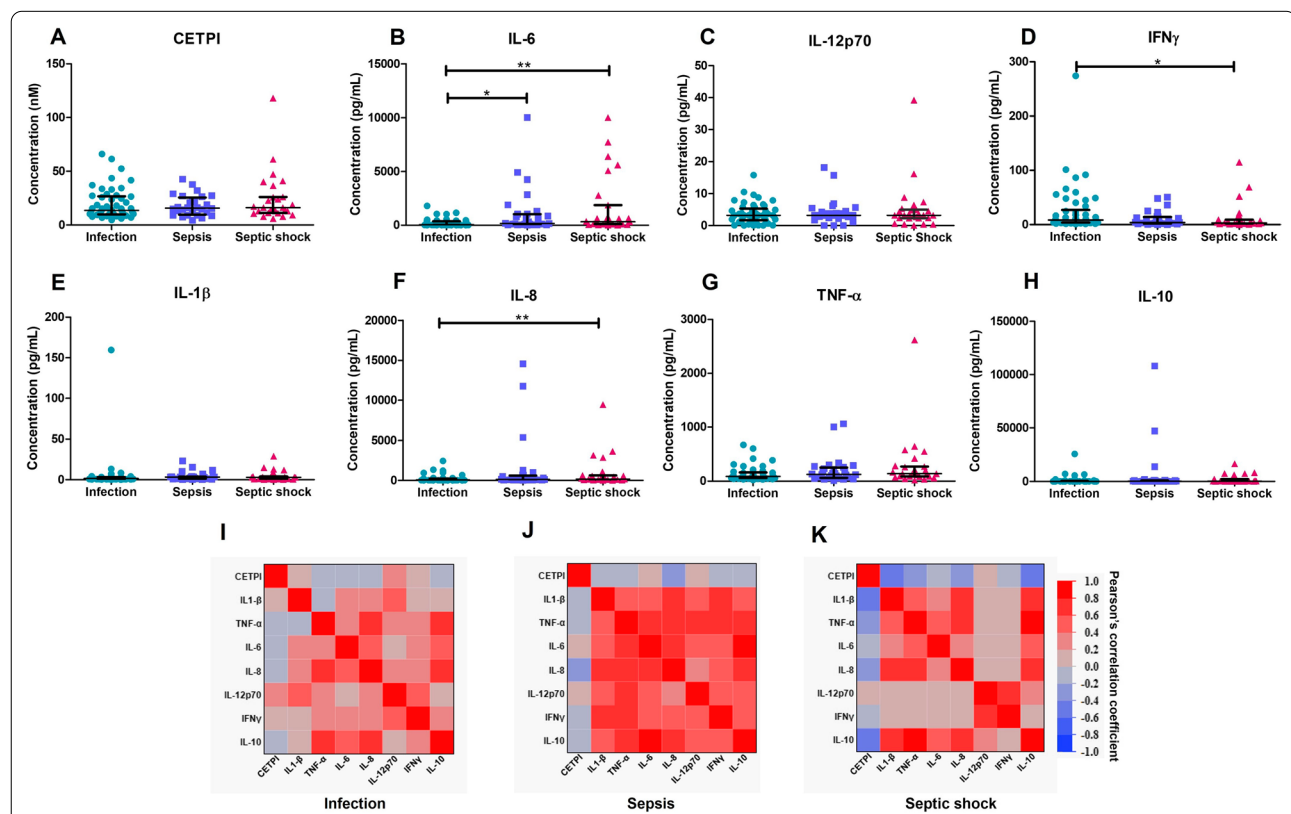


Fig. 3 CETPI and cytokines plasma levels in patients with infection, sepsis, and septic shock due to Gram-negative bacteria. **A** CETPI. **B** Interleukin-6 (IL-6). **C** Interleukin-12p70 (IL-12p70). **D** Interferon γ (IFN γ). **E** Interleukin-1 beta (IL-1 β). **F** Interleukin-8 (IL-8). **G** Tumor necrosis factor-alpha (TNF- α). **H** Interleukin-10 (IL-10). Data are shown as median with IQR; * $p<0.05$, ** $p<0.01$; Differences between groups were assessed using Kruskal-Wallis test and subsequent Dunn's Multiple Comparison test. **I** Pearson's correlation values between the 7 cytokines and CETPI in patients with infection, **J** sepsis, and **K** septic shock. The red color indicates a positive correlation, and the blue color a negative correlation

with sepsis (Fig. 3J), and with IL-1 β , TNF- α , IL-6, and IL-8 in patients with septic shock (Fig. 3K) (Additional file 1: Table S2 and S3). Interestingly, there were negative correlations between CETPI with IL-1 β , IL-8, and IL-10 in septic shock patients (Fig. 3K) (Additional file 1: Table S3).

Patients with liver dysfunction present increased plasma concentrations of LPS and CETPI

Considering that the main site of infection in all patients studied corresponds to an intra-abdominal origin (Table 1), and that hepatic cells are involved in the clearance of LPS of intestinal origin, we analyzed the levels of LPS and CETPI in the plasma of patients with and without liver dysfunction (Fig. 4). Plasma LPS levels were higher in patients that presented liver dysfunction (Fig. 4A–C), with differences in patients with infection versus patients with infection but without liver dysfunction (577.90 pg/mL [487.20–1136.00] vs 214.90 pg/mL [105.90–400.70], $p < 0.05$) (Fig. 4A). Interestingly, the plasma concentration of CETPI was also found to be higher in infection (31.19 nM [20.07–40.58]), and sepsis patients (28.21 nM [24.34–34.65]) with liver dysfunction compared with patients with infection (12.35 nM [9.50–17.41]) and sepsis (14.45 nM [9.04–19.39]) without this comorbidity (Fig. 4D, E). Although the differences

showed not to be statistically significant, a similar increase in CETPI concentration was observed in septic shock patients (24.10 nM [13.54–44.07]) with respect to patients without liver dysfunction (14.84 nM [10.29–23.44]) (Fig. 4F). Besides, it is shown that a high plasma CETPI and LPS levels correlate in patients with infection and sepsis due to Gram-negative bacteria (Additional file 1: Fig. S2).

Proteolytic activity upon CETPI is associated with disease severity

We analyzed the CETPI expression employing a Western Blot analysis in plasma samples of both controls and patients (Fig. 5). In the plasma of controls, it was detected the expected band of 69 kDa (Fig. 5A), whereas, when plasma samples from patients were analyzed, together with the regular protein band corresponding to CETPI (69 kDa), a lower molecular weight protein band (\sim 67 kDa) appeared (Fig. 5B). Although a basal level of CETPI was detected in control plasma samples, it did not show any type of correlation with the negligible concentration of inflammatory cytokines (Fig. 5C, D). However, when plasma samples from patients with infection were analyzed, the presence of the 67 kDa band was associated with the increased level of inflammatory cytokines, especially with IL-6 (Fig. 5E, F) (Additional file 1: Table S4).

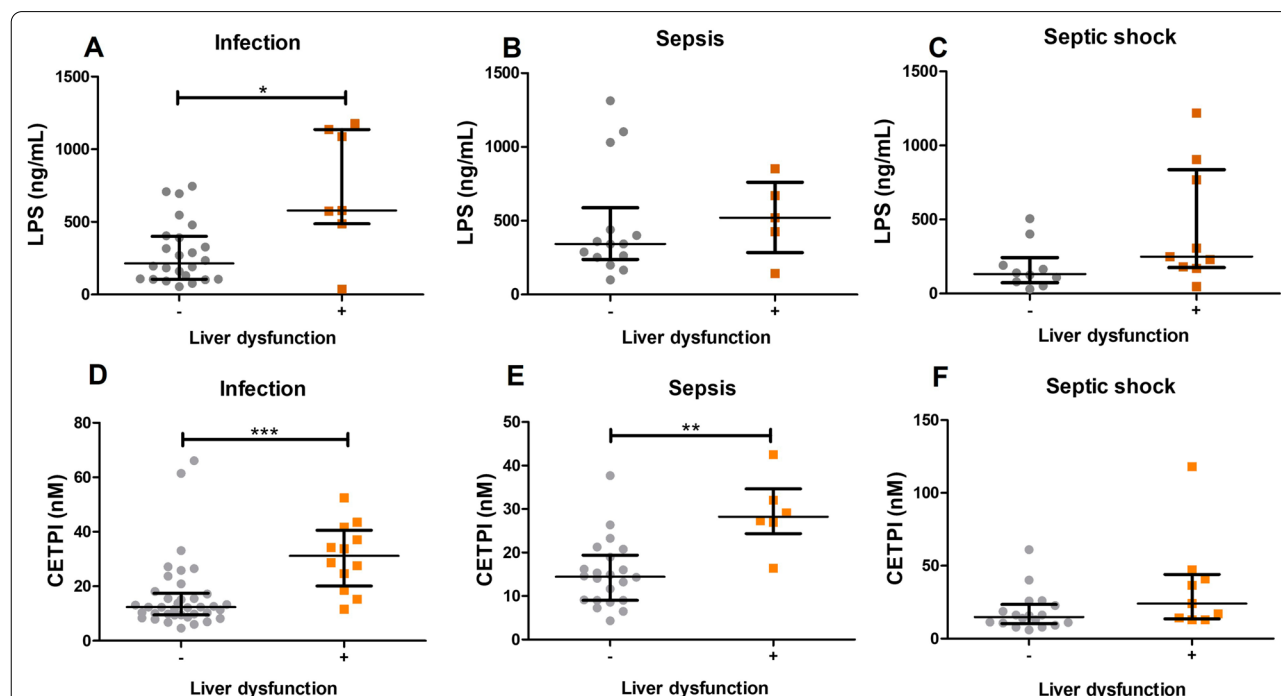


Fig. 4 LPS and CETPI plasma levels in patients with or without liver dysfunction. LPS plasma levels from patients with **A** Infection ($n=31$); **B** Sepsis ($n=19$); **C** Septic shock ($n=19$), classified according to the presence or absence of liver dysfunction. CETPI plasma levels from patients with **D** Infection ($n=50$); **E** Sepsis ($n=28$); **F** Septic shock ($n=27$), classified according to the presence or absence of liver dysfunction. Differences between groups were assessed using Mann–Whitney test. Data are shown as median with IQR. * $p < 0.05$, ** $p < 0.01$, *** $p < 0.001$

Moreover, when plasma samples from patients with sepsis and septic shock were analyzed, this phenomenon was exacerbated showing a clear association with the presence of the ~67 kDa accessory protein band, and a marked increase in IL-6 and IL-10 (Fig. 5G, H) (Additional file 1: Table S4).

In order to find out the origin of the ~67 kDa band observed in the Western blot analysis, we employed HPLC-mass spectrometry. Interestingly, sequences directly related to the sequence for CETPI were found (Fig. 6A). However, the question arises, how an anti-CETPI antibody raised against the C-terminal sequence of CETPI, not present in CETP, permitted us to identify a second band in the western blot analysis? We found that the largest percentage of peptides identified by HPLC-mass spectrometry analysis of the ~67 kDa band, corresponds to sequences belonging to albumin, a well-known protein that readily binds peptides. Therefore, we decided to find out if contained in the plasma of sepsis and septic shock patients, albumin that normally shows an average molecular weight of 66.5 kDa, might contain bound-peptides derived from the C-terminal segment of CETPI. For this purpose, following a procedure to eliminate albumin from the plasma of sepsis and septic shock patients, samples were eluted through columns containing an albumin-binding resin. Interestingly, we do not detect the ~67 kDa in the albumin-depleted plasma samples (Fig. 6B). Considering that the elution of the albumin of the columns was done employing harsh conditions, peptides initially bound to albumin most probably became detached and eliminated, and therefore not detected in association with albumin (Fig. 6B). This set of experiments, confirm that peptides derived from the C-terminal region of CETPI, when bound to albumin are responsible for the positive Western blot signal found at ~67 kDa (Fig. 6B).

Overall, these results suggest the possibility that the activation of proteolytic enzymes might occur in the plasma of patients with sepsis and septic shock, therefore, the proteolytic activity upon CETPI could be generating peptides that eventually end up binding to albumin. In order to further explore this possibility, an analysis of the most susceptible sites for proteolytic cleavage at the C-terminal domain of CETPI was carried out. Interestingly, we found such positions where enzymes matrix-metallopeptidase-2 (MMP-2), elastase-2, chymotrypsin

A, and matrix-metallopeptidase-9 (MMP-9) might act (Fig. 6C). This analysis and the increased protease activity found in the plasma samples from all patient groups, in comparison with controls (Fig. 6D), support the hypothesis that the 67 kDa accessory protein band, corresponding to albumin, contains cleaved peptides derived from the C-terminal segment of CETPI, and therefore identified by the anti-CETPI antibody.

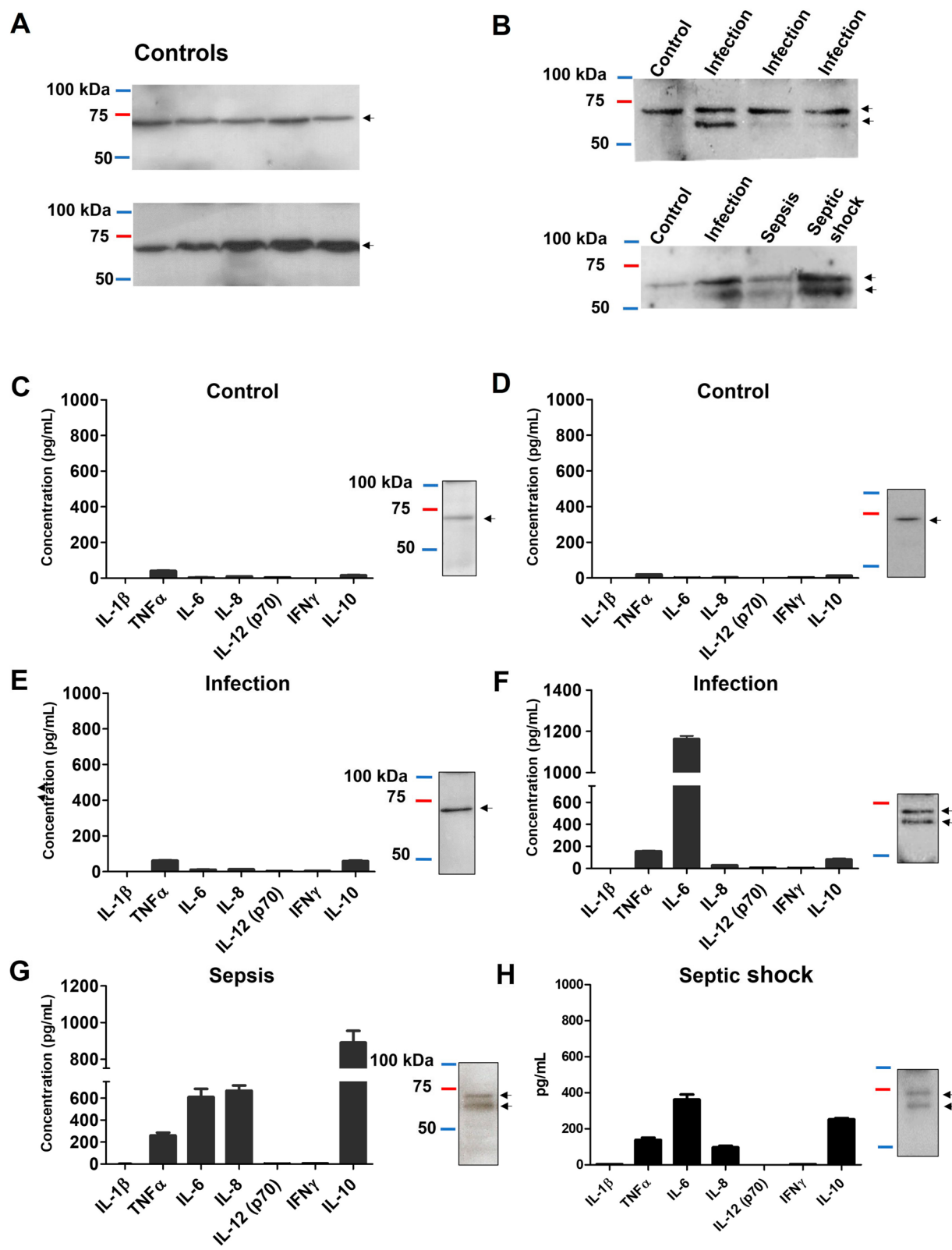
Discussion

Sepsis as a life-threatening syndrome with important variations in terms of incidence and mortality across the world, affects according to the World Health Organization, around 50 million people every year associated with 11 million deaths (WHO 2020). Therefore, this syndrome is responsible for approximately 20% of total deaths in the world in a single year (Rudd et al. 2020). Several pathophysiological alterations are present in sepsis, where a balanced response to the infection is essential to improve the survival rate. In this study, we describe the existing correlation between the severity of the disease, CETPI and LPS plasma levels during Gram-negative bacteraemia.

Our results show the presence of a high plasma CETPI concentration in the patients with an infectious process due to Gram-negative bacteria, in comparison to the control group. Since we have previously reported the presence of CETPI in the plasma of healthy subjects (Alonso et al. 2003), here as increased concentrations of CETPI have been found in patients with Gram-negative bacteraemia, we consider its role as a potential LPS-binding protein, and therefore as a participant in the physiological response to LPS. Although no direct differences were found in the concentration of CETPI between patients, an important correlation was found between CETPI concentrations and the SOFA score, indicating an association with the degree of organ dysfunction/failure (Lambden et al. 2019). A direct correlation between the SOFA score and IL-6, TNF- α , IL-8, and IL-10 was also observed. Interestingly, TNF- α and IL-6 as cytokines involved in endothelial damage, and multiple organ dysfunction syndrome, are often used as biomarkers for sepsis (Miguel-Bayarri et al. 2012; Molano Franco et al. 2019; Grondman et al. 2020). Whereas, IL-8 has been proposed as a prognostic factor in septic patients (Livaditi et al. 2006; Anderson et al. 2019), and IL-10 has been

(See figure on next page.)

Fig. 5 Association between cytokine plasma levels, and the presence of CETPI in the plasma of representative samples from control subjects and patients. **A** CETPI expression in plasma samples from control subjects. **B** Top: CETPI expression in plasma samples from control subjects and patients with infection. Down: CETPI expression in plasma samples from control subjects and patients with infection, sepsis, and septic shock. **C, D** Plasma samples obtained from control subjects; **E, F** patients with infection; **G** sepsis; and **H** septic shock. Left panels show the level of IL-1 β , TNF α , IL-6, IL-8, IL-12 (p70), IFN γ , and IL-10 (Data are presented as mean \pm SEM). At the right of each graph, the protein band that corresponds to CETPI (arrow tips) determined by western blot analysis, is shown. The same plasma samples were used for both measurements of plasma cytokines and CETPI

**Fig. 5** (See legend on previous page.)

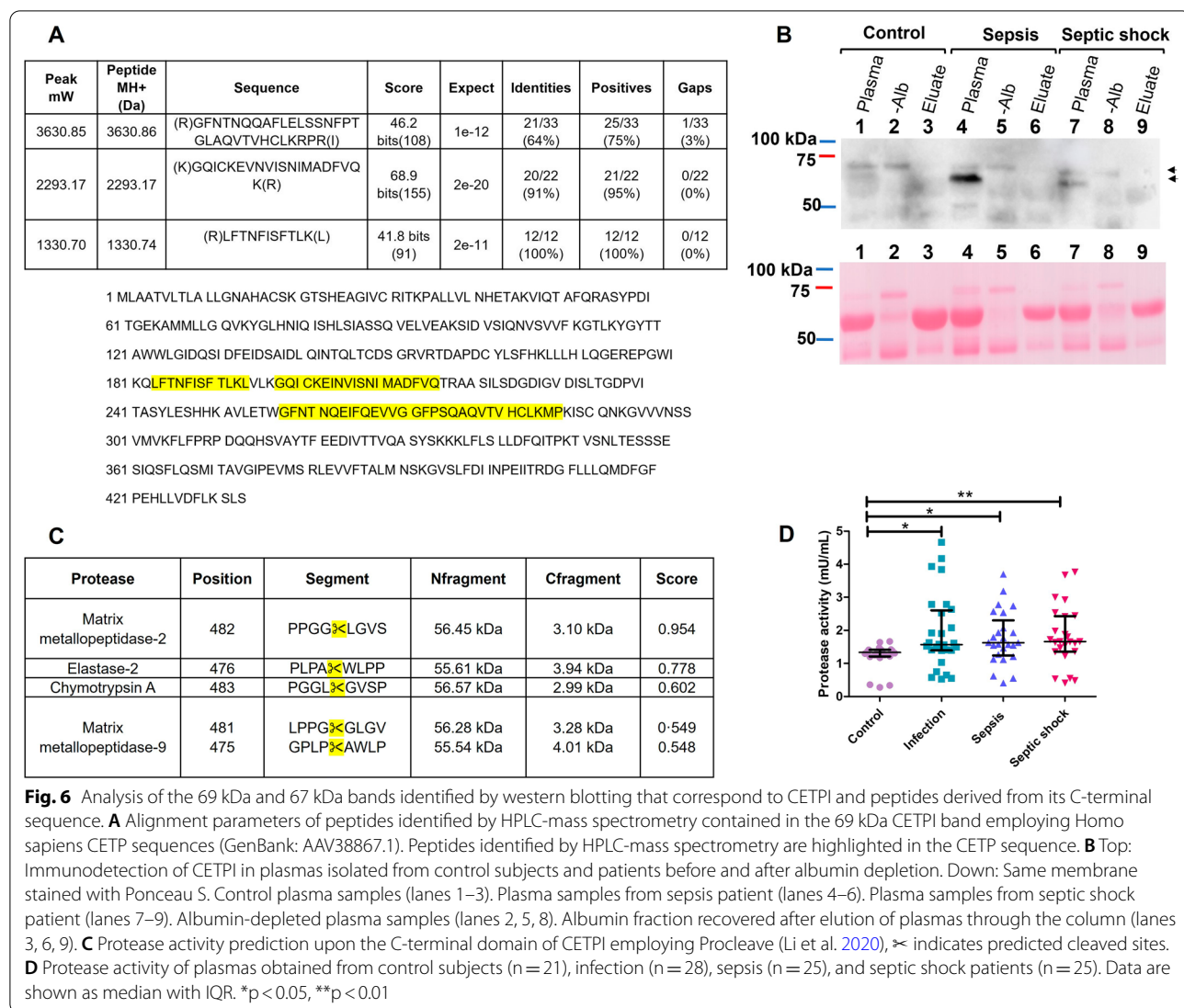


Fig. 6 Analysis of the 69 kDa and 67 kDa bands identified by western blotting that correspond to CETPI and peptides derived from its C-terminal sequence. **A** Alignment parameters of peptides identified by HPLC-mass spectrometry contained in the 69 kDa CETPI band employing Homo sapiens CETP sequences (GenBank: AAV38867.1). Peptides identified by HPLC-mass spectrometry are highlighted in the CETP sequence. **B** Top: Immunodetection of CETPI in plasmas isolated from control subjects and patients before and after albumin depletion. Down: Same membrane stained with Ponceau S. Control plasma samples (lanes 1–3). Plasma samples from sepsis patient (lanes 4–6). Plasma samples from septic shock patient (lanes 7–9). Albumin-depleted plasma samples (lanes 2, 5, 8). Albumin fraction recovered after elution of plasmas through the column (lanes 3, 6, 9). **C** Protease activity prediction upon the C-terminal domain of CETPI employing Procleave (Li et al. 2020). **x** indicates predicted cleaved sites. **D** Protease activity of plasmas obtained from control subjects ($n=21$), infection ($n=28$), sepsis ($n=25$), and septic shock patients ($n=25$). Data are shown as median with IQR. * $p<0.05$, ** $p<0.01$

used as an indicator of a hypoinflammatory phenotype (Barichello et al. 2022). On the other hand, IFN γ that negatively correlates with the SOFA score, is known to be required during the host defense against pathogens, therefore contributing to a worse prognosis if the infection is not being controlled (Ono et al. 2018). Patients with septic shock present higher IL-6 and IL-8 plasma levels and lower levels of IFN γ than patients with infection, showing that an impaired immune response contributes to a worse prognosis. Our results also show a positive correlation between IL-10 and pro-inflammatory cytokines, whose simultaneous presence has been associated with the pathogenesis of sepsis (Matsumoto et al. 2018).

Experiments from our group where LPS-treated rabbits were administered with a peptide derived from the carboxy-end segment of CETPI, showed attenuated

circulating levels of pro-inflammatory molecules (Luna-Reyes et al. 2021). During the present investigation, based on the high levels of CETPI found in patients with Gram-negative bacteraemia, we explored its relationship with the cytokine plasma levels, and found negative correlations between CETPI with IL-1 β , IL-8, and IL-10. These results are consistent with the LPS-binding role of CETPI, showing an interesting correlation with the release of IL-8 by the gut (García-González, et al. 2015; Luna-Reyes et al. 2021; Liu et al. 2006; Angrisano et al. 2010).

An in vitro study carried out by our group several years ago, shows a clear correlation between an increase in CETPI expression by Caco-2 cells and small intestine cells, under LPS stimulation (García-González, et al. 2015). Considering that CETPI apparently is only synthesized by intestinal cells, the increased level of LPS in

circulation could promote the overexpression of CETPI in the intestinal epithelium as an early protective mechanism against the harmful action of LPS. Since LPS either entering the circulatory system from the intestinal tract through the portal circulation, or due to the antibiotic action upon bacteria, find their way to the liver, a key organ in the deactivation and clearance of LPS (Pérez-Hernández et al. 2021; Shao et al. 2007), our results are consistent with the fact that patients presenting liver dysfunction show an increased LPS plasma level (Bode et al. 1987; Parlesak et al. 2000; Thuy et al. 2008; Nier et al. 2020). This finding associated with the fact that patients showing liver dysfunction present even higher plasma CETPI levels, place CETPI as a promising biomarker of disease severity.

We consider this a clear response to infection and endotoxemia caused by the presence of LPS in the bloodstream following antimicrobial treatment, and/or when the intestinal epithelium starts to be compromised. Although endotoxemia might have other origins such as trauma, if we consider the gut as a major source of infection, the alteration of the intestinal barrier might be considered an important cause for this clinical condition (Pérez-Hernández et al. 2021).

The overexpression of CETPI associated with the formation of peptides secondary to proteolytic cleavage, seems to represent what it can be considered, a true emergency response system, switched-on at the start of an infection, and further developed in sepsis and septic shock. As consistently shown here with our western blot analysis of plasmas from all patient groups, the correlation between the appearance of the ~67 kDa electrophoretic band associated with the presence of proteolysis and generation of CETPI derived peptides, higher IL-6 levels, and organic failure, can be concurrent with other indicators of disease severity (Schulte et al. 2013; Fan et al. 2016).

Since the presence of systemic proteolysis has been associated with a high mortality rate in septic shock patients (Bauzá-Martínez et al. 2018), the fact that we did not find significant differences between infection, sepsis, and septic shock patients, seems to be related to the low mortality rate (4.8%) observed by us. Taking into account that CETPI is expressed in small intestine cells (Alonso et al. 2003), associated with the fact that the main source of infection in our patients is abdominal, proteolysis of CETPI by matrix metalloproteinases (MMPs) and serine proteases cannot be ruled out. In support of this possibility, the analysis for protease prediction performed by us shows that the C-terminal domain of CETPI presents potential cleavage sites for chymotrypsin A, elastase-2, MMP-9, and MMP-2.

Considering that CETPI might correspond to a protein that binds LPS in vivo, one of the limitations of this study is that we only included patients with positive blood cultures for Gram-negative bacteria. Therefore, it will be also of interest to explore the physiological role of CETPI in patients presenting other etiologies and a non-infectious systemic inflammatory response. Also, data presented here, corresponds to clinical data and plasma samples obtained within 12 h of ICU admission, thus, both the clinical information and the analysis of plasmas collected 48 h after admission, are currently being studied and should be reported soon.

Conclusion

This study provides new insights into the role of CETPI in sepsis due to Gram-negative bacteria. Given that a fine balance control given by diverse immune responses is essential in the prognosis of a septic patient, CETPI can be considered as a new LPS-binding protein, and therefore as a novel player in the pathophysiology of sepsis.

Abbreviations

CETPI: Isoform of the cholesteryl-ester transfer protein; LPS: Lipopolysaccharides; IL-1 β : Interleukin-1 beta; TNF α : Tumor necrosis factor-alpha; IL-6: Interleukin-6; IL-8: Interleukin-8; IL-12p70: Interleukin-12p70; IFN γ : Interferon γ ; IL-10: Interleukin-10; SOFA: Sequential Organ Failure Assessment; ICU: Intensive care unit; HDL: High-density lipoproteins; LDL: Low-density lipoproteins; CETP: Cholesteryl-ester transfer protein; ELISA: Enzyme-linked immunosorbent assay; INCMNSZ: Instituto Nacional de Ciencias Médicas y Nutrición "Salvador Zubirán"; CRP: C-reactive protein; PCT: Procalcitonin; RT: Room temperature; PBS: Phosphate-Buffered Saline; SD: Standard deviation; IQR: Interquartile range; MMP-2: Matrix-metallopeptidase-2; MMP-9: Matrix-metallopeptidase-9; MMPs: Matrix metalloproteinases.

Supplementary Information

The online version contains supplementary material available at <https://doi.org/10.1186/s10020-022-00585-3>.

Additional file 1: Figure S1. Empirical cumulative distribution of the CETPI measurements. Empirical cumulative distribution of CETPI plasma concentration of controls ($n=47$) and patients with infection ($n=50$), sepsis ($n=28$), and septic shock ($n=27$), with a positive blood culture for Gram-negative bacteria. **Figure S2.** LPS correlates with CETPI plasma levels in patients with Gram-negative bacteraemia. Correlation between LPS with CETPI levels in patients with A infection ($n=31$), B sepsis ($n=19$), and C septic shock ($n=19$). Spearman correlations show associations between LPS and CETPI in patients with infection and sepsis. **Table S1.** Probability of correlation between cytokines and CETPI in patients with infection shown in Fig. 3I. **Table S2.** Probability of correlation between cytokines and CETPI in patients with sepsis shown in Fig. 3J. **Table S3.** Probability of correlation between cytokines and CETPI in patients with septic shock shown in Fig. 3K. **Table S4.** Clinical parameters of patients with E, F infection, G sepsis, and H septic shock shown in Fig. 5.

Acknowledgements

We would like to express a special thanks to Tzipe Govezensky for her expert advice in the statistical analysis of data. We also thank Georgina Díaz-Herrera, and Dra. Hilda Vázquez-López for experimental assistance. Also, Aurey Galván and Manuel Ortiz for technical support. Eréndira G. Pérez-Hernández

received a scholarship from CONACYT (465348) in support of her PhD studies. Ismael Luna-Reyes is currently receiving a scholarship from CONACYT (2019-000037-02NACF-25744) for the development of his PhD studies.

Author contributions

EGP-H performed experiments, contributed to analysis of results, and manuscript preparation. VP-D contributed to sample acquisition, clinical design, and analysis of results. IL-R performed experiments and contributed to the analysis of results. B.D-C. contributed to the analysis of results. JS-O contributed to the design and development of all clinical aspects of the study, and to the analysis of results. JM-O conceived the study and guided it throughout, contributed to the analysis of results, and wrote the paper. All authors read and approved the final manuscript.

Funding

This work was supported by grants UNAM-PAPIIT IN207121, UNAM-PAPIIT IN206619, and Estímulo a Investigaciones Médicas "Miguel Alemán Valdés", Fundación Miguel Alemán A.C.

Availability of data and materials

All data generated or analyzed during this study are included in the paper and its supplementary information files. Also, relevant data are available from the authors upon reasonable request.

Declarations

Ethics approval and consent to participate

This study was approved by INCMSZ's Research Ethics Committee (Reference number: 2252) and performed in accordance with the Declaration of Helsinki. Written informed consents were obtained from all participants before data and biological specimen collection.

Consent for publication

Not applicable.

Competing interests

J.M.-O. is inventor on patent application PCT/MX2014/00087 related to this study, "Peptides derived from the C-terminal domain of CETPI as molecules blocking the lipopolysaccharide-induced effect in sepsis and septic shock", submitted to the World Intellectual Property Organization and held by Universidad Nacional Autónoma de México. IL-R, E.G.P-H., VP-D, B.D-C., JS-O declare no competing conflict of interest.

Author details

¹Instituto de Fisiología Celular, Universidad Nacional Autónoma de México, 04510 Ciudad de Mexico, Mexico. ²Departamento de Medicina Interna, Instituto Nacional de Ciencias Médicas y Nutrición "Salvador Zubirán", 14080 Ciudad de Mexico, Mexico. ³Dirección de Medicina, Instituto Nacional de Ciencias Médicas y Nutrición "Salvador Zubirán", 14080 Ciudad de Mexico, Mexico.

Received: 7 June 2022 Accepted: 4 December 2022

Published online: 19 December 2022

References

- Alonso AL, Zentella-Dehesa A, Mas-Oliva J. Characterization of a naturally occurring new version of the cholesterol ester transfer protein (CETP) from small intestine. *Mol Cell Biochem*. 2003;245:173–82.
- Anderson BJ, Calfee CS, Liu KD, Reilly JP, Kangelaris KN, Shashaty MGS, et al. Plasma sTNFR1 and IL8 for prognostic enrichment in sepsis trials: a prospective cohort study. *Crit Care*. 2019;23:400.
- Angrisano T, Pero R, Peluso S, Keller S, Sacchetti S, Bruni CB, et al. LPS-induced IL-8 activation in human intestinal epithelial cells is accompanied by specific histone H3 acetylation and methylation changes. *BMC Microbiol*. 2010;10:172.
- Barichello T, Generoso JS, Singer M, Dal-Pizzol F. Biomarkers for sepsis: more than just fever and leukocytosis—a narrative review. *Crit Care*. 2022;26:14.
- Bauzá-Martínez J, Aletti F, Pinto BB, Ribas V, Odena MA, Díaz R, et al. Proteolysis in septic shock patients: plasma peptidomic patterns are associated with mortality. *Br J Anaesth*. 2018;121:1065–74.
- Beamer LJ. Structure of human BPI (bactericidal/permeability-increasing protein) and implications for related proteins. *Biochem Soc Trans*. 2003;31:791–4.
- Bode C, Kugler V, Bode JC. Endotoxemia in patients with alcoholic and non-alcoholic cirrhosis and in subjects with no evidence of chronic liver disease following acute alcohol excess. *J Hepatol*. 1987;4:8–14.
- Cecconi M, Evans L, Levy M, Rhodes A. Sepsis and septic shock. *The Lancet*. 2018;392:75–87.
- Fan SL, Miller NS, Lee JJ, Remick DG. Diagnosing sepsis—the role of laboratory medicine. *Clin Chim Acta*. 2016;460:203–10.
- Font MD, Thyagarajan B, Khanna AK. Sepsis and Septic Shock—basics of diagnosis, pathophysiology and clinical decision making. *Med Clin North Am*. 2020;104:573–85.
- García-González V, Gutiérrez-Quintanar N, Mas-Oliva J. The C-terminal domain supports a novel function for CETPI as a new plasma lipopolysaccharide-binding protein. *Sci Rep*. 2015;5:16091.
- Grondman I, Pirvu A, Riza A, Ioana M, Netea MG. Biomarkers of inflammation and the etiology of sepsis. *Biochem Soc Trans*. 2020;48:1–14.
- Krasity BC, Troll JV, Weiss JP, McFall-Ngai MJ. LBP/BPI proteins and their relatives: conservation over evolution and roles in mutualism. *Biochem Soc Trans*. 2011;39:1039–44.
- Lambden S, Laterre PF, Levy MM, Francois B. The SOFA score—development, utility and challenges of accurate assessment in clinical trials. *Crit Care*. 2019;23:374.
- Li F, Leier A, Liu Q, Wang Y, Xiang D, Akutsu T, et al. Procleave: predicting protease-specific substrate cleavage sites by combining sequence and structural information. *Genomics Proteomics Bioinformatics*. 2020;18:52–64.
- Liu YW, Chen CC, Tseng HP, Chang WC. Lipopolysaccharide-induced transcriptional activation of interleukin-10 is mediated by MAPK- and NF-κB-induced CCAAT/enhancer-binding protein δ in mouse macrophages. *Cell Signal*. 2006;18:1492–500.
- Livaditi O, Kotanidou A, Psarra A, Dimopoulos I, Sotiropoulou C, Augustatou K, et al. Neutrophil CD64 expression and serum IL-8: sensitive early markers of severity and outcome in sepsis. *Cytokine*. 2006;36:283–90.
- Luna-Reyes I, Pérez-Hernández EG, Delgado-Coello B, Ávila-Rodríguez MÁ, Mas-Oliva J. Peptide VSAK maintains tissue glucose uptake and attenuates pro-inflammatory responses caused by LPS in an experimental model of the systemic inflammatory response syndrome: a PET study. *Sci Rep*. 2021;11:14752.
- Matsumoto H, Ogura H, Shimizu K, Ikeda M, Hirose T, Matsuura H, et al. The clinical importance of a cytokine network in the acute phase of sepsis. *Sci Rep*. 2018;8:13995.
- Miguel-Barriá V, Casanoves-Laparra EB, Pallás-Beneyto L, Sancho-Chinesta S, Martín-Osorio LF, Tormo-Calandín C, et al. Prognostic value of the biomarkers procalcitonin, interleukin-6 and C-reactive protein in severe sepsis. *Med Intensive*. 2012;36:556–62.
- Molano Franco D, Arevalo-Rodríguez I, Roqué i Figuls M, Montero Oleas NG, Nuvials X, Zamora J. Plasma interleukin-6 concentration for the diagnosis of sepsis in critically ill adults. *Cochrane Database Syst Rev*. 2019;4:CD011811.
- Nier A, Huber Y, Labenz C, Michel M, Bergheim I, Schattenberg JM. Adipokines and endotoxemia correlate with hepatic steatosis in non-alcoholic fatty liver disease (NAFLD). *Nutrients*. 2020;12:699.
- Ono S, Tsujimoto H, Hiraki S, Aosasa S. Mechanisms of sepsis-induced immunosuppression and immunological modification therapies for sepsis. *Ann Gastroenterol Surg*. 2018;2:351–8.
- Parlesak A, Schäfer C, Schütz T, Bode JC, Bode C. Increased intestinal permeability to macromolecules and endotoxemia in patients with chronic alcohol abuse in different stages of alcohol-induced liver disease. *J Hepatol*. 2000;32:742–7.
- Pérez-Hernández EG, Delgado-Coello B, Luna-Reyes I, Mas-Oliva J. New insights into lipopolysaccharide inactivation mechanisms in sepsis. *Biomed Pharmacother*. 2021;141: 111890.
- Reinhart K, Daniels R, Kissoon N, Machado FR, Schachter RD, Finfer S. Recognizing sepsis as a global health priority—a WHO resolution. *N Engl J Med*. 2017;377:414–7.

- Rudd KE, Johnson SC, Agesa KM, Shackelford KA, Tsoi D, Kievlan DR, et al. Global, regional, and national sepsis incidence and mortality, 1990–2017: analysis for the Global Burden of Disease Study. *Lancet.* 2020;395:200–11.
- Schulte W, Bernhagen J, Bucala R. Cytokines in sepsis: potent immunoregulators and potential therapeutic targets—an updated view. *Mediators Inflamm.* 2013;2013: 165974.
- Shao B, Lu M, Katz SC, Varley AW, Hardwick J, Rogers TE, et al. A host lipase detoxifies bacterial lipopolysaccharides in the liver and spleen. *J Biol Chem.* 2007;282:13726–35.
- Singer M, Deutschman CS, Seymour C, Shankar-Hari M, Annane D, Bauer M, et al. The third international consensus definitions for sepsis and septic shock (sepsis-3). *JAMA.* 2016;315:801–10.
- Thuy S, Ladurner R, Volynets V, Wagner S, Strahl S, Königsrainer A, et al. Nonalcoholic fatty liver disease in humans is associated with increased plasma endotoxin and plasminogen activator inhibitor 1 concentrations and with fructose intake. *J Nutr.* 2008;138:1452–5.
- Van Der Poll T, Van De Veerdonk FL, Scicluna BP, Netea MG. The immunopathology of sepsis and potential therapeutic targets. *Nat Rev Immunol.* 2017;17:407–20.
- Vreugdenhil ACE, Snoek AMP, Van'T Veer C, Greve JWM, Buurman WA. LPS-binding protein circulates in association with apoB-containing lipoproteins and enhances endotoxin-LDL/VLDL interaction. *J Clin Invest.* 2001;107:225–34.
- WHO. Service delivery and safety: improving the prevention, diagnosis and clinical management of sepsis. <https://www.who.int/news-room/fact-sheets/detail/sepsis> (2020). Accessed 23 May 2022.

Publisher's Note

Springer Nature remains neutral with regard to jurisdictional claims in published maps and institutional affiliations.

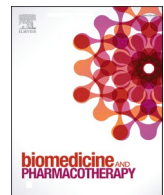
Ready to submit your research? Choose BMC and benefit from:

- fast, convenient online submission
- thorough peer review by experienced researchers in your field
- rapid publication on acceptance
- support for research data, including large and complex data types
- gold Open Access which fosters wider collaboration and increased citations
- maximum visibility for your research: over 100M website views per year

At BMC, research is always in progress.

Learn more biomedcentral.com/submissions





New insights into lipopolysaccharide inactivation mechanisms in sepsis

Eréndira Guadalupe Pérez-Hernández, Blanca Delgado-Coello, Ismael Luna-Reyes,
Jaime Mas-Oliva*

Instituto de Fisiología Celular, Universidad Nacional Autónoma de México, 04510 Mexico City, Mexico



ARTICLE INFO

Keywords:

Sepsis
Lipopolysaccharide
Gut-liver axis
Dysbiosis
CETPI

ABSTRACT

The complex pathophysiology of sepsis makes it a syndrome with limited therapeutic options and a high mortality rate. Gram-negative bacteria containing lipopolysaccharides (LPS) in their outer membrane correspond to the most common cause of sepsis. Since the gut is considered an important source of LPS, intestinal damage has been considered a cause and a consequence of sepsis. Although important in the maintenance of the intestinal epithelial cell homeostasis, the microbiota has been considered a source of LPS. Recent studies have started to shed light on how sepsis is triggered by dysbiosis, and an increased inflammatory state of the intestinal epithelial cells, expanding the understanding of the gut-liver axis in sepsis. Here, we review the gut-liver interaction in Gram-negative sepsis, exploring the mechanisms of LPS inactivation, including the recently described contribution of an isoform of the cholesterol-ester transfer protein (CETPI). Although several key questions remain to be answered when the pathophysiology of sepsis is reviewed, new contributions coming to light exploring the way LPS might be inactivated *in vivo*, suggest that new applications might soon reach the clinical setting.

1. Introduction

Sepsis, a syndrome where a dysregulated host response to infection conduces to physiological abnormalities, and eventually, to life-threatening organ dysfunction [1], corresponds to an important health problem accounting for 19.7% of global deaths [2]. Many cases of sepsis and septic shock have their origin in the abdominal cavity, where a series of intestine-related alterations have been considered a key factor in triggering sepsis and the multiple organ dysfunction syndrome (MODS) [3,4]. Since the intestine and the liver are closely related through the gut-liver axis composed of the portal vein, the biliary tract, and several systemic mediators [5], this review explores the contribution of the mechanisms known to be activated in these two organs that counteract the deleterious effects of LPS in sepsis.

The role of the gut as a key factor in triggering sepsis and multiple organ dysfunction is first presented, highlighting the contribution of the intestinal barrier disruption associated with the presence in plasma of gut-derived LPS. Later, we describe the recognition and processing of LPS by the liver. Finally, we focus on the gut and liver LPS-inactivation mechanisms, where the participation of proteins such as the bactericidal/permeability-increasing protein (BPI), the lipopolysaccharide-binding protein (LBP), and the cholesterol-ester transfer protein (CETP) is discussed; including the newly described

CETP isoform (CETPI), proposed by our group to participate in the inactivation of LPS in the plasma of patients with sepsis and septic shock.

2. Intestinal barrier disruption and the role of microbiota in sepsis

LPS are the major component present in the outer membrane of Gram-negative bacteria, constituted by lipid A, core sugars, and the O-antigen [6]. Lipid A is the most conserved molecule, and the main responsible for LPS bioactivity [7]. The main source of endotoxin in sepsis is secondary to a Gram-negative bacterial infection, and in many cases directly related to a deficiency in the barrier function of the intestine [8]. The disruption of the intestinal barrier leads to increased intestinal permeability, gut-derived LPS translocation to the lymphatic system, transport of LPS to the liver by the portal vein (gut-liver axis), and the development of immune responses by hepatic cells [9].

Under normal conditions, the gut lumen hosts the microbiota, comprising bacteria, archaea, fungi, protozoa, and viruses [10]. Although important in the maintenance of intestinal epithelial cell (IECs) homeostasis, the microbiota has been considered a source of LPS [11,12]. The normal microbiota regulates the production of antimicrobial molecules, as well as mucins [11,13], components of the mucus layer, functioning as a physical barrier that separates the microbiota

* Corresponding author.

E-mail address: jmas@ifc.unam.mx (J. Mas-Oliva).

from the IECs [14]. In the colon, the mucus layer is composed by an inner layer normally absent of bacteria, and an outer mucus layer colonized by anaerobic bacteria where the phyla *Firmicutes* and *Bacteroidetes* are the most abundant, followed by facultative species such as *Escherichia coli*, that can be present in low concentrations [15]. Pathogens and several commensal intestinal bacteria have mucolytic activity, but only facultative species can penetrate the inner mucus layer [13]. In an inflammatory microenvironment, there is an increase in the abundance of facultative anaerobic bacteria, whereas the proportion of strictly anaerobic decreases, altering the composition of the gut microbiota (dysbiosis) and promoting the accentuation of the inflammatory process [16]. This is evident in patients presenting the systemic inflammatory response syndrome, where a decrease of obligate anaerobes and an increase in pathogenic bacteria in the intestine has been observed [17].

Underneath the mucus layer, in the luminal surface of the small intestine protrude a series of structures called villi, separated between them by tubular invaginations known as crypts. At the base of the crypts, there are columnar stem cells that differentiate into diverse types of epithelial cells, comprising enterocytes, goblet cells, entero-endocrine cells, and Paneth cells (Fig. 1a). Considered as the main intestinal barrier to infection, the apical glycocalyx containing cell surface mucins, together with the presence of epithelial tight junctions, adherens junctions, and desmosomes [13,19], belong to a system of key defense structures. Among the causes that lead to the disruption of these structural components of the intestinal barrier; infection, trauma, ischemia/reperfusion events, and immune cell dysregulation, have been recognized as important ones [20,21]. Also, as a consequence of the damage caused by these cell disturbances, dysbiosis becomes present, as shown in patients with septic shock [22], in patients that receive antibiotic treatment [23,24], and in general, in critically ill patients [25,26].

Evidence showing an association between alterations of the microbiota and subsequent admission of patients to the hospital due to sepsis, mainly includes those with dysbiosis produced by infection-related hospitalization, and antibiotic administration [27,28]. When dysbiosis becomes present, among other alterations, an increase in the intestinal permeability is observed, most of the time associated with an alteration of cell-cell adhesion properties of IECs. Then, as a result of infection or dysbiosis, a pro-inflammatory environment is developed, and tight junctions become disrupted, turning the epithelial barrier leaky [29] (Fig. 1b).

This phenomenon explains the transmigration of bacteria, LPS, and other harmful metabolites from the lymphatic system and portal circulation to the systemic circulation and other organs causing MODS [30–32]. The mesenteric lymph vessel conducts pathogen-associated

molecular patterns (PAMPs), or intracellular molecules released from damaged or dying cells (called damage-associated molecular patterns or DAMPs). These molecules associated with gut-derived pathogens continue towards the systemic circulation and eventually the lungs producing the acute respiratory distress syndrome and distant organ injury [33–35].

Associated to the barrier function of IECs limiting the translocation of bacteria and therefore their contact with intestinal immune cells [36], the participation of the microbiota has been defined as an important line of defense against invading pathogens. The relationship between IECs and the normal bacteria present in the intestine contributes to the maintenance of the intestinal barrier function through the production of microbiota-derived inositol phosphate [37], and the fermentation of undigested carbohydrates, such as the end-products of high fiber diets, producing short-chain fatty acids (SCFAs), propionate, acetate, and butyrate. Butyrate, as the main energy source for epithelial cells, promotes cell survival, and proliferation [38]. In addition, SCFAs maintain the intestinal barrier after LPS exposure, through the stimulation of the mechanisms that overexpress tight-junction proteins such as claudin-1 and ZO-1, and also through the inhibition of the NLRP3 inflammasome, autophagy, and NF-κB activation [39,40].

Since an important risk factor to develop sepsis correlates with the presence of low concentrations of butyrate-producing bacteria in the intestinal lumen [41], fecal microbiota transplantation to mice with sepsis has shown to promote a protective effect associated with the restoration of normal levels of butyrate [42]. Also, the relationship achieved between the microenvironment promoted by the gut microbiota, and its effects on LPS production has been proven in atherosclerosis-prone mice, where LPS synthesis is reduced in mice treated with live *Bacteroides*, reducing the expression of the Toll-like receptor 4 (TLR4), and contributing to maintain the gut-barrier integrity [43]. Although the precise mechanisms by which microbiota contributes to the LPS fecal levels remains unclear, a lower abundance of *Bacteroides* is related to inflammatory diseases as in sepsis [44]. In addition, the gut microbiota and their metabolites reduce LPS-induced inflammation in distant organs like the lung and the liver. In this sense, the process of inflammation induced by LPS in the liver has been shown to decrease in mice when treated with molecules known to be synthesized by the gut microbiota, such as the aromatic heterocyclic compound indole [45]. Also, recent results indicate the protective effect of the intestinal microbiota in regulating immunity of LPS-induced acute lung injury, by modulating the TLR4/NF-κB signaling pathway associated to the induction of inflammation and oxidative stress [46].

On the other hand, it has been established that high-fat diets enhance intestinal permeability contributing to LPS translocation from the gut to

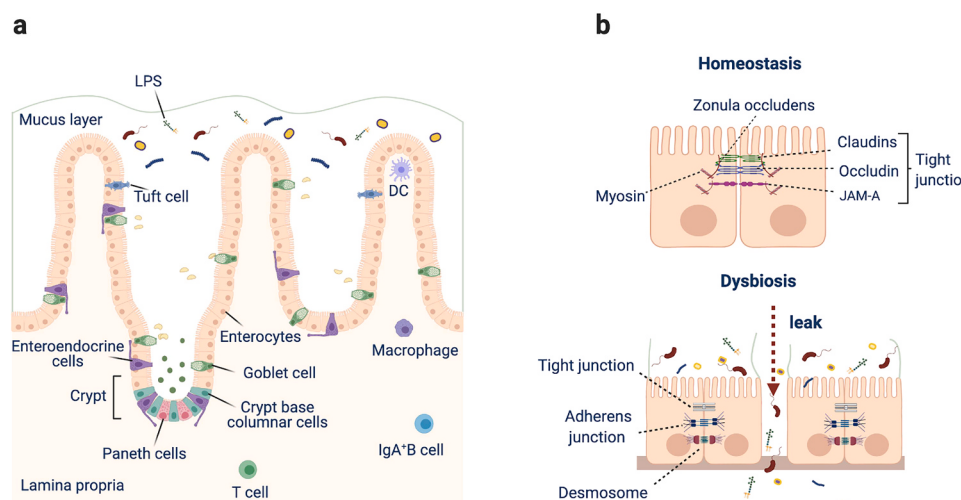


Fig. 1. Disruption of the intestinal barrier as a mechanism closely related to the development of sepsis. a) Under healthy conditions, the gut presents a single layer of intestinal epithelial cells (IECs) provided with microvilli, that act both, as a physical barrier, and as a cell system that transports nutrients and exchanges ions [18]. While IECs are covered with a dense layer of mucus synthesized by goblet cells, Paneth cells producing essential growth factors and antimicrobial peptides protect columnar stem cells. b) When the normal homeostatic equilibrium of the microbiota is altered, epithelial cells lose tight junctions, and dysbiosis occurs producing free routes for the migration of bacteria and their metabolites to the liver and other organs, starting the septic process. LPS, lipopolysaccharides; DC, dendritic cells; JAM-A, junctional adhesion molecule-A.

plasma, triggering the onset of low-grade inflammation [47]. Since during the postprandial period, dietary long-chain fats are absorbed following their incorporation into chylomicrons, LPS can be incorporated also, therefore facilitating their absorption and contributing to postprandial inflammation [48–50]. The administration of high-fat diets to mice has been also related to a reduced expression in IECs of genes coding for tight junction proteins, such as ZO-1 and occludin [51]. High-fat diets promote the release of inflammatory mediators, and activate mast cells in the intestinal mucosa, affecting the transcellular and paracellular intestinal permeability [52,53]. In absence of a pathogen agent, administration to mice of a fat-rich diet low in fiber, causes a high susceptibility to develop sepsis after antibiotic exposure and surgical injury [54]. Moreover, employing an LPS-induced sepsis model, it has been observed that mice fed with a western diet are susceptible to develop immunoparalysis [55].

3. The liver response to LPS

Although several of the main functions carried out by the liver comprise the metabolism of nutrients, the production of clotting factors, and detoxification; its immune function is critical to maintain tolerance and protection against pathogens carried via the portal system. As the first line of defense, this immune function is particularly important against systemic and intestine-derived pathogens. In this sense, it has been found that the concentration of LPS in the portal circulation is higher than the LPS concentration in the peripheral blood [56,57]. Therefore, the anatomical disposition of the liver and the intestine, reveals the critical connection role of these two organs in the process of detoxification of gut-derived LPS [57]. Hepatic cells participate in a network system designed to detect, capture, and prime the adequate immune response against circulating microorganisms. For this purpose and in association with hepatocytes, a large population of macrophages, neutrophils, natural killer cells, lymphocytes, dendritic cells, B cells, hepatic stellate cells (HSC), and liver sinusoidal endothelial cells (LSEC), contribute to the liver response in sepsis [58,59]. In septic patients, it has been shown that bacterial clearance by the liver is important to reduce plasma LPS levels, which in parallel lowers the severity of the immune response and improves the patient's outcome [58,60].

So far, the main molecules involved in LPS-sensing are LBP, CD14, MD-2, and TLR4 [61], which initiate the activation of intracellular signal transduction networks in subdomains of the plasma membrane rich in phosphatidylinositol 4,5-biphosphate [62]. The sorting adaptors, TIRAP and TRAM, interact with these regions sensing dimerized TLR4 at the cell surface or on endosomes, inducing the myddosome formation or TRIF signaling, respectively [63,64]. (Fig. 2). The myddosome elicits the production of pro-inflammatory mediators by activating inflammatory transcription factors, such as NF- κ B and AP-1; whereas the TLR4 internalized in endosomes engage TRAM and TRIF, initiating IRF3-dependent type-I IFN production [61] (Fig. 2). On the other hand, several other cellular responses to LPS have been described, involving phagocytosis [65], autophagy [66], and mitochondrial reactive oxygen species production [67]. In the macrophage, intracellular LPS triggers the noncanonical inflammasome, well known to correspond to a TLR4-independent response (Fig. 2). During this cellular response, caspase-11 recognizes intracellular LPS, leading to the generation of IL-1 β , IL-18, and to pyroptosis, which further contributes to the severity of sepsis [68,69]. Therefore, it has been reported that the use of activation antagonists of human caspases 4 and 5 (the orthologs of mouse caspase-11), may result beneficial for septic patients [69,70].

Regarding the distribution of TLR4 as the main receptor mediating the LPS effect, TLR4 transcripts are abundantly expressed in Kupffer cells (KCs), followed by LSEC, and poorly expressed in hepatocytes, in both mouse and human liver [71]. In vivo, it is assumed that LPS interact first with KCs and LSEC in the sinusoid, and eventually, with HSC in the space of Disse. Given the key role that KCs and LSEC play in the recognition and clearance of LPS, they also contain the scavenger

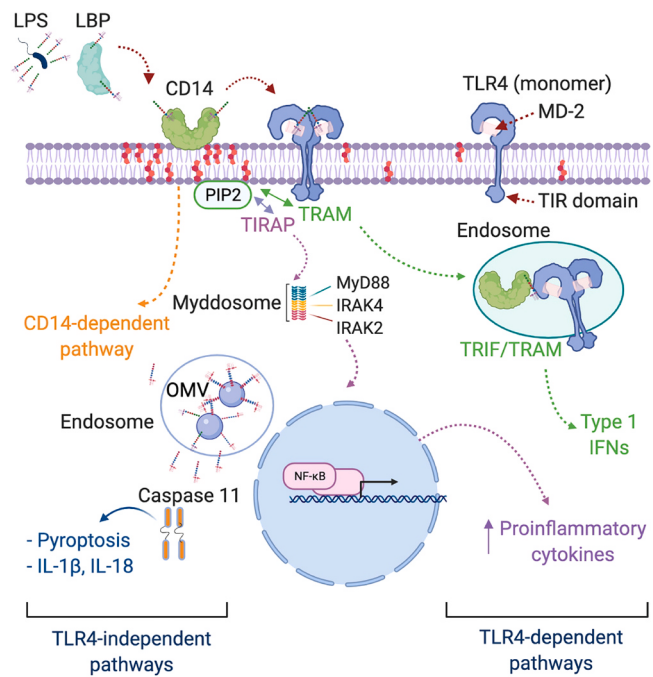


Fig. 2. Schematic diagram of the LPS/TLR4 signaling pathway. The cascade of cellular events mediated through the LPS/TLR4 signaling pathway initiates with the interaction of LPS with LBP and CD14, facilitating the subsequent signaling events by the TLR4-MD2 complex. The sorting adaptors TIRAP and TRAM induce the myddosome formation or TRIF signaling, resulting in the production of pro-inflammatory cytokines and type 1 IFNs, respectively. An alternative mechanism mediated by caspase 11 has been also described, where outer membrane vesicles (OMV) produced by Gram-negative bacteria, are endocytosed, and LPS is delivered into the cytosol of host cells, conduced to IL-1 β and IL-8 production, and to pyroptosis. TLR4, Toll-like receptor 4; LPS, lipopolysaccharides; LBP, lipopolysaccharide-binding protein; IFNs, interferons.

receptor class B type 1 (SR-B1), and the activin receptor-like kinase (ALK-1), known to participate in the process (Fig. 3). SR-B1 corresponds to the high-density lipoprotein (HDL) receptor, considered to be highly expressed in hepatocytes being at least 5-fold more abundant in LSEC and poorly expressed in KCs and HSC [72]. In addition to the main role of SR-B1 in the reverse transport of cholesterol through the cell uptake of cholesterol-esters from HDL, during the course of sepsis SR-B1 also contributes to LPS clearance in the liver [73].

Recent work has attracted attention to the role of the bone morphogenetic protein-9, a cytokine member of the TGF- β superfamily produced by HSC that binds ALK-1, showing a role as a modulator of the in vitro response of human LSEC evoked by LPS. Transcripts for ALK-1 are mainly expressed in LSEC and KCs, and very low levels are found in the hepatocytes of both mice and humans [71].

4. Mechanisms of lipopolysaccharide neutralization

The gut mucosa presents several mechanisms that participate in LPS inactivation, where besides being a physical barrier, prevents LPS from coming in close contact with the apical side of IECs. Among the molecules that participate, the following have been well studied: mucins, intestinal alkaline phosphatase (IAP), antimicrobial peptides (AMPs), IgA, bile acids, and a series of LPS binding proteins (Fig. 4a). Among the different secreted mucins, both in humans and mice, mucin 2 (Muc2) corresponds to the major component preventing the translocation of intestinal bacteria [74,75]. An investigation studying Muc2^{-/-} mice shows that when treated with sublethal doses of LPS, these experimental animals present a high mortality rate associated with impaired iron homeostasis, and an increased bacterial translocation [76]. IAP corresponds to a mucosal defense enzyme that, through the removal of

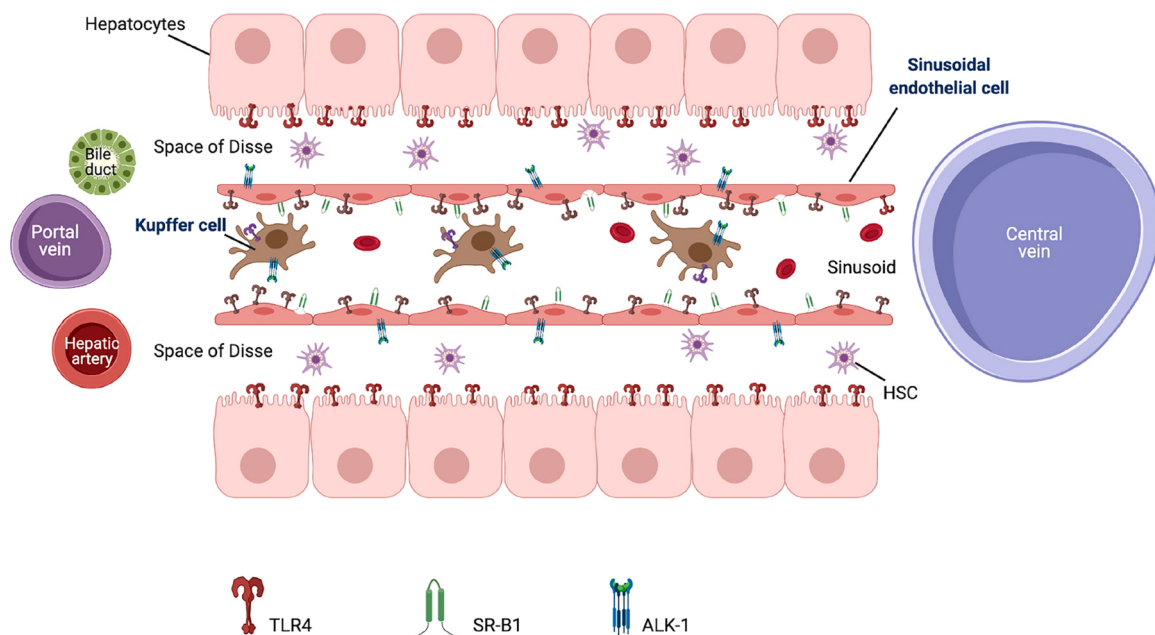


Fig. 3. Participation of different hepatic cell types in the recognition and clearance of LPS during sepsis. Although hepatocytes and non-parenchymal cells when exposed to LPS trigger an inflammatory response, Kupffer cells and liver sinusoidal endothelial cells, play an outstanding role in clearing LPS and the restoration of homeostasis. LPS, lipopolysaccharides; TLR4, Toll-like receptor 4; SR-B1, high-density lipoprotein receptor class B type 1; ALK-1, activating receptor-like kinase; HSC, hepatic stellate cells.

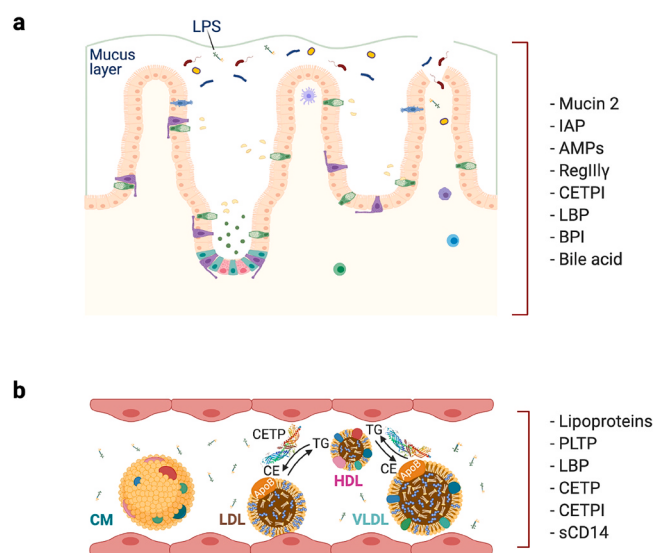


Fig. 4. Mechanisms of LPS inactivation present in the gut-liver axis. a) The intestine presents several mechanisms to limit the entrance of LPS to intestinal lymphatics and portal circulation. In the presence of an inflammatory micro-environment such as the one present during sepsis, these mechanisms are bypassed. b) LPS present in the intestinal lymphatics bind to chylomicrons (CM) being transporting to the portal circulation, whereas LPS in the blood bind to lipoproteins, which are constantly being restructured, and taken up by Kupffer cells (KCs) and liver sinusoidal endothelial cells (LSEC). TG, triglycerides; CE, cholesterol esters.

phosphate groups coupled to glucosamines, detoxifies LPS [77], promoting mucosal tolerance to resident bacteria, and protecting the host from sepsis during inflammatory conditions [78,79]. In animal models of sepsis and patients with sepsis, the administration of IAP attenuates LPS toxicity and prolongs survival time [80–83].

AMPs are secreted by Paneth cells in response to bacteria and LPS, and they spread into the mucus layer of the gut. Alpha-defensins, the

most abundant antimicrobial peptides in the human intestine, are secreted in response to LPS [11,84], and their interaction inhibits TLR-mediated inflammation. Also, Paneth cells detect gut bacteria through cell-autonomous MyD88 activation, triggering the expression of antimicrobial factors, such as RegIII γ , RegIII β , and RELM β , all expressed after oral administration of LPS to germ-free mice [85].

Five LPS-binding proteins belonging to the family of lipid transfer/LPS-binding proteins (LTP/LBP) have been described: the phospholipid transfer protein (PLTP), LBP, BPI, CETP [86], and a new isoform of CETP described by our group, named CETPI [87,88]. LBP is a component of the intestinal mucosal defense system secreted by intestinal epithelial cells [89], and it is present in the secretory granules of Paneth cells [90]. While CD14 has been recognized as the receptor for the complex formed between LBP/LPS [91], promoting an exacerbated inflammatory response mediated by TLR4, a high concentration of LBP also contributes to neutralizing LPS. BPI is present in neutrophils and expressed in human epithelial cells (oral, pulmonary, and intestinal) [92], where it shows a bactericidal action and a neutralizing activity against LPS. In the intestinal epithelium, BPI expression increases in response to changes in the levels of intracellular potassium caused by cell damage, whereas neither PAMPs, such as LPS nor cytokines, induce BPI expression [93,94]. These findings suggest that DAMPs regulate BPI expression instead of PAMPs, important in limiting the translocation of commensal bacteria during epithelial damage [94], and also protecting mucosal surfaces against the endotoxin of Gram-negative bacteria [93].

While gut-derived LPS molecules enter the bloodstream, proteins such as PLTP, LBP, and sCD14 promote their binding to lipoproteins, therefore facilitating their transport to the liver for further elimination (Fig. 4b). The liver as the main source of CETP also synthesizes acute-phase proteins, such as LBP and sCD14 [95]. The role of CETP in sepsis-like conditions has been evaluated by us studying small intestine cells in culture. We found that following incubation with LPS, these cells that normally do not synthesize CETP, start to produce the protein [88]. Moreover, the role of CETP as a mediator of the excessive inflammatory response to LPS has been described employing RAW 264.7 murine macrophages, where TNF- α production increases upon incubation with LPS, but decreases in a dose-dependent manner when human CETP is

added to the medium [96,97]. Since cholesterol esters are transferred between lipoproteins by CETP in exchange for triglycerides from HDL to LDL and very low-density lipoproteins (VLDL), the resulting triglyceride-enriched HDL are easily degraded by hepatic lipases decreasing the level of circulating HDL-cholesterol (HDL-C) (Fig. 4b). Considering that HDL-C plasma levels are inversely associated with the risk of cardiovascular disease, for some time it has been thought that the presence of a low HDL-C concentration mediated by a high plasma CETP concentration could be detrimental in those individuals affected with cardiovascular disease. In association with these findings, the clinical trial testing the CETP inhibitor torcetrapib, expected to lower the activity of CETP and therefore increase plasma HDL-C, was not concluded due to an unanticipated high mortality rate found associated with cardiovascular and non-cardiovascular complications. Interestingly, among the non-cardiovascular causes, the presence of infection was directly found to be established with the use of this inhibitor [98].

Soon after the clinical trials studying the effects of CETP inhibitors upon cardiovascular disease were interrupted, its potential interaction of torcetrapib with LBP and BPI was explored. It was shown that this inhibitor does not affect LPS binding ability to LBP and BPI, in the same way as LPS do not affect CETP function. It was also shown that LPS strongly induces the expression of TNF- α in ex vivo blood assays, even in the presence of torcetrapib [99]. These results suggest that HDL-remodeling mediated by CETP is a crucial component in the response to Gram-negative infections. Accordingly, a low HDL-C plasma concentration has been associated with an unfavorable outcome during the development of sepsis [100]. A recent meta-analysis shows the relation between low HDL plasma levels and a high mortality rate in patients with sepsis [101]. In support of these data, studying patients that present the CETP genetic variant rs1800777 (allele A), which is a gain-of-function variant of CETP associated with abnormally low HDL-C levels, it was observed that in the presence of sepsis these patients are not able to downregulate CETP, and therefore the transfer of cholesterol-esters from HDL to LDL and VLDL is increased. This condition leads patients to become more susceptible to organ failure associated to a low survival rate [102].

For some time, it has been considered that CETP is synthesized in the hepatocyte the predominant cell type in the liver, however, nowadays we know that CETP is mainly expressed in a specific population of resting KCs displaying surface proteins known as Clec4f and Vsig4 [104–106]. Apparently, as an early mechanism to counteract the harmful effects of LPS, the expression of these proteins is reduced when KCs are LPS-activated, in parallel with a decrease in CETP and an increase in plasma HDL-C [106] (Fig. 5). While the important inactivation

of LPS in plasma mediated by their association with lipoproteins such as HDL, is directly related to the insertion of lipid A into the outer phospholipid layer of this lipoprotein [107], lipoprotein-bound LPS are removed from the bloodstream by liver cells through the LDL receptor (LDLR), the LDLR-related protein-1 [108,109], and SR-B1 [73].

Since the uptake of LPS-HDL complexes by KCs, is slower than free LPS [110], LSEC are considered the main cell type involved in the clearance of these LPS-HDL complexes probably through the interaction with SR-B1 [111]. Nevertheless, the relevance of LPS clearance mediated by SR-B1 in patients with sepsis still shows inconsistent results [73, 112,113]. On the other hand, although TLR4 located in the hepatocyte membrane has been shown to contribute in sepsis to the clearance of LPS from circulation [60], due to the complex role of TLR4 in the septic process, the use in the clinic of TLR4 antagonist has ended with controversial results [114]. Finally, a key detoxification mechanism for LPS is carried out by the enzymes lipid A-phosphatase and acyloxyacyl-hydrolase present in KCs and LSEC, as a preliminary step for excretion into the bile [110,111].

Furthermore, the contribution of KCs in sepsis is relevant considering that in contrast to monocyte-derived macrophages, KCs have proliferative capacity, allowing them to regenerate themselves [115]. Besides, KCs having the capability to polarize specific activation states, perform diverse functions in different microenvironments with the ability to change from the M1 phenotype (classical activation) to the alternative M2 phenotype [116]. Since M1-polarized KCs predominate in sepsis producing a large amount of pro-inflammatory cytokines like TNF- α , and IL-6 (Fig. 5), new therapeutic approaches have been employed to inhibit M1 polarization with the use of mesenchymal stem cells and chromone derivatives [117,118].

5. CETPI a new lipopolysaccharide-binding protein

CETPI corresponds to a new protein described by our group, that apparently when studied in the rabbit as the experimental model, seems to be exclusively expressed in the small intestine [87]. Although it is present in human plasma, it is still not known if in the human, the intestine is the only organ that synthesizes CETPI. Nevertheless, the fact that under normal conditions CETPI is found in plasma is most probably related to its lipid binding properties, and therefore to the possibility that while being synthesized by the enterocyte, CETPI binds to the newly formed chylomicrons, following in association, a normal excretion pathway into the lacteal [119].

The main structural difference between CETP and CETPI resides in its C-terminal domain, where the last 24 C-terminal residues present in

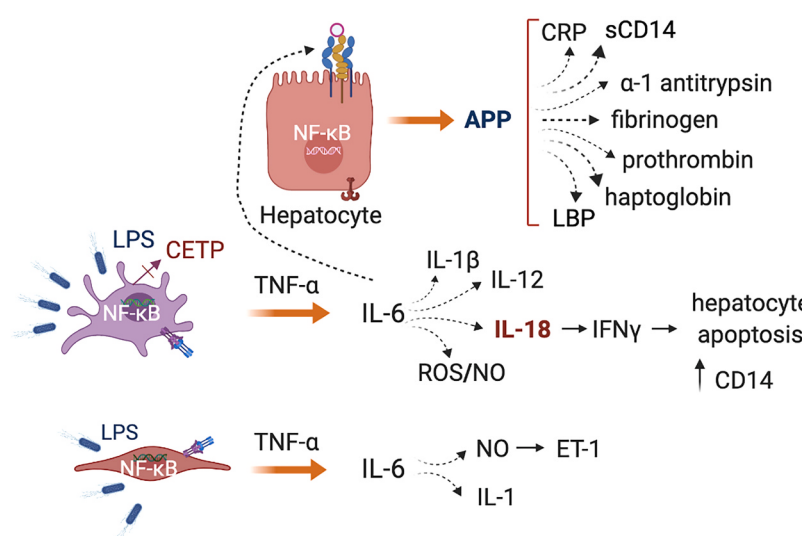


Fig. 5. Role of CETP in the liver's response to LPS. When LPS from Gram-negative bacteria activate KCs, they stop producing CETP, and therefore, circulating HDL levels increase. As a response to LPS, hepatic cells produce pro-inflammatory cytokines and trigger different signaling pathways. Among the interleukins produced by KCs, IL-18 seems to be the main factor provoking liver damage by stimulating the secretion of interferon-gamma (IFN- γ), which leads hepatocytes to apoptosis. Also, liver sinusoidal endothelial cells (LSEC) produce nitric oxide (NO) that induces the secretion of endothelin-1 (ET-1), known to be involved in the inflammatory response [103]. Moreover, hepatocytes respond to the TNF- α /IL-6 signal carried out by KCs and LSEC, by producing further inflammatory acute-phase proteins (APP).

CETP are substituted by 18 new ones. This new sequence in CETPI including prolines and positively charged amino acids, confer this domain with a disordered structure and a net positive electrostatic charge [87,88]. Peptide VSAK (for the first four aa of the 18 aa peptide V474-P491), derived from the C-terminal domain of CETPI interacts with LPS, protects macrophages against the cytotoxic effects of LPS, and in vitro prevents the generation of oxidative stress [88]. Interestingly, the stimulation of colon-derived cells (Caco-2) and small intestine cells (FHs74Int) with LPS, increases CETPI expression [88], indicating an important role of this protein in mediating the cytotoxic effects of LPS present in the intestine. The presence of CETPI in plasma reflects its key function in sepsis and septic shock, since plasma CETPI levels have been shown to be in parallel increased in intensive care unit patients presenting both conditions in comparison to healthy subjects [120]. While as mentioned above, the normal excretion of CETPI to circulation might be explained by its association with chylomicrons, under a pathological condition involving inflammation of the intestine, protein translocation is known to take place due to structural changes of the epithelial layer [121].

Since the heterogeneous response of patients to infection is one of the main obstacles for an early diagnosis and treatment of the disease, the use of biomarkers related to the diagnosis, disease severity, and prognostic aspects of sepsis represents a key point to improve the outcome of patients [122]. Although several biomarkers of the septic process have been reported, their use in clinical practice is still limited. Among the biomarkers frequently detected during the acute phase of sepsis, the C-reactive protein, procalcitonin, and IL-6, have been identified as important ones [123]. Interestingly, we have demonstrated that CETPI and peptides derived from the carboxy-end segment of this protein, such as peptide VSAK, might be also considered as a new set of biomarkers to define disease severity during the transition from infection, sepsis, to septic shock [120].

Recent results from our laboratory employing Positron Emission Tomography, have also shown that peptides derived from the carboxy-end segment of CETPI, including peptide VSAK, when injected intravenously reduce the detrimental effects produced by LPS in Dutch dwarf rabbits, used as an animal model to develop a systemic inflammatory response syndrome associated to septic shock [124]. Included in the same report, employing molecular dynamics, we have shown that peptide VSAK irreversibly binds to LPS, a process that most probably deactivates the endotoxin, preventing inflammation through activation of the TLR4/NF- κ B signaling pathway. Treatment with peptide VSAK prevented the onset of changes in serum levels of glucose and insulin associated with the establishment of an insulin resistance-like syndrome in all septic animals studied. Also, treatment with peptide VSAK showed an important attenuation in the circulating levels of pro-inflammatory molecules increased in LPS treated animals. As a whole, our data suggest that peptide VSAK might be considered not only as a new marker molecule of disease severity, but also as a candidate in the development and use of a new therapeutic strategy focused on mitigating the harmful effects produced by LPS during sepsis and septic shock. A better understanding of the way molecules such as CETPI and peptide VSAK are involved in the neutralization of LPS, will help to develop new and improved management schemes to control sepsis and septic shock in the setting of the Intensive Care Unit.

6. Outstanding questions

The disruption of the intestinal barrier in sepsis plays a key role by affecting the homeostasis established with the microbiota, the crosstalk between the gut and other organs such as the liver, and by promoting the presence of LPS in the bloodstream. Therefore, new knowledge is needed to clarify: (1) The contribution of the gut-liver and gut-lung axis in MODS, considering the contribution of DAMPs and PAMPs. (2) The use of probiotics, prebiotics, and fecal microbiota transplantation to counteract the effect of antibiotics administered to patients with sepsis. (3)

The participation of CETP in the equilibrium of lipoproteins in the pathophysiology of sepsis. (4) The possibility for the use of CETPI and peptides derived from CETPI as biomarkers of organ failure and disease severity in patients with sepsis and septic shock. (5) The potential therapeutic use of LPS-binding peptides that could restore immune-dysregulation during the acute stages of sepsis.

6.1. Search strategy and selection criteria

References cited in this review were identified employing PubMed and Google Scholar. The search strategy included articles published in English from January 1977 to May 2021, using the terms: "gut microbiota", "gut-derived sepsis", "lipopolysaccharide inactivation", "gut-translocation", "liver injury", "Gram-negative sepsis", "multiple organ dysfunction" and "gut-liver axis". The selection criteria employed to include articles were originality and their impact in the field.

Funding

This work was supported by grants awarded to Jaime Mas-Oliva from Universidad Nacional Autónoma de México-PAPIIT México (IN205717 and IN206619).

Author contributions

Eréndira G. Pérez-Hernández and Jaime Mas-Oliva participated with conceptualization, literature search, writing, and critical review. Blanca Delgado-Coello contributed with literature search, figure design, and critical review. Ismael Luna-Reyes contributed with literature search, writing, and critical review.

Conflict of interest statement

The authors declare no competing conflict of interest.

Acknowledgments

Eréndira G. Pérez-Hernández received a scholarship from CONACYT (465348) in support of her Ph.D. studies. Ismael Luna-Reyes is receiving a scholarship from CONACYT (2019-000037-02NACF-25744) for the development of his Ph.D. studies.

Figures were created with Biorender.com.

References

- [1] M. Singer, C.S. Deutschman, C.W. Seymour, M. Shankar-Hari, D. Annane, M. Bauer, R. Bellomo, G.R. Bernard, J.D. Chiche, C.M. Coopersmith, R. S. Hotchkiss, M.M. Levy, J.C. Marshall, G.S. Martin, S.M. Opal, G.D. Rubenfeld, T. van der Poll, J.L. Vincent, D.C. Angus, The third international consensus definitions for sepsis and septic shock (Sepsis-3), *JAMA* 315 (2016) 801–810.
- [2] K.E. Rudd, S.C. Johnson, K.M. Agesa, K.A. Shackelford, D. Tsui, D.R. Kievlan, D. V. Colombara, K.S. Ikuta, N. Kisssoon, S. Finfer, C. Fleischmann-Struzek, F. R. Machado, K.K. Reinhart, K. Rowan, C.W. Seymour, R.S. Watson, T.E. West, F. Marinho, S.I. Hay, R. Lozano, A.D. Lopez, D.C. Angus, C. Murray, M. Naghavi, Global, regional, and national sepsis incidence and mortality, 1990–2017: analysis for the global burden of disease study, *Lancet* 395 (2020) 200–211.
- [3] N.J. Klingensmith, C.M. Coopersmith, The gut as the motor of multiple organ dysfunction in critical illness, *Crit. Care Clin.* 32 (2016) 203–212.
- [4] S. Ahlawat, Asha, K.K. Sharma, Gut-organ axis: a microbial outreach and networking, *Lett. Appl. Microbiol.* 72 (2021) 636–668.
- [5] A. Tripathi, J. Debelius, D.A. Brenner, M. Karin, R. Loomba, B. Schnabl, R. Knight, The gut-liver axis and the intersection with the microbiome, *Nat. Rev. Gastroenterol. Hepatol.* 15 (2018) 397–411.
- [6] X. Wang, P. Quinn, Endotoxins: lipopolysaccharides of gram-negative bacteria, in: X. Wang, P. Quinn (Eds.), *Endotoxins: Structure, Function and Recognition*, Springer, 2010, pp. 3–25.
- [7] E.T. Rietschel, T. Kirikae, F.U. Schade, A.J. Ulmer, O. Holst, H. Bräde, G. Schmidt, U. Mamat, H.D. Grimmecke, S. Kusumoto, The chemical structure of bacterial endotoxin in relation to bioactivity, *Immunobiology* 187 (1993) 169–190.
- [8] K. Buttenschoen, P. Radermacher, H. Brädt, Endotoxin elimination in sepsis: physiology and therapeutic application, *Lange Arch. Surg.* 395 (2010) 597–605.

- [9] S.Y. Kim, E. Seki, Toll-like receptors in liver disease, in: I.M. Arias, H.J. Alter, J. L. Boyer (Eds.), *The Liver: Biology and Pathobiology*, sixth ed., John Wiley & Sons, 2020, pp. 737–745.
- [10] X.V. Li, I. Leonardi, I.D. Iliev, Gut mycobiota in immunity and inflammatory disease, *Immunity* 50 (2019) 1365–1379.
- [11] C.L. Bevins, N.H. Salzman, Paneth cells, antimicrobial peptides and maintenance of intestinal homeostasis, *Nat. Rev. Microbiol.* 9 (2011) 356–368.
- [12] J.C. Clemente, L.K. Ursell, L.W. Parfrey, R. Knight, The impact of the gut microbiota on human health: an integrative view, *Cell* 148 (2012) 1258–1270.
- [13] M.A. McGuckin, S.K. Lindén, P. Sutton, T.H. Florin, Mucin dynamics and enteric pathogens, *Nat. Rev. Microbiol.* 9 (2011) 265–278.
- [14] M.E. Johansson, H. Sjövall, G.C. Hansson, The gastrointestinal mucus system in health and disease, *Nat. Rev. Gastroenterol. Hepatol.* 10 (2013) 352–361.
- [15] P.B. Eckburg, E.M. Bik, C.N. Bernstein, E. Purdom, L. Dethlefsen, M. Sargent, S. R. Gill, K.E. Nelson, D.A. Relman, Diversity of the human intestinal microbial flora, *Science* 308 (2005) 1635–1638.
- [16] S.E. Winter, M.G. Winter, M.N. Xavier, P. Thienimirit, V. Poon, A.M. Keestra, R. C. Laughlin, G. Gomez, J. Wu, S.D. Lawhon, I.E. Popova, S.J. Parikh, L.G. Adams, R.M. Tsolis, V.J. Stewart, A.J. Bäumler, Host-derived nitrate boosts growth of *E. coli* in the inflamed gut, *Science* 339 (2013) 708–711.
- [17] K. Shimizu, H. Ogura, M. Goto, T. Asahara, K. Nomoto, M. Morotomi, K. Yoshiya, A. Matsushima, Y. Sumi, Y. Kuwagata, H. Tanaka, T. Shimazu, H. Sugimoto, Altered gut flora and environment in patients with severe SIRS, *J. Trauma* 60 (2006) 126–133.
- [18] T. Pelaseyed, G.C. Hansson, Membrane mucins of the intestine at a glance, *J. Cell Sci.* (2020) 133, jcs240929.
- [19] R. Okumura, K. Takeda, Roles of intestinal epithelial cells in the maintenance of gut homeostasis, *Exp. Mol. Med.* 49 (2017) 338.
- [20] L.A. Ding, J.S. Li, Y.S. Li, N.T. Zhu, F.N. Liu, L. Tan, Intestinal barrier damage caused by trauma and lipopolysaccharide, *World J. Gastroenterol.* 10 (2004) 2373–2378.
- [21] G. Son, M. Kremer, I.N. Hines, Contribution of gut bacteria to liver pathobiology, *Gastroenterol. Res. Pract.* 2010 (2010) 453–563.
- [22] Y.D. Wan, R.X. Zhu, Z.Q. Wu, S.Y. Lyu, L.X. Zhao, Z.J. Du, X.T. Pan, Gut microbiota disruption in septic shock patients: a pilot study, *Med. Sci. Monit.* 24 (2018) 8639–8646.
- [23] S. Kim, A. Covington, E.G. Pamer, The intestinal microbiota: antibiotics, colonization resistance, and enteric pathogens, *Immunol. Rev.* 279 (1) (2017) 90–105.
- [24] L. Liu, Q. Wang, H. Lin, R. Das, S. Wang, H. Qi, J. Yang, Y. Xue, D. Mao, Y. Luo, Amoxicillin increased functional pathway genes and beta-lactam resistance genes by pathogens bloomed in intestinal microbiota using a simulator of the human intestinal microbial ecosystem, *Front. Microbiol.* 11 (2020) 1213.
- [25] A. Yeh, M.B. Rogers, B. Firek, M.D. Neal, B.S. Zuckerbraun, M.J. Morowitz, Dysbiosis across multiple body sites in critically ill adult surgical patients, *Shock* 46 (2016) 649–654.
- [26] A. Reintam Blaser, J.C. Preiser, S. Fruhwald, A. Wilmer, J. Werner, C. Benstoem, M.P. Casaeer, J. Starkopf, A. van Zanten, O. Rooyackers, S.M. Jakob, C.I. Loudet, D.E. Bear, G. Elke, M. Kott, I. Lautenschläger, J. Schäper, J. Gunst, C. Stoppe, L. Nobile, V. Fuhrmann, M.M. Berger, H.M. Oudemans-van Straaten, Y. M. Arabi, A.M. Deane, E. Working Group on Gastrointestinal Function within the Section of Metabolism, Endocrinology and Nutrition (MEN Section) of, Gastrointestinal dysfunction in the critically ill: a systematic scoping review and research agenda proposed by the section of metabolism, endocrinology and nutrition of the European society of intensive care medicine, *Crit. Care* 24 (1) (2020) 224.
- [27] H.C. Prescott, R.P. Dickson, M.A. Rogers, K.M. Langa, T.J. Iwashyna, Hospitalization type and subsequent severe sepsis, *Am. J. Respir. Crit. Care Med.* 192 (2015) 581–588.
- [28] J. Baggs, J.A. Jernigan, A.L. Halpin, L. Epstein, K.M. Hatfield, L.C. McDonald, Risk of subsequent sepsis within 90 days after a hospital stay by type of antibiotic exposure, *Clin. Infect. Dis.* 66 (2018) 1004–1012.
- [29] M.A. Odenwald, J.R. Turner, The intestinal epithelial barrier: a therapeutic target? *Nat. Rev. Gastroenterol. Hepatol.* 14 (2017) 9–21.
- [30] L. Wang, C. Llorente, P. Hartmann, A.M. Yang, P. Chen, B. Schnabl, Methods to determine intestinal permeability and bacterial translocation during liver disease, *J. Immunol. Methods* 421 (2015) 44–53.
- [31] F. Rainer, A. Horvath, T.D. Sandahl, B. Leber, B. Schmerboeck, A. Blesl, A. Groselj-Strele, R.E. Stauber, P. Fickert, P. Stiegler, H.J. Möller, H. Grönbaek, V. Stadlbauer, Soluble CD163 and soluble mannose receptor predict survival and decompensation in patients with liver cirrhosis, and correlate with gut permeability and bacterial translocation, *Aliment. Pharm. Ther.* 47 (2018) 657–664.
- [32] J. Yang, S.Y. Lim, Y.S. Ko, H.Y. Lee, S.W. Oh, M.G. Kim, W.Y. Cho, S.K. Jo, Intestinal barrier disruption and dysregulated mucosal immunity contribute to kidney fibrosis in chronic kidney disease, *Nephrol. Dial. Transpl.* 34 (3) (2019) 419–428.
- [33] E.A. Deitch, Gut-origin sepsis: evolution of a concept, *Surgeon* 10 (2012) 350–356.
- [34] S.F. Assimakopoulos, C. Triantos, K. Thomopoulos, F. Fligou, I. Maroulis, M. Marangos, C.A. Gogos, Gut-origin sepsis in the critically ill patient: pathophysiology and treatment, *Infection* 46 (2018) 751–760.
- [35] Y. Ma, X. Yang, V. Chatterjee, M.H. Wu, S.Y. Yuan, The gut-lung axis in systemic inflammation. Role of mesenteric lymph as a conduit, *Am. J. Respir. Cell Mol. Biol.* 64 (2021) 19–28.
- [36] L.W. Peterson, D. Artis, Intestinal epithelial cells: regulators of barrier function and immune homeostasis, *Nat. Rev. Immunol.* 14 (2014) 141–153.
- [37] S.E. Wu, S. Hashimoto-Hill, V. Woo, E.M. Eshleman, J. Whitt, L. Engleman, R. Karns, L.A. Denison, D.B. Haslam, T. Alenghat, Microbiota-derived metabolite promotes HDAC3 activity in the gut, *Nature* 586 (2020) 108–112.
- [38] G. Shen, J. Wu, B.C. Ye, N. Qi, Gut microbiota-derived metabolites in the development of diseases, *Can. J. Infect. Dis. Med. Microbiol.* 2021 (2021), 6658674.
- [39] Y. Feng, Y. Wang, P. Wang, Y. Huang, F. Wang, Short-chain fatty acids manifest stimulative and protective effects on intestinal barrier function through the inhibition of NLRP3 inflammasome and autophagy, *Cell Physiol. Biochem.* 49 (2018) 190–205.
- [40] J. Fu, G. Li, X. Wu, B. Zang, Sodium butyrate ameliorates intestinal injury and improves survival in a rat model of cecal ligation and puncture-induced sepsis, *Inflammation* 42 (2019) 1276–1286.
- [41] M.W. Adelman, M.H. Woodworth, C. Langelier, L.M. Busch, J.A. Kempker, C. S. Kraft, G.S. Martin, The gut microbiome's role in the development, maintenance, and outcomes of sepsis, *Crit. Care* 24 (2020) 278.
- [42] S.M. Kim, J.R. DeFazio, S.K. Hyoju, K. Sangani, R. Keskey, M.A. Krezalek, N. N. Khodarev, N. Sangwan, S. Christley, K.G. Harris, A. Malik, A. Zaborin, R. Bouziati, D.R. Ranao, M. Wiegerink, J.D. Ernest, B.A. Shakhssheer, I. D. Fleming, R.R. Weichselbaum, D.A. Antonopoulos, J.A. Gilbert, L.B. Barreiro, O. Zaborina, B. Jabri, J.C. Alverdy, Fecal microbiota transplant rescues mice from human pathogen mediated sepsis by restoring systemic immunity, *Nat. Commun.* 11 (2020) 2354.
- [43] N. Yoshida, T. Emoto, T. Yamashita, H. Watanabe, T. Hayashi, T. Tabata, N. Hoshi, N. Hatanaka, G. Ozawa, N. Sasaki, T. Mizoguchi, H.Z. Amin, Y. Hirota, W. Ogawa, T. Yamada, K.I. Hirata, *Bacteroides vulgatus* and *bacteroides dorei* reduce gut microbial lipopolysaccharide production and inhibit atherosclerosis, *Circulation* 138 (2018) 2486–2498.
- [44] N. Yoshida, T. Yamashita, S. Kishino, H. Watanabe, K. Sasaki, D. Sasaki, T. Tabata, Y. Sugiyama, N. Kitamura, Y. Saito, T. Emoto, T. Hayashi, T. Takahashi, M. Shinohara, R. Osawa, A. Kondo, T. Yamada, J. Ogawa, K. I. Hirata, A possible beneficial effect of *Bacteroides* on faecal lipopolysaccharide activity and cardiovascular diseases, *Sci. Rep.* 10 (2020) 13009.
- [45] M. Beaumont, A.M. Neyrinck, M. Olivares, J. Rodríguez, A. de Rocca Serra, M. Roumain, L.B. Bindels, P.D. Cani, P. Evenepoel, G.G. Muccioli, J.B. Demoulin, N.M. Delzenne, The gut microbiota metabolite indole alleviates liver inflammation in mice, *FASEB J.* 32 (2018), 201800544 fJ201800544.
- [46] J. Tang, L. Xu, Y. Zeng, F. Gong, Effect of gut microbiota on LPS-induced acute lung injury by regulating the TLR4/NF-κB signaling pathway, *Int. Immunopharmacol.* 91 (2021), 107272.
- [47] P.D. Cani, A.M. Neyrinck, F. Fava, C. Knauf, R.G. Burcelin, K.M. Tuohy, G. R. Gibson, N.M. Delzenne, Selective increases of bifidobacteria in gut microflora improve high-fat-diet-induced diabetes in mice through a mechanism associated with endotoxaemia, *Diabetologia* 50 (2007) 2374–2383.
- [48] S. Ghoshal, J. Witt, J. Zhong, W. de Villiers, E. Eckhardt, Chylomicrons promote intestinal absorption of lipopolysaccharides, *J. Lipid Res.* 50 (2009) 90–97.
- [49] F. Laugeronette, C. Vors, A. Géloën, M.A. Chauvin, C. Soulage, S. Lambert-Porcheron, N. Peretti, M. Alliger, R. Burcelin, M. Laville, H. Vidal, M. C. Michalski, Emulsified lipids increase endotoxemia: possible role in early postprandial low-grade inflammation, *J. Nutr. Biochem.* 22 (2011) 53–59.
- [50] M. Clemente-Postigo, M.I. Queipo-Ortuño, M. Murri, M. Boto-Ordoñez, P. Perez-Martinez, C. Andres-Lacueva, F. Cardona, F.J. Tinahones, Endotoxin increase after fat overload is related to postprandial hypertriglyceridemia in morbidly obese patients, *J. Lipid Res.* 53 (2012) 973–978.
- [51] P.D. Cani, R. Bibiloni, C. Knauf, A. Waget, A.M. Neyrinck, N.M. Delzenne, R. Burcelin, Changes in gut microbiota control metabolic endotoxemia-induced inflammation in high-fat diet-induced obesity and diabetes in mice, *Diabetes* 57 (2008) 1470–1481.
- [52] Y. Ji, Y. Sakata, P. Tso, Nutrient-induced inflammation in the intestine, *Curr. Opin. Clin. Nutr. Metab. Care* 14 (2011) 315–321.
- [53] T. Suzuki, Regulation of the intestinal barrier by nutrients: the role of tight junctions, *Anim. Sci. J.* 91 (2020) 13357.
- [54] S.K. Hyoju, A. Zaborin, R. Keskey, A. Sharma, W. Arnold, F. van den Berg, S. M. Kim, N. Gottel, C. Bethel, A. Charnot-Katsikas, P. Jianxin, C. Adriaansens, E. Papazian, J.A. Gilbert, O. Zaborina, J.C. Alverdy, Mice fed an obesogenic western diet, administered antibiotics, and subjected to a sterile surgical procedure develop lethal septicemia with multidrug-resistant pathogens, *mBio* 10 (2019) e00903-e00919.
- [55] B.A. Napier, M. Andres-Terre, L.M. Massis, A.J. Hryckowian, S.K. Higginbottom, K. Cumnock, K.M. Casey, B. Haileselassie, K.A. Lugo, D.S. Schneider, J. L. Sonnenburg, D.M. Monack, Western diet regulates immune status and the response to LPS-driven sepsis independent of diet-associated microbiome, *Proc. Natl. Acad. Sci. U.S.A.* 116 (2019) 3688–3694.
- [56] A.J. Jacob, P.K. Goldberg, N. Bloom, G.A. Degenshein, P.J. Kozinn, Endotoxin and bacteria in portal blood, *Gastroenterology* 72 (1977) 1268–1270.
- [57] P. Kubes, C. Jenne, Immune responses in the liver, *Annu. Rev. Immunol.* 36 (2018) 247–277.
- [58] J. Yan, S. Li, S. Li, The role of the liver in sepsis, *Int. Rev. Immunol.* 33 (2014) 498–510.
- [59] P. Strnad, F. Tacke, A. Koch, C. Trautwein, Liver - guardian, modifier and target of sepsis, *Nat. Rev. Gastroenterol. Hepatol.* 14 (2017) 55–66.
- [60] M. Deng, M.J. Scott, P. Loughran, G. Gibson, C. Sodhi, S. Watkins, D. Hackam, T. R. Billiar, Lipopolysaccharide clearance, bacterial clearance, and systemic

- inflammatory responses are regulated by cell type-specific functions of TLR4 during sepsis, *J. Immunol.* 190 (2013) 5152–5160.
- [61] Y. Tan, J.C. Kagan, A cross-disciplinary perspective on the innate immune responses to bacterial lipopolysaccharide, *Mol. Cell* 54 (2014) 212–223.
- [62] J.C. Kagan, R. Medzhitov, Phosphoinositide-mediated adaptor recruitment controls Toll-like receptor signaling, *Cell* 125 (2006) 943–955.
- [63] M. Yamamoto, S. Sato, H. Hemmi, K. Hoshino, T. Kishio, H. Sanjo, O. Takeuchi, M. Sugiyama, M. Okabe, K. Takeda, S. Akira, Role of adaptor TRIF in the MyD88-independent toll-like receptor signaling pathway, *Science* 301 (2003) 640–643.
- [64] K.S. Bonham, M.H. Orzalli, K. Hayashi, A.I. Wolf, C. Glanemann, W. Weninger, A. Iwasaki, D.M. Knipe, J.C. Kagan, A promiscuous lipid-binding protein diversifies the subcellular sites of toll-like receptor signal transduction, *Cell* 156 (2014) 705–716.
- [65] J.M. Blander, R. Medzhitov, Regulation of phagosome maturation by signals from toll-like receptors, *Science* 304 (2004) 1014–1018.
- [66] Y. Xu, C. Jagannath, X.D. Liu, A. Sharafkhaneh, K.E. Kolodziejska, N.T. Eissa, Toll-like receptor 4 is a sensor for autophagy associated with innate immunity, *Immunity* 27 (2007) 135–144.
- [67] A.P. West, I.E. Brodsky, C. Rahner, D.K. Woo, H. Erdjument-Bromage, P. Tempst, M.C. Walsh, Y. Choi, G.S. Shadel, S. Ghosh, TLR signalling augments macrophage bactericidal activity through mitochondrial ROS, *Nature* 472 (2011) 476–480.
- [68] J.A. Hagar, D.A. Powell, Y. Aachoui, R.K. Ernst, E.A. Miao, Cytoplasmic LPS activates caspase-11: implications in TLR4-independent endotoxic shock, *Science* 341 (2013) 1250–1253.
- [69] N. Kayagaki, M.T. Wong, I.B. Stowe, S.R. Ramani, L.C. Gonzalez, S. Akashi-Takamura, K. Miyake, J. Zhang, W.P. Lee, A. Muszyński, L.S. Forsberg, R. W. Carlson, V.M. Dixit, Noncanonical inflammasome activation by intracellular LPS independent of TLR4, *Science* 341 (2013) 1246–1249.
- [70] A. Pfalzgraff, G. Weindl, Intracellular lipopolysaccharide sensing as a potential therapeutic target for sepsis, *Trends Pharm. Sci.* 40 (2019) 187–197.
- [71] H. Gaitantzi, J. Karch, L. Germann, C. Cai, V. Rausch, E. Birgin, N. Rahbari, T. Seitz, C. Hellerbrand, C. König, H.G. Augustin, C. Mogler, C. de la Torre, N. Gretz, T. Itzel, A. Teufel, M. Ebert, K. Breitkopf-Heinlein, BMP-9 modulates the hepatic responses to LPS, *Cells* 9 (2020) 617.
- [72] L.P. Ganesan, J.M. Mates, A.M. Cheplowitz, C.L. Avila, J.M. Zimmerer, Z. Yao, A. Maisyeu, M.V. Rajaram, J.M. Robinson, C.L. Anderson, Scavenger receptor B1, the HDL receptor, is expressed abundantly in liver sinusoidal endothelial cells, *Sci. Rep.* 6 (2016) 20646.
- [73] L. Guo, Z. Zheng, J. Ai, B. Huang, X.A. Li, Hepatic scavenger receptor BI protects against polymicrobial-induced sepsis through promoting LPS clearance in mice, *J. Biol. Chem.* 289 (2014) 14666–14673.
- [74] G.C. Hansson, Mucins and the microbiome, *Annu. Rev. Biochem.* 89 (2020) 769–793.
- [75] M.A. Borisova, K.M. Achasova, K.N. Morozova, E.N. Andreyeva, E.A. Litvinova, A. A. Ogienko, M.V. Morozova, M.B. Berkova, E. Kiseleva, E.N. Kozhevnikova, Mucin-2 knockout is a model of intercellular junction defects, mitochondrial damage and ATP depletion in the intestinal epithelium, *Sci. Rep.* 10 (2020) 21135.
- [76] M. Kumar, A. Leon Coria, S. Cornick, B. Petri, S. Mayengbam, H.B. Jijon, F. Moreau, J. Shearer, K. Chadee, Increased intestinal permeability exacerbates sepsis through reduced hepatic SCD-1 activity and dysregulated iron recycling, *Nat. Commun.* 11 (2020) 483.
- [77] J.M. Bates, J. Åkerlund, E. Mittge, K. Guillemin, Intestinal alkaline phosphatase detoxifies lipopolysaccharide and prevents inflammation in zebrafish in response to the gut microbiota, *Cell Host Microbe* 2 (2007) 371–382.
- [78] K. Geddes, D.J. Philpott, A new role for intestinal alkaline phosphatase in gut barrier maintenance, *Gastroenterology* 135 (2008) 8–12.
- [79] S.B. Singh, A. Carroll-Portillo, C. Coffman, N.L. Ritz, H.C. Lin, Intestinal alkaline phosphatase exerts anti-inflammatory effects against lipopolysaccharide by inducing autophagy, *Sci. Rep.* 10 (2020) 3107.
- [80] F. Su, R. Brands, Z. Wang, C. Verdant, A. Bruhn, Y. Cai, W. Raaben, M. Wulferink, J.L. Vincent, Beneficial effects of alkaline phosphatase in septic shock, *Crit. Care Med.* 34 (2006) 2182–2187.
- [81] S. Heemskerk, R. Masereeuw, O. Moesker, M.P. Bouw, J.G. van der Hoeven, W. H. Peters, F.G. Russel, P. Pickkers, G. APSEP Study, Alkaline phosphatase treatment improves renal function in severe sepsis or septic shock patients, *Crit. Care Med.* 37 (2009) 417–423, 417-e1.
- [82] P. Pickkers, S. Heemskerk, J. Schouten, P.F. Laterre, J.L. Vincent, A. Beishuizen, P.G. Jorens, H. Spapen, M. Bulitta, W.H. Peters, J.G. van der Hoeven, Alkaline phosphatase for treatment of sepsis-induced acute kidney injury: a prospective randomized double-blind placebo-controlled trial, *Crit. Care* 16 (2012) 14.
- [83] F. Hümmeke-Oppers, P. Hemelaar, P. Pickkers, Innovative drugs to target renal inflammation in sepsis: alkaline phosphatase, *Front. Pharm.* 10 (2019) 919.
- [84] T. Ayabe, D.P. Satchell, C.L. Wilson, W.C. Parks, M.E. Selsted, A.J. Ouellette, Secretion of microbicidal alpha-defensins by intestinal Paneth cells in response to bacteria, *Nat. Immunol.* 1 (2000) 113–118.
- [85] S. Vaishnava, C.L. Behrendt, A.S. Ismail, L. Eckmann, L.V. Hooper, Paneth cells directly sense gut commensals and maintain homeostasis at the intestinal host-microbial interface, *Proc. Natl. Acad. Sci. U.S.A.* 105 (2008) 20858–20863.
- [86] L.J. Beamer, Structure of human BPI (bactericidal/permeability-increasing protein) and implications for related proteins, *Biochem. Soc. Trans.* 31 (2003) 791–794.
- [87] A.L. Alonso, A. Zentella-Dehesa, J. Mas-Oliva, Characterization of a naturally occurring new version of the cholesterol ester transfer protein (CETP) from small intestine, *Mol. Cell. Biochem.* 245 (2003) 173–182.
- [88] V. García-González, N. Gutiérrez-Quintanar, J. Mas-Oliva, The C-terminal domain supports a novel function for CETPI as a new plasma lipopolysaccharide-binding protein, *Sci. Rep.* 5 (2015) 16091.
- [89] A.C. Vreugdenhil, A.M. Snoek, J.W. Greve, W.A. Buurman, Lipopolysaccharide-binding protein is vectorially secreted and transported by cultured intestinal epithelial cells and is present in the intestinal mucus of mice, *J. Immunol.* 165 (2000) 4561–4566.
- [90] G.H. Hansen, K. Rasmussen, L.L. Niels-Christiansen, E.M. Danielsen, Lipopolysaccharide-binding protein: localization in secretory granules of Paneth cells in the mouse small intestine, *Histochem. Cell Biol.* 131 (2009) 727–732.
- [91] S.D. Wright, R.A. Ramos, P.S. Tobias, R.J. Ulevitch, J.C. Mathison, CD14, a receptor for complexes of lipopolysaccharide (LPS) and LPS binding protein, *Science* 249 (1990) 1431–1433.
- [92] G. Cann, O. Levy, G.T. Furuta, S. Narravula-Alipati, R.B. Sisson, C.N. Serhan, S. P. Colgan, Lipid mediator-induced expression of bactericidal/ permeability-increasing protein (BPI) in human mucosal epithelia, *Proc. Natl. Acad. Sci. U.S.A.* 99 (2002) 3902–3907.
- [93] G. Cann, E. Cario, A. Lennartsson, U. Gullberg, C. Brennan, O. Levy, S.P. Colgan, Functional and biochemical characterization of epithelial bactericidal/ permeability-increasing protein, *Am. J. Physiol. Gastrointest. Liver Physiol.* 290 (2006) G557–G567.
- [94] A. Balakrishnan, D. Chakravortty, Epithelial cell damage activates bactericidal/ permeability increasing-protein (BPI) expression in intestinal epithelium, *Front. Microbiol.* 8 (2017) 1567.
- [95] S. Bas, B.R. Gauthier, U. Spenuo, S. Stingelin, C. Gabay, CD14 is an acute-phase protein, *J. Immunol.* 172 (2004) 4470–4479.
- [96] P.M. Cazita, D.F. Barbeiro, A.I. Moretti, E.C. Quintão, F.G. Soriano, Human cholesterol ester transfer protein expression enhances the mouse survival rate in an experimental systemic inflammation model: a novel role for CETP, *Shock* 30 (2008) 590–595.
- [97] T.M. Venancio, R.M. Machado, A. Castoldi, M.T. Amano, V.S. Nunes, E. C. Quintão, N.O. Camara, F.G. Soriano, P.M. Cazita, CETP lowers TLR4 expression which attenuates the inflammatory response induced by LPS and polymicrobial sepsis, *Mediat. Inflamm.* 2016 (2016), 1784014.
- [98] P.J. Barter, M. Caulfield, M. Eriksson, S.M. Grundy, J.J. Kastelein, M. Komajda, J. Lopez-Sendon, L. Mosca, J.C. Tardif, D.D. Waters, C.L. Shear, J.H. Revkin, K. A. Buhr, M.R. Fisher, A.R. Tall, B. Brewer, I. ILLUMINATE, Effects of torcetrapib in patients at high risk for coronary events, *New Engl. J. Med.* 357 (2007) 2109–2122.
- [99] R.W. Clark, D. Cunningham, Y. Cong, T.A. Subash, G.T. Tkalcic, D.B. Lloyd, J. G. Boyd, B.A. Chrunky, G.A. Karam, X. Qiu, I.K. Wang, O.L. Francone, Assessment of cholesterol ester transfer protein inhibitors for interaction with proteins involved in the immune response to infection, *J. Lipid Res.* 51 (2010) 967–974.
- [100] C.M. Grion, L.T. Cardoso, T.F. Perazolo, A.S. Garcia, D.S. Barbosa, H.K. Morimoto, T. Matsuo, A.J. Carrilho, Lipoproteins and CETP levels as risk factors for severe sepsis in hospitalized patients, *Eur. J. Clin. Investig.* 40 (2010) 330–338.
- [101] S.H. Liu, H.Y. Liang, H.Y. Li, X.F. Ding, T.W. Sun, J. Wang, Effect of low high-density lipoprotein levels on mortality of septic patients: a systematic review and meta-analysis of cohort studies, *World J. Emerg. Med.* 11 (2020) 109–116.
- [102] M. Trinder, K.R. Genga, H.J. Kong, L.L. Blauw, C. Lo, X. Li, M. Cirstea, Y. Wang, P. Rensen, J.A. Russell, K.R. Walley, J.H. Boyd, L.R. Brunham, Cholesterol ester transfer protein influences high-density lipoprotein levels and survival in sepsis, *Am. J. Respir. Crit. Care Med.* 199 (2019) 854–862.
- [103] E.A. Woźnica, M. Inglot, R.K. Woźnica, L. Łysenko, Liver dysfunction in sepsis, *Adv. Clin. Exp. Med.* 27 (2018) 547–551.
- [104] Z. Li, Y. Wang, R.J. van der Sluis, J.W. van der Hoorn, H.M. Princen, M. Van Eck, T.J. Van Berkel, P.C. Rensen, M. Hoekstra, Niacin reduces plasma CETP levels by diminishing liver macrophage content in CETP transgenic mice, *Biochem. Pharm.* 84 (2012) 821–829.
- [105] Y. Wang, S. van der Tuin, N. Tjeerdema, A.D. van Dam, S.S. Rensen, T. Hendrikx, J.F. Berbée, B. Atanasovska, J. Fu, M. Hoekstra, S. Bekkering, N.P. Riksen, W. A. Buurman, J.W. Greve, M.H. Hofker, R. Shiri-Sverdlov, O.C. Meijer, J.W. Smit, L.M. Havekes, K.W. van Dijk, P.C. Rensen, Plasma cholesterol ester transfer protein is predominantly derived from Kupffer cells, *Hepatology* 62 (2015) 1710–1722.
- [106] S.J.L. van der Tuin, Z. Li, J.F.P. Berbée, I. Verkouter, L.E. Ringnalda, A.E. Neele, J. B. Klinken, S.S. Rensen, J. Fu, M. de Winther, A.K. Groen, P. Rensen, K. Willems van Dijk, Y. Wang, Lipopolysaccharide lowers cholesterol ester transfer protein by activating F4/80⁺Clec4F⁺Vsig4⁺Ly6C⁺ Kupffer cell subsets, *J. Am. Heart Assoc.* 7 (2018), e008105.
- [107] L.L. Blauw, Y. Wang, K. Willems van Dijk, P.C.N. Rensen, A novel role for CETP as immunological gatekeeper: raising HDL to cure sepsis? *Trends Endocrinol. Metab.* 31 (2020) 334–343.
- [108] H.W. Harris, S.E. Brady, J.H. Rapp, Hepatic endosomal trafficking of lipoprotein-bound endotoxin in rats, *J. Surg. Res.* 106 (2002) 188–195.
- [109] P.M. Grin, D.J. Dwivedi, K.M. Chatheley, B.L. Trigatti, A. Prat, N.G. Seidah, P. C. Liaw, A.E. Fox-Robichaud, Low-density lipoprotein (LDL)-dependent uptake of Gram-positive lipoteichoic acid and Gram-negative lipopolysaccharide occurs through LDL receptor, *Sci. Rep.* 8 (2018) 10496.
- [110] B. Shao, R.S. Munford, R. Kitchens, A.W. Varley, Hepatic uptake and deacylation of the LPS in bloodborne LPS-lipoprotein complexes, *Innate Immun.* 18 (2012) 825–833.
- [111] Z. Yao, J.M. Mates, A.M. Cheplowitz, L.P. Hammer, A. Maisyeu, G.S. Phillips, M. D. Wewers, M.V. Rajaram, J.M. Robinson, C.L. Anderson, L.P. Ganesan, Blood-borne lipopolysaccharide is rapidly eliminated by liver sinusoidal endothelial cells via high-density lipoprotein, *J. Immunol.* 197 (2016) 2390–2399.

- [112] J. Li, K. Xia, M. Xiong, X. Wang, N. Yan, Effects of sepsis on the metabolism of sphingomyelin and cholesterol in mice with liver dysfunction, *Exp. Ther. Med.* 14 (2017) 5635–5640.
- [113] E. Pandey, A.S. Nour, E.N. Harris, Prominent receptors of liver sinusoidal endothelial cells in liver homeostasis and disease, *Front. Physiol.* 11 (2020) 873.
- [114] N.N. Kuzmich, K.V. Sivak, V.N. Chubarev, Y.B. Porozov, T.N. Savateeva-Lyubimova, F. Peri, TLR4 signaling pathway modulators as potential therapeutics in inflammation and sepsis, *Vaccines* 5 (2017) 34.
- [115] Y. Wen, J. Lambrecht, C. Ju, F. Tacke, Hepatic macrophages in liver homeostasis and diseases-diversity, plasticity and therapeutic opportunities, *Cell. Mol. Immunol.* 18 (2021) 45–56.
- [116] A.T. Nguyen-Lefebvre, A. Horuzsko, Kupffer cell metabolism and function, *J. Enzym. Metab.* 1 (2015) 101.
- [117] X. Liang, T. Li, Q. Zhou, S. Pi, Y. Li, X. Chen, Z. Weng, H. Li, Y. Zhao, H. Wang, Y. Chen, Mesenchymal stem cells attenuate sepsis-induced liver injury via inhibiting M1 polarization of Kupffer cells, *Mol. Cell. Biochem.* 452 (2019) 187–197.
- [118] F. Xu, Y. Ma, W. Huang, J. Gao, M. Guo, J. Li, L. Kong, G. Liang, R. Du, Q. Xu, X. Wu, Typically inhibiting USP14 promotes autophagy in M1-like macrophages and alleviates CLP-induced sepsis, *Cell Death Dis.* 11 (2020) 666.
- [119] J.B. Dixon, Mechanisms of chylomicron uptake into lacteals, *Ann. N.Y. Acad. Sci.* 1207 (2010) E52–E57.
- [120] E.G. Pérez-Hernández, V.M. De la Puente- Díaz de León, I. Luna-Reyes, J. Sifuentes-Osornio, J. Mas-Oliva, New Biomarkers in Sepsis and Septic Shock. CETPI and peptides derived from its C-terminal Segment as Defining Molecules of Disease Severity. (Submitted).
- [121] K.R. Groschwitz, S.P. Hogan, Intestinal barrier function: molecular regulation and disease pathogenesis, *J. Allergy Clin. Immunol.* 124 (2009) 3–22.
- [122] T.S.R. van Engelen, W.J. Wiersinga, B.P. Scicluna, T. van der Poll, Biomarkers in sepsis, *Crit. Care Clin.* 34 (2018) 139–152.
- [123] C. Pierrakos, D. Velissaris, M. Bisdorff, J.C. Marshall, J.L. Vincent, Biomarkers of sepsis: time for a reappraisal, *Crit. Care* 24 (2020) 287.
- [124] I. Luna-Reyes, E.G. Pérez-Hernández, B. Delgado-Coello, M.A. Ávila-Rodríguez, J. Mas-Oliva, Peptide VSAK maintains tissue glucose uptake and attenuates pro-inflammatory responses caused by LPS in an experimental model of the Systemic Inflammatory Response Syndrome; a PET study. (Submitted).

Article

Lipid Modulation in the Formation of β -Sheet Structures. Implications for De Novo Design of Human Islet Amyloid Polypeptide and the Impact on β -Cell Homeostasis

Israel Martínez-Navarro ^{1,†}, Raúl Díaz-Molina ¹ , Angel Pulido-Capiz ^{1,2,†}, Jaime Mas-Oliva ³ , Ismael Luna-Reyes ³, Eustolia Rodríguez-Velázquez ^{4,5}, Ignacio A. Rivero ⁶, Marco A. Ramos-Ibarra ⁷ , Manuel Alatorre-Meda ⁸  and Victor García-González ^{1,*} 

¹ Departamento de Bioquímica, Facultad de Medicina Mexicali, Universidad Autónoma de Baja California, Mexicali 21000, Baja California, Mexico; israel.martinez.navarro@uabc.edu.mx (I.M.-N.); rauldiaz@uabc.edu.mx (R.D.-M.); pulido.angel@uabc.edu.mx (A.P.-C.)

² Laboratorio de Biología Molecular, Facultad de Medicina Mexicali, Universidad Autónoma de Baja California, Mexicali 21000, Baja California, Mexico.

³ Instituto de Fisiología Celular, Universidad Nacional Autónoma de México, Ciudad de Mexico 04510, Mexico; jmas@ifc.unam.mx (J.M.-O.); ismaelluna.biome@gmail.com (I.L.-R.)

⁴ Facultad de Odontología, Universidad Autónoma de Baja California, Tijuana 22390, Mexico; eustolia.rodriguez@uabc.edu.mx

⁵ Tecnológico Nacional de México/I.T. Tijuana, Centro de Graduados e Investigación en Química-Grupo de Biomateriales y Nanomedicina, Tijuana 22510, Mexico

⁶ Tecnológico Nacional de México/Instituto Tecnológico de Tijuana, Centro de Graduados e Investigación en Química, Tijuana 22510, Baja California, Mexico; irivero@tectijuana.mx

⁷ Facultad de Ciencias Químicas e Ingeniería, Universidad Autónoma de Baja California, Tijuana 22390, Baja California, Mexico; mramos@uabc.edu.mx

⁸ Cátedras CONACyT- Tecnológico Nacional de México/I.T. Tijuana, Centro de Graduados e Investigación en Química-Grupo de Biomateriales y Nanomedicina, Tijuana 22510, Mexico; manuel_alatorre@yahoo.com.mx

* Correspondence: vgarcia62@uabc.edu.mx; Tel.: +52-68-6557-1622

† These authors contributed equally to this work.

Received: 17 July 2020; Accepted: 4 August 2020; Published: 19 August 2020



Abstract: Human islet amyloid polypeptide (hIAPP) corresponds to a 37-residue hormone present in insulin granules that maintains a high propensity to form β -sheet structures during co-secretion with insulin. Previously, employing a biomimetic approach, we proposed a panel of optimized IAPP sequences with only one residue substitution that shows the capability to reduce amyloidogenesis. Taking into account that specific membrane lipids have been considered as a key factor in the induction of cytotoxicity, in this study, following the same design strategy, we characterize the effect of a series of lipids upon several polypeptide domains that show the highest aggregation propensity. The characterization of the C-native segment of hIAPP (residues F₂₃-Y₃₇), together with novel variants F₂₃R and I₂₆A allowed us to demonstrate an effect upon the formation of β -sheet structures. Our results suggest that zwitterionic phospholipids promote adsorption of the C-native segments at the lipid-interface and β -sheet formation with the exception of the F₂₃R variant. Moreover, the presence of cholesterol did not modify this behavior, and the β -sheet structural transitions were not registered when the N-terminal domain of hIAPP (K₁-S₂₀) was characterized. Considering that insulin granules are enriched in phosphatidylserine (PS), the property of lipid vesicles containing negatively charged lipids was also evaluated. We found that these types of lipids promote β -sheet conformational transitions in both the C-native segment and the new variants. Furthermore, these PS/peptides arrangements are internalized in Langerhans islet β -cells, localized in the endoplasmic reticulum, and trigger critical pathways such as unfolded protein response (UPR), affecting insulin secretion. Since this phenomenon was associated with the presence of cytotoxicity on Langerhans

islet β -cells, it can be concluded that the anionic lipid environment and degree of solvation are critical conditions for the stability of segments with the propensity to form β -sheet structures, a situation that will eventually affect the structural characteristics and stability of IAPP within insulin granules, thus modifying the insulin secretion.

Keywords: hIAPP; amyloidogenesis; insulin granules; endoplasmic reticulum; anionic lipids; F₂₃R variant; β -sheet transitions; β -cell cytotoxicity; unfolded protein response

1. Introduction

Human islet amyloid polypeptide (hIAPP) is a hormone that slows down gastric emptying and participates in the regulation of plasmatic glucose associated with functions such as glucagon-release inhibition and leptin sensitization [1,2]. hIAPP is a monomeric peptide processed in the Golgi complex and secreted in insulin granules in response to β -cell secretagogues [3]. However, amyloid fibril formation in hIAPP could trigger an amplified toxicity response that leads to failure of pancreatic β -cells, a hallmark of type 2 diabetes mellitus (T2DM). Several variants of hIAPP modify their stability accelerating amyloid formation; for instance, in Asian populations, the S₂₀G mutation has been associated with early-stage cases of DM2 [4]. Likewise, variants have been described in the Maori populations of New Zealand [5]. By contrast, rat IAPP (rIAPP) containing structural differences with hIAPP in six residues situated in region 18–29 (H₁₈R, F₂₃L, A₂₅P, I₂₆V, S₂₈P, and S₂₉P) show a diminished trend to produce amyloid fibrils [6]. Although these changes allowed the development of pramlintide, an amylinomimetic peptide with three variants (A₂₅P, S₂₈P, and S₂₉P) used in DM2 therapy; the propensity to aggregation of this sequence is not completely avoided.

Several reports suggest that the C-native segment of IAPP (residues 23–37) is a critical domain in the structural transitions that trigger amyloid formation [6], hence, it could be a target for the development of strategies to reduce aggregation. Based on multiple sequence alignment among N- and C-domains on 240 sequences of different species, the N-domain (residues 1–20) has been described as a conserved sequence among a wide variety of organisms, while the C-domain (residues 22–37) has been restricted to phylogenetically close groups [7]. Therefore, we proposed a panel of optimized IAPP sequences, which could reduce aggregation with only one residue substitution [7].

Localized changes in the secondary structure of proteins and peptides are believed to work as a molecular switch regulating function or, in some cases, as a trigger for misfolding. In this context, we have described these conditions by studying the cholesteryl-ester transfer protein (CETP) and a series of apolipoproteins [8–13]. In addition, other studies have reported that phosphatidylserine (PS) vesicles could increase the peptide/aggregation ratio, suggesting an electrostatic factor as a triggering condition for the induction of conformational changes [14,15]. In this sense, within insulin secretory granules derived from the endoplasmic reticulum (ER) [16], the concentration of PS and phosphatidylinositol has been described to be fivefold higher compared to that of the cell membrane [17]. Therefore, lipids could be a factor that promotes structural changes in hIAPP, inducing misfolding phenomena.

However, highly sophisticated mechanisms that modulate protein structure and function have evolved to maintain cellular homeostasis and counteract misfolding [11]. Perturbations in these mechanisms can lead to protein dysfunction as well as deleterious cell processes. Specifically, imbalances in secretory protein synthesis pathways lead to a condition known as ER stress, which elicits the adaptive unfolded protein response (UPR) [11], a phenomenon that could be critical during insulin maturation. Importantly, proinsulin is folded in the ER by chaperones such as protein disulfide isomerases (PDI) and binding immunoglobulin protein (BiP) or GRP-78 [18]. Therefore, the transducers of the UPR pathway, IRE1, ATF6 α , and PERK, promote the translation of target chaperones through XBPIs, ATF6 α , and CHOP transcription factors, respectively, when unfolded proteins accumulate in the lumen [19]. The three branches of UPR are essential in cell homeostasis to reduce ER stress and

to ensure adequate synthesis of peptides such as insulin [20]. Indeed, in several reports, we have described the effect of metabolic overload on the dysregulation of UPR arms [21,22].

Given this situation, the initial events of misfolding and amyloid aggregation promote a cascade of pathological processes considered the hallmark in the progression of several chronic degenerative diseases [8–13] that might be associated with conditions related to metabolic overload [21,22]. Having this in mind, we herein characterized the role of lipid systems on the conformational transitions of the most aggregative C-terminal domain of hIAPP, and through a biomimetic approach, evaluated this condition on variants F₂₃R and I₂₆A that potentially could reduce aggregation. In addition, we also characterized the association with cell responses involved in protein homeostasis such as UPR.

2. Materials and Methods

2.1. De Novo IAPP Sequences

Based on network analysis, different residues from 240 species reported in the NCBI database were replaced on the hIAPP sequence. The effect of the substitutions was characterized through physicochemical assays, as well as by the computational identification of regions with a high intrinsic propensity for aggregation [7]. Aggregation propensity range was obtained considering the aggregation value of hIAPP as a reference, based on the AGGRESCAN algorithm (Na4vSS) [23].

2.2. Materials

Cell culture reagents were purchased from Thermo Fisher (Carlsbad, CA, USA), while tissue culture plates and other plastic materials were obtained from Corning Inc. (Corning, NY, USA). Salts and buffers were obtained from Sigma-Aldrich (St. Luis, MI, USA), as well as Thioflavin T (ThT), black Sudan B, Congo red, sodium dodecyl sulfate (SDS), and 3-(4,5-dimethylthiazol-2-yl)-2,5-diphenyltetrazolium bromide (MTT). L- α -phosphatidylcholine (PC), L- α -phosphatidylserine (PS), L- α -phosphatidyl-ethanolamine (PE), 1-oleoyl-2-hydroxy-sn-glycero-3-phosphate (LPA), 1-palmitoyl-2-oleoyl-sn-glycerol (POPG), and cholesterol were obtained from Avanti Polar Lipids, Inc. (Alabaster, AL, USA). Antibodies anti-XBP1s and anti-BiP/GRP78 were purchased from Abcam (Cambridge, UK) and anti- β -actin was obtained from Santa Cruz Biotechnology (Dallas, TX, USA). Anti-PDI was donated by Dr. Marco A. Ramos Ibarra.

2.3. Peptide Synthesis and Preparation

Several peptides were synthesized considering the physicochemical properties of hIAPP such as: N-native segment (¹KCNTATCATQRLANFLVHSS²⁰); C-native segment (²³FGAILSSTNVGSNTY³⁷); F₂₃R variant (²³RGAILSSTNVGSNTY³⁷); and I₂₆A variant (²³FGAALSSTNVGSNTY³⁷) (Figure 1). Likewise, the aggregative core of amyloid beta (A β) peptide was used as a control ²⁵GSNKGAIIGLM³⁵. All solutions were filtered through 0.22 μ m membrane filters (Millipore, Burlington, MA, USA) before the experiments. Peptide purity greater than 98% was confirmed by mass spectrometry and HPLC (GenScript, Piscataway, NY, USA). The best condition for peptide solubilization was the use of ultrapure H₂O (600 μ g/mL), subsequently diluted in phosphate buffer pH 7.4 (60 μ g/mL).

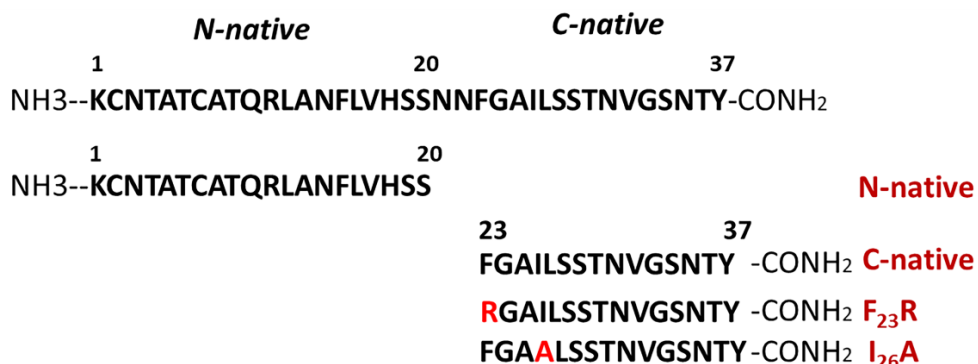


Figure 1. Representation of the primary structure of human islet amyloid polypeptide (hIAPP) and peptides corresponding to N-native and C-native domains, as well as new variants of hIAPP.

2.4. Preparation of Small Unilamellar Vesicles (SUVs)

SUVs were prepared from PC, PS, PE, cholesterol, and POPG (600 µg/mL) upon their mixing and conditioning at varying concentrations. PC, PS, PE, cholesterol, and POPG were dissolved in chloroform and dried for 90 min under a gentle stream of N₂ with an additional incubation of 5 h at 30 °C in an Eppendorf Vacufuge concentrator (Eppendorf, Hamburg, Germany), according to protocols established by our working group [9]. After drying, samples were hydrated in phosphate buffer to pH 7.4 and processed through 4 cycles of freezing in liquid N₂ and thawing at 37 °C, and finally subjected to a sonication process (for 10 min under 15 s on/30 s off cycles at 9.5–10 W) in a Cole-Parmer Ultrasonic Homogenizer (Vernon Hills, IL, USA). Samples were stabilized for 1 h at 25 °C and centrifuged at 13,000 rpm for 10 min.

LPA samples in chloroform were placed under a gentle flow of N₂ for 90 min and additional 12 h in a vacuum equipment. The samples were hydrated in phosphate buffer and afterwards processed through 4 cycles of freezing in liquid N₂ and thawing at 37 °C. Solutions were left to equilibrate for 2 h and centrifuged at 13,000 rpm for 10 min.

2.5. Preparation of Large Unilamellar Vesicles (LUVs)

LUVs were prepared from PC and PS by the reverse-phase evaporation methodology [24], with some adaptations. Specifically, PC LUVs were prepared by dissolving the lipid (600 µg/mL) in a 1:3 mixture of diethylether:phosphate buffer (pH 7.4). Then, the solution was sonicated for 5 min in an ultrasonic homogenizer. Finally, the solution was added to a rotary evaporator working at an initial pressure of 400 mmHg for 5 min, followed by a final pressure of 650 mmHg until complete removal of diethylether. Likewise, PS LUVs were prepared by dissolving the lipid (600 µg/mL) in chloroform and drying the resulting solution for 90 min under a gentle stream of N₂ with an additional incubation of 2 h at 30 °C in an Eppendorf Vacufuge concentrator, according to protocols established by our working group [9]. After drying, samples were hydrated in phosphate buffer, pH 7.4, and processed through 4 cycles of freezing in liquid N₂ and thawing at 37 °C. Finally, samples were subjected to a sonication process (for 5 min under 15 s on/30 s off cycles at 9.5–10 W) in an ultrasonic homogenizer.

2.6. Dynamic Light Scattering Experimentation and Optical Density Characterization

In the characterization of vesicle size, PC (300 µM) and PS (300 µM) vesicles were evaluated. The hydrodynamic diameter (Dh) and Z-Potential of the vesicles were assessed by dynamic light scattering (DLS), employing a Zetasizer Nanoseries spectrophotometer (Malvern Instruments, Malvern, UK). All measurements were carried out at 25 °C using polystyrene disposable cells and folded capillary cells for the size and ζ potential measurements, respectively. Before their characterization, the samples were vortexed for 10 s and left to rest for 30 min at 25 °C. The results are the average of five measurements. In another batch of vesicles (PS), we completed the characterization by using a

Microtrac equipment. In a complementary way, we performed the optical density characterization of vesicles employing a BioRad Smart spectrophotometer with diode array (Hercules, CA, USA).

2.7. Peptide Bond Conformational Changes

Experiments were performed through the characterization of optical density at 218 nm, which is associated with conformational changes along the formation of β -sheet structures [8,10]. The effect of lipid vesicles composed of several lipids on conformational changes of hIAPP-derived peptides was evaluated. Measurements were obtained using the above-described BioRad Smart spectrophotometer, employing a peptide concentration of 60 $\mu\text{g}/\text{mL}$ and then evaluating the effect of the lipid vesicles.

2.8. Congo Red Birefringence Spectroscopy

Assays were performed based on a previous protocol [8], employing 10.6 μM Congo red and 60 $\mu\text{g}/\text{mL}$ peptides solutions. The optical density was measured at 494 nm, employing the above-described BioRad Smart spectrophotometer, under varying solution conditions.

2.9. ThT-Fluorescence Assay

β -sheet structures of peptides were characterized through the ThT-fluorescence assay. Samples were incubated for 12 h at 37 °C and monitored with the ThT (20 μM) treatment. Fluorescence emission spectra were registered at 25 °C from 460 to 610 nm with an excitation wavelength of 450 nm in a Cary Eclipse Fluorescence spectrophotometer (Agilent Technologies, Inc., Santa Clara, CA, USA).

2.10. Circular Dichroism (CD)

CD experiments were performed at a peptide concentration of 120 $\mu\text{g}/\text{mL}$ in a 1-mm path length quartz cuvette, using the CD neural network (CDNN) based software. Spectra were recorded with a 1-mm bandwidth, using 1 nm increments and 2.5 s accumulation time. CD spectra were recorded with an AVIV 62DS spectropolarimeter (AVIV Instruments, Lakewood, NJ, USA) at 25 °C employing far UV wavelengths (190–260 nm). CD results were reported as mean molar ellipticity ($\deg \text{cm}^2 \text{dmol}^{-1}$).

2.11. Lipid–Peptide Interactions

Lipid/peptide samples were analyzed with a nondenaturing electrophoresis technique adapted by our group for lipid–peptide characterization. We established a new methodology through the use of 0.8–15% native gradient gel electrophoresis [8]. Later, gels were stained following the Sudan black and silver nitrate protocols [8].

2.12. Molecular Dynamics

Peptide-membrane systems were generated with the CHARMM-GUI input generator. For all systems, a MARTINI force field for polarizable amino acids and water was used. In our assays, we used the peptides in a simple lipid bilayer system, each lipid bilayer consisting of a homogenous array of 8 × 8 lipid molecules of PS (DIPS 18:2–18:2) or PC (3:1, DPOC 16:1–18:1 and POPC 16:0–18:0). Peptide models of N-native, C-native, and variants F₂₃R and I₂₆A were generated using the ITASSER online server; for all peptides, we used the predicted model with highest TM value. The systems were minimized using steepest descent and conjugate gradient methods. Then, five equilibration steps were performed for each system. Simulations were conducted in a 1:1 peptide-membrane system during 3000 ns at 303.15 K and 1 atm pressure. For each system, we evaluated the lipid bilayer lateral displacement from lipids as an indicator of bilayer fluidity. Our analysis was based on the GROMACS built-in function for MSD analysis. To this end, we used the built-in functions of GROMACS, which are calculated using the following equation:

$$D_{At} = \frac{1}{6} \lim_{t \rightarrow \infty} \langle \| \mathbf{r}_i(t) - \mathbf{r}_i(0) \|^2 \rangle_{i \in a}$$

where $\mathbf{r}_i(t)$ indicates molecule position at time t , $\mathbf{r}_i(0)$ indicates the position at molecules at time zero, and is calculated for molecules included in A set of molecules. Additionally, $6D_A t$ represents diffusion coefficient over time (t) for A set of molecules, using Einstein correlation adjusted for long simulations.

In this sense, the analysis along the membrane was performed in one single plane. Before analysis of MSD, periodic boundary conditions were converted used built-in conversion functions to ensure the continuous trajectory of molecules.

In a complementary way, we performed molecular dynamics reruns, started from previously equilibrated systems that were used in original reported simulations. The systems were evaluated under the same conditions of temperature, pressure, and number of molecules. The simulation time was reduced to 30,000 ps; 100 consecutive simulations were performed for each system where the previous simulation was used as a starting point for the subsequent one. All trajectories obtained from short simulations were joined using built-in functions of GROMACS to reach the same simulation time reported previously; the resulting trajectory file was converted into a continuous trajectory file. MSD analysis for this system is reported in Figures S3 and S6. This strategy was based on previous reports [25,26].

2.13. Cell Culture

β -cell line RIN-m5F (American Type Culture Collection) was grown using RPMI-1640 culture medium supplemented with 10% fetal bovine serum, 10 U/mL penicillin, 10 μ g/mL streptomycin, and 25 μ g/mL amphotericin B. Cultures were maintained at 37 °C in a humidified atmosphere of 95% air and 5% CO₂.

2.14. Cell Viability Assay

Peptide cytotoxicity was assessed through MTT assays RIN-m5F cells, under different peptide and lipid-peptide treatments. Cells were seeded into 96-well plates at a density of 20,000 cells/well and allowed to grow to 90% of confluence. Next, the culture medium was replaced with Opti-MEM medium. After 1 h under this condition, cells were incubated under the different treatments and subsequently processed according to previous protocols [8].

2.15. Western Blotting Analysis

Under different peptide and PS-SUVs treatments, the expression of proteins associated with the UPR pathway and insulin folding were evaluated. After experimentation on RIN-m5F cells, proteins were extracted from cell cultures using ice-cold protein lysis buffer (150 mM NaCl, 10 mM Tris, pH 7.4, 1% Triton X-100, 0.5% NP40, 1 mM EDTA, 1 mM EGTA, 0.2 mM sodium orthovanadate, 10 mM benzamidine, 10 μ g/mL leupeptin, 10 μ g/mL aprotinin, and 250 μ M PMSF). An average of 25 μ g of protein lysates were separated on 8% SDS-PAGE electrophoresis and transferred to polyvinylidene difluoride (PVDF) membranes. The membranes were blocked with 5% nonfat milk in Tris-buffered saline 0.1% Tween-20 (TBS-T) for 1 h at 37 °C and incubated at 4 °C overnight with primary antibody (anti-XBP1s, anti-BiP/GRP78, anti-PDI, anti-SERCA2, and anti- β -actin). Following washing with TBS-T, the membranes were further incubated for 1.5 h at 37 °C with the corresponding horseradish peroxidase-conjugated secondary antibodies. Proteins were detected with the enhanced chemiluminescence reagent (Immobilon Western from Millipore, Burlington, MA, USA).

2.16. Endoplasmic Reticulum Isolation

ER fractions were obtained from RIN-m5F cells under several PS/peptides treatments. The methodology was based on the report of Prajapati et al. [27]. Cells were proliferated in 100 mm cell culture plates at a density of 2.3×10^5 cells/mL. Cells were maintained in proliferation for 72 h to reach 95% of confluence, and later, different treatments were performed on a volume of 5 mL. Later, culture cells were washed with PBS 1x, recovered, and treated with 1 mL of homogenizer buffer (30 mM Tris-HCl pH 7.4, 225 mM mannitol, 75 mM sucrose, 0.5 mM EGTA, protease inhibitor,

and 0.5% BSA). Homogenates were briefly sonicated (two cycles of 15 s on/30 s off at 9.5–10 W). Then, the homogenate was centrifuged at $630 \times g$ for 5 min at 4 °C. Supernatant was collected and conserved, and the pellet was newly processed by sonication and centrifuged under the same conditions. The combined supernatant was centrifuged again at $630 \times g$ for 5 min at 4 °C (nuclei-free lysate), and 150 µL was conserved. Then, the nuclei-free lysate fraction was centrifuged at $6300 \times g$ for 10 min. The supernatant was transferred into a new tube, and then, it was centrifuged at $20,000 \times g$ for 30 min at 4 °C. The supernatant was recovered and centrifuged at $100,000 \times g$ for 60 min at 4 °C, using a S140-AT 2555 rotor. The supernatant corresponds to the cytoplasm fraction, whereas the pellet corresponds to the ER fraction. Protein markers (anti-BiP, anti-PDI, anti-SERCA2, and anti-β-actin) were used to evaluate the quality of the isolations (Figure S9).

2.17. Fabrication of Vesicles Composed of PS (30 µM) and the Fluorescent Probe BODIPY-Leu (6 µM)

BODIPY-Leu probe was synthesized according to protocols developed by our group [22]. Then, the required quantities of L-α-phosphatidylserine and BODIPY-Leu were dissolved in chloroform and mixed vigorously to obtain a clear solution. Then, the solution was dried for 90 min under a gentle stream of N₂ with an additional incubation of 5 h at 30 °C in an Eppendorf Vacufuge concentrator, according to protocols established by our working group [9]. After drying, samples were hydrated in phosphate buffer pH 7.4 and processed through 4 cycles of freezing in liquid N₂ and thawing at 37 °C, and finally subjected to a sonication process (for 10 min under 15 s on/30 s off cycles at 9.5–10 W) in an ultrasonic homogenizer. Samples were stabilized for 1 h at 25 °C and centrifuged at 13,000 rpm for 10 min.

2.18. Confocal Microscopy

A LEICA TCS-SP8 confocal scanning biological microscope (LEICA Microsystems Heidelberg GmbH, Nussloch, Germany) was employed in the characterization of the subcellular localization of PS/BODIPY-Leu vesicles (PS 30 µM/BODIPY-Leu 6 µM). RIN-m5F cells were proliferated to 90% of confluence and treated with PS/BODIPY-Leu vesicles and hIAPP-derived peptides for 20 h. Later, culture cells were washed with HBSS buffer, and then, the ER-tracker probe (1 µM) was added and incubated for 25 min at 37 °C. Cells were washed once with HBSS buffer and fixed with 4% formaldehyde for 2 min at 37 °C and mounted for observation. Macroscopically different zones were recorded, preferentially at the center of the specimens, to depict representative images. Images were recorded at excitation/emission wavelengths of 488/495–545 and 552/562–700 nm for detection of PS 30 µM/BODIPY-Leu (green) and ER-tracker (red), respectively.

2.19. Insulin ELISA Assays

Cells were proliferated in 100 mm cell culture plates at a density of 2.3×10^5 cells/mL. Cells were maintained in proliferation for 72 h, and later, different treatments were performed on a volume of 5 mL. Cell culture medium was recovered and centrifuged for 5 min at 5000 rpm. The supernatant medium was recovered and diluted (1/3) in PBS. Insulin concentrations were quantified with the Rat Ultrasensitive Insulin ELISA kit (80-INSRTU-E01, E10; ALPCO Diagnostics, Salem, NH, USA) through several adaptations according to manufacturer's recommendations. Absorbance readings were performed at 450 nm, and results were reported as ng/mL.

2.20. Statistical Analysis

Data were expressed as mean ± SD. The statistical analyses were conducted with one-way ANOVA. In MTT assays data were expressed as mean ± SD.

3. Results

3.1. Secondary Structure Characterization of hIAPP Peptides

In a previous report, we proposed a panel of 113 hIAPP variants, 30 of which could reduce aggregation propensity with only one substitution on the hIAPP sequence [7], compared to the pramlintide drug (3 substitutions) and several hIAPP analogs generated by substituting up to four arginine residues at positions F₂₃-I₂₆ [28]. Our results suggested that the 23 and 26 positions maintain secondary structure stability [7]. To assess changes in these positions, F₂₃R and I₂₆A variants were evaluated and compared to the highly aggregative hIAPP C-native residues (²³FGAILSSTNVGSNTY³⁷). Through ThT-fluorescence assays, the F₂₃R variant showed the lowest fluorescence values corresponding to a reduced β -sheet structure formation compared with the C-native and the I₂₆A variant (Figure 2A). Most probably, the result found with F₂₃R is associated with the electrostatic charge of the arginine-side chain (position 23) that exerts a repulsive effect among peptide monomers.

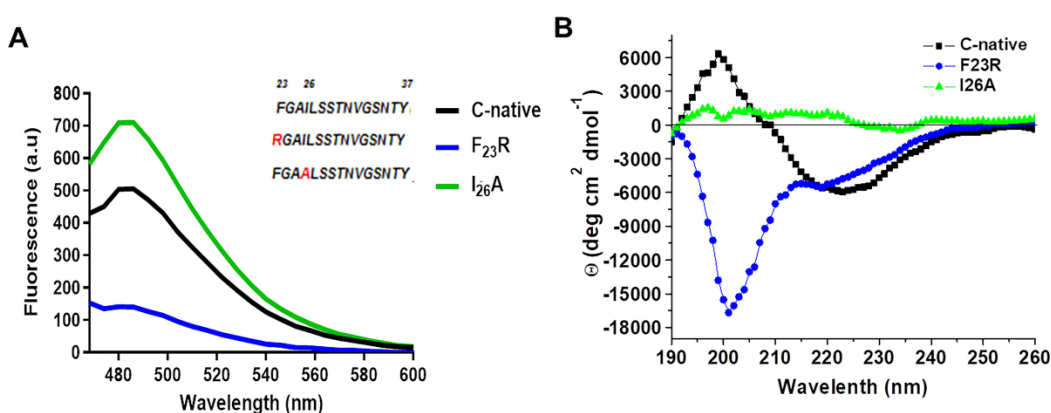


Figure 2. Structural characterization of C-terminal IAPP-derived peptides shows the inhibition of β -structures by the new F₂₃R variant. (A) Fluorescence emission spectra through ThT assays on IAPP variants (60 μ g/mL). The characteristic emission peak was registered at 482 nm. (B) Circular dichroism (CD) spectra of hIAPP variants (190–260 nm). In this representative experiment, the peptide concentration was 120 μ g/mL.

The substitution of only F₂₃R could reduce β -sheet structure formation. In the I₂₆A variant, as opposed to the expected, a slightly higher signal than in the C-native segment was detected (Figure 2A). Although aggregation propensity values (AGGRESCAN Index) for I₂₆A (-8.2) suggest a low tendency to generate β -structures, parameters such as hydrophobicity and isoelectric point are similar in both fragments (Table 1). Characterization of peptides was completed by CD analysis (Figure 2B), in which the C-native spectrum indicated a β -sheet structure formation. For the F₂₃R variant, a peak at 190 nm and two minima at 202 and 219 nm were registered, typical of a mixture of α -helix, disordered structures, and minimal β -sheet structures. I₂₆A showed an atypical behavior since the spectrum did not represent a defined secondary structure, possibly associated with amorphous aggregation.

Table 1. Physicochemical parameters of evaluated peptides.

ID	Sequence	AGGRESCAN Value ¹	Hydropathy (kcal/mol)	Charge pH 7.4	Hydrophobicity (kcal/mol)	pI	μ H kcal/mol
C-native	²³ FGAILSSTNGSNTY ³⁷	6.6	0.28	0	0.29	5.92	0.18
F ₂₃ R variant	²³ RGAILSSTNGSNTY ³⁷	-0.3	-0.21	1	0.21	9.84	0.04
I ₂₆ A variant	²³ FGAALSTSSTNGSNTY ³⁷	-8.2	0.1	0	0.24	5.92	0.13
N-native	¹ KCNTATCATQRLANFLVHSS ²⁰	-6.3	-0.04	3	-0.02	9.14	0.27

¹ Negative values are associated with a low propensity to form amyloid fibrils, whereas positive ones are associated with higher propensity. Red identifies the residue variants.

In amyloidogenic peptides, the stability of antiparallel β -sheet structures is determined by hydrogen bonds, salt bridges, and weak polar interactions among side chains of residues [29]. Under our working conditions, the net charge of +1 for the F₂₃R sequence at pH 7.4 could be a determining factor in the low propensity to aggregation, due to the likely appearance of electrostatic repulsions. In turn, I₂₆A and the C-native segment showed a neutral charge at a pH range of 3.0 to 8.5 with an intrinsic tendency to aggregation, a situation that has been discussed in several reports as a problem with the therapeutics of hIAPP [30]. Therefore, a balance among the dynamic secondary structure of the hIAPP C-native segment, the net charge, and the physicochemical properties of the lipid microenvironment could define the type of the adopted secondary structure [10].

3.2. Effect of Lipids on the Secondary Structure of hIAPP Peptides

The effect of lipids on the secondary structure of hIAPP peptides was characterized through the use of SUVs. In a first approach, PC-SUVs were employed as a model system and their effect on the C-native segment as well as the F₂₃R and I₂₆A variants was assessed through spectroscopy at 218 nm and birefringence with the Congo red assay (Figure 3). PC was chosen in the first instance since it is the most abundant zwitterionic phospholipid of the outer plasma membrane. Under incubation with increasing concentrations of PC-SUVs, the F₂₃R variant did not show significant changes in the β -sheet structure content where minimal absorbance values were recorded for peptide-bond characterization. In addition, an evident difference in birefringence values compared to the C-native segment was registered (Figure 3A,B). The behavior of the I₂₆A variant was comparable to the C-native segment suggesting β -sheet formation, a phenomenon associated with physicochemical parameters such as isoelectric point, hydrophobicity, and electrostatic charge (Table 1). Our data agree with the results of Cho et al., 2008, employing PC liposomes, wherein the aggregation effect of IAPP was evident [31]. By contrast, when assessing the effect of these PC SUVs on the N-native segment (¹KCNTATCATQRLANFLVHSS²⁰), β -structure formation was not found (Figure S1A–C), therefore, suggesting that structural transitions leading to β -sheet formation in hIAPP fundamentally occur on the C-native domain. Remarkably, this β -sheet structural transition exclusive to the C-native segment was likewise observed when working with PC-based large unilamellar vesicles (PC LUVs), also studied to extend the characterization of the effect of this lipid (Figure S2). While stored in β -cell granules at a pH near 5.5, the aggregation of hIAPP is inhibited; however, aggregation propensity increases when hIAPP is released into the extracellular compartment at pH 7.4 [32]. Taking into account that the effect of lipids was studied at pH 7.4, the induction of β -structures was evident on the C-native segment when incubated with PC vesicles, both SUVs and LUVs (Figure 3C,D). Interestingly, this phenomenon did not occur when the F23R variant was used (Figure 3E,F). Since several studies have reported that cholesterol (Chol) functions as a trigger factor of amyloid formation [33,34], unilamellar PC/Chol vesicles (prepared at a 3/2 molar ratio) were evaluated. Despite the increase of PC/Chol SUVs concentration (0–180 μ M), our data suggest that PC/Chol vesicles do not promote β -sheet formation on the F₂₃R variant (Figure 3G,H), whereas the I₂₆A variant shows the formation of β -sheet structures (Figure 3G,H).

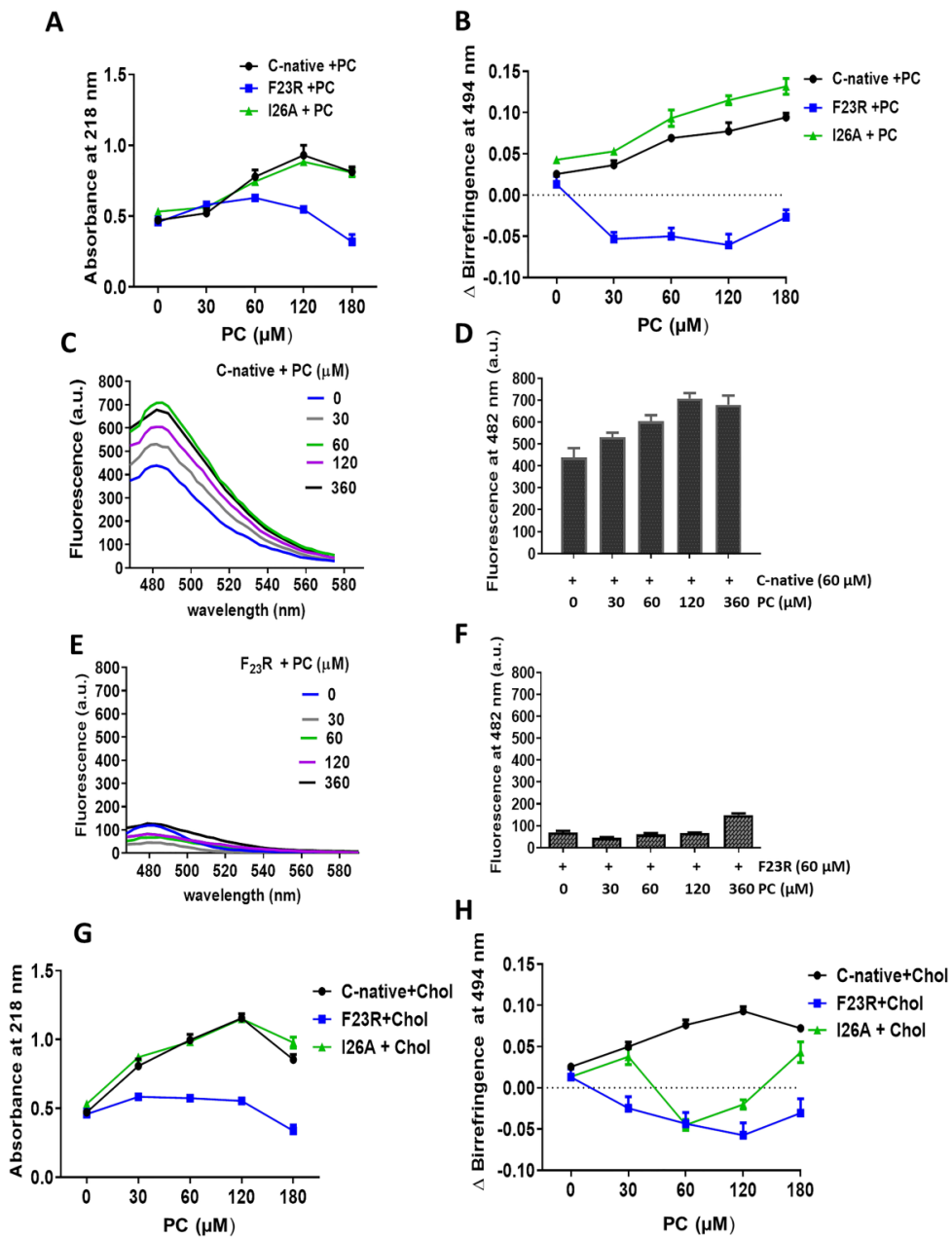


Figure 3. Effect of zwitterionic L- α -phosphatidylcholine-small unilamellar vesicles (PC-SUVs) on the secondary structure of IAPP-peptides. (A) Peptide bond absorbance of the C-native segment, F₂₃R, and I₂₆A under incubation with PC-SUVs. (B) Peptide characterization by birefringence with Congo red assay. (C) Interaction of the C-native segment under increasing concentrations of PC-vesicles evaluated by ThT assay. (D) Values of ThT-fluorescence emission at 482 nm. (E) Interaction between F₂₃R under increasing concentrations of PC. (F) Values of ThT-fluorescence emission at 482 nm. Characterization of the C-native segment, F₂₃R, and I₂₆A under the incubation of SUVs composed of PC and cholesterol (Chol) through peptide bond absorbance at 218 nm (G) and Congo red assay (H).

In a complementary way, we performed molecular dynamic simulations according to our experimental conditions using PC molecules. Simulations were conducted in the presence of modeled peptides (C-native segment, variants F₂₃R, I₂₆A, and N-native segment) and lipid bilayers with no peptides used as control. We ran simulations during 3000 ns in all systems, and the peptide molecule was situated at 30 Å from the top of the membrane. Although the three peptides derived from the hIAPP C-terminal domain (C-native, F₂₃R, and I₂₆A) adsorb at the membrane surface at less than

500 ns (Figure 4A–F), we found a slightly lower displacement for the C-native segment concerning the F₂₃R and I₂₆A during the evaluation of the displacement of phospholipids and peptide MSD (mean square deviation) on the z-axis, suggesting that interactions between C-native/lipids generate a movement restriction (Figure 4I). This phenomenon could be related to peptide interactions on the hydrophilic/hydrophobic interface of membranes. Moreover, to robust our experimental system and in order to discard false-positive bias, complementary MSD analysis (Figure S3) was performed through 100 consecutive short simulations (30 ns) for each system. According to the obtained results, the displacement of phospholipids and peptides derived from IAPP on the z-axis, follows the same behavior described in Figure 4I (Figure S3).

Several reports indicate that the region that initially interacts with cell membranes is the N-terminal of hIAPP [35]; our simulations suggest that the adsorption phenomenon of the N-native segment at the lipid interface (Figure 4G,H) presents an even greater restriction of movement with respect to peptides derived from the C-domain segment (Figure 4I).

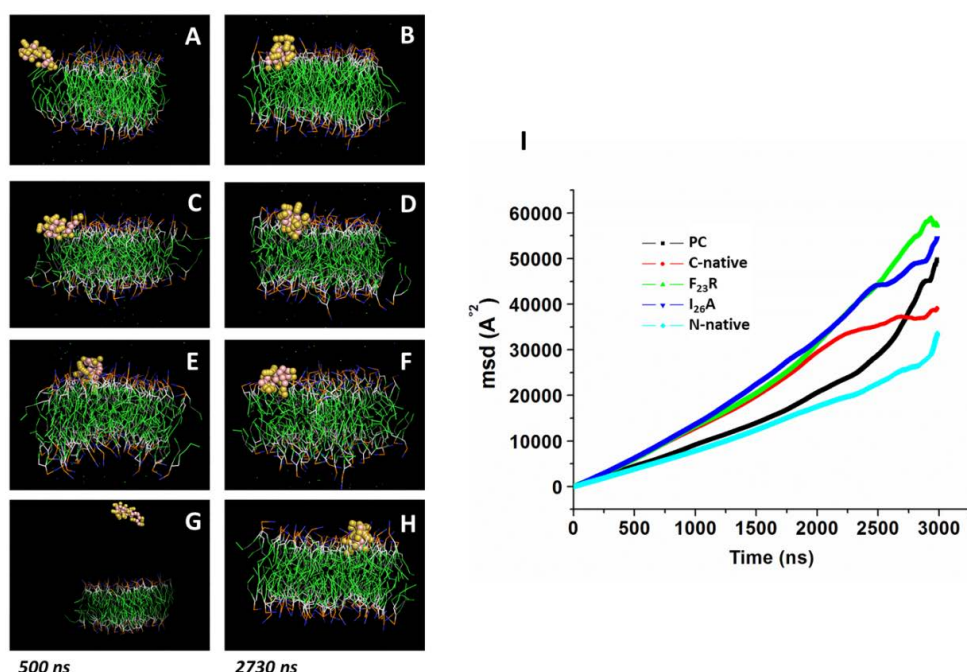


Figure 4. Displacement of peptides derived from IAPP on the z-axis of PC-bilayers (mean square deviation, MSD). Representative snapshots of PC bilayers associated with the C-native fragment of IAPP at 500 ns (A) and 2730 ns (B), F₂₃R (C,D), I₂₆A (E,F), and the N-native fragment (G,H). (I) Behavior of mean square deviation (Å^2) through a 3000 ns simulation employing coarse grain methodology.

3.3. Structure Modulation Dependent on Negative Electrostatic Surface in hIAPP Peptides

Insulin secretory granules are derived from the ER membrane, contain high levels of PS and phosphatidylinositol in comparison to the plasmatic membrane [16], and show an important dynamic behavior [17]. Therefore, in order to evaluate the impact of anionic electrostatic charge, PS and POPG vesicles were evaluated (Figure 5). In a first assay, our results suggest a modulation by PS-SUVs on the C-native segment, wherein a significant increase in ThT-fluorescence values dependent on PS concentration was identified (Figure 5A,B). The F₂₃R variant showed the same β -sheet formation from the lowest PS concentration (30 μM) (Figure 5C,D), a result that contrasts with the effect found when zwitterionic PC and PC/Chol vesicles are used. In complementary experimentation, the same tendency was registered through peptide bond spectrophotometry and Congo red assays (Figure 5E,F). Results confirm the propensity of the F₂₃R variant to show β -sheet transitions induced by PS-SUVs, supporting the fact that the fibrillation process begins when monomers change to oligomers and that, in general, the formation of mature fibrils follow a sigmoidal behavior [36].

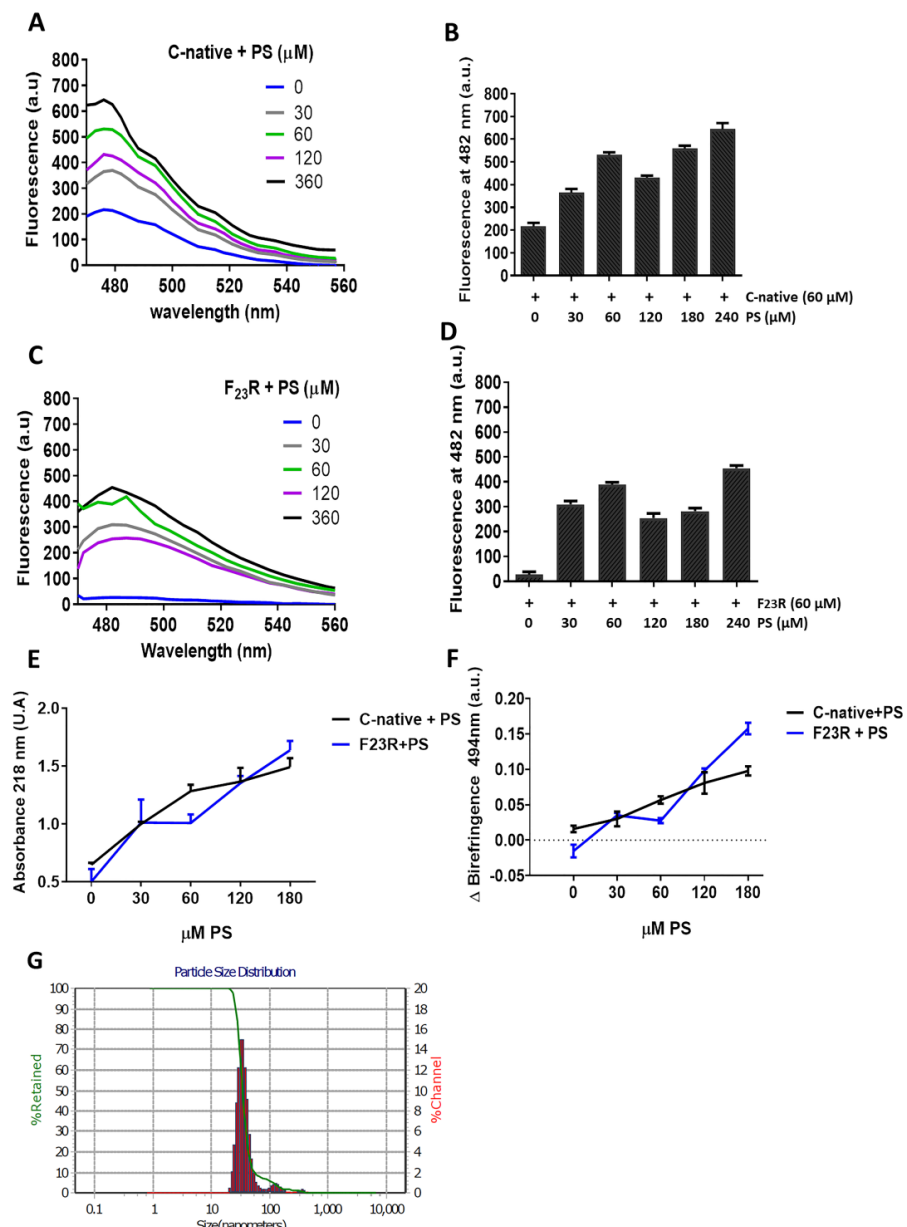


Figure 5. PS-SUVs promote the formation of β -sheet structures on the C-terminal-derived peptides of IAPP. (A) Interaction of the C-native segment at increasing concentrations of PS evaluated by ThT-fluorescence assays. (B) Same experimentation as in A, ThT-fluorescence at 482 nm. (C) Fluorescence emission spectra obtained through ThT assays on the F₂₃R variant under increasing concentrations of PS. (D) Same experimentation as in (C), ThT-fluorescence at 482 nm. (E) Evaluation of the PS-effect on the secondary structure of peptides through peptide-bond absorbance at 218 nm, and by Congo red birefringence at 494 nm (F). (G) Dispersion of the size of PS-SUVs used in this experimentation by DLS.

Moreover, although we registered the effect of PS-SUVs on β -sheet conformational transitions in hIAPP-derived peptides, we performed several efforts to obtain a homogenate LUV-preparation, however, considering the intrinsic PS-property to form SUVs, we designed a protocol based in freezing/thawing and a slightly sonication process (Materials and Methods). Then, we obtained a mixture of SUVs and LUVs. Results suggest the presence of the same β -sheet transitions registered in the C-native and F₂₃R variant under treatment with SUVs/LUVs mixtures (Figure S4).

To perform an approximation to the nucleation phenomenon of hIAPP-derived peptides at a 1/2 peptide/PS ratio, peptide bond conformation was monitored along with time (Figure 6A).

Data suggest that the incubation with PS-SUVs triggers a conformational transition to β -sheet formation, shortening the lag phase [37,38]. Variant F₂₃R shows the same tendency under the interaction with anionic PS-vesicles (Figure 6B). Complementary results obtained through CD confirmed the same phenomenon with the C-native segment and the F₂₃R variant (Figure 6D,E). Once the lag phase is surpassed, the oligomeric structures establish interchain electrostatic interactions to evolve into more ordered structures and amyloid fibrils [36]. In this case, this phenomenon was critical for the F₂₃R variant, showing an eightfold increase in the CD signal at 222 nm, corresponding to the formation of β -sheet structures. In this sense, arginine and cationic residues have been described to interact with PS membranes due to high affinity of the side chains for anionic lipids [39]. These β -sheet transitions were not evident in the N-domain segment despite of positive charge content (Figure 6C) at neutral pH (Table 1); however, according to CD spectra, this interaction facilitates α -helix formation (Figure 6F). Furthermore, the structural transitions promoted by PS (Figure 6A,B) were not evidenced when vesicles composed of phosphatidyl-ethanolamine in both the C-native and N-native segments were evaluated (Figure S5). Then, the cationic lipid surface is not a critical factor for β -sheet aggregation on hIAPP segments.

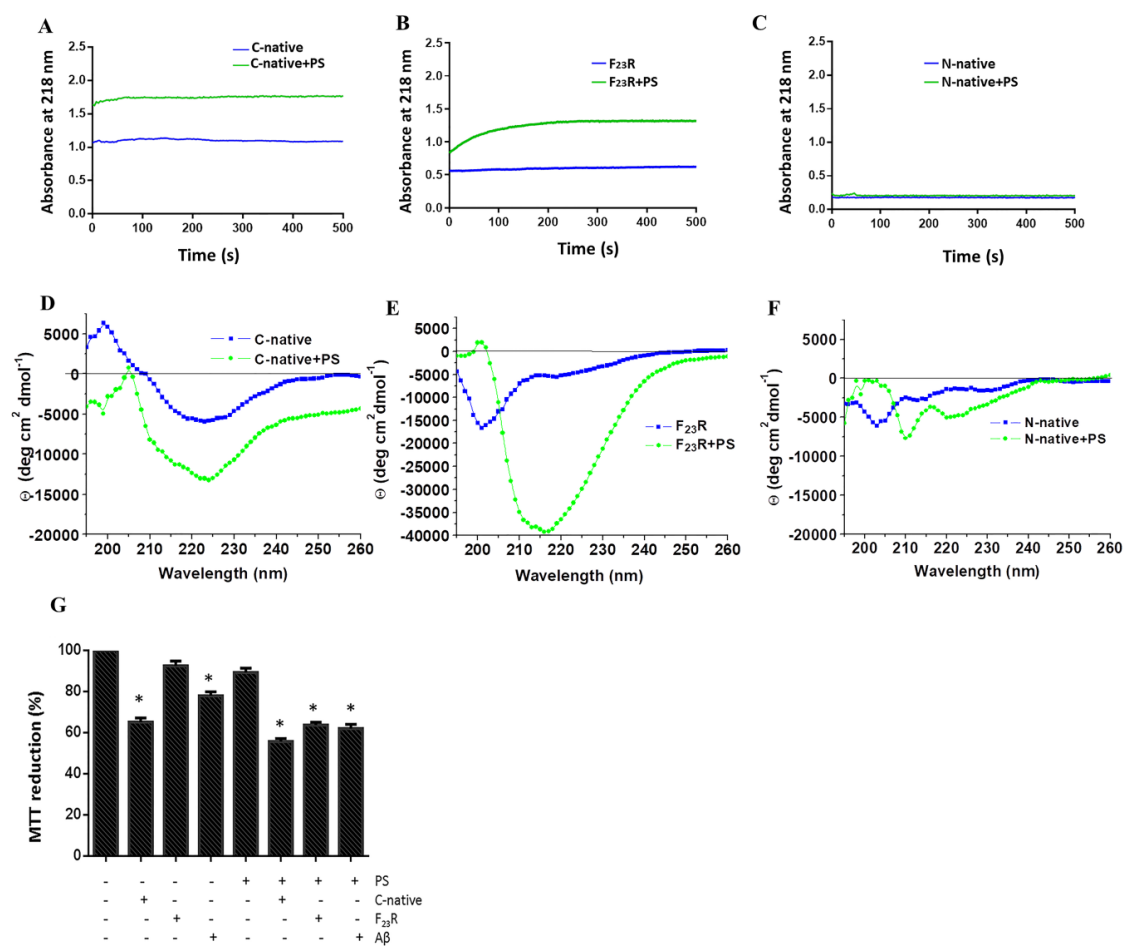


Figure 6. The anionic lipid surface as the critical factor for β -sheet aggregation on C-terminal peptides. Effect of PS on nucleation of the C-native segment (**A**), F₂₃R variant (**B**), and the N-native segment (**C**). Same experimentation as in **A**, **B**, and **C**, the effect of PS on the secondary structure of the C-native segment (**D**), F₂₃R variant (**E**), and N-native segment (**F**), evaluated by CD. (**G**) Cell viability evaluation on RIN-m5F cells treated under different stimuli of peptides/PS vesicles (7.5/15 μ M). Data are expressed as mean \pm SD ($n = 6$) * $p < 0.005$.

Strikingly, on the other hand, variants F₂₃R and I₂₆A showed aggregation upon their interaction with the anionic lipid system (PS), as evidenced by CD spectra (Figure 6E). These results appear to be contradictory considering the AGGRESCAN values (Na4vSS), −5.3 for F₂₃R and −8.2 for I₂₆A (Table 1), which predict that the formation of β -structures should be inhibited, in association with reports suggesting that membranes of β -cells are composed of anionic lipids (2.5–13%) [40]. Taking into account this rather unexpected outcome, cell viability assays were performed in a model of Langerhans islet β -cells (RIN-m5F cells) to assess the effect of peptide/PS vesicles mixtures at the cellular level. Results pointed out that F₂₃R/PS mixtures decreased cell viability compared to controls. Likewise, when the anionic vesicles are present, the C-native segment and the F₂₃R fragment showed cytotoxicity properties (Figure 6G). In this experimental design, the A β peptide was used as a control.

As a complementary test, we performed dynamic simulations of IAPP-derived peptides in the presence of a preassembled PS bilayer during 3000 ns, wherein the peptide molecule was situated at 30 Å above the top of the membrane in all systems (Figure 7). In the evaluation of the displacement of the interacting species (PS and peptides), we found a considerable diminution in MSD for the F₂₃R variant with respect to the C-terminal segment and I₂₆A (Figure 7A), which is possibly associated with an electrostatic factor. Indeed, in the analysis of the trend line, the F₂₃R slope showed the lowest value compared to results obtained with other peptides (data not showed). In the same way that of the PC system, a complementary MSD analysis through 100 consecutive short simulations (30 ns) for each PS-system was performed, and results obtained from these short simulations follow the same tendency (Figure S6). Moreover, A β -peptide was incorporated as a control. Importantly, through the simulation time, the collapse of the simulations was not registered. Thus, interactions between the F₂₃R and lipids generate a restriction in movement modifying the lipid packing and show the F₂₃R peptide situated deeper within the lipid bilayer (Figure 7D,E). According to our CD experimentation, this is possibly a critical condition for the propensity modulation towards the formation of β -sheet structures.

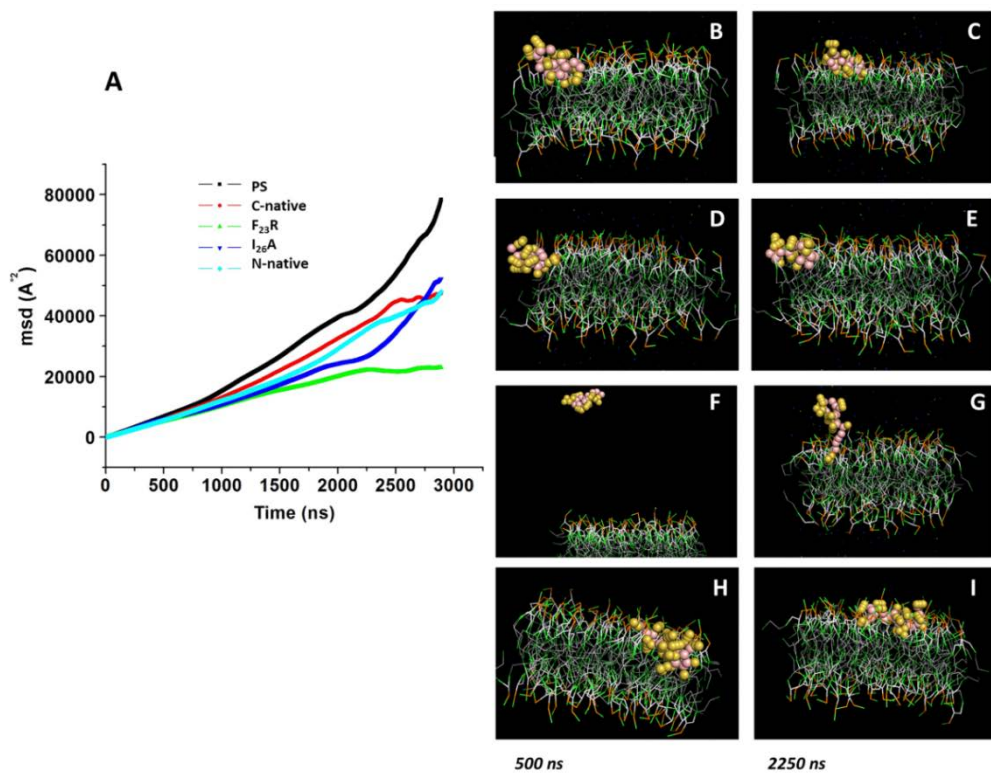


Figure 7. Displacement of peptides derived from the IAPP C-terminal on the z-axis of PS-bilayer. (A) MDS values on PS bilayer under the incubation of peptides-derived of IAPP through 3000 ns of simulation. Representative snapshots of the PS model with the C-native segment at 500 ns (**B**) and 2250 ns (**C**). Snapshots of F₂₃R (**D,E**), I₂₆A (**F,G**), and the N-native segment (**H,I**) under the same conditions.

To determine whether the PS anionic environment is the factor that leads to the formation of β -structures, other anionic lipid vesicles were evaluated. To this end, vesicles of PC and anionic-POPG were prepared at a 3 to 1 molar ratio, for which, the characterization of the peptide bond at 218 nm showed for the C-native segment, F₂₃R, and I₂₆A variants, an increase in peptide bond absorbance, demonstrating a phosphatidyl-glycerol (POPG)-modulation dependent response (Figure S7A). In the same way, the three fragments, C-native segment, F₂₃R, and I₂₆A, incubated with POPG enhanced cytotoxicity on β -cells (Figure S7B). Likewise, a control with A β -peptide was included. To extend this characterization using peptide-bond spectroscopy, anionic SUVs were evaluated by increasing the molar concentration of POPG (0–100%). A strong modulation of POPG on the β -structure of the C-native fragment and both F₂₃R and I₂₆A was observed (Figure S7C). Therefore, it seems that anionic electrostatic charges prove to play an important role in amyloidogenesis, as further demonstrated by the evaluation of a representative A β -peptide (Figure S7C).

Although the structure of IAPP could change according to the physicochemical properties of lipids [7], in an attempt to characterize the role of lipid surfaces on the conformational transitions of β -sheets, we evaluated the influence of solvation determined by the presence of a free hydroxyl group in position 2 of phospholipid heads. Our results indicate that treatment with lysophosphatidic acid (LPA) micelles under a neutral pH promotes conformational transitions towards β -sheet structures only in the C-native segment and F₂₃R variant (Figure S8). For the case of the N-native segment, a spectrum corresponding to an α -helix signal was registered, reflecting the avoidance of β -sheet structure formation. These results appear to confirm that β -structure modulation is localized at the C-native domain of IAPP (Figure S8). Results that are in concordance with the proposal that amyloidogenicity and cytotoxicity are induced by two different regions of the hIAPP sequence [41]. Likewise, these findings are in agreement with previous results from our laboratory where we described that incubation with LPA promotes conformational transitions in the C-terminal domain of cholesteryl ester transfer protein (CETP) [10].

4. Discussion

During the course of the present investigation, employing a biomimetic approach, we have been able to develop and evaluate new variants of IAPP with the property to show fewer propensities to form β -sheet structures. New sequences such as F₂₃R have shown to increase the stability of the C-native segment of IAPP, with an important involvement of the anionic nature lipids. This behavior can be associated at pH 7.4 with charged lipids that contributed to structural changes towards the β -sheet formation, whereas the I₂₆A variant shows a neutral charge and an isoelectric point similar to the C-native segment, promoting a strong interaction with anionic phospholipids. Molecular dynamics showing an absorption phenomenon of F₂₃R at the surface of lipid bilayer indicate the possibility for the formation of peptide-PS aggregates that, by means of lipotoxicity, could have contributed to the observed cytotoxicity (Figure 6G). Further experiments are nowadays in progress in our laboratories to confirm this assumption (data to be published).

The content of anionic phospholipids in β -cell membranes is reported to range from 2.5% to 13.2%, a proportion mainly situated in the inner leaflet of the membrane [38], proportion much similar as found in insulin secretory granules where a higher content of PS and phosphatidylinositol has been described [17,42], which are derived from ER membranes during insulin maturation. This contributes to the possibility that hIAPP aggregation could be increased at the intracellular space, especially during the process of maturation of insulin secretory granules. The phenomenon of membrane asymmetry that could enhance hIAPP amyloid formation and membrane damage *in vivo* [43] could modify the PS-biodisponibility and, therefore, triggers the β -sheets formation.

Therefore, considering the critical role of PS in the promotion of β -sheet conformational transitions on hIAPP-derived peptides, the impact of phospholipid negative-electrostatic charge on UPR regulation was characterized. In this sense, PS-SUVs with the hIAPP-derived peptides under a 1 to 2 peptide/PS ratio were incubated on β -cell cultures for 20 h. In the first case, critical UPR-targets were evaluated

under the peptide/PS treatments in complete cellular lysates (Figure 8A) results suggest the slight activation of XBPIs, a transcription factor of the activation of IRE1-arm of UPR. Likewise, an increase in the expression of chaperone BiP under peptides/PS treatments was registered, and this phenomenon was more evident under the C-native treatment. Possibly, these modifications could be partly related to a cellular compensatory response aimed to maintain protein homeostasis in ER (Figure 8A), as well as critical functions in the physiology of β -cells. Importantly, when insulin concentrations were evaluated in extracellular media, we found a diminution of the insulin levels upon treatment with the peptide/PS mixtures (Figure 8B).

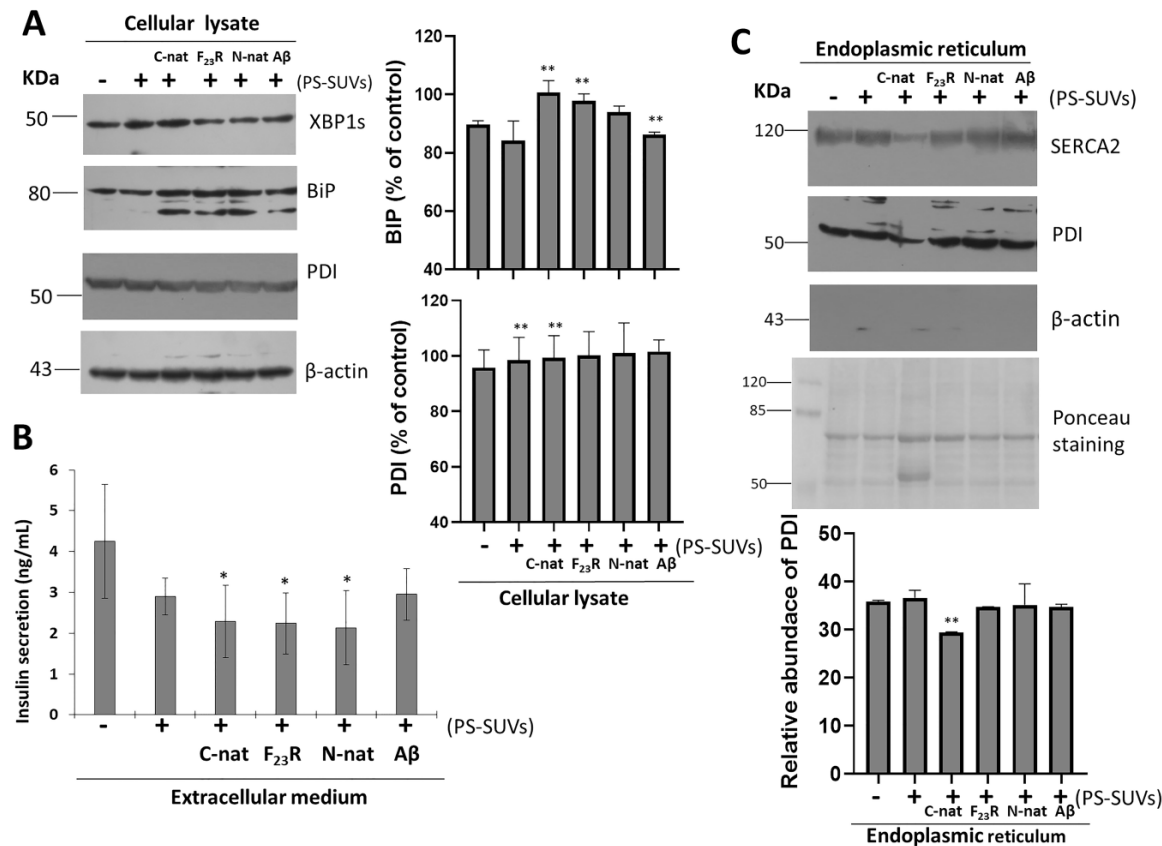


Figure 8. Unfolded protein response is activated under the treatment of hIAPP-derived peptides/PS vesicles mixtures. (A) Effect of hIAPP-derived peptides/PS on the expression of XBP1s and binding immunoglobulin protein (BiP) targets of unfolded protein response (UPR), as well as protein disulfide isomerase (PDI) expression on complete cell lysates. Densitometry analysis of (BiP) and PDI immunoblots, results are reported as means \pm SD and expressed as % of control, ** $p < 0.05$. $A\beta$ -peptide was used as a control. β -actin was used as a loading control. (B) Insulin concentrations (ng/mL) in extracellular media, * $p < 0.1$. (C) Under the same experimental conditions, the ER was purified and the expression of sarco/endoplasmic reticulum Ca^{2+} -ATPase-2 (SERCA2), PDI, and β -actin were characterized. Polyvinylidene difluoride (PVDF) membranes were stained with Ponceau. Densitometry analysis of PDI immunoblots; results are reported as means \pm SD and expressed as relative abundance; ** $p < 0.05$.

PDI is a chaperone that regulates folding of proinsulin, participates in disulfide bond formation, and maintains ER redox homeostasis [44]. In our conditions, when total β -cell lysates were evaluated under peptide/PS treatments, we did not find changes in PDI expression (Figure 8A). Constituting a chaperone-protein with critical functions, high expression levels of PDI have been found in the ER lumen, to a lower extend in the cytosol, and also in different cellular membranes. [45]. In addition,

we have also detected PDI in the extracellular medium of β -cells treated with peptide/PS mixtures (data not shown). However, more experimental evidence is required to establish a mechanistic proposal.

To dissect the role of PDI, we performed the isolation of ER of β -cells cultures, evaluating sarco/endoplasmic reticulum Ca^{2+} -ATPase-2 (SERCA2) and β -actin as controls of ER isolations. Results indicated the isolation of pure ER-fractions (Figure S9). Then, under the same treatments of hIAPP-peptides/PS-SUVs, we characterized the expression of PDI. We found that the PDI levels diminished upon treatment with C-native/PS, as well as the levels of SERCA2 resident of ER (Figure 8C). Results suggest that the affection of SERCA2 and PDI under C-native/PS treatment might be related to both their ER localization and the activation of UPR, affecting insulin secretion.

ER-lumen and the function of chaperones BiP and PDI are critical during proinsulin folding. Considering our results, and in an attempt to characterize the effect of the PS vesicles and possibly trace their cellular localization, confocal microscopy experiments were carried out. To this end, we prepared PS and peptide/PS vesicles ($30 \mu\text{M}$) tagged with the green fluorescent probe BODIPY-Leu [46] ($6 \mu\text{M}$) (referred to as BODIPY-Leu/PS and BODIPY-Leu/peptides/PS vesicles, respectively), with which RIN-m5F cells were treated. In the first instance, our results demonstrated that BODIPY-Leu/PS vesicles are internalized in RIN-m5F cells (Figure 9A–C, stained in green). Then, we used ER-tracker (red staining) for characterize the colocalizing in ER sites (Figure 9D–I). Results suggest that the system is located in the ER. Importantly, when we evaluated the localization of the BODIPY-Leu/PS vesicles incubated with hIAPP-derived peptides (C-native and F₂₃R variant) under a molar relationship (1/2; peptide/vesicle), the BODIPY-Leu/PS signal was localized under C-native treatment in ER sites (Figure 9J–L), however, the signal diminished slightly under F₂₃R treatment (Figure 9M–O). In an important way, C-native/PS treatment promoted the higher levels of cytotoxicity in the studied cells (Figure 6G), affecting insulin secretion (Figure 8B). Moreover, these phenomena coincide with UPR activation and affection of localization of PDI and SERCA2 in the ER (Figure 8C). Therefore, it appears that the localization of peptide/PS is a critical condition to induce the alterations in homeostasis of the ER. This phenomenon was evidenced after treatment with the C-native/PS system, whereupon the higher fluorescence signal of the BODIPY-Leu/PS vesicles along the ER very likely corresponds with the alterations in localization of PDI, SERCA2, and the insulin secretion. This phenomenon was not evident upon treatment with the F₂₃R variant.

Therefore, our results suggest that the lipid-anionic electrostatic charge is a critical condition that could modulate the UPR pathway and the conformational transition of IAPP-derived peptides. Thus, a negative electrostatic-charge environment could be critical in insulin secretion as well. Interestingly, the content of anionic lipids of β -cells and insulin secretory granules has been related to an altered glucose-stimulated insulin exocytosis [17,43]. Therefore, a condition of metabolic overload also has been associated with the biodisponibility of fatty acids [22], very likely contributing to the deleterious phenomenon correlated with the concentration of anionic phospholipids, promoting misfolded transitions on hIAPP. Having in mind this phenomenon, our group has generated new materials of polymeric films of polyvinyl dimethylazlactone (PVDMA) and polyethylene imine (PEI) to evaluate the effect of fatty acids on β -cell membranes [47] and diverse critical physiological functions.

In a complementary way, current results of our laboratory suggest that the induction of oligomers at the C-native domain of IAPP accelerates β -sheet formation when treated with oleic acid/PC vesicles. By contrast, when palmitic acid/PC vesicles are used, this result is not found (data not shown). Then, considering that unsaturation and shorter fatty acids of phospholipids facilitate the curvature and fluidity of membranes favoring their fusion [17], although increasing the risk of aggregation, there is a subtle regulation in the conservation of the structure of the hIAPP. Moreover, a report reveals synergic implications of free fatty acids and hIAPP in ER stress and apoptosis of islet β -cells [48]. In this context, we have documented the role of metabolic overload by saturated fatty acids on proteostasis and its impact on insulin secretion, specifically the dysregulation of targets that control intracellular calcium homeostasis [22], as also documented in this report for SERCA2.

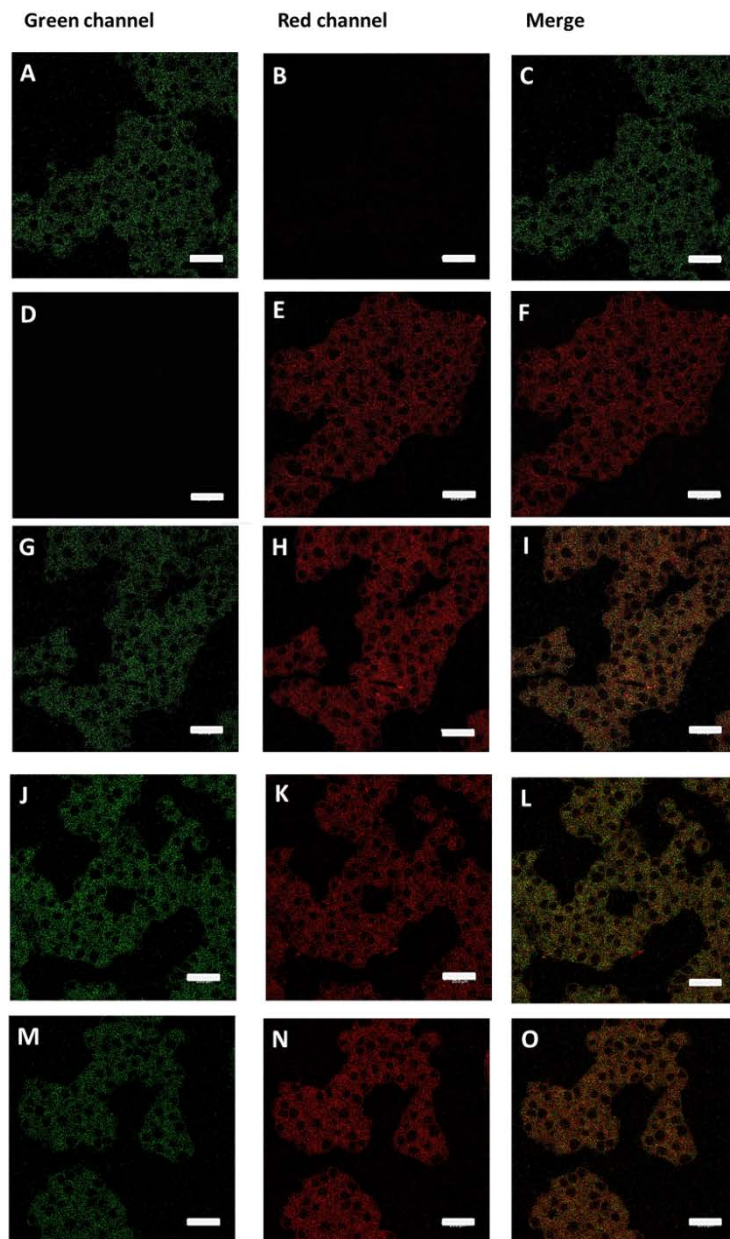


Figure 9. BODIPY-Leu/PS vesicles (green) colocalize with ER-tracker (red). (A–C) Langerhans islet β -cells (RIN-m5F cells) treated with BODIPY-Leu/PS vesicles. (D–F) Cells treated with ER-tracker. (G–I) Cells treated jointly with BODIPY-Leu/PS vesicles and ER-tracker. (J–L) Effect of C-native treatment on localization of BODIPY-Leu/PS vesicles and ER-tracker. (M–O) Effect of F₂₃R peptide treatment on localization of BODIPY-Leu/PS vesicles and ER-tracker. Scale bars correspond to 25 μ m.

Recently, following peptidomimetic design strategies, research has been developed to find a way to inhibit the formation of β -sheet structures in segments of an important series of polypeptides and proteins as a therapeutic way to fight amyloid disease. There is still a field of action in amyloidogenesis design. Although prolines residues in rIAPP promote disordered structures, results of coincubation of rIAPP and hIAPP suggest that rat amylin does not block β -sheet and also forms its own β -sheet, most probably on the outside of the human fibrils [49], revealing the complex behavior in the development of an amyloid fibril inhibitor. We and other authors have documented that it is critical to consider the impact of lipid environment. In the light of our results, the F₂₃R variant of IAPP showed a low propensity to form β -sheet structures even under the effect of zwitterionic lipids. However, anionic charge of lipid vesicles and degree of solvation were factors for the modulation of β -sheet formation of

the F₂₃R and I₂₆A variants, as well as in the C-native segment of IAPP, all associated to the cytotoxicity phenomena of β -cells. In conclusion, our results show the potential implications of modulating the structure and stability of IAPP for the design of analog therapeutics based on peptides and proteins.

Supplementary Materials: The following are available online at <http://www.mdpi.com/2218-273X/10/9/1201/s1>, Figure S1. Incubation with SUVs composed of phosphatidylcholine does not induce conformational transitions on the N-native segment (¹KCNTATCATQRLANFLVHSS²⁰) of hIAPP. Figure S2. Effect of PC-LUVs on the secondary structure of peptides derived from hIAPP. Figure S3. Displacement of peptides on the z-axis of PC-bilayers (MSD) obtained by short simulations. Figure S4. Mixtures of LUVs/SUVs composed of PS facilitate the formation of β -sheet structures. Figure S5. The cationic lipid surface is not a critical factor for β -sheet aggregation on hIAPP segments. Figure S6. Displacement of peptides on the z-axis of PS-bilayers (MSD) obtained by short simulations. Figure S7. Effect of SUVs composed of 1-palmitoyl-2-oleoyl-sn-glycerol (POPG) on the structure of IAPP variants. Figure S8. Effect of lysophosphatidic acid incubation on the secondary structure of C-native (A), F₂₃R variant (B), and N-native (C). Figure S9. Characterization of several fractions obtained during endoplasmic reticulum (ER) isolation.

Author Contributions: I.M.-N., A.P.-C., and V.G.-G., conceived and designed the experiments; I.M.-N., A.P.-C., I.L.-R., E.R.-V., M.A.-M., and J.M.-O., performed experiments; I.M.-N., A.P.-C., J.M.-O., I.L.-R., R.D.-M., and V.G.-G., analyzed data; J.M.-O., M.A.R.-I., I.A.R., and V.G.-G., contributed reagents/materials/analysis tools; A.P.C. and V.G.-G., wrote the paper. All authors have read and agreed to the published version of the manuscript.

Funding: This research was funded by the Coordinación de Posgrado e Investigación-UABC grant 106/2/N/57/1 (1983), Fondo Sectorial de Investigación para la Educación CB 2017-2018 (A1-S-28653/SEP/CONACYT), and 21a. Convocatoria Interna de Apoyo a Proyectos de Investigación (Coordinación General de Investigación y Posgrado/UABC). We thank DGTIC-UNAM for granting access to the supercomputing cluster MIZTLI (project: LANCAD-UNAM-DGTIC-352 granted to JM-O).

Acknowledgments: Authors thank Blanca Delgado-Coello for expert technical assistance and the administrative support of Josue Villegas-Sandoval and Mónica López-Valladares. Authors thank Ernesto Beltran-Partida and Benjamin Valdes-Salas for participation in DLS experimentation. Authors thank Santa Cruz Biotechnology for the donation of anti-SERCA2. M.A.-M. thanks funding from CONACyT (Mexico) through Research Projects INFR-2015-251863 and PDCPN-2015-89.

Conflicts of Interest: The authors declare no conflict of interest.

References

1. Koda, J.E.; Fineman, M.; Rink, T.J.; Dailey, G.E.; Muchmore, D.B.; Linarelli, L.G. Amylin concentrations and glucose control. *Lancet* **1992**, *339*, 1179–1180. [[CrossRef](#)]
2. Percy, A.J.; Trainor, D.A.; Rittenhouse, J.; Phelps, J.; Koda, J.E. Development of sensitive immunoassays to detect amylin and amylin-like peptides in unextracted plasma. *Clin. Chem.* **1996**, *42*, 576–585. [[CrossRef](#)] [[PubMed](#)]
3. Novials, A.; Sarri, Y.; Casamitjana, R.; Rivera, F.; Gomis, R. Regulation of islet amyloid polypeptide in human pancreatic islets. *Diabetes* **1993**, *42*, 1514–1519. [[CrossRef](#)] [[PubMed](#)]
4. Xu, W.; Jiang, P.; Mu, Y. Conformation preorganization: Effects of S20G mutation on the structure of human islet amyloid polypeptide segment. *J. Phys. Chem. B* **2009**, *113*, 7308–7314. [[CrossRef](#)] [[PubMed](#)]
5. Poa, N.R.; Cooper, G.J.; Edgar, P.F. Amylin gene promoter mutations predispose to Type 2 diabetes in New Zealand Maori. *Diabetologia* **2003**, *46*, 574–578. [[CrossRef](#)] [[PubMed](#)]
6. Berhanu, W.M.; Hansmann, U.H. Inter-species cross-seeding: Stability and assembly of rat-human amylin aggregates. *PLoS ONE* **2014**, *9*, e97051. [[CrossRef](#)]
7. Pulido-Capiz, A.; Diaz-Molina, R.; Martinez-Navarro, I.; Guevara-Olaya, L.A.; Casanueva-Perez, E.; Mas-Oliva, J.; Rivero, I.A.; Garcia-Gonzalez, V. Modulation of Amyloidogenesis Controlled by the C-Terminal Domain of Islet Amyloid Polypeptide Shows New Functions on Hepatocyte Cholesterol Metabolism. *Front. Endocrinol.* **2018**, *9*, 331. [[CrossRef](#)]
8. Garcia-Gonzalez, V.; Gutierrez-Quintanar, N.; Mas-Oliva, J. The C-terminal Domain Supports a Novel Function for CETPI as a New Plasma Lipopolysaccharide-Binding Protein. *Sci. Rep.* **2015**, *5*, 16091. [[CrossRef](#)]
9. Garcia-Gonzalez, V.; Gutierrez-Quintanar, N.; Mendoza-Espinosa, P.; Brocos, P.; Pineiro, A.; Mas-Oliva, J. Key structural arrangements at the C-terminus domain of CETP suggest a potential mechanism for lipid-transfer activity. *J. Struct. Biol.* **2014**, *186*, 19–27. [[CrossRef](#)]

10. Garcia-Gonzalez, V.; Mas-Oliva, J. Amyloid fibril formation of peptides derived from the C-terminus of CETP modulated by lipids. *Biochem. Biophys. Res. Commun.* **2013**, *434*, 54–59. [[CrossRef](#)]
11. Diaz-Villanueva, J.F.; Diaz-Molina, R.; Garcia-Gonzalez, V. Protein Folding and Mechanisms of Proteostasis. *Int. J. Mol. Sci.* **2015**, *16*, 17193–17230. [[CrossRef](#)] [[PubMed](#)]
12. Garcia-Gonzalez, V.; Mas-Oliva, J. Amyloidogenic properties of a D/N mutated 12 amino acid fragment of the C-terminal domain of the Cholesteryl-Ester Transfer Protein (CETP). *Int. J. Mol. Sci.* **2011**, *12*, 2019–2035. [[CrossRef](#)] [[PubMed](#)]
13. Mendoza-Espinosa, P.; Garcia-Gonzalez, V.; Moreno, A.; Castillo, R.; Mas-Oliva, J. Disorder-to-order conformational transitions in protein structure and its relationship to disease. *Mol. Cell. Biochem.* **2009**, *330*, 105–120. [[CrossRef](#)] [[PubMed](#)]
14. Knight, J.D.; Hebda, J.A.; Miranker, A.D. Conserved and cooperative assembly of membrane-bound alpha-helical states of islet amyloid polypeptide. *Biochemistry* **2006**, *45*, 9496–9508. [[CrossRef](#)]
15. Jayasinghe, S.A.; Langen, R. Lipid membranes modulate the structure of islet amyloid polypeptide. *Biochemistry* **2005**, *44*, 12113–12119. [[CrossRef](#)]
16. Suckale, J.; Solimena, M. The insulin secretory granule as a signaling hub. *Trends Endocrinol. Metab.* **2010**, *21*, 599–609. [[CrossRef](#)]
17. MacDonald, M.J.; Ade, L.; Ntambi, J.M.; Ansari, I.U.; Stoker, S.W. Characterization of phospholipids in insulin secretory granules and mitochondria in pancreatic beta cells and their changes with glucose stimulation. *J. Biol. Chem.* **2015**, *290*, 11075–11092. [[CrossRef](#)]
18. Saito Michiko, S.Y. ER Stress, Secretory Granule Biogenesis, and Insulin. In *Ultimate Guide to Insulin*; IntechOpen: London, UK, 2019. [[CrossRef](#)]
19. Schuck, S.; Prinz, W.A.; Thorn, K.S.; Voss, C.; Walter, P. Membrane expansion alleviates endoplasmic reticulum stress independently of the unfolded protein response. *J. Cell. Biol.* **2009**, *187*, 525–536. [[CrossRef](#)]
20. Meyerovich, K.; Ortis, F.; Allagnat, F.; Cardozo, A.K. Endoplasmic reticulum stress and the unfolded protein response in pancreatic islet inflammation. *J. Mol. Endocrinol.* **2016**, *57*, R1–R17. [[CrossRef](#)]
21. Galindo-Hernandez, O.; Cordova-Guerrero, I.; Diaz-Rubio, L.J.; Pulido-Capiz, A.; Diaz-Villanueva, J.F.; Castaneda-Sanchez, C.Y.; Serafin-Higuera, N.; Garcia-Gonzalez, V. Protein translation associated to PERK arm is a new target for regulation of metainflammation: A connection with hepatocyte cholesterol. *J. Cell. Biochem.* **2019**, *120*, 4158–4171. [[CrossRef](#)]
22. Acosta-Montano, P.; Rodriguez-Velazquez, E.; Ibarra-Lopez, E.; Frayde-Gomez, H.; Mas-Oliva, J.; Delgado-Coello, B.; Rivero, I.A.; Alatorre-Meda, M.; Aguilera, J.; Guevara-Olaya, L.; et al. Fatty Acid and Lipopolysaccharide Effect on Beta Cells Proteostasis and its Impact on Insulin Secretion. *Cells* **2019**, *8*, 884. [[CrossRef](#)] [[PubMed](#)]
23. Conchillo-Sole, O.; de Groot, N.S.; Aviles, F.X.; Vendrell, J.; Daura, X.; Ventura, S. AGGRESCAN: A server for the prediction and evaluation of "hot spots" of aggregation in polypeptides. *BMC Bioinform.* **2007**, *8*, 65. [[CrossRef](#)] [[PubMed](#)]
24. Szoka, F., Jr.; Papahadjopoulos, D. Comparative properties and methods of preparation of lipid vesicles (liposomes). *Annu. Rev. Biophys. Bioeng.* **1980**, *9*, 467–508. [[CrossRef](#)] [[PubMed](#)]
25. Knapp, B.; Ospina, L.; Deane, C.M. Avoiding False Positive Conclusions in Molecular Simulation: The Importance of Replicas. *J. Chem. Theory Comput.* **2018**, *14*, 6127–6138. [[CrossRef](#)]
26. Losasso, V.; Pietropaolo, A.; Zannoni, C.; Gustincich, S.; Carloni, P. Structural role of compensatory amino acid replacements in the alpha-synuclein protein. *Biochemistry* **2011**, *50*, 6994–7001. [[CrossRef](#)]
27. Prajapati, P.; Wang, W.X.; Nelson, P.T.; Springer, J.E. Methodology for Subcellular Fractionation and MicroRNA Examination of Mitochondria, Mitochondria Associated ER Membrane (MAM), ER, and Cytosol from Human Brain. *Methods Mol. Biol.* **2020**, *2063*, 139–154. [[CrossRef](#)]
28. Patil, S.M.; Alexandrescu, A.T. Charge-Based Inhibitors of Amylin Fibrillization and Toxicity. *J. Diabetes Res.* **2015**, *2015*, 946037. [[CrossRef](#)]
29. Balbach, J.J.; Ishii, Y.; Antzutkin, O.N.; Leapman, R.D.; Rizzo, N.W.; Dyda, F.; Reed, J.; Tycko, R. Amyloid fibril formation by A beta 16–22, a seven-residue fragment of the Alzheimer's beta-amyloid peptide, and structural characterization by solid state NMR. *Biochemistry* **2000**, *39*, 13748–13759. [[CrossRef](#)]
30. Smaoui, M.R.; Waldispuhl, J. Complete characterization of the mutation landscape reveals the effect on amylin stability and amyloidogenicity. *Proteins* **2015**, *83*, 1014–1026. [[CrossRef](#)]

31. Cho, W.J.; Jena, B.P.; Jeremic, A.M. Nano-scale imaging and dynamics of amylin-membrane interactions and its implication in type II diabetes mellitus. *Methods Cell. Biol.* **2008**, *90*, 267–286. [[CrossRef](#)]
32. Khemtemourian, L.; Domenech, E.; Doux, J.P.; Koorengevel, M.C.; Killian, J.A. Low pH acts as inhibitor of membrane damage induced by human islet amyloid polypeptide. *J. Am. Chem. Soc.* **2011**, *133*, 15598–15604. [[CrossRef](#)] [[PubMed](#)]
33. Cho, W.J.; Trikha, S.; Jeremic, A.M. Cholesterol regulates assembly of human islet amyloid polypeptide on model membranes. *J Mol Biol* **2009**, *393*, 765–775. [[CrossRef](#)] [[PubMed](#)]
34. Simons, K.; Toomre, D. Lipid rafts and signal transduction. *Nat. Rev. Mol. Cell. Biol.* **2000**, *1*, 31–39. [[CrossRef](#)] [[PubMed](#)]
35. Skeby, K.K.; Andersen, O.J.; Pogorelov, T.V.; Tajkhorshid, E.; Schiott, B. Conformational Dynamics of the Human Islet Amyloid Polypeptide in a Membrane Environment: Toward the Aggregation Prone Form. *Biochemistry* **2016**, *55*, 2031–2042. [[CrossRef](#)] [[PubMed](#)]
36. DeToma, A.S.; Salamekh, S.; Ramamoorthy, A.; Lim, M.H. Misfolded proteins in Alzheimer’s disease and type II diabetes. *Chem. Soc. Rev.* **2012**, *41*, 608–621. [[CrossRef](#)]
37. Kelly, J.W. Mechanisms of amyloidogenesis. *Nat. Struct. Biol.* **2000**, *7*, 824–826. [[CrossRef](#)]
38. Xu, W.; Wei, G.; Su, H.; Nordenskiold, L.; Mu, Y. Effects of cholesterol on pore formation in lipid bilayers induced by human islet amyloid polypeptide fragments: A coarse-grained molecular dynamics study. *Phys. Rev. E* **2011**, *84*, 051922. [[CrossRef](#)]
39. Vorobyov, I.; Allen, T.W. On the role of anionic lipids in charged protein interactions with membranes. *Biochim. Biophys. Acta* **2011**, *1808*, 1673–1683. [[CrossRef](#)]
40. Platre, M.P.; Jaillais, Y. Anionic lipids and the maintenance of membrane electrostatics in eukaryotes. *Plant Signal. Behav.* **2017**, *12*, e1282022. [[CrossRef](#)]
41. Martel, A.; Antony, L.; Gerelli, Y.; Porcar, L.; Fluit, A.; Hoffmann, K.; Kiesel, I.; Vivaudou, M.; Fragneto, G.; de Pablo, J.J. Membrane Permeation versus Amyloidogenicity: A Multitechnique Study of Islet Amyloid Polypeptide Interaction with Model Membranes. *J. Am. Chem. Soc.* **2017**, *139*, 137–148. [[CrossRef](#)]
42. Saitta, F.; Signorelli, M.; Fessas, D. Dissecting the effects of free fatty acids on the thermodynamic stability of complex model membranes mimicking insulin secretory granules. *Colloids Surf. B Biointerfaces* **2019**, *176*, 167–175. [[CrossRef](#)] [[PubMed](#)]
43. Zhang, X.; St Clair, J.R.; London, E.; Raleigh, D.P. Islet Amyloid Polypeptide Membrane Interactions: Effects of Membrane Composition. *Biochemistry* **2017**, *56*, 376–390. [[CrossRef](#)] [[PubMed](#)]
44. Jang, I.; Pottekat, A.; Poonthong, J.; Yong, J.; Lagunas-Acosta, J.; Charbono, A.; Chen, Z.; Scheuner, D.L.; Liu, M.; Itkin-Ansari, P.; et al. PDIA1/P4HB is required for efficient proinsulin maturation and ss cell health in response to diet induced obesity. *eLife* **2019**, *8*. [[CrossRef](#)] [[PubMed](#)]
45. Ali Khan, H.; Mutus, B. Protein disulfide isomerase a multifunctional protein with multiple physiological roles. *Front Chem.* **2014**, *2*, 70. [[CrossRef](#)]
46. Avelino Jorge, G.-G.V.; Alatorre-Meda, M.; Rodríguez-Velázquez, E.; Rivero, I.A. Synthesis of BODIPY-amino acids and the potential applications as specific dyes for the cytoplasm of Langerhans β -cells. 2020, (in review).
47. Avila-Cossio, M.E.; Rivero, I.A.; Garcia-Gonzalez, V.; Alatorre-Meda, M.; Rodriguez-Velazquez, E.; Calva-Yanez, J.C.; Espinoza, K.A.; Pulido-Capiz, A. Preparation of Polymeric Films of PVDMA-PEI Functionalized with Fatty Acids for Studying the Adherence and Proliferation of Langerhans beta-Cells. *ACS Omega* **2020**, *5*, 5249–5257. [[CrossRef](#)]
48. Gao, L.P.; Chen, H.C.; Ma, Z.L.; Chen, A.D.; Du, H.L.; Yin, J.; Jing, Y.H. Fibrillation of human islet amyloid polypeptide and its toxicity to pancreatic beta-cells under lipid environment. *Biochim. Biophys. Acta Gen. Subj.* **2020**, *1864*, 129422. [[CrossRef](#)]
49. Middleton, C.T.; Marek, P.; Cao, P.; Chiu, C.C.; Singh, S.; Woys, A.M.; de Pablo, J.J.; Raleigh, D.P.; Zanni, M.T. Two-dimensional infrared spectroscopy reveals the complex behaviour of an amyloid fibril inhibitor. *Nat. Chem.* **2012**, *4*, 355–360. [[CrossRef](#)]

